

2

WHOI-88-16

**Summer Study Program
in
Geophysical Fluid Dynamics
Order and Disorder in Planetary Dynamos**

by

Willem V.R. Malkus

Edited by
Mary Evans Berry

Woods Hole Oceanographic Institution
Woods Hole, Massachusetts 02543

May 1988

Technical Report

Funding was provided by the Office of Naval Research under contract Number N00014-82-G-0079,
and the National Science Foundation under grant Number DMS-85-04166.

Reproduction in whole or in part is permitted for any purpose of the
United States Government. This report should be cited as:
Woods Hole Oceanog. Inst. Tech. Rept., WHOI-88-16.

Approved for publication; distribution unlimited.

Approved for Distribution:

DTIC
ELECTE
JUN 27 1988
S D H

Charles D. Hollister

Charles D. Hollister
Dean of Graduate Studies

1987 Summer Study Program

in

Geophysical Fluid Dynamics

ORDER AND DISORDER IN

PLANETARY DYNAMOS

Woods Hole Oceanographic Institution
Woods Hole, Massachusetts

GEOPHYSICAL FLUID DYNAMICS PROGRAM

Summer 1987

Staff and Visitors

NAME	AFFILIATION
Bayly, Bruce J.	Courant Institute of Mathematical Sciences
Berger, Mel S.	University of Massachusetts at Amherst
Bloxham, Jeremy	Harvard University
Bolton, Edward W.	Yale University
Cattaneo, Fausto	JILA, University of Colorado at Boulder
Childress, Stephen	Courant Institute of Mathematical Sciences
Fields, George B.	Harvard University
Flierl, Glenn R.	Massachusetts Institute of Technology
Griffa, Annalisa	Scripps Institution of Oceanography
Hide, Raymond	Meteorological Office, Bracknell, U.K.
Hughes, David	DAMTP, University of Cambridge
Ierley, Glenn R.	Michigan Technological University
Krasny, Robert	Courant Institute of Mathematical Sciences
Malkus, Willem V.R.	Massachusetts Institute of Technology
Proctor, Michael R.E.	Cambridge University
Salmon, Richard L.	University of California, San Diego
Shepherd, Theodore G.	DAMTP, University of Cambridge
Sommeria, Joel	University of Grenoble
Soward, Andrew M.	University of Newcastle-upon-Tyne
Spiegel, Edward A.	Columbia University
Stern, Melvin E.	Florida State University
Strauss, Henry R.	Courant Institute of Mathematical Sciences
Veronis, George	Yale University
Weiss, Nigel O.	Cambridge University
Young, William R.	Massachusetts Institute of Technology

Fellows

Brazell, Lorna C.	Emmanuel College, University of Cambridge
Gilbert, Andrew D.	Gonville & Caius College, University of Cambridge
Hollerbach, Rainer	Scripps Institution of Oceanography
Hu, Bin Bin	Columbia University
Jennings, Richard L.	University of Newcastle upon Tyne
Klapper, Isaac	Courant Institute of Mathematical Sciences
McMillan, Jack F.	University of Hawaii
Yano, Jun-Ichi	Kyoto University



Row 1: R. Jennings, A. Gilbert, M. Stern, B. Bayly, R. Salmon, G. Veronis,
A. Soward, A. Griffa, R. Hide

Row 2: J. McMillan, R. Hollerbach, J. Sommeria, B. Young, G. Ierley, J. Yano,
S. Childress, I. Klapper, B. Hu, L. Brazell, W. Malkus, N. Weiss, K. Rooth

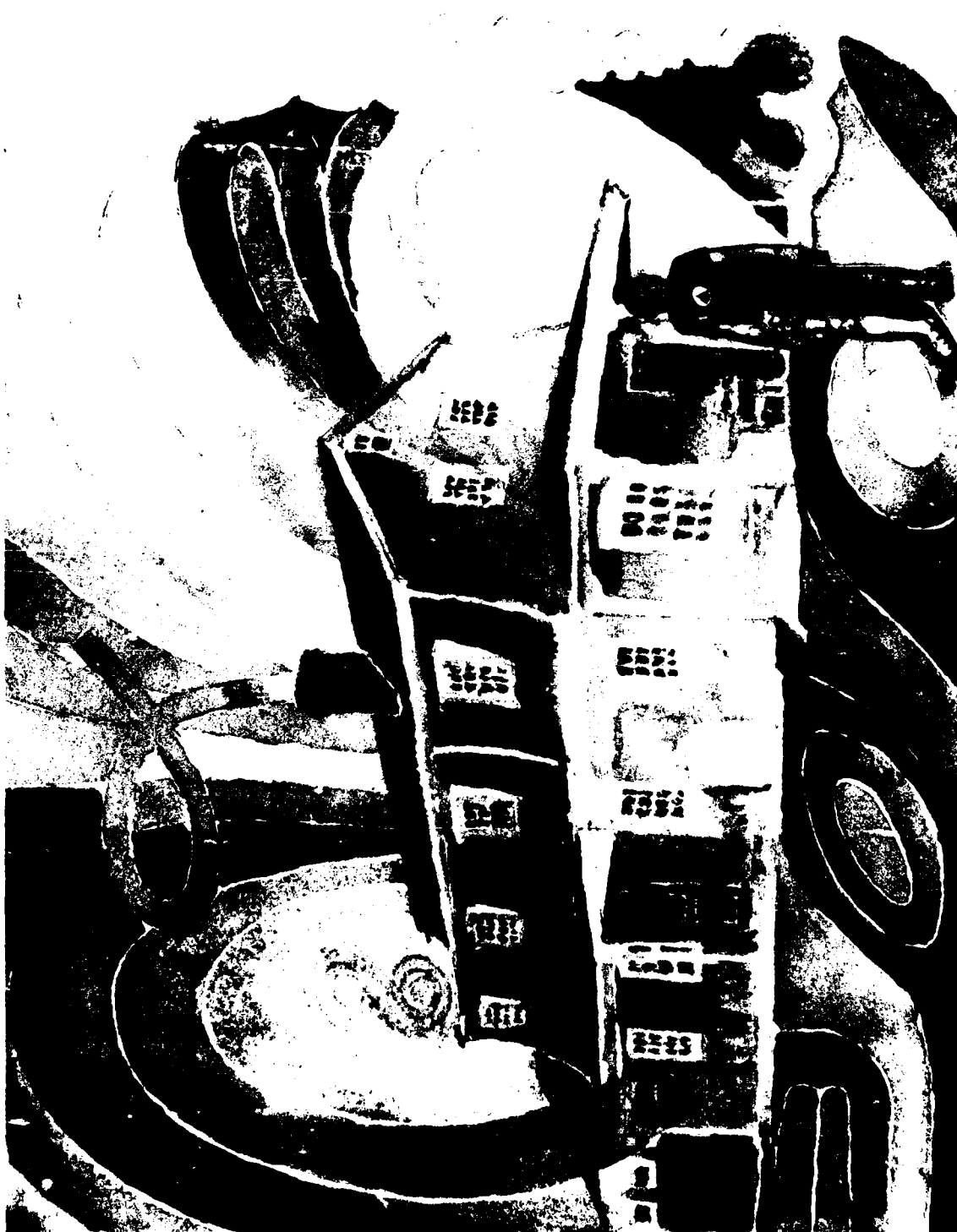


J. Whitehead, G. Field, E. Spiegel, M. Proctor, H. Strauss, T. Shepherd,
J. Gollub

ton For	
RA&I	<input checked="" type="checkbox"/>
B	<input type="checkbox"/>
need	<input type="checkbox"/>
uation	

By		
Distribution/		
Availability Codes		
Dist	Avail and/or	Special
A1		





The Magnetic Cottage by Stephen Childress, Principal Lecturer

PREFACE

Our principal lecturer, Stephen Childress, can be seen on a preceding page emerging from the "magnetic cottage" he constructed to edify those of us who attended G.F.D. '87. His central theme was the kinematic properties of the "fast" dynamo, one whose growth rate is insensitive to electrical conductivity. These novel studies, and the seminars given by Andrew Soward and others, offer assurance of more mechanistic understanding of evolving magnetic fields in stars and planets. The timely juxtaposition of Childress' lectures on kinematic fast dynamos and the seminars by Bruce Bayly on inertial three-dimensional instabilities of shear flow, may lead soon to a dynamic fast-fast dynamo.

Faster than convecting continents, slower than Antarctic bottom water, waves in the Earth's magnetic field move to the west. Geophysicists' knowledge of the underlying process appears to advance at a similar pace. Yet the dynamos of the summer season already have suggested hydromagnetic flows which offer hope both of realizeable laboratory dynamos and more realistic planetary models. Perhaps the pace of testable predictions will quicken?

The Fellowship lectures were more confined to the summer topic than is usual. Several of the Fellows reported on exciting discoveries of the season, several reported on sound extensions of work discussed in the principal lectures, and several struggled with problems which resisted swift resolution. The record of these lectures found in this volume may appear quite polished for a first paper, yet they have not been formally edited and must be treated as unpublished manuscripts. A reader who wishes to quote material found here should seek the permission of the author.

We are indebted to the Office of Naval Research and to three branches of the National Science Foundation for financial support for the summer program. The polished execution of initial editing and \LaTeX format of the principal lectures is due to Mary Berry. We are grateful to Mary and A. L. Peirson for their thoughtful administration of our program.

Willem V.R. Malkus
Director

Contents

1 A Brief Tour of Dynamo Theory 1919 - 1978	7
1.1 Introduction	7
1.2 Derivation of the Induction Equation	8
1.3 The Disc Dynamo	9
1.4 Toroidal-Poloidal Decomposition of Fields	10
1.5 A Simple Induction Problem	12
1.6 Summary	13
1.7 References	13
2 The Alpha-Effect (How to Smooth a Rough Problem)	15
2.1 Introduction	15
2.2 Parker's Cyclonic Events	17
2.3 Roberts' 2-D Cellular Flow (1972)	17
2.4 Braginskii's Models	21
2.5 References	26
3 Induction at Large and Infinite R	27
3.1 Cauchy's Solution for $R = \infty$	27
3.2 The Effect of Diffusion	32
3.3 References	36
4 Asymptotics for Large R in Steady Flow	37
4.1 Flux Expulsion	37
4.2 Alpha Effect at large R in Cellular Flow	40
4.3 Cat's Eyes	44
4.4 Another Modification	49
4.5 Third Example of α -Effect in the Limit $R \rightarrow \infty$	50
4.6 The Density of Dynamos in One Model	50
4.7 References	51
5 The Genesis of the Fast Dynamos	53
5.1 Introduction	53
5.2 The Role of Diffusion	53
5.3 Liapunov Exponents	54
5.4 Some Models of Fast Dynamos	56
5.5 The Rope Dynamo	57
5.6 Problems Facing Fast Dynamos	59
5.7 Conclusions	61
5.8 References	61

6	Fast Dynamos I: Steady Flow	63
6.1	Introduction	63
6.2	Numerical studies of Beltrami's Flow	66
6.3	Some Aspects of the Geometry of the ABC Flows	68
6.4	Soward's Analysis of Fast Dynamo Activity	72
6.5	References	73
7	Fast Dynamos II: Analysis of Complex Flows	75
7.1	Soward's Analysis of Cellular Flow in the Limit $R \rightarrow \infty$	75
7.2	Heuristic Model	75
7.3	Boundary Layer Structure	77
7.4	Ponomarenko's Helical Dynamo	78
7.5	Dynamos from Non-Magnetic Instabilities	79
7.6	Possible Approaches to Fast Dynamos	81
7.7	Overlapping Cat's Eyes	83
7.8	Blinking Eyes	83
7.9	Other Systems Worth Considering	83
7.10	References	85
8	Fast Dynamos III: Methods Based on Unsteady Maps and Flows	87
8.1	Introduction	87
8.2	The Stretch-Fold-Shear (SFS) Map	87
8.3	Mapping the Magnetic Field	88
8.4	Digression on the "Tent Map"	90
8.5	Some Graphical Results	91
8.6	Some Analysis of the Model	96
8.7	References	96
9	Dynamo Concepts Applied to Vortex Stretching	97
9.1	Preamble	97
9.2	General Introduction	97
9.3	Possible Singularities of Euler and Navier-Stokes Flows	99
9.4	The Taylor-Green Problem	101
9.5	Discussion	101
9.6	Vortex Tube Models of the Energy Cascade	102
9.7	Vortical Automata	104
9.8	References	107

ABSTRACTS OF PARTICIPANTS

Fast Dynamos in Chaotic Flow Bruce Bayly	109
Observational Constraints on Theories of the Geodynamo Jeremy Bloxham	111
Nonlinear Convection in a Spherical Shell Edward W. Bolton	113
Low Order Model of the Solar Dynamo Fausto Cattaneo	115
Current Sheets in Force-Free Magnetic Fields George Field	117
Wind-Driven Circulation and Free Equilibrium States in a Closed Basin Annalisa Griffa	120
The Determination of Topographic Core-Mantle Coupling from Geophysical Data Raymond Hide	121
The Nonlinear Breakup of a Magnetic Layer David W. Hughes	123
Macrodynamic Equilibration and Eigenflows Glenn Ierley	125
Computation of Vortex Sheet Roll-Up Robert Krasny	127
Shunted Homopolar Dynamo - Analytic Approach to a Poincaré Map Ya Yan Lu	131
Inertial Modes in Laboratory Spheroids Willem V.R. Malkus	133
Strong Spatial Resonance and Travelling Waves in Bénard Convection M.R.E. Proctor	135
A Review of Hamiltonian Fluid Mechanics Rick Salmon	137

Nonlinear Stability and Some of its Implications	
T.G. Shepherd	139
Vortices in a Turbulent Shear: A Model of the Great Red Spot of Jupiter	
Joël Sommeria	145
Aspects of Fast Dynamo Theory	147
Application of the Wiener-Hopf Method to Fast Dynamos	
Andrew Soward	149
The Loss of Integrability	
E. A. Spiegel	153
Evolution of a Locally Unstable Shear Flow Near a Wall or a Coast	
Melvin E. Stern	155
Turbulent Fast Dynamos	156
Current Sheets in the Solar Corona	
Henry Strauss	157
Ocean Circulation Driven by Wind and Buoyancy	
George Veronis	159
Toy Systems and Stellar Dynamos	
Nigel Weiss	161
Nonlinear Corner Flows on a β-Plane	
William R. Young	164

FELLOWS PROJECT REPORTS

**The Instability of an Elliptical Flow in the
Presence of a Magnetic Field**

Lorna Brazell

F1.1 - F1.18

The Ponomarenko Dynamo

Andrew D. Gilbert

F2.1 - F2.12

**A Numerical Model of α^2 and $\alpha\omega$ Dynamos
in the Limit of Asymptotically Small Viscosity**

Rainer Hollerbach

F3.1 - F3.16

**Elliptical Instability Modes in Rigid Container Growth Rate
and Reynold Stresses**

Bin Bin Hu

F4.1 - F4.18

Symmetry Breaking in the Solar Dynamo

Richard Jennings

F5.1 - F5.16

Topology and Ergodics in Chaotic Fast Dynamos

Isaac Klapper

F6.1 - F6.14

A Quasi-Dynamical Dynamo Model

Jack McMillan

F7.1 - F7.21

**How I Managed to set an Isolated Monopole Vortex in
Quasi-Geostrophic Zonal Shear Flow**

Jun-Ichi Yano

F8.1 - F8.24

1987 Summer Study Program

in

Geophysical Fluid Dynamics

ORDER AND DISORDER IN

PLANETARY DYNAMOS

LECTURES

Stephen Childress

Courant Institute of Mathematical Sciences

Lecture 1

A Brief Tour of Dynamo Theory 1919 - 1978

1.1 Introduction

The principal problems motivating the study of dynamo theory are those of the Earth's and the Sun's dynamos. Many and various theories were put forward to explain these; Larmor was the earliest to propose that some form of fluid dynamo action was responsible for generating the observed magnetic fields, in 1919. The emphasis in at least the early lectures of this series will be on the kinematic dynamo problem; although a treatment not involving the dynamics of the system can never be satisfactory, the state of knowledge of the dynamics and the complexity of the governing equations are such that the comparatively simplistic, kinematic approach – where the velocity field is specified considering only in passing whether or not it might be physically realistic – is still a useful one. An additional justification is that in the initial state where the seed magnetic field is too small to affect the velocity field, a kinematic treatment is consistent with the dynamics of the problem, given a force field to set up the flow.

The kinematic dynamo problem consists in finding solutions to the equations

$$\frac{\partial \mathbf{B}}{\partial t} + \mathbf{u} \cdot \nabla \mathbf{B} - \mathbf{B} \cdot \nabla \mathbf{u} - \eta \nabla^2 \mathbf{B} = 0 \quad \text{- the induction equation} \quad (1.1)$$

$$\nabla \cdot \mathbf{B} = 0 \quad (1.2)$$

where $\mathbf{u}(\mathbf{r}, t)$ is the given (or guessed!) velocity field

$\mathbf{B}(\mathbf{r}, t)$ is the magnetic field

η is the magnetic diffusivity, having dimension of $[L^2/T]$,

and is the principal parameter of interest. For a conducting fluid with conductivity σ and magnetic permeability μ , the magnetic diffusivity is defined as

$$\eta = \frac{1}{\sigma \mu} \quad (1.3)$$

In addition, consider the fluid to be incompressible, i.e.

$$\nabla \cdot \mathbf{u} = 0 \quad (1.4)$$

The system being considered is as shown in (Figure 1.1).

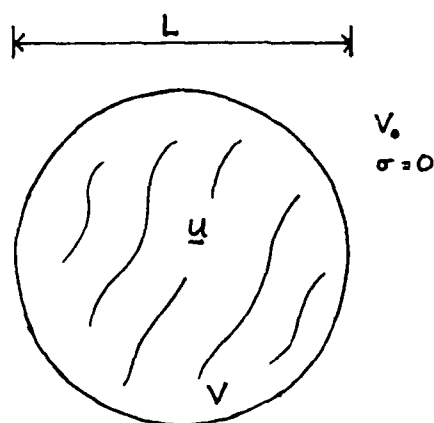


Figure 1.1: A spherical volume of fluid.

Let U be a typical speed of the fluid. Then the magnetic Reynolds number R (sometimes denoted by R_m) is defined by

$$R \equiv \frac{UL}{\eta} \approx \frac{|\nabla \wedge (u \wedge B)|}{|\eta \nabla^2 B|} = \frac{\text{advective term}}{\text{diffusive term}} \quad (1.5)$$

The case where $R \gg 1$ leads, for a flux tube of material, to the "frozen flux" approximation where

$$\frac{d}{dt} \int_{\text{surface of tube end}} B \cdot n ds = 0 \quad (1.6)$$

so that stretching of the tube will lead to amplification of the magnetic field. The dynamo problem is not solved, however, since fields generated this way must then be reassembled into a whole, and that is less straightforward.

If $u = 0$, the characteristic timescale on which a magnetic field in an isolated system will decay is

$$\tau = \frac{L^2}{\eta} \quad (1.7)$$

The basic evidence for dynamo activity in the Earth is the presence of a periodic or aperiodic cycle persisting longer than this natural decay time (in the Earth's case, by a factor of about 10^3 ; the power spectrum of the field has been discussed by Lowes (1973)). R is typically large in astrophysical bodies, of the order of 100 or more. For the sun R is much larger, and the main evidence of dynamo action there is the *solar cycle*.

1.2 Derivation of the Induction Equation

Equation (1) is derived from the so-called pre-Maxwell equations:

$$J = \sigma(E + u \wedge B) \quad \text{- Ohm's Law} \quad (1.8)$$

where J is the electric current

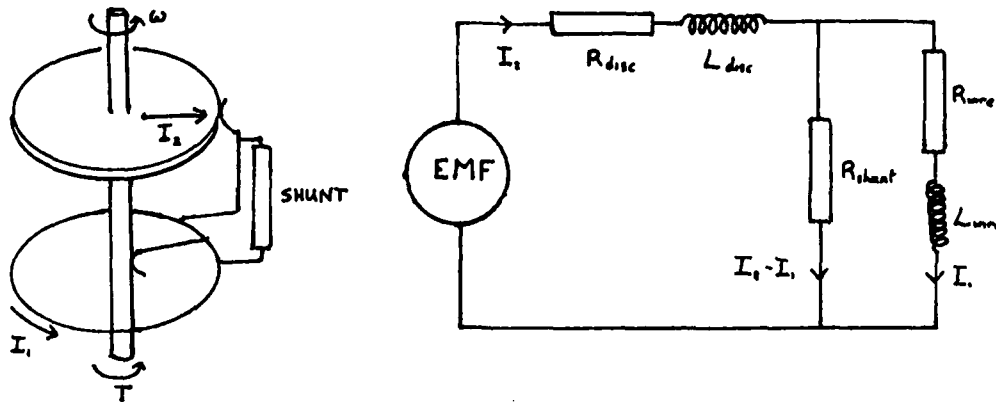


Figure 1.2

\mathbf{E} is the electric field and

$\mathbf{u} \wedge \mathbf{B}$ gives the electromotive force due to the fluid crossing lines of force;

$$\nabla \wedge \mathbf{E} = \frac{-\partial \mathbf{B}}{\partial t} \quad \text{- Faraday's Law} \quad (1.9)$$

which says that the circulation of $\mathbf{E} = -$ flux of rate-of-change of \mathbf{B}

$$\nabla \wedge \mathbf{B} = \mu \mathbf{J} \quad \text{- Ampere's Law} \quad (1.10)$$

which says that the circulation of \mathbf{B} is proportional to the flux of current. Substituting for \mathbf{E} from (1.8) into (1.9) gives

$$\frac{\partial \mathbf{B}}{\partial t} = \nabla \wedge (\mathbf{u} \wedge \mathbf{B}) - \nabla \wedge \left(\frac{\mathbf{J}}{\sigma} \right); \quad (1.11)$$

and substituting for \mathbf{J} from (1.10) and using (1.2) and (1.3) gives (1) as stated. Implicit in the induction equation is the role of stirring of the field by global fluid motions as a source of disorder, whether the motions are regular or turbulent.

The global motions of the Earth's core fluid are believed to produce such a source of disorder.

1.3 The Disc Dynamo

The simplest dynamo that exhibits chaotic, aperiodic sequence of normal and reversed states similar to that seen in the Earth is the disc dynamo as shown in figure 1.2.

The behavior of the disc dynamo is governed by the following equations:

$$M\omega I_1 = L_{disc} \frac{dI_2}{dt} + R_{disc} I_2 + R_{shunt} (I_2 - I_1) \quad (1.12)$$

where M is the mutual inductance of the disc and the wire

$$\begin{aligned}(I_2 - I_1)R_{shunt} &= L_{wire} \frac{dI_1}{dt} + I_1 R_{wire} \\ C \frac{d\omega}{dt} &= T + M I_1 I_2 - \nu \omega\end{aligned}\quad (1.13)$$

where C is the moment of inertia

T is the driving torque

$\nu \omega$ is a viscous damping term

These equations map to the Lorenz system as follows:

$$[t, \omega, I_1, I_2] \rightarrow [\tau t, (\frac{R}{\nu} - \frac{R_s}{M} - z)\delta, \beta x, \alpha y] \quad (1.14)$$

where $\tau = \frac{L_{disc}}{R_{disc}}$

$$\delta = (R_{wire} + R_{shunt})(R_{disc} + R_{shunt})/M R_{shunt}$$

$$\alpha^2 = (R_{wire} + R_{shunt})/M R_{shunt} \nu \delta$$

$$\beta = R_{shunt} \alpha / (R_{wire} + R_{shunt})$$

In this system the equations become

$$dx/dt = R - yz - \nu x$$

$$dy/dt = \sigma(z - y)$$

$$dz/dt = xy - z$$

Figure 1.3 shows the oscillations of the system in phase space.

The disc dynamo works by virtue of a very specific topology that is far removed from the broadly homogeneous, single, conducting mass that forms the dynamo system for either the Earth or Sun.

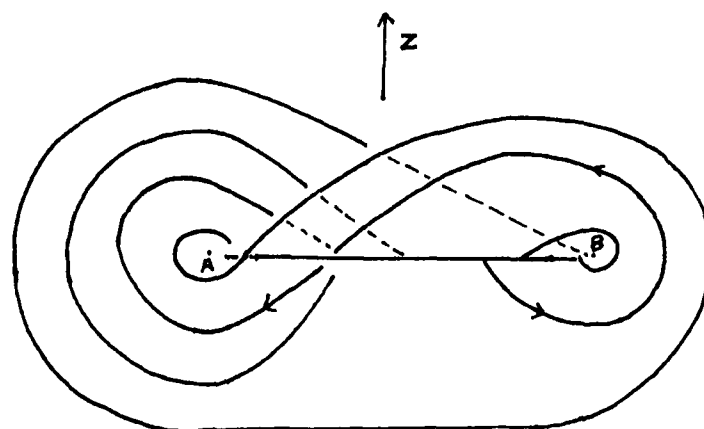
1.4 Toroidal-Poloidal Decomposition of Fields

In a typical spherical system, \mathbf{B} and \mathbf{u} may be written as a sum of poloidal and toroidal components as shown in Figure 1.4.

Mathematically, this decomposition is expressed as

$$\mathbf{B} = \underbrace{\nabla \wedge T \mathbf{r}}_{\mathbf{B}_T} + \underbrace{\nabla \wedge \nabla \wedge S \mathbf{r}}_{\mathbf{B}_P} \quad (1.15)$$

This structure is natural to a spherical system. The poloidal and toroidal components are converted into each other during the dynamo processes, either sequentially or simultaneously; an early success was Backus' (1958) sequence of interactions by which $\mathbf{B}_P \rightarrow \mathbf{B}_T \rightarrow \mathbf{B}_P$. The scalars T and S which describe the toroidal and poloidal parts respectively are both functions of all three spherical coordinates. The decomposition as shown is uniquely possible only if both scalars are stipulated to have zero mean over spherical surfaces.



$$A: (I_1, I_2) = (-C_1, -C_2)$$

$$B: (I_1, I_2) = (C_1, C_2)$$

Figure 1.3

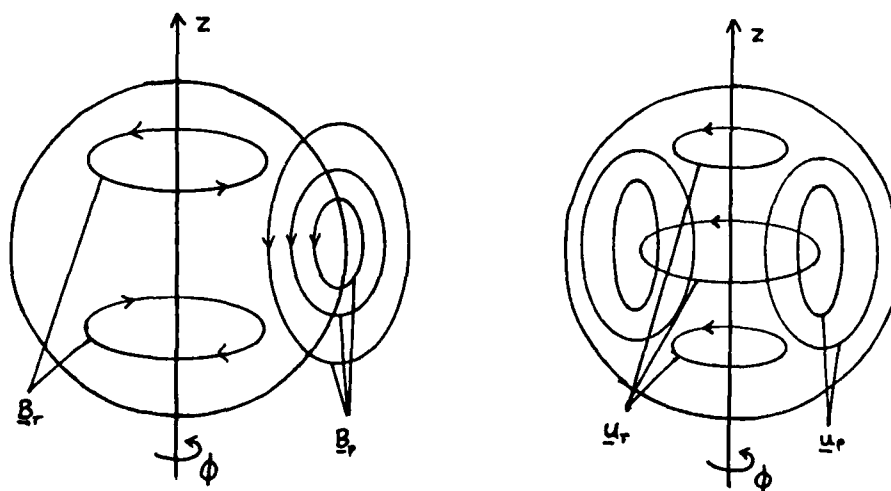


Figure 1.4

1.5 A Simple Induction Problem

Consider a system with axial symmetry and take a toroidal velocity:

$$\mathbf{u} = \omega(r)r \sin \theta \mathbf{i}_\phi; \quad \omega(r_0) = 0 \quad (1.16)$$

Let

$$\mathbf{B} = \mathbf{B}_0 + \mathbf{B}' \quad (1.17)$$

where

$$\begin{aligned} \mathbf{B}_0 &= i_z B_0 \quad \text{as } r \rightarrow \infty \text{ is a steady external field} \\ \mathbf{B}' &= \underbrace{\nabla \wedge T\mathbf{r}}_{\mathbf{B}_T} + \underbrace{\nabla \wedge \nabla \wedge S\mathbf{r}}_{\mathbf{B}_P} \end{aligned} \quad (1.18)$$

subject to the uniqueness condition

$$\frac{1}{4\pi^2} \int_{\text{unit sphere}} S, T d\Omega = 0$$

In the steady case,

$$\begin{aligned} \mathbf{B} &= \nabla \phi, \quad r > r_0, \\ \nabla \wedge \mathbf{B} &= \nabla \wedge \nabla \wedge T\mathbf{r} + \nabla \wedge \nabla \wedge \nabla \wedge S\mathbf{r}, \quad r < r_0 \end{aligned} \quad (1.19)$$

But

$$\begin{aligned} \nabla \wedge S\mathbf{r} &= \nabla S \wedge \mathbf{r} \\ \nabla \wedge (\nabla S \wedge \mathbf{r}) &= \mathbf{r} \cdot \nabla (\nabla S) - (\nabla S \cdot \nabla) \mathbf{r} - \mathbf{r} (\nabla^2 S) + 3 \nabla S \\ &= -\mathbf{r} \nabla^2 S + \nabla (S + \mathbf{r} \cdot \nabla S) \\ \Rightarrow \nabla \wedge \nabla \wedge \nabla \wedge S\mathbf{r} &= \nabla \wedge (-\nabla^2 S \mathbf{r}) \end{aligned} \quad (1.20)$$

So

$$\begin{aligned} \nabla \wedge \nabla \wedge \mathbf{B} &= \nabla \wedge (-\nabla^2 T \mathbf{r}) + \nabla \wedge \nabla \wedge (-\nabla^2 S \mathbf{r}) \\ &= \sigma \mu \nabla \wedge (\mathbf{u} \wedge \mathbf{B}) \\ &= \frac{1}{\eta} \nabla \wedge \left(\frac{B_0}{3} \omega' r P_2(\cos \theta) \right) \mathbf{r} \end{aligned} \quad (1.21)$$

So in conductor

$$\nabla^2 T = -\frac{B_0}{3} \frac{\omega' r}{3\eta} P_2(\cos \theta)$$

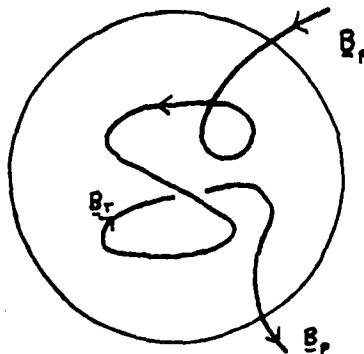
and

$$\nabla^2 S = 0 \quad (1.22)$$

Outside the conductor,

$$\nabla \wedge \mathbf{B} = 0 \Rightarrow \nabla^2 S = T = 0 \quad (1.23)$$

The boundary conditions at $r = r_0$ are thus that B_n , B_t and E_r are continuous on the boundary and that $J_n = 0$ there. (E_n is not continuous since a build-up of charges may occur.)

Figure 1.5: The ω effect.

Hence $T = 0$ on the boundary.

The equations are solved by variation of parameters

$$T = \frac{-B_0}{3} \frac{P_2(\cos \theta)}{\eta r^3} \left[\int_0^r r^4 \omega(r) dr - \frac{r^5}{r_0^5} \int_0^{r_0} r^4 \omega(r) dr \right] \quad (1.24)$$

in the conductor and zero outside.

$S = \frac{1}{2} r \cos \theta$ everywhere (uniform poloidal field).

By the action of the angular velocity, ω , it is therefore easy to create energy in the toroidal component if energy is present in the poloidal part, as shown in Figure 1.5. For a uniform field, no effect is observed outside the conductor.

1.6 Summary

At a macroscopic level, the magnetohydrodynamics of the dynamo 'climate' can exhibit aperiodicities of most nonlinear systems.

Fortunately there is also some order: the " ω - effect" is naturally present in symmetric rotating systems. Thorough reviews of the problem are given in Moffatt (1978) and Parker (1979).

1.7 References

- Backus, G., (1958). "A class of self-sustaining dissipative spherical dynamos," *Annals of Physics*, **4**, 372-447.
- Lowes, F.J., (1973). "Spatial power spectrum of the main geomagnetic field, and extrapolation to the core," *Geophys. J.R. Astr. Soc.*, **36**, 717-730.
- Moffatt, H.K., (1978). *Magnetic field generation in electrically conducting fluids*, Cambridge University Press.
- Parker, E.N., (1979). *Cosmical magnetic fields*, Oxford University Press.

Notes submitted by Lorna Brazell

Lecture 2

A Brief Tour Continued: The Alpha-Effect (How to Smooth a Rough Problem)

2.1 Introduction

Planetary dynamos are naturally associated with rotating, approximately spherical systems, which have a very accessible omega effect. This produces toroidal field components if poloidal field components are present: $B_P \xrightarrow{\omega} B_T$. However, the omega effect, in isolation, cannot produce a dynamo. Some possible modifications are:

- Include plausible convective motions in \mathbf{u} and solve the eigenvalue problem for the growth rate of a magnetic field numerically (Bullard and Gellman, 1954).
- Add further components to \mathbf{u} and treat a more general axisymmetric problem. However Cowling (1934) showed that such dynamos, with *both* velocity and magnetic fields axisymmetric, are impossible.
- Break the symmetry of the conductor, for example, to give a kind of disc dynamo. This is probably unrealistic for planetary cores.
- Combine simple rotors embedded in a conducting sphere (Figure 2.1). This gave the first proof of steady dynamo action in a homogeneous medium (Herzenberg, 1958). Note that a boundary to V_0 is essential for two similar rotors, but is not needed for two dissimilar rotors, nor for three or more (Gibson, 1968).

The hard problem is to produce poloidal fields from toroidal fields, $B_T \rightarrow B_P$, and thus close the cycle. If C is a closed loop of poloidal field, spanned by a surface, S , (Figure 2.2) then:

$$\int_C \mathbf{B} \cdot d\mathbf{s} = \frac{1}{\mu} \int_S \mathbf{J} \cdot d\mathbf{S} \quad (2.1)$$

and so a current flows through S . Thus poloidal fields are generated by toroidal currents, and the problem is to generate currents *aligned* with the toroidal field. This is an example of the "alpha effect".

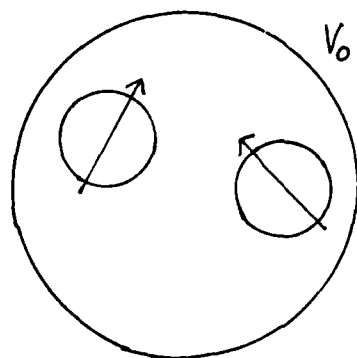


Figure 2.1

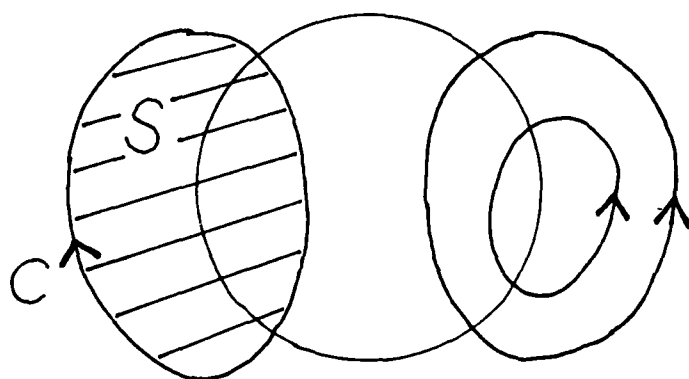


Figure 2.2

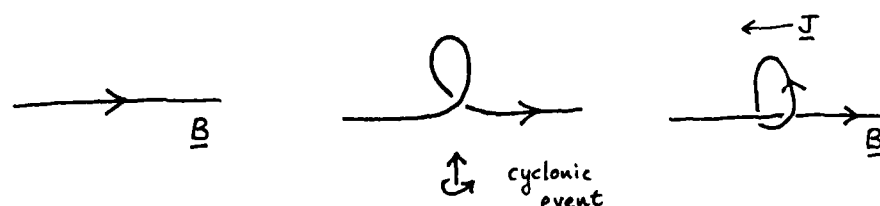


Figure 2.3

2.2 Parker's Cyclonic Events

A mechanism giving an alpha effect was first suggested by Parker (1955), who considered rising blobs of buoyant fluid. Such blobs would rotate as they rise, because of Coriolis forces, and these "cyclonic events" would lift and twist magnetic field lines (Figure 2.3). The process generates loops of flux perpendicular to the original field line, and thus a current parallel to the original field. This demonstrates that *helical* motions are a possible way of realizing an alpha effect. The analysis of Steenbeck, Krause and Rädler (1966) showed how such effects arise by averaging over small scale events, in a variety of circumstances.

2.3 Roberts' 2-D Cellular Flow (1972)

We consider now as a model which uses smoothing at *low* local magnetic Reynolds numbers and provides an example illustrating Parker's ideas. Take the velocity field:

$$\begin{aligned} \mathbf{u} &= (\psi_y, -\psi_x, K\psi) \\ \psi &= \frac{U}{k} \sin kx \sin ky \end{aligned} \quad (2.2)$$

This is cellular flow; in each cell the particle paths are helical, sweeping out nested cylinders (Figure 2.4).

What is the effect of this flow on an ambient, constant field, $B_0 i$? Set $\mathbf{B} = B_0 i + \mathbf{b}$ in the induction equation:

$$\frac{\partial \mathbf{b}}{\partial t} + \mathbf{u} \cdot \nabla \mathbf{b} - B_0 \frac{\partial \mathbf{u}}{\partial x} - \mathbf{b} \cdot \nabla \mathbf{u} - \eta \nabla^2 \mathbf{b} = 0 \quad (2.3)$$

with orders: $b/t, Ubk, B_0 U k, Ubk, \eta k^2 b$. Assume that \mathbf{b} is steady, and the local magnetic Reynolds number is small, $R \equiv U/k\eta \ll 1$. Then $\mathbf{b} \sim B_0 U/k\eta \ll B_0$, and

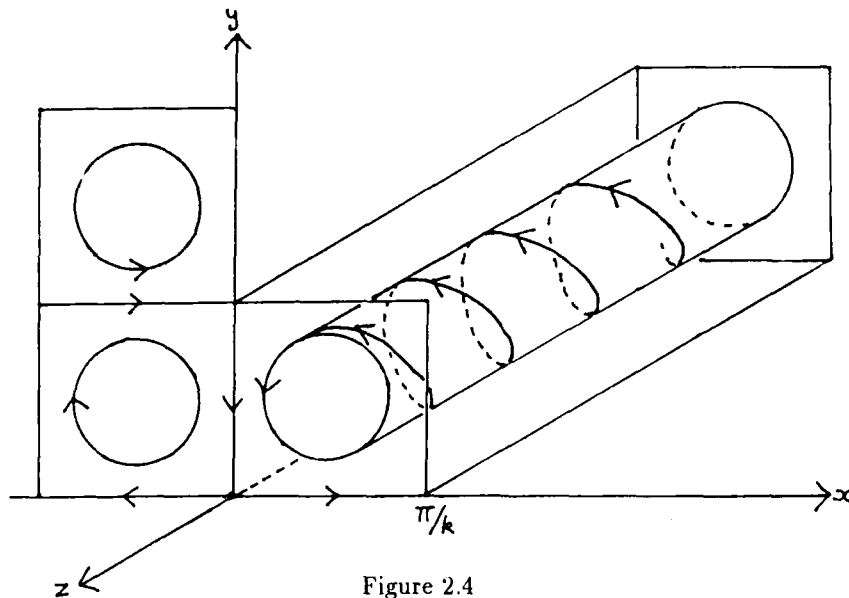


Figure 2.4

$$\mathbf{b} \simeq -\frac{B_0}{\eta} \nabla^{-2} \frac{\partial \mathbf{u}}{\partial x} = \frac{B_0}{2\eta k^2} \frac{\partial \mathbf{u}}{\partial x} \quad (2.4)$$

Now we calculate the average (over many cells) of $\mathbf{u} \wedge \mathbf{B}$:

$$\langle \mathbf{u} \wedge \mathbf{B} \rangle = \langle \mathbf{u} \wedge \mathbf{b} \rangle = -\frac{B_0 K}{\eta k^2} \mathbf{i} \langle \psi_x^2 \rangle = -\frac{B_0 U^2 K}{4\eta k^2} \mathbf{i} \quad (2.5)$$

With $K = k$, the motion induces an emf $\alpha B_0 \mathbf{i}$, with $\alpha = -U^2/4\eta k$, and a corresponding current parallel to the mean field, as envisaged by Parker. Note that $\alpha = O(RU)$, having the dimensions of velocity.

For a general uniform mean field, \mathbf{B}_0 , the effect of this flow is to give the emf:

$$\langle \mathbf{u} \wedge \mathbf{B} \rangle = \langle \mathbf{u} \wedge \mathbf{b} \rangle = \boldsymbol{\alpha} \cdot \mathbf{B}_0 \quad (2.6)$$

where

$$\boldsymbol{\alpha} = -\frac{KU^2}{4\eta k^2} \begin{pmatrix} 1 & 0 & 0 \\ 0 & 1 & 0 \\ 0 & 0 & 0 \end{pmatrix} \quad (2.7)$$

is a pseudo-tensor. The helical structure of the flow may be measured by the "helicity" (Moffatt, 1969):

$$H = \langle \mathbf{u} \cdot \nabla \wedge \mathbf{u} \rangle \quad (2.8)$$

For this flow, $H = U^2 K$, so that $\alpha = -H/\eta k^2$, and the alpha effect is seen to be closely related to the helicity in the fluid flow. This cellular flow realizes, at low R , what Parker had envisaged at high R (Figure 2.5). The magnetic field line is deformed diffusively into a helical shape.

Let us apply the same ideas to the flow:

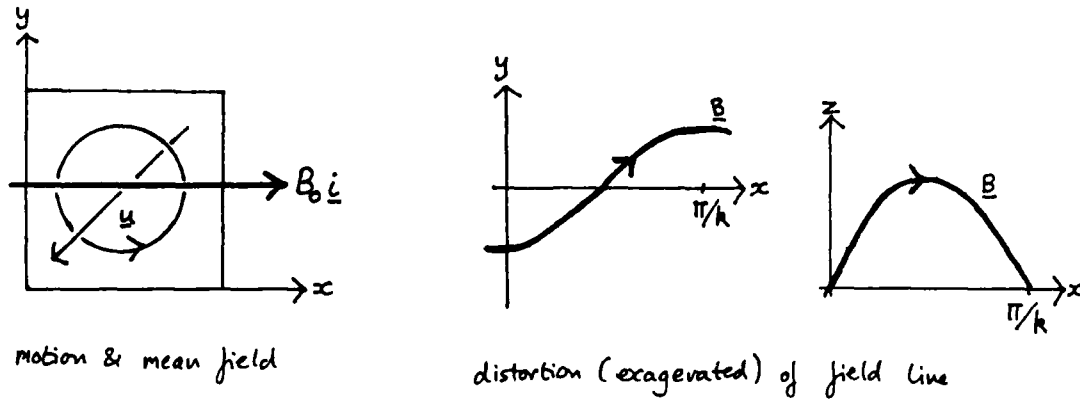


Figure 2.5

$$\mathbf{u} = \mathbf{u}^{(1)} + \mathbf{u}^{(2)} \quad (2.9)$$

with

$$\begin{aligned} \mathbf{u}^{(1)} &= U(0, \cos kx, \sin kx), \\ \mathbf{u}^{(2)} &= U(\sin ky, 0, \cos ky). \end{aligned}$$

This flow may be written as:

$$\mathbf{u} = (\psi_y, -\psi_x, -k\psi) \quad (2.10)$$

with

$$\psi = \frac{2U}{k} \sin\left(\frac{k}{2}(x+y) + \frac{\pi}{4}\right) \sin\left(\frac{k}{2}(y-x) - \frac{\pi}{4}\right)$$

and is thus equivalent to Roberts' flow (with $K = -k$) under a rotation, translation and change of scale.

Both components, $\mathbf{u}^{(1)}, \mathbf{u}^{(2)}$ satisfy $\nabla \wedge \mathbf{u}^{(i)} = -k\mathbf{u}^{(i)}$ and are called "Beltrami waves". Their sum, \mathbf{u} , also satisfies this relation and is called a "Beltrami field" (Beltrami (1889).

The effect of $\mathbf{u}^{(1)}$ on any uniform magnetic field, \mathbf{B}_0 , is to generate a weak field, \mathbf{b} , given, for small R , by:

$$-\eta \nabla^2 \mathbf{b} = \mathbf{B}_0 \cdot \nabla \mathbf{u} = U k B_{0x} (0, -\sin kx, \cos kx) \quad (2.11)$$

$$\mathbf{b} = \frac{U B_{0x}}{\eta k} (0, -\sin kx, \cos kx) \quad (2.12)$$

and

$$\mathbf{u} \wedge \mathbf{b} = \frac{B_{0x} U^2}{\eta k} \mathbf{i} \quad (2.13)$$

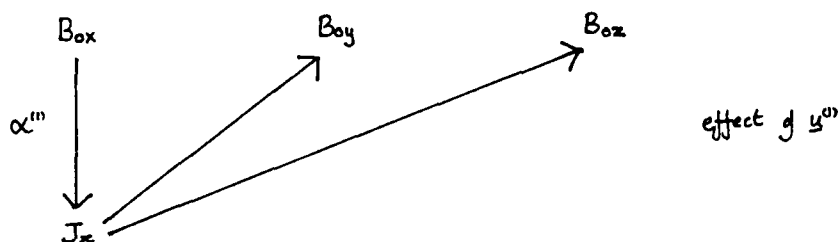


Figure 2.6

Thus $u^{(1)}$ acts only on B_{0x} , to generate a parallel mean current. This mean current corresponds to mean fields in the y and z directions (Figure 2.6). This is not a closed cycle, and, alone, cannot give a dynamo. However if we now include $u^{(2)}$, which generates a current in the y direction from B_{0y} , we obtain Figure 2.7. Thus the cycle may be closed, and it is possible to create an α^2 dynamo from two or more Beltrami waves, as in Roberts' cellular dynamo. To show this, suppose that the mean field, $\langle \mathbf{B} \rangle \equiv \mathbf{B}_0$, varies over large scales, $L \gg k^{-1}$, the size of the cells. Taking the mean of the induction equation gives:

$$\frac{\partial}{\partial t} \langle \mathbf{B} \rangle - \eta \nabla^2 \langle \mathbf{B} \rangle = \nabla \wedge (\alpha \cdot \langle \mathbf{B} \rangle) \quad (2.14)$$

Since $\langle \mathbf{B} \rangle$ is approximately uniform on the scale of the cells, α is given by the above local calculation.

For Roberts' flow, with $\langle \mathbf{B} \rangle$ as a function of z and t alone:

$$\frac{\partial}{\partial t} \langle \mathbf{B} \rangle - \eta \frac{\partial^2}{\partial z^2} \langle \mathbf{B} \rangle = \frac{\partial}{\partial z} (i_z \wedge \alpha \langle \mathbf{B} \rangle) \quad (2.15)$$

To solve this set $\mathbf{B} = \langle B_x \rangle + i \langle B_y \rangle$ so that:

$$\frac{\partial B}{\partial t} - \eta \frac{\partial^2 B}{\partial z^2} = i \alpha \frac{\partial B}{\partial z}. \quad (2.16)$$

Setting $B \propto e^{pt+i\lambda z}$ gives the growth rate,

$$p = -\alpha\lambda - \eta\lambda^2 = \frac{U^2 K}{4\eta k^2} \lambda - \eta\lambda^2 \quad (2.17)$$

if we non-dimensionalize variables via: $p^* = p/\eta k^2$, $\lambda^* = \lambda/k$, $K/k = \mathcal{H}$ then $p^* = R^2 \mathcal{H} \lambda^* - \lambda^{*2}$ with $R \ll 1$. For a growing magnetic field, $p^* > 0$, we require $\lambda^* \leq O(R^2)$ and $\mathcal{H} > 0$. Thus dynamo action can occur, with growing mean fields on a much larger scale (by a factor $O(R^{-2})$) than that of the cellular flow. Note that although the magnetic Reynolds number

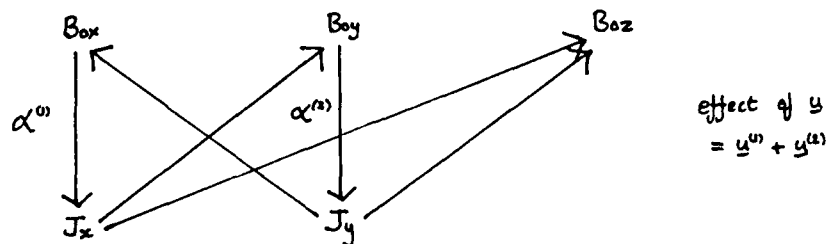


Figure 2.7

based on the cell size, $R = U/k\eta$, is small, the magnetic Reynolds number based on the scale of the growing field, $U/\lambda\eta \sim R^{-1}$, is large.

The theory is valid for small R . As R is increased, numerical computations (Roberts, 1972) show that the scale of the most unstable mode, $1/\lambda^*$, decreases; the growth rate, p^* , first increases, but then begins to decrease (Figure 2.8). The dynamo becomes less effective for large R . Remarks:

- Related smoothing procedures utilize unsteady flows with $kU/\omega < 1$.
- Smoothing can be given a fairly complete mathematical basis.
- We stopped at "first-order smoothing", since $\alpha \neq 0$ was realized. There is a theory of n^{th} order smoothing.
- This is a nice application of two-scale asymptotics; we deal with the microscale separately from the macroscale.
- Many systems of astrophysical interest (for example, the sun) have

$$U/k\eta \gg 1, U\omega \geq 1 \quad (2.18)$$

The asymptotics we have used are for the opposite limits!

2.4 Braginskii's Models

This theory (Braginskii 1964, 1965, 1976, see also Roberts 1971, Soward 1972, Moffatt 1978), is motivated by the near axial symmetry of the Earth's (and Jupiter's) magnetic field, and large values of the magnetic Reynolds number, $R \sim 10^2 - 10^3$. The analysis combines both limits; as $R \rightarrow \infty$, the dominant fields are axisymmetric and toroidal (figure 2.9); thus $u_T \wedge B_T = 0$.

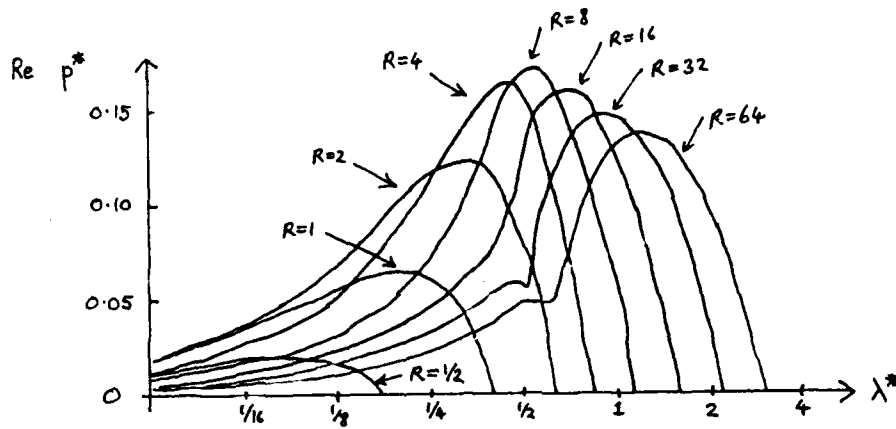


Figure 2.8

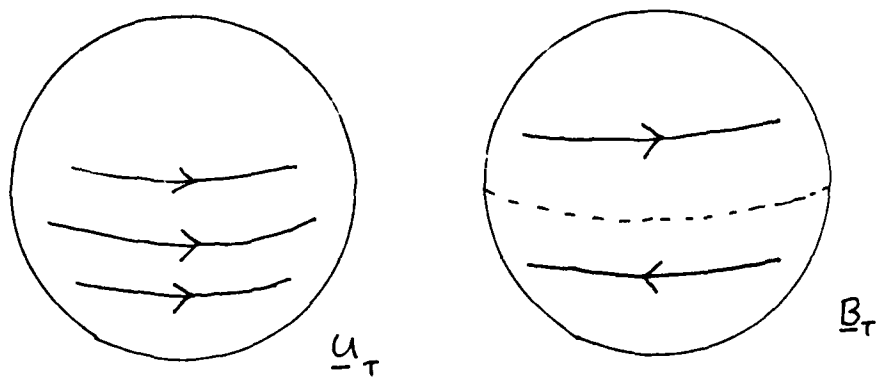


Figure 2.9

The omega effect is built in from the start in that B_T results from the stretching and twisting of a weak symmetric poloidal field, B_P , of order $1/R$. The complete model consists of these basic axisymmetric fields, with small axisymmetric and non-axisymmetric corrections, whose orders in R are carefully chosen.

For the expansion set $\rho = r \sin \theta$ and $\tau = t/R$, a reduced time, with t measured in units of L/U . Set:

$$\mathbf{B} = \underbrace{B(z, \rho, \tau) \mathbf{i}_\phi}_{\text{toroidal, } B_T} + \underbrace{R^{-1} \nabla \wedge (A(z, \rho, \tau) \mathbf{i}_\phi)}_{\text{poloidal, } B_P} + \underbrace{\sum_i R^{-i/2} \mathbf{B}^{(i)}(z, \rho, \phi, t, \tau)}_{\text{non-axisymmetric}} \quad (2.19)$$

$$\mathbf{u} = \underbrace{W(z, \rho) \mathbf{i}_\phi}_{\text{toroidal, } u_T} + \underbrace{R^{-1} \mathbf{v}(z, \rho, \tau)}_{\text{poloidal, } u_P} + \underbrace{\sum_i R^{-i/2} \mathbf{u}^{(i)}(z, \rho, \phi, t, \tau)}_{\text{non-axisymmetric}} \quad (2.20)$$

and let $\mathbf{v} = \nabla \wedge (\psi(z, \rho, \tau) \mathbf{i}_\phi)$. A system of equations is obtained by angle-averaging over ϕ , denoted by $\langle \cdot \rangle$; the $O(1/R)$ equation is:

$$\frac{\partial B}{\partial \tau} + \rho v_{eff} \cdot \nabla \frac{B}{\rho} = (\nabla^2 - \frac{1}{\rho^2}) B + \underbrace{\nabla \frac{W}{\rho} \wedge \nabla \rho A_{eff}}_{\text{omega effect}} \quad (2.21)$$

and the equation for A_{eff} , at $O(1/R^2)$, is:

$$\frac{\partial A_{eff}}{\partial \tau} + \rho^{-1} v_{eff} \cdot \nabla \rho A_{eff} = (\nabla^2 - \frac{1}{\rho^2}) A_{eff} + \underbrace{\alpha B}_{\text{alpha effect}} \quad (2.22)$$

Here, $A_{eff} = A + \gamma B$, $\psi_{eff} = \psi + \gamma B$, $v_{eff} = \nabla \wedge (\psi_{eff}(z, \rho, \tau) \mathbf{i}_\phi)$ and α, γ are quadratic functionals of the velocity field.

Thus we have coupled equations for the magnetic fields in a sphere, incorporating alpha and omega effects. These may be solved numerically to obtain magnetic fields that grow exponentially on a time scale $\tau = t/R$ (t being the turnover time of the flow).

The analysis of Soward (1972, see also Moffatt 1978) leads to further insights into Braginskii's model. The $O(R^{-1/2})$ non-axisymmetric terms in \mathbf{u} and \mathbf{B} ($\mathbf{u}^{(1)}, \mathbf{B}^{(1)}$) are closely linked, and also diffusion plays no role at this order. Hence \mathbf{B} , up to $O(R^{-1/2})$ terms, is a slightly perturbed, near axisymmetric field, which can be mapped back into axisymmetric form by a near identity transformation, $M(t, \tau)$ (Figure 2.10). M may be chosen so that the diffusionless induction equation is *invariant*. The exact equation (with $\eta \neq 0$) produces new terms under M ; however, since the dependent variables are now axisymmetric (to higher order), the transformed equations may be angle-averaged. The average produces the alpha effect term. The effective variables come from expressing the new axisymmetric components (obtained under M) in terms of the original components.

Braginskii's approach carries over to the full MHD system. Relative to rotating axes (in the steady case):

$$\begin{aligned} \nabla p + 2\Omega \wedge \mathbf{u} + \frac{1}{\mu \rho_0} \mathbf{B} \wedge \nabla \wedge \mathbf{B} &= \mathbf{F} \\ \nabla \cdot \mathbf{u} &= 0 \end{aligned} \quad (2.23)$$

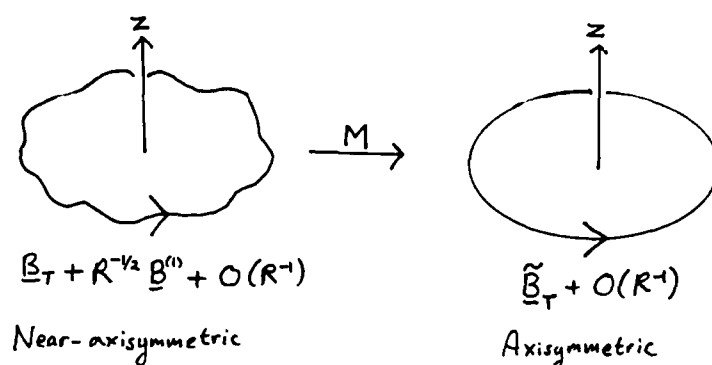


Figure 2.10

where F includes inertial terms (probably small in the Earth's core) and driving forces (convection, for example) the ϕ -component of this equation is

$$\frac{1}{\rho} \frac{\partial p}{\partial \phi} + 2\Omega u_\rho + \frac{1}{\mu\rho_0} (\mathbf{B} \wedge \nabla \wedge \mathbf{B})_\phi = F_\phi \quad (2.24)$$

in cylindrical polar coordinates (ρ, ϕ, z) . Now integrate this equation around the cylinder, $\rho = \text{constant}$ (Figure 2.11). Then:

$$\int_{z_A}^{z_B} dz \int_0^{2\pi} d\phi \left(\frac{1}{\rho} \frac{\partial p}{\partial \phi} + 2\Omega u_\rho + \frac{1}{\mu\rho_0} (\mathbf{B} \wedge \nabla \wedge \mathbf{B})_\phi - F_\phi \right) = 0 \quad (2.25)$$

The first term integrates to zero around the cylinder, and the second term gives zero, since the total radial flux through the cylinder must be zero by incompressibility, $\nabla \cdot \mathbf{u} = 0$. We are thus left with "Taylor's constraint" (Taylor 1963):

$$\int_{z_A}^{z_B} dz \int_0^{2\pi} d\phi \left(\frac{1}{\mu\rho_0} (\mathbf{B} \wedge \nabla \wedge \mathbf{B})_\phi - F_\phi \right) = 0; \quad (2.26)$$

the total torque on any cylinder of fluid must vanish. Furthermore if the magnetic field and F_ϕ are given, this constraint determines the velocity field uniquely.

Analyses of the full MHD equations, in which the velocity field is generated by convection in a rotating system, typically give the bifurcation diagram shown in Figure 2.12 (Eltayeb and Roberts 1970). As the Rayleigh number, Q , is increased from zero, the kinetic and magnetic energies are zero until $Q = Q'$. For $Q' < Q < Q''$, convection occurs, but is not strong enough to give dynamo action. For $Q \gtrsim Q''$, dynamo action gives a magnetic field which saturates at a low energy. Note, however, that steady convection is also possible at values of $Q < Q'$, with strong magnetic and velocity fields.

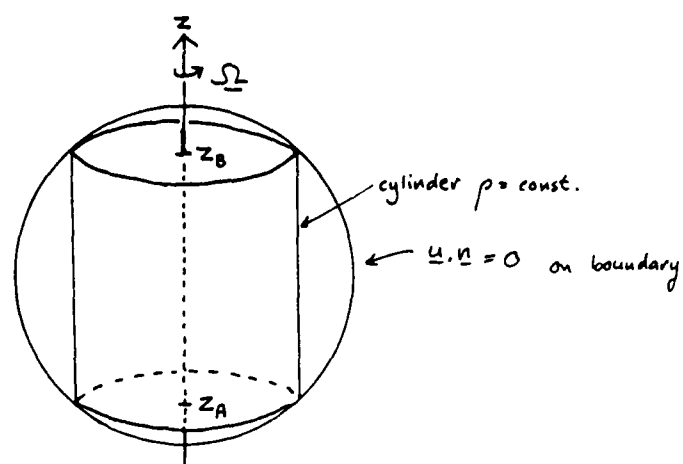


Figure 2.11

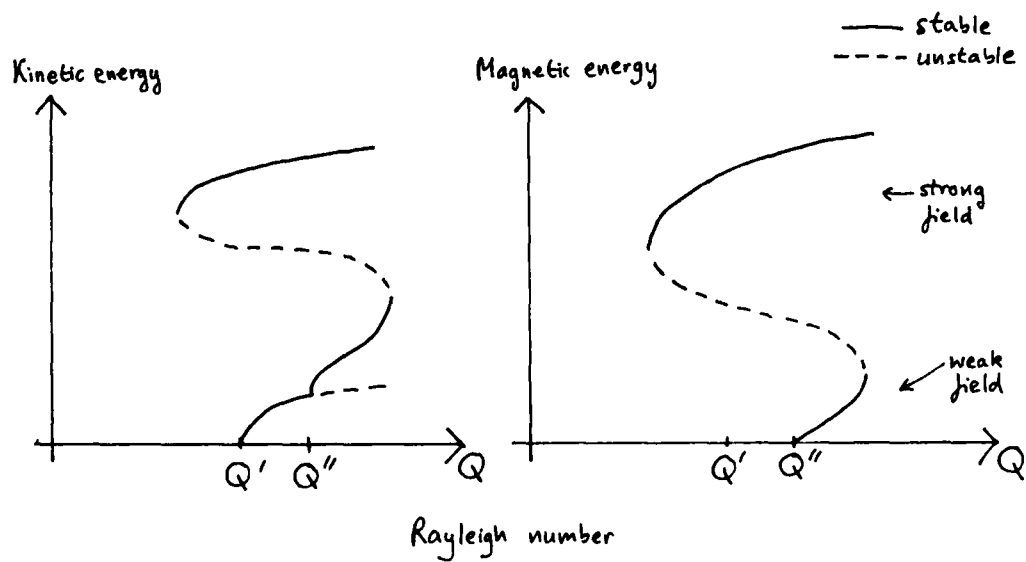


Figure 2.12

2.5 References

- Beltrami, E., "Opera Matematiche", vol. 4, p. 304, (1889).
- Braginskii, S.I., 1964. "Kinematic models of the Earth's hydromagnetic dynamo", *Geomagnetism and Astronomy*, IV, 572.
- Braginskii, S.I., 1965. "Self-excitation of a magnetic field during the motion of a highly conducting fluid," *Sov Phys. JETP*, vol. 20, 726.
- Braginskii, S.I., 1976. "On the nearly axially-symmetrical model of the hydromagnetic dynamo of the earth," *Phys. Earth Planet. Int.*, 11, 191.
- Bullard, E.C. and Gellman, H., 1954. "Homogeneous dynamos and terrestrial magnetism," *Phil. Trans. Roy. Soc.*, A247, 213.
- Cowling, T.G., 1934. "The magnetic field of sunspots," *Mon. Not. Roy. Astr. Soc.*, 94, 39.
- Eltayeb, I.A. and Roberts, P.H., 1970. "On the hydromagnetics of rotating fluids," *Astrophys. J.*, 162, 699.
- Gibson, R.D., 1968. "The Herzenberg dynamo I," *Q. J. Mech. Appl. Math.*, 21, 243.
- Herzenberg, A., 1958. "Geomagnetic dynamos," *Phil. Trans. Roy. Soc.*, A250 543.
- Moffatt, H.K., 1969. "The degree of knottedness of tangled vortex lines," *J. Fluid Mech.*, 35, 117.
- Moffatt, H.K., 1978. *Magnetic field generation in electrically conducting fluids*, Cambridge University Press.
- Parker, E. N., 1955. "Hydrodynamic dynamo models," *Astrophys. J.*, 122, 293.
- Roberts, G. O., 1972. "Dynamo action of fluid motions with two-dimensional periodicity," *Phil. Trans. Roy. Soc.*, A271, 411.
- Roberts, P.H., 1971. "Dynamo Theory," in *Mathematical problems in the Geophysical Sciences*, ed. W. H. Reid, AMS, vol. 2, p. 129.
- Soward, A. M., 1972. "A kinematic dynamo theory of large magnetic Reynolds number dynamos," *Phil. Trans. Roy. Soc.*, A272, 431.
- Steenbeck, M. F., Krause, F. and Rädler, K. H., 1966. "A calculation of the mean electromotive force in an electrically conducting fluid in turbulent motion, under the influence of Coriolis forces," *Z. Naturforsch.*, 21A, 369.
- Taylor, J. B., 1963. "The magnetohydrodynamics of a rotating fluid and the earth's dynamo problem," *Proc. Roy. Soc.*, A274, 274.

Lecture 3

Induction at Large and Infinite R

3.1 Cauchy's Solution for $R = \infty$

Dropping the diffusion term from the induction equation, we get

$$\frac{\partial \mathbf{B}}{\partial t} - \nabla \wedge (\mathbf{u} \wedge \mathbf{B}) = 0 \quad (3.1)$$

$$\frac{\partial \mathbf{B}}{\partial t} - \mathbf{B} \cdot \nabla \mathbf{u} + \mathbf{u}(\nabla \cdot \mathbf{B}) - \mathbf{u} \cdot \nabla \mathbf{B} - \mathbf{B}(\nabla \cdot \mathbf{u}) = 0 \quad (3.2)$$

But, since

$$\nabla \cdot \mathbf{u} = \nabla \cdot \mathbf{B} = 0, \quad (3.3)$$

$$\frac{D\mathbf{B}}{Dt} = \mathbf{B} \cdot \nabla \mathbf{u} \quad (3.4)$$

or, using subscript notation,

$$\frac{DB_i}{Dt} = B_k \frac{\partial u_i}{\partial x_k} \quad (3.5)$$

We wish to solve (3.4) subject to the initial conditions

$$B_i(\mathbf{x}, 0) = B_i^{(0)}(\mathbf{x}) \quad (3.6)$$

We begin by introducing Lagrangian coordinates $\mathbf{x}(\mathbf{a}, t)$ defined by

$$\frac{\partial \mathbf{x}}{\partial t} |_{\mathbf{a}} = \mathbf{u}(\mathbf{x}(\mathbf{a}, t), t), \quad \mathbf{x}(\mathbf{a}, 0) = \mathbf{a} \quad (3.7)$$

Then, the Jacobian determinant $J_{ij} = \frac{\partial x_i}{\partial a_j}$ satisfies Eq 4 since we have

$$\frac{D}{Dt} J_{ij} = \frac{\partial}{\partial t} J_{ij} |_{\mathbf{a}} = \frac{\partial}{\partial t} \left(\frac{\partial x_i}{\partial a_j} \right) |_{\mathbf{a}} = \frac{\partial}{\partial a_j} \left(\frac{\partial x_i}{\partial t} \right) |_{\mathbf{a}} = \frac{\partial u_i}{\partial a_j} = \frac{\partial u_i}{\partial x_k} \cdot \frac{\partial x_k}{\partial a_j} = J_{kj} \frac{\partial u_i}{\partial x_k} \quad (3.8)$$

However, it doesn't satisfy Eq 5, so we try the linear combination $J_{ij} \cdot B_j^{(0)}(\mathbf{a})$, which still satisfies Eq 4 since $\partial/\partial t B_j^{(0)}(\mathbf{a}) |_{\mathbf{a}} = 0$ and so it comes out of the differentiation in Eq 7 and then just gets carried along. Furthermore, since $J_{ij}(\mathbf{a}, 0) = \partial a_i / \partial a_j = \delta_{ij}$, $J_{ij} \cdot B_j^{(0)}(\mathbf{a})$ also satisfies Eq 5, and so (assuming uniqueness) the solution is

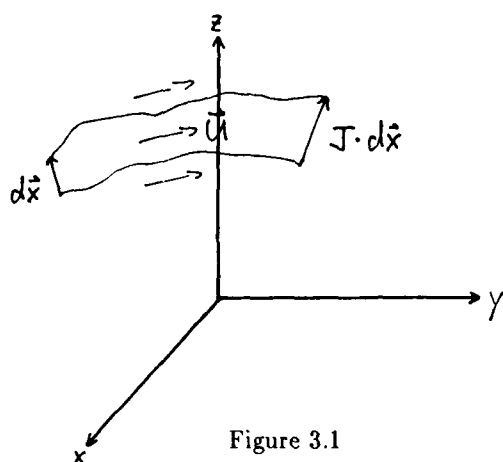


Figure 3.1

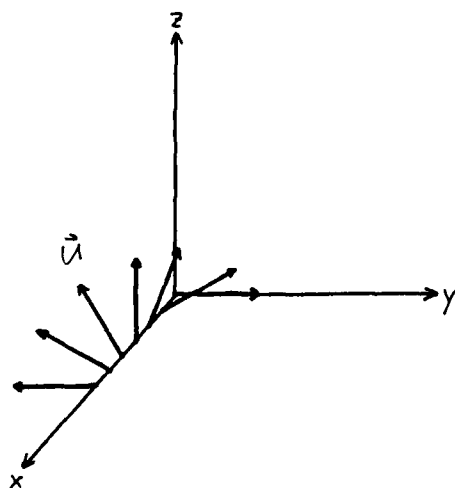


Figure 3.2: Example 1: Beltrami Wave

$$B_i(\mathbf{a}, t) = J_{ij}(\mathbf{a}, t) \cdot B_j(\mathbf{a}, 0) \quad (3.9)$$

Now, what is the physical interpretation of this result? If we consider a small material line element $d\mathbf{x}$ at time 0, at time t it will have transformed into $J \cdot d\mathbf{x}$ and we see that the magnetic field transforms in exactly the same manner. Thus, we say that the magnetic field is frozen into the fluid. (See Figure 3.1).

Next, we will consider some special cases where we can solve for the Lagrangian variables explicitly, and thereby use Cauchy's solution to further understand the α -effect. (See Figure 3.2).

Take $\mathbf{u} = \cos x \mathbf{j} + \sin x \mathbf{k}$, then the equations for the Lagrangian variables become

$$\frac{\partial \mathbf{x}}{\partial t} = 0 \Rightarrow \mathbf{x} = \mathbf{a}_1 \quad (3.10)$$

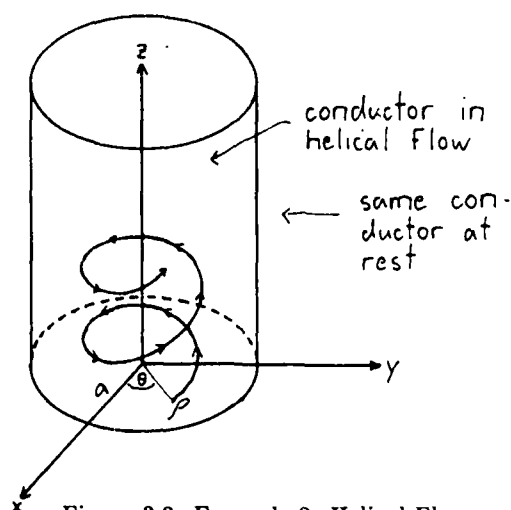


Figure 3.3: Example 2: Helical Flow

$$\begin{aligned}\frac{\partial y}{\partial t} &= \cos x = \cos a_1 \Rightarrow y = a_2 + t \cos a_1 \\ \frac{\partial z}{\partial t} &= \sin x = \sin a_1 \Rightarrow z = a_3 + t \sin a_1\end{aligned}$$

and so

$$J = \begin{vmatrix} 1 & 0 & 0 \\ -t \sin a_1 & 1 & 0 \\ t \cos a_1 & 0 & 1 \end{vmatrix} \quad (3.11)$$

Thus, if we take $B^0 = B_0 \hat{i}$, then

$$B = B_0 \hat{i} - B_0 t \sin a_1 \hat{j} + B_0 t \cos a_1 \hat{k} \quad (3.12)$$

and so

$$u \wedge B = \begin{vmatrix} \hat{i} & \hat{j} & \hat{k} \\ 0 & \cos a_1 & \sin a_1 \\ B_0 & -B_0 t \sin a_1 & B_0 t \cos a_1 \end{vmatrix} = B_0 t \hat{i} + B_0 \sin a_1 \hat{j} - B_0 \cos a_1 \hat{k} \quad (3.13)$$

Then, averaging this result over all a_1 , we get

$$\langle u \wedge B \rangle = B_0 t \hat{i} \quad (3.14)$$

and so the α -effect in this case grows linearly with time. Physically, it is caused by the initially straight field lines being distorted into helices of ever-increasing radii and thereby inducing an ever-increasing emf along the x-axis.

Take

$$u = \begin{cases} \rho \omega(\rho) \hat{i}_\theta + W(\rho) \hat{i}_z & \rho < a \\ 0 & \rho > a \end{cases} \quad \text{with } \omega(a) = W(a) = 0 \quad (3.15)$$

then the equations for the Lagrangian variables become

$$\frac{\partial \rho}{\partial t} = 0 \Rightarrow \rho = \rho_0$$

$$\begin{aligned}\frac{\partial \theta}{\partial t} &= \omega(\rho) = \omega(\rho_0) \Rightarrow \theta = \theta_0 + \omega(\rho_0)t \\ \frac{\partial z}{\partial t} &= W(\rho) = W(\rho_0) \Rightarrow z = z_0 + W(\rho_0)t\end{aligned}\quad (3.16)$$

so in Cartesian coordinates

$$\begin{aligned}x &= \rho_0 \cos(\theta_0 + \omega(\rho_0)t) \\ y &= \rho_0 \sin(\theta_0 + \omega(\rho_0)t) \\ z &= z_0 + W(\rho_0)t\end{aligned}\quad (3.17)$$

Then, using the chain rule (that is

$$\frac{\partial x}{\partial x_0} = \frac{\partial x}{\partial \rho_0} \cdot \frac{\partial \rho_0}{\partial x_0} + \frac{\partial x}{\partial \theta_0} \cdot \frac{\partial \theta_0}{\partial x_0} \quad (3.18)$$

etc.) one gets after a little algebra

$$J = \begin{vmatrix} \cos \omega_0 t - \rho_0 \omega'_0 t \cos \theta_0 \sin \theta & -\sin \omega_0 t - \rho_0 \omega'_0 t \sin \theta_0 \sin \theta & 0 \\ \sin \omega_0 t + \rho_0 \omega'_0 t \cos \theta_0 \cos \theta & \cos \omega_0 t + \rho_0 \omega'_0 t \sin \theta_0 \cos \theta & 0 \\ t \cos \theta_0 W'_0 & t \sin \theta_0 W'_0 & 1 \end{vmatrix} \quad (3.19)$$

where $\omega_0 = \omega(\rho_0)$, $\omega'_0 = \omega'(\rho_0)$, etc.

So, if we take $\mathbf{B}^0 = \hat{i}$, then

$$\mathbf{B} = (\cos \omega_0 t - \rho_0 \omega'_0 t \cos \theta_0 \sin \theta) \hat{i} + (\sin \omega_0 t + \rho_0 \omega'_0 t \cos \theta_0 \cos \theta) \hat{j} + t \cos \theta_0 W'_0 \hat{k} \quad (3.20)$$

and so

$$\mathbf{u} \wedge \mathbf{B} = \begin{vmatrix} \hat{i} & \hat{j} & \hat{k} \\ -\rho_0 \omega_0 \sin \theta & \rho_0 \omega_0 \cos \theta & W_0 \\ (\cos \omega_0 t - \rho_0 \omega'_0 t \cos \theta_0 \sin \theta) & (\sin \omega_0 t + \rho_0 \omega'_0 t \cos \theta_0 \cos \theta) & t \cos \theta_0 W'_0 \end{vmatrix} \quad (3.21)$$

$$\begin{aligned} &= i[\rho_0 t \cos \theta_0 \cos \theta (\omega_0 W'_0 - \omega'_0 W_0) - W_0 \sin \omega_0 t] \\ &+ j[\rho_0 t \cos \theta_0 \sin \theta (\omega_0 W'_0 - \omega'_0 W_0) + W_0 \cos \omega_0 t] \\ &- k \rho_0 \omega_0 \cos \theta_0 \end{aligned} \quad (3.22)$$

Then, averaging this result over all ρ_0 and θ_0 (and remembering that $\theta = \theta_0 + \omega_0 t$), we get

$$\begin{aligned} \langle \mathbf{u} \wedge \mathbf{B} \rangle &= \frac{1}{\pi a^2} \int_0^a \int_0^{2\pi} \mathbf{u} \wedge \mathbf{B} d\theta_0 \rho_0 d\rho_0 \\ &= i \frac{1}{\pi a^2} \int_0^a 2\pi \left[\frac{1}{2} \rho_0 t \cos \omega_0 t (\omega_0 W'_0 - \omega'_0 W_0) - W_0 \sin \omega_0 t \right] \rho_0 d\rho_0 \\ &+ j \frac{1}{\pi a^2} \int_0^a 2\pi \left[\frac{1}{2} \rho_0 t \sin \omega_0 t (\omega_0 W'_0 - \omega'_0 W_0) + W_0 \cos \omega_0 t \right] \rho_0 d\rho_0 \end{aligned} \quad (3.23)$$

Now, we integrate the $\omega'_0 W_0$ terms by parts using $u = \rho_0^2 W_0$ and noting that since $W_0(a) = 0$ the integrated parts vanish, leaving

$$\langle \mathbf{u} \wedge \mathbf{B} \rangle = i \frac{1}{a^2} \int_0^a \rho_0^2 W'_0 (\omega_0 t \cos \omega_0 t + \sin \omega_0 t) d\rho_0 \quad (3.24)$$

$$+ j \frac{1}{a^2} \int_0^a \rho_0^2 W'_0 (\omega_0 t \sin \omega_0 t - \cos \omega_0 t) d\rho_0 \quad (3.25)$$

We now consider some examples:

a) Following Ponomarenko (1973), we pick

$$\begin{aligned}\omega &= \omega_0 H(a - \rho) \\ W &= W_0 H(a - \rho)\end{aligned}\quad (3.26)$$

that is, the cylinder is in a solid-body corkscrew motion. (Actually, because $\omega_0 W'_0$ appears in the integrand we have to be a little careful and give W a somewhat smoother profile. However, all we are interested in is concentrating the shear at the cylinder boundary, so whether W is an exact step-function, or a slightly smoothed step-function doesn't much matter.) Then,

$$\langle \mathbf{u} \wedge \mathbf{B} \rangle = -W_0 [i(\omega_0 t \cos \omega_0 t + \sin \omega_0 t) + j(\omega_0 t \sin \omega_0 t - \cos \omega_0 t)] \quad (3.27)$$

and so we get linearly growing oscillations in the α -effect. The reason they grow indefinitely is that the field at the boundary is stretched indefinitely, thereby inducing an ever-growing emf.

b) Next, to avoid this infinite shear at the cylinder boundary, we pick

$$\begin{aligned}\omega &= \omega_0 \frac{a - \rho}{a} \\ W &= W_0 \frac{a^2 - \rho^2}{a^2}\end{aligned}\quad (3.28)$$

Then,

$$\begin{aligned}\langle \mathbf{u} \wedge \mathbf{B} \rangle &= -i \frac{1}{a^2} \int_0^a \rho^2 \frac{W_0}{a^2} 2\rho \left(\frac{a - \rho}{a} \omega_0 t \cos \left(\frac{a - \rho}{a} \omega_0 t \right) + \sin \left(\frac{a - \rho}{a} \omega_0 t \right) \right) d\rho \\ &\quad - j \frac{1}{a^2} \int_0^a \rho^2 \frac{W_0}{a^2} 2\rho \left(\frac{a - \rho}{a} \omega_0 t \sin \left(\frac{a - \rho}{a} \omega_0 t \right) - \cos \left(\frac{a - \rho}{a} \omega_0 t \right) \right) d\rho\end{aligned}\quad (3.29)$$

Let

$$\begin{aligned}q &= \frac{a - \rho}{a} \omega_0 t \text{ then} \\ \langle \mathbf{u} \wedge \mathbf{B} \rangle &= -i \frac{2W_0}{\tau} \int_0^\tau \left(1 - \frac{q}{\tau}\right)^3 (q \cos q + \sin q) dq \\ &\quad - j \frac{2W_0}{\tau} \int_0^\tau \left(1 - \frac{q}{\tau}\right)^3 (q \sin q - \cos q) dq\end{aligned}\quad (3.30)$$

where $\tau = \omega_0 t$. Then, after several integrations by parts, we finally get

$$\begin{aligned}\langle \mathbf{u} \wedge \mathbf{B} \rangle &= iW_0 \left(-\frac{24}{\tau^3} - \frac{12}{\tau^3} \cos \tau + \frac{36}{\tau^4} \sin \tau \right) \\ &\quad + jW_0 \left(-\frac{6}{\tau^2} - \frac{12}{\tau^3} \sin \tau + \frac{36}{\tau^4} (1 - \cos \tau) \right)\end{aligned}\quad (3.31)$$

which incidentally remains finite for $\tau \rightarrow 0$ and in fact takes the form $-i W_0/5\tau + j W_0/2$. Thus, we get initially growing oscillations in the α -effect, but ultimately we get decay. The reason for this decay is that the differential rotation and advection twist up the magnetic field lines so completely that there is tremendous cancellation in the average.

Finally, we can integrate this α -effect with respect to time. After evaluating several contour integrals, we get

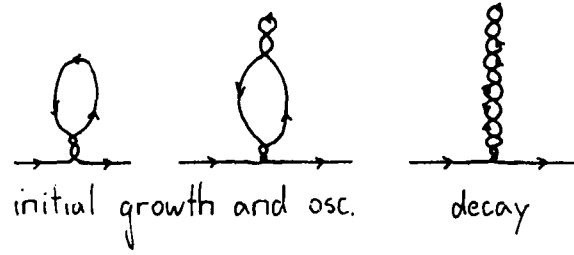


Figure 3.4

$$\int_0^\infty \langle \mathbf{u} \wedge \mathbf{B} \rangle dt = -2 \frac{W_0}{\omega_0} \hat{\mathbf{i}} \quad (3.32)$$

so we get a non-zero integrated α even in the absence of diffusion. This suggests the following dynamo mechanism: Run a number of such cells at large (but not infinite) R until this integrated α -effect has been achieved and the field lines have become all twisted up. Then wait while diffusion presumably wipes out all these twisted-up field lines and then start again. This idea of motion-stasis-motion-stasis was used by Backus (1958) to prove unsteady dynamo action in a sphere, and it has long been a useful technique in dynamo theory.

3.2 The Effect of Diffusion

Just now we asserted without proof that once the field lines got all twisted up diffusion would wipe them out. So now we want to examine the effect of a little diffusion in somewhat more detail. Taking the same solid-body helical motion as before, that is $\mathbf{u} = \rho \omega \hat{\mathbf{i}}_\theta + W \hat{\mathbf{i}}_z$, the induction equations in cylindrical coordinates become

$$\frac{\partial B_\rho}{\partial t} + \omega \frac{\partial B_\rho}{\partial \theta} + W \frac{\partial B_\rho}{\partial z} - \eta \left(\nabla^2 B_\rho - \frac{1}{\rho^2} B_\rho - \frac{2}{\rho^2} \frac{\partial B_\theta}{\partial \theta} \right) = 0 \quad (3.33)$$

$$\frac{\partial B_\theta}{\partial t} + \omega \frac{\partial B_\theta}{\partial \theta} + W \frac{\partial B_\theta}{\partial z} - \eta \left(\nabla^2 B_\theta - \frac{1}{\rho^2} B_\theta + \frac{2}{\rho^2} \frac{\partial B_\rho}{\partial \theta} \right) = 0 \quad (3.34)$$

$$\frac{\partial B_z}{\partial t} + \omega \frac{\partial B_z}{\partial \theta} + W \frac{\partial B_z}{\partial z} - \eta \nabla^2 B_z = B_\rho W \delta(a - \rho) \quad (3.35)$$

Then, since we are looking for steady-state solutions independent of z , we set $\frac{\partial}{\partial t} = \frac{\partial}{\partial z} = 0$. Also, we introduce a potential A , so

$$\mathbf{B} = (B_\rho, B_\theta, B_z) = \left(-\frac{1}{\rho} \frac{\partial A}{\partial \theta}, \frac{\partial A}{\partial \rho}, B \right) \quad (3.36)$$

then

$$\omega \frac{\partial A}{\partial \theta} = \eta \nabla^2 A \quad (3.37)$$

$$\omega \frac{\partial B}{\partial \theta} = \eta \nabla^2 B - \frac{1}{\rho} \frac{\partial A}{\partial \theta} W \delta(a - \rho) \quad (3.38)$$

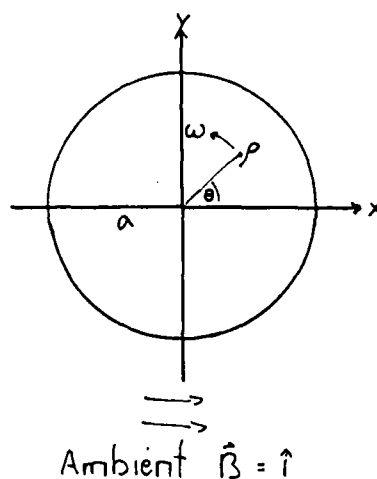


Figure 3.5

where Eq 37 follows by taking the inverse curl of $(i \cdot 33 + j \cdot 34)$. These equations, of course, only apply for $\rho \leq a$. For $\rho > a$ we have $\nabla^2 A = \nabla^2 B = 0$. Also, we have as boundary conditions that $A, \partial A / \partial \theta$, and B must be continuous across $\rho = a$ and $A \rightarrow -\rho \sin \theta, B \rightarrow 0$ as $\rho \rightarrow \infty$.

Then, assuming $\eta \nabla^2 A$ is small, Eq 37 yields $\partial A / \partial \theta \approx 0$, so to first order $A = A_0(\rho)$. Reinserting this result into Eq 35 and integrating, we thus get

$$\int_0^{2\pi} \omega \frac{\partial A}{\partial \theta} d\theta = \eta \int_0^{2\pi} \frac{1}{\rho} \frac{\partial}{\partial \rho} \left(\rho \frac{\partial A_0}{\partial \rho} \right) d\theta \quad (3.39)$$

$$0 = 2\pi \eta \frac{1}{\rho} \frac{\partial}{\partial \rho} \left(\rho \frac{\partial A_0}{\partial \rho} \right) \quad (3.40)$$

$$A_0 = C \ln \rho + C' \quad (3.41)$$

But now C must be 0 to avoid a singularity at the origin, and of course C' is just an irrelevant constant, so in fact $A_0 = 0$ for $\rho \leq a$.

And then, to satisfy the various boundary conditions, we must have

$$A = -\left(\rho - \frac{a^2}{\rho}\right) \sin \theta \text{ for } \rho > a \quad (3.42)$$

Also, since

$$\frac{\partial A}{\partial \theta} \Big|_{\rho=a} = 0 \quad (3.43)$$

Eq 38 is completely unforced, and so $B = 0$ everywhere. Thus we see that the field is expelled from the cylinder.

This result will be referred to here as the Prandtl-Batchelor-Lagerstrom theorem.

The above result is just fine except for one little detail: $\partial A / \partial \rho = B_\theta$ is discontinuous across $\rho = a$, being 0 for a^- and $-2 \sin \theta$ for a^+ . But then $\mathbf{J} = \nabla \wedge \mathbf{B}$ is infinite, which is unphysical. Thus, there must be some small boundary layer at the cylinder wall. It is this boundary layer structure which we now wish to examine. We begin by defining a stretched coordinate $\zeta = (\rho - a) \sqrt{\omega / 2\eta}$ to measure the distance from the cylinder wall.

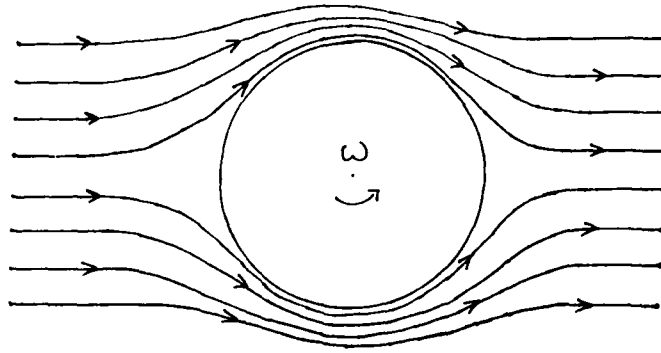


Figure 3.6

Then, within the boundary layer we try a solution of the form

$$A = \sqrt{\frac{2\eta}{\omega}} [\sin \theta A_s(\zeta) + \cos \theta A_c(\zeta)] \quad (3.44)$$

Inserting this into Eq 35 and approximating ∇^2 as $\partial^2/\partial \rho^2 = \omega/2\eta \partial^2/\partial \zeta^2$, we get after equating coefficients of $\sin \theta$ and $\cos \theta$

$$A_s = \frac{1}{2} A_c'', \quad A_c = -\frac{1}{2} A_s'' \quad (3.45)$$

The associated boundary conditions are

$$\frac{\partial A}{\partial \rho} \big|_{\rho=a} = -2 \sin \theta \Rightarrow A_s'(0) = -2, \quad A_c'(0) = 0 \quad (3.46)$$

$$A_s, A_c \rightarrow 0 \text{ as } \zeta \rightarrow -\infty \quad (3.47)$$

The solution is

$$A_s = -e^\zeta (\cos \zeta + \sin \zeta), \quad A_c = -e^\zeta (\sin \zeta - \cos \zeta) \quad (3.48)$$

And of course, we must now put this A into Eq 38 and solve for B . As before, we try a solution of the form

$$B = \sin \theta B_s(\zeta) + \cos \theta B_c(\zeta) \quad (3.49)$$

and get

$$B_s - \frac{1}{2} B_c'' = -\frac{W}{a\omega} \delta(\zeta) A_s(\zeta), \quad B_c + \frac{1}{2} B_s'' = -\frac{W}{a\omega} \delta(\zeta) A_c(\zeta) \quad (3.50)$$

Suitably decaying (as $\zeta \rightarrow -\infty$) solutions are

$$B_s = C_1 e^\zeta \sin \zeta + C_2 e^\zeta \cos \zeta, \quad B_c = -C_1 e^\zeta \cos \zeta + C_2 e^\zeta \sin \zeta \quad (3.51)$$

and by integrating Eq 50 from a^- to a^+ we get as boundary conditions

$$B'_s(0) = B'_c(0) = \frac{2W}{a\omega} \quad (3.52)$$

which yield $C_1 = 0$, $C_2 = \frac{2W}{a\omega}$, and so

$$B = \frac{2W}{a\omega} e^\zeta (\sin \theta \cdot \cos \zeta + \cos \theta \cdot \sin \zeta) \quad (3.53)$$

Unfortunately, we are still not quite finished, since now $A, \partial A / \partial \theta$ and B are no longer continuous across $\rho = a$. Thus, for $\rho > a$ we must have

$$A = \sqrt{\frac{2\eta}{\omega}} \left[(-\sin \theta + \cos \theta) \frac{a}{\rho} - \left(\rho - \frac{a^2}{\rho} \right) \sin \theta \right] \quad (3.54)$$

$$B = \frac{2W}{\omega \rho} \sin \theta \quad (3.55)$$

Thus, to this order the boundary layer structure is

inside field extends an $\mathcal{O}(aR^{-1/2})$ distance and has magnitudes	correction to dipole Field outside extends an $\mathcal{O}(a)$ distance and has magnitudes
$B_\rho \sim \mathcal{O}(R^{-1/2})$	$B_\rho \sim \mathcal{O}(R^{-1/2})$
$B_\theta \sim \mathcal{O}(1)$	$B_\theta \sim \mathcal{O}(R^{-1/2})$
$B_z \sim \mathcal{O}(1)$	$B_z \sim \mathcal{O}(1)$

Finally, we can compute the asymptotic α -effect due to this boundary layer

$$\begin{aligned}
 \alpha_{xx} &= \frac{1}{\pi a^2} \int_0^a \int_0^{2\pi} (U_y B_z - U_z B_y) d\theta \rho d\rho \\
 &= \frac{1}{\pi a^2} \int_0^a \int_0^{2\pi} \left((\rho \omega \cos \theta B - W \left(-\frac{1}{\rho} \frac{\partial A}{\partial \theta} \sin \theta + \frac{\partial A}{\partial \rho} \cos \theta \right)) \right) d\theta \rho d\rho \\
 &\approx \frac{1}{a^2} \int_0^a (\rho \omega B_c(\zeta) - W A'_c(\zeta)) \rho d\rho \\
 &\approx \frac{1}{a^2} \int_{-\infty}^0 (a\omega B_c - W A'_c) a \sqrt{\frac{2\eta}{\omega}} d\zeta \\
 &= -2 \frac{W}{a} \sqrt{\frac{2\eta}{\omega}} \\
 &= -2\sqrt{2} W R^{-\frac{1}{2}} \text{ as } R \rightarrow \infty
 \end{aligned} \quad (3.56)$$

3.3 References

- Backus, G.E., 1958. "A class of self-sustaining dissipative spherical dynamos", *Ann. Phys.*, 4, 372-447.
- Ponomarenko, Y. B., 1973. "On the theory of the hydromagnetic dynamo", *Zh. Prikl. Mech. Tech. Fiz. (USSR)*, 6, 775.

Notes submitted by Rainer Hollerbach.

Lecture 4

Asymptotics for Large R in Steady Flow

4.1 Flux Expulsion

As $R \rightarrow \infty$, one important effect is the magnetic flux expulsion for flows with steady closed streamlines, because the induced current produces an additional field, which tends to offset the applied field. Weiss (1966) has computed a variety of solutions of the induction equation in the 2-dimensional case, where, in dimensionless form, with t measured in eddy turnover times (L/U), the equation for the magnetic potential is

$$\frac{\partial A}{\partial t} + \mathbf{u} \cdot \nabla A = \frac{1}{R} \nabla^2 A, \text{ where } \mathbf{B} = \nabla \times (A(x, y) \mathbf{e}_z) \quad (4.1)$$

for either a single eddy or a regular array of eddies (see Figure 4.1). He showed that the time needed to expel the magnetic field is proportional to $R^{1/3}L/U$, much shorter than the diffusion time RL/U . Moffatt and Kamkar (1983) discussed the origins of this ordering, and Rhines and Young (1983) gave a full discussion for various geometries.

We consider, first, the simple case of a rotor in a steady incompressible velocity field. Here we have

$$\mathbf{u} = \rho \omega(\rho) \hat{\mathbf{e}}_\phi \quad (4.2)$$

and (4.1) becomes (with D^2 the Laplacian in polar coordinates)

$$\frac{\partial A}{\partial t} + \omega(\rho) \frac{\partial A}{\partial \theta} - \frac{1}{R} D^2 A = 0 (\rho < a) \quad (4.3)$$

Letting:

$$A = \sum_{n=-\infty}^{\infty} A_n(\rho, t) e^{in(\theta - \omega(\rho)t)} \quad (4.4)$$

We substitute (4.4) into (4.3), this yields:

$$\frac{\partial A_n}{\partial t} - \frac{1}{R} \left(\frac{\partial^2 A_n}{\partial \rho^2} + \frac{1}{\rho} \frac{\partial A_n}{\partial \rho} - \frac{A_n}{\rho^2} \right) = - \frac{A_n n^2 \omega_\rho^2 t^2}{R} - \frac{2in t \omega_\rho A_{n\rho}}{R} - \frac{in \omega_\rho A_n t}{\rho} - \frac{in \omega_{\rho\rho} t}{R} A_n \quad (4.5)$$

i.e.

$$\frac{\partial A_n}{\partial t} = - \frac{A_n n^2 \omega_\rho^2 t^2}{R} + \text{terms proportional to } t^1 \text{ or } t^0 \quad (4.6)$$

Since we assume many eddy turnover times, $\omega_\rho t \gg 1$, we only need keep the t^2 term in (4.6) (for $\omega_\rho \neq 0$):

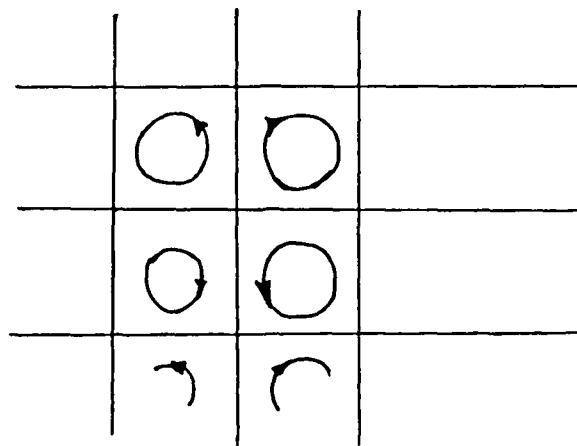


Figure 4.1

$$\frac{\partial A_n}{\partial t} \cong -\frac{A_n n^2 \omega_p^2 t^2}{R} \quad (4.7)$$

From the solution of (4.7), (4.4) we obtain

$$A(\rho, \theta, t) \simeq \sum_{n=-\infty}^{\infty} e^{-\frac{n^2 \omega_p^2 t^3}{3R}} e^{in(\theta - \omega(\rho)t)} \tilde{A}_n(\rho) \quad (4.8)$$

The $n=0$ terms yield

$$\tilde{A}_0(\rho, t) \simeq \frac{1}{2\pi} \int_{\theta}^{2\pi} A(\rho, \theta, 0) d\theta + \dots \quad (4.9)$$

where the dots stand for intermittency corrections for points ρ where $\omega_p = 0$.

Note that if $A(\rho, \theta, 0) = \rho \sin \theta$, then $\tilde{A}_0(\rho, t) \cong 0$, so complete expulsion of field occurs when a uniform field is applied. Actually the $n = 0$ term corresponds to parallel velocity and magnetic field, a configuration which survives this phase of the process, a sort of advective "spin-up" for the field. Once $t \gg R^{1/3}$, another phase of diffusive equilibration begins. However the spin-up phase accounts for the expulsion of the flux, to the extent permitted by the initial condition.

4.1.1 Slow Diffusion Phase

The remaining field diffuses slowly on a timescale $t \sim R$. $A_0(\rho)$ provides the initial condition for this phase. Since this is a slow process, the interaction with the exterior ($\rho > a$, also diffusive) is not negligible. In general, the P-B-L state is obtained after this slow diffusion phase. There is an interesting analogy in vortex dynamics.

Suppose a number of vortex patches carrying circulation Γ_i , are released at $t = 0$ (Figure 4.2) then, a spiral pattern is formed on eddy-turnover scale. Fast diffusion occurs on time scale $\sim R^{1/3}$, leaving a single rotationally symmetric vortex, carrying the net circulation $\sum \Gamma_i$, which slowly evolves on a diffusive timescale. This problem was studied by Lundgren (see Lecture 6).

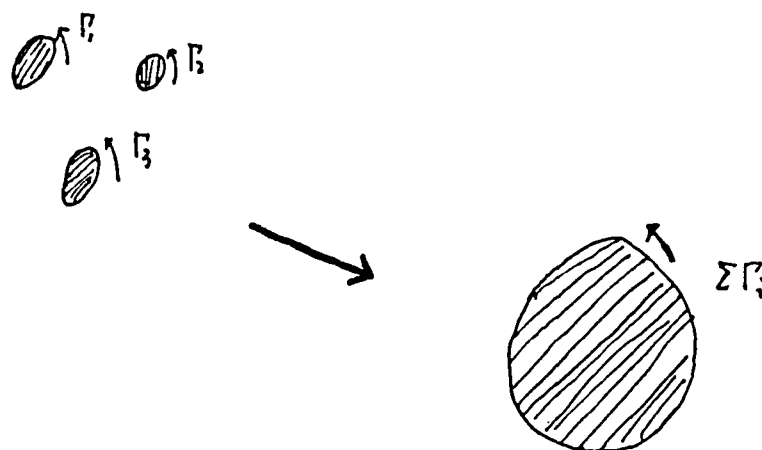


Figure 4.2

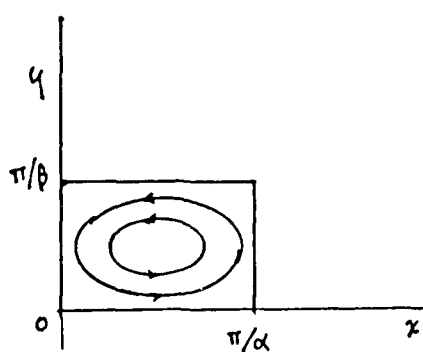


Figure 4.3

4.1.2 Spinup Phase of a General eddy

We assume that $\mathbf{u} = (\psi_y, -\psi_x)$ where $\psi = \text{stream function} = \psi(x, y)$. Then the induction is described by

$$\frac{\partial A}{\partial t} + q \frac{\partial A}{\partial s} - \frac{1}{R} \nabla^2 A = 0 \quad (4.10)$$

where $q = |\mathbf{u}|$, is the speed and s is arc length.

We now introduce new coordinates, Θ, ψ . If $a(\psi) = \text{area within a contour}$, then we have

$$a_\psi(\psi_0) = \int_{\psi=\psi_0} \frac{1}{q} ds \quad (4.11)$$

$$\text{proof: } \frac{\Delta a}{\Delta \psi} = \oint \frac{\Delta n ds}{\Delta \psi} = \oint \frac{ds}{q}$$

Now let

$$A(x, y, t) = \tilde{A}(\psi, \theta - \frac{t}{a_\psi}, t) = \tilde{A}(\psi, \Theta, t) \quad (4.12)$$

where

$$\theta = \frac{2\pi}{a_\psi} \left(\int_0^s \frac{ds}{q} \right) \quad 0 \leq \theta \leq 2\pi \quad (4.13)$$

Then:

$$A_t \cong \left(\nabla \frac{1}{a_\psi} \right)^2 \frac{t^2}{R} \tilde{A} \Theta_\Theta = \frac{a_{\psi\psi}^2}{a_\psi^2} q^2 \frac{t^2}{R} \tilde{A} \Theta_\Theta \quad (4.14)$$

with $\tau = \frac{1}{3} \frac{t^3}{R}$, we have:

$$\tilde{A}_\tau = \left[\frac{a_{\psi\psi}}{a_\psi^2} q(\Theta, \psi) \right]^2 \tilde{A}_{\Theta\Theta} = D(\Theta, \psi) \tilde{A}_{\Theta\Theta} \quad (4.15)$$

Since $D > 0$, (4.14) being a parabolic diffusion equation, \tilde{A} will become independent of Θ as $\tau \rightarrow \infty$, on the timescale $t \sim R^{1/3}$.

4.2 Alpha Effect at large R in Cellular Flow

We now want to study the development of $\langle \mathbf{u} \wedge \mathbf{B} \rangle$, (the average over the plane of the cells), once flux expulsion has occurred, with $R \gg 1$. In the following discussion, we assume a system independent of z , and a steady magnetic field.

Robert's (1972) numerical calculation gave the function $\alpha(R)$ in

$$\alpha = \begin{pmatrix} \alpha(R) & 0 \\ 0 & \alpha(R) \end{pmatrix} \quad (4.16)$$

up to $R \sim 64$, but how does $\alpha(R)$ behave as $R \rightarrow \infty$?

To study this, we take a general flow (Childress, 1979)

$$\mathbf{u} = (\psi_y, -\psi_x, W(\psi)) \quad (4.17)$$

Assuming $\langle \mathbf{B} \rangle = \mathbf{i}$, $R \gg 1$ we take it for granted that flux expulsion has occurred, so that the flux is concentrated near the boundary of the cells with:

$$\mathbf{B} = (A_y, -A_x, B) \quad (4.18)$$

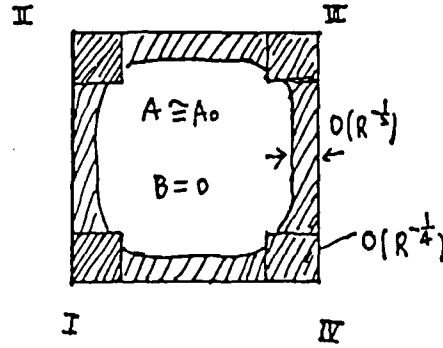


Figure 4.4

Then (4.1) becomes

$$q \frac{\partial A}{\partial s} = \frac{1}{R} \nabla^2 A \cong \frac{1}{R} \frac{\partial^2 A}{\partial n^2} \cong \frac{q^2}{R} \frac{\partial^2 A}{\partial \psi^2} \quad (4.19)$$

where again $q = |\mathbf{u}|$. We now introduce the Von-Mises Coordinates.

$$\sigma = \int_0^s q ds \quad \zeta = R^{1/2} \psi \quad (4.20)$$

where s is the arc length. We get from 4.19, as $R \rightarrow \infty$

$$\frac{\partial A}{\partial \sigma} = \frac{\partial^2 A}{\partial \zeta^2} \quad (4.21)$$

$$\frac{\partial B}{\partial \sigma} - \frac{\partial^2 B}{\partial \zeta^2} = W'(0) \frac{\partial A}{\partial \sigma} \quad (4.22)$$

So, our problem has essentially reduced to a heat conduction problem in one dimension.

Consider now the boundary conditions to be imposed on solutions of 4.22, are Figure 4.4:

$$\begin{aligned} A = -\pi/2\beta \quad B = 0 \quad \text{on} \quad 0 < x < \pi/\alpha, y = 0 \\ A = \pi/2\beta \quad B = 0 \quad \text{on} \quad 0 < x < \pi/\alpha, y = \pi/\beta \\ \frac{\partial A}{\partial x} = 0 \quad B = 0 \quad \text{on} \quad x = 0, \pi/\alpha, 0 < y < \pi/\beta \end{aligned} \quad (4.23)$$

Once A is known, we can obtain B from

$$B = \frac{1}{2} \zeta \frac{\partial A}{\partial \zeta} W'(0) \quad (4.24)$$

Consequently the solution of the boundary-layer problem is fully determined by A . At the corners of the rectangle the boundary layers join and the preceding limit is not valid. The corner regions insure the continuity of A and B with respect to σ , and are therefore referred to as transition regions (see figures 4.4 and 4.5).

At a transition region, we have $q \sim$ distance from corner (take this as the origin) and also $\psi \sim xy \sim R^{-1/2}$. So $x, y \sim R$ and $\mathbf{u} \cdot \nabla A \sim A_0$, $R^{-1} \nabla^2 A \sim A_0 R^{-1/2}$, and the latter

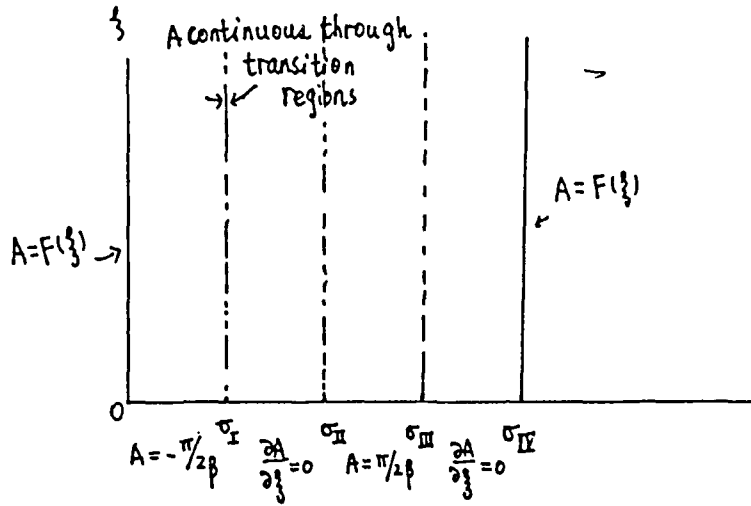


Figure 4.5

term is negligible. Therefore, in the transition regions, excluding the streamline $\psi = 0$, the variables satisfy the equations

$$\frac{\partial A}{\partial x} \frac{\partial \psi}{\partial y} - \frac{\partial A}{\partial y} \frac{\partial \psi}{\partial x} = 0 \quad \text{and} \quad \frac{\partial B}{\partial x} \frac{\partial \psi}{\partial y} - \frac{\partial B}{\partial y} \frac{\partial \psi}{\partial x} = 0 \quad (4.25)$$

Let σ_i $i = 1, 2, 3, 4$ denote the value of σ at the corner. Then (4.23) becomes

$$A = -\frac{\pi}{2\beta}, 0 < \sigma < \sigma_1, A = \frac{\pi}{2\beta}, \sigma_2 < \sigma < \sigma_3, \frac{\partial A}{\partial \xi} = 0, \sigma_1 < \sigma < \sigma_2 \quad \text{and} \quad \sigma_3 < \sigma < \sigma_4 \quad (4.26)$$

This is just a description of a semi-infinite bar which is, at its free end, alternating cooled, insulated, heated, insulated, etc. The problem is to find temperature which is repeated after one cycle. Obviously, it is not necessary that $A \rightarrow 0$ as $\xi \rightarrow \infty$; in general, a nonzero A_0 will be determined as part of solution.

The final result for the α -effect is (Childress, 1979)

$$\langle \mathbf{u} \wedge \mathbf{B} \rangle = \alpha_0 \cdot \langle \mathbf{B} \rangle + O(R^{-1/2}) \quad (4.27)$$

$$\alpha_0 = R^{-1/2} \begin{bmatrix} \mu_1 & \delta \\ \delta & \mu_2 \end{bmatrix} \langle \mathbf{u} \wedge \mathbf{B} \rangle_x \simeq \int -\psi_x B + W A_x dx \quad (4.28)$$

as $\mathbf{u} = (\psi_y, -\psi_x, K\psi)$ where $\psi = \sin x \sin y + \delta \cos x \cos y$ $|\delta| \leq 1$. The physical mechanism for the α -effect involves the pulling out of "tongues" of flux in the layers, which then interact with the small z -component of velocity to produce a mean emf. We suggest this process in Figure 4.6

This result has also been studied by Anufriyev and Fishman (1982), and Soward (1987). Soward has found that the key integral equation has an exact explicit solution by the Wiener-

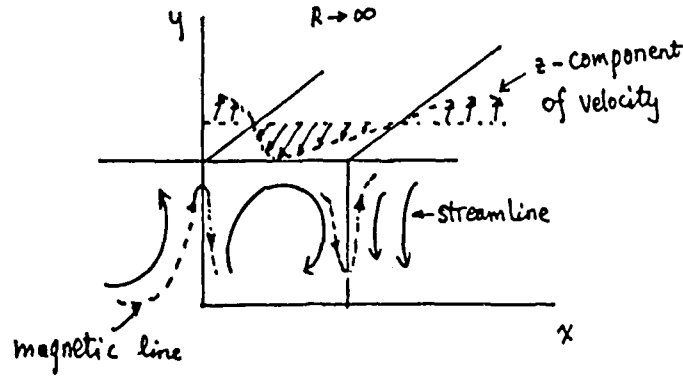


Figure 4.6

Hopf method. He let $A = \frac{\pi}{2}a(\xi, \sigma)$, then obtained a heat conduction problem in the form

$$a(\xi, 4) = \int_0^\infty [S(\xi - u) - S(\xi + u)]a(\xi, 2)du, \quad (4.29)$$

$$a(\xi, 2) = \text{Erf}\left(\frac{\xi}{\sqrt{8}}\right) - 1 - \int_0^\infty [S(\xi - u) - S(\xi + u)]a(\xi, 4)du, \quad (4.30)$$

$$\text{where } S(x) = \frac{1}{\sqrt{8\pi}}e^{-x^2/8}. \quad (4.31)$$

Let

$$\phi(\xi) = a_\xi(\xi, 2) + ia_\xi(\xi, 4) \quad (\xi \geq 0) \quad (4.32)$$

$$\phi(\xi) = \frac{1+\Gamma}{\sqrt{2\pi}}e^{-\xi^2/8} + i \int_0^\infty (\phi(u)S(\xi - u) - \phi^*(u)S(\xi - u))du \quad (4.33)$$

$$\text{Then } \phi(-\xi) = \phi^*(\xi) \quad (4.34)$$

gives the extension to $\xi < 0$. So

$$l + i\Gamma = \int_0^\infty \phi(\xi)d\xi \text{ and } \alpha_o = -\frac{1}{2} \int_0^\infty \xi \text{Im}[\phi(\xi)]d\xi. \quad (4.35)$$

From the solution of 4.33, he obtained

$$\alpha_{(o)} = \alpha \begin{bmatrix} 1 & 0 \\ 0 & 1 \end{bmatrix} \text{ where} \quad (4.36)$$

$$\alpha_o = -\frac{K}{\sqrt{R}} \sqrt{\frac{2}{\pi}} \sum_{n=1}^\infty \frac{(-1)^n}{\sqrt{2n+1}} = -0.533 \frac{K}{\sqrt{R}} \quad (4.37)$$

In figure 4.7 we compare (4.37), an estimate given by Childress (1979) and the numerical results of Roberts (1972).

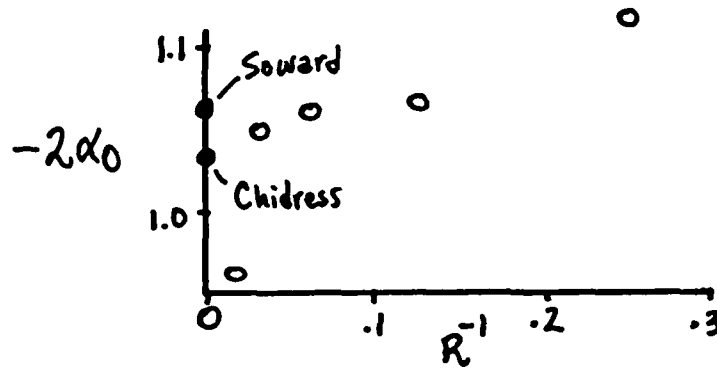


Figure 4.7: Open circles are Roberts' numerical results; Soward's value is the correct theoretical asymptote.

4.2.1 Application to the Dynamo

Let $\langle B_x + iB_y \rangle = \exp[inz + pt]$. Assuming that

$$\psi = \sin x \sin y, \quad \mathbf{u} = (\psi_y, -\psi_x, K\psi), \quad (4.38)$$

we obtain an equation for the growth rate p of the form

$$p + \frac{n^2}{R} = \frac{\alpha_0 n}{\sqrt{R}}, \quad \alpha_0 = -0.533. \quad (4.39)$$

This derivation assumes that the α -effect computation, which neglected z -dependence of \mathbf{B} , still holds as long as

$$\frac{2\pi}{n} \gg \frac{1}{\sqrt{R}}, \quad \text{or} \quad \frac{n}{\sqrt{R}} \ll 1 \quad (4.40)$$

Then, if $\beta = n/\sqrt{R}$, we have

$$\begin{aligned} p &= \beta\alpha_0 - \beta^2 \\ &\simeq \beta\alpha_0, \quad \beta \ll 1. \end{aligned} \quad (4.41)$$

The double limit $\beta \rightarrow 0, R \rightarrow \infty$ must be analyzed further in order to see how close the result given here, $p = o(1), R \rightarrow \infty$, can come to giving a finite p in the limit. We will study this point further in Lecture 7.

4.3 Cat's Eyes

We consider the so-called "cat's eye" flow with $\psi = \sin x \sin y + \delta \cos x \cos y$, $0 \leq |\delta| \leq 1$, $\mathbf{u} = (\psi_y, -\psi_x, K\psi)$. We will consider here some preliminary results of

β	$R^{1/2}(\alpha_1 - \alpha_2)$	$R^{1/2}(\alpha_2 - \alpha_1)$	$RD\text{et}(\alpha)$
0	-.533	.533	.284
.5	-2.255	1.383	.311
1.0	-1.118	3.378	.400
1.5	-.077	7.204	.550
2.0	-.054	13.370	.715
3.0	-.030	34.300	1.030

Table 4.1

Childress and Soward (unpublished).

First consider $\delta = \pm 1$, $\psi = \cos(x \mp y)$.

With $\langle \mathbf{B} \rangle = \mathbf{i}$, we find that

$$\begin{aligned} A &= y - \frac{R}{2} \sin(x \mp y) \\ B &= -\frac{R}{2} K \sin(x \mp y) \end{aligned} \quad (4.42)$$

The symmetry again assumes that

$$\alpha = \begin{bmatrix} \alpha_1 & \alpha_2 \\ \alpha_2 & \alpha_1 \end{bmatrix}, \quad (4.43)$$

where, from the induction equation,

$$\begin{aligned} B_{01}\alpha_1 + B_{02}\alpha_2 &= \frac{1}{\pi^2} \int_D \int (U_y B_z - U_z B_y) dx dy \\ B_{01}\alpha_2 + B_{02}\alpha_1 &= \frac{1}{\pi^2} \int_D \int (U_z B_x - U_x B_z) dx dy \end{aligned} \quad (4.44)$$

Since $\mathbf{B} = (A_y, -A_x, B)$, we may substitute (4.41) into (4.43) to obtain

$$\alpha = -\frac{RK}{2} \begin{bmatrix} 1 & \mp 1 \\ \mp 1 & 1 \end{bmatrix} \quad (4.45)$$

For this case, the magnetic growth rate is given by

$$p + \frac{1}{R} n^2 = \sqrt{\det(\alpha)} n = 0 \quad (4.46)$$

which shows no dynamo action for $\delta = \pm 1$.

But what about the $|\delta| < 1$ case? In Table 4.1 and Figure 4.8 we show the numerical results for the cat's-eye flows.

The values in the first column are probably not to be trusted above $\beta = 2.0$. The values for $D\text{et}(\alpha)$ are also uncertain above this point. The analysis of this model is continuing and reliable results for large β may be accessible by boundary-layer asymptotics.

4.3.1 P-B-L Analysis

Let

$$H[A] \equiv \left(q \frac{\partial}{\partial s} - R^{-1} \nabla^2 \right) A = 0$$

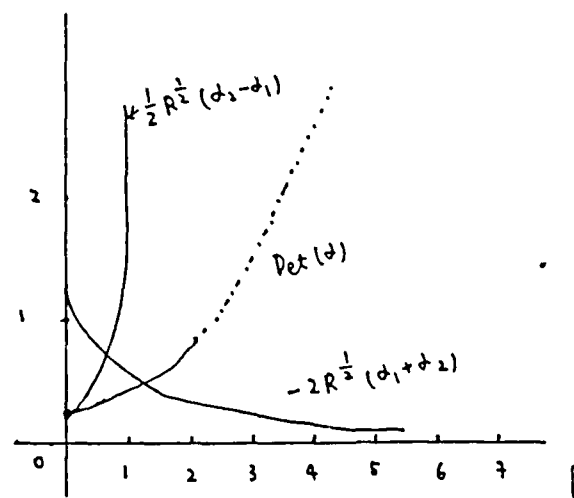


Figure 4.8

$$\begin{aligned}
 q &= |\mathbf{u}| \\
 \mathbf{u} &= (\psi_y, -\psi_x) \\
 H[B] &= K \frac{\partial(\psi, A)}{\partial(x, y)}
 \end{aligned} \tag{4.47}$$

Consider first the region of closed streamlines, shown in Figure 4.9. Assume $A = A_0 + R^{-1}A_1 + \dots$ where $A_0 = O(1)$. Insert this series into (4.47).

The R^0 term gives $q \frac{\partial A_0}{\partial s} = 0$, i.e. $A_0 = A_0(\psi)$, a function of ψ only.

The R^{-1} term gives $q \partial A_1 / \partial s = \nabla^2 A_0$. Thus from

$$\oint_{C(\psi)} \frac{1}{q} \nabla^2 A_0 ds = 0 \tag{4.48}$$

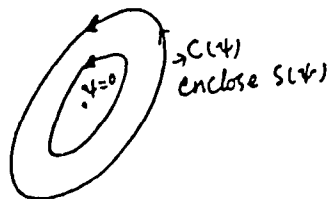


Figure 4.9

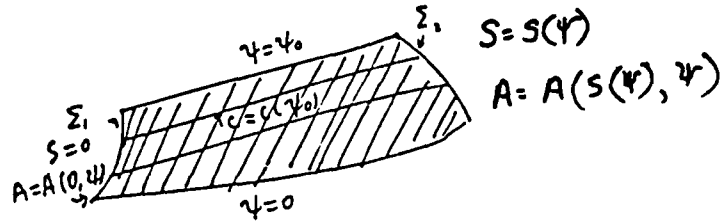


Figure 4.10

we get

$$\frac{d}{d\psi} \oint_{C(\psi)} \frac{1}{q} \nabla^2 A_0 ds d\psi = 0 \quad (4.49)$$

or

$$\frac{d}{d\psi} \iint S(\psi) \nabla^2 A_0 dx dy = \frac{d}{d\psi} \oint_{C(\psi)} \frac{\partial A_0}{\partial n} ds = \frac{d}{d\psi} \left[\gamma(\psi) \frac{dA_0}{d\psi} \right] = 0 \quad (4.50)$$

where

$$\gamma(\psi) = \oint q ds \quad (4.51)$$

Consequently

$$\gamma(\psi) \frac{dA_0}{d\psi} = \text{const.} \quad (4.52)$$

Since $\gamma(0) = 0$, it follows that $dA_0/d\psi = 0$, i.e. A_0 is independent of ψ inside a region of nested closed streamlines. In a similar way we find that $A = \text{const} + O(R^{-N})$ for any $N > 0$, as $R \rightarrow \infty$.

4.3.2 Analysis of Finite Channel

Now we consider the family of streamlines $C(\psi)$, $0 < \psi < \psi_0$ shown in Figure 4.10, where the streamlines connect two arcs $\Sigma_{1,2}$, on which the values of A value are given. We also take ψ and the arc length $s = s(\psi)$ as independent variables. We then try to solve equation

$$u \frac{\partial A}{\partial s} - R^{-1} \nabla^2 A = 0 \quad (4.53)$$

For the channel there is a flux which is $O(1)$ through the cell. These field lines get stretched out by the channel flow, producing fields of order R .

Thus we take $A = RA_0 + A_1 + \dots$ putting this into (4.54), the

R^1 term gives $A_0 = A_0(\psi)$, while the

R^0 term gives $u \partial A_1 / \partial s = \nabla^2 A_0$.

Thus (et. Figure 4.11)

$$\int_{C(\psi)} q^{-1} \nabla^2 A_0 ds = A_1(\Sigma(\psi), x) - A_1(0, \psi) \equiv [A_1] \quad (4.54)$$

Since $dx dy \Leftrightarrow q^{-1} ds d\psi$, (4.55) may be transformed as above to give

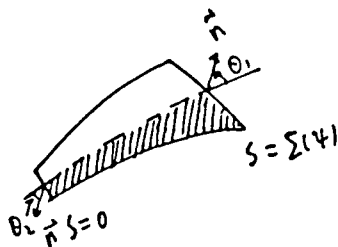


Figure 4.11

$$[A_1] = \frac{\partial}{\partial \psi} \int \int_{S(\psi)} q^{-1} A_0 ds d\psi = \frac{\partial}{\partial \psi} \int \int \nabla^2 A_0 dx dy \quad (4.55)$$

where $S(\psi)$ is the domain bounded by $C(\psi)$, the lowest streamline $C(0)$, and the arcs $\sum_{1,2}$.
Now

$$[A_1] = \frac{\partial}{\partial x} \int \int \nabla^2 A_0 dx dy = \frac{\partial}{\partial \psi} \oint \nabla A_0 ds = \frac{\partial}{\partial \psi} (\gamma(\psi) \frac{\partial A_0}{\partial \psi}) + \Delta_0(\psi) \quad (4.56)$$

where γ is given by (4.51) and

$$\Delta_0(\psi) = \frac{\partial A_0}{\partial \psi} [q(\sum(\psi), \psi) \sin \theta_1 - q(0, \psi) \sin \theta_2]. \quad (4.57)$$

The angles θ_1, θ_2 are shown in Figure 4.11.

For the cat's eye flow, $\psi = \sin x \sin y + \delta \cos x \cos y$. The channel is as shown as Figure 4.12. Over one period, because of symmetry and periodicity we have (with $B_0 = (1, -1)$), and $A = x + y + \tilde{A}$, \tilde{A} periodic. Thus $\Delta_0 = 0$ $[A_1] = 2\pi$. Also

$$\gamma(\psi) = 2 \int_0^\pi (\delta^2 - \psi^2 + (1 - \delta^2) \sin^2 u)^{1/2} du, \quad |\psi| \leq \delta \quad (4.58)$$

Similarly, for B_0 , we also have:

$$q \frac{\partial B_0}{\partial s} = -Kq \frac{\partial A_0}{\partial s} = 0 \quad (4.59)$$

$$q \frac{\partial B_1}{\partial s} - \nabla^2 B_0 = -Kq \frac{\partial A_1}{\partial s} \quad (4.60)$$

$$- \int_{C(\psi)} \frac{1}{q} \nabla^2 B_0 ds = -K[A_1] \quad (4.61)$$

From (4.44)

$$\alpha = \begin{pmatrix} \alpha_1 & \alpha_2 \\ \alpha_2 & \alpha_1 \end{pmatrix} \quad (4.62)$$

$$\begin{aligned} \alpha_1 - \alpha_2 &= \frac{1}{\pi^2} \int_0^\pi \int_0^\pi (A_x K \psi - \psi_x B) dx dy, \\ &\simeq \frac{R}{\pi^2} \int_0^\pi \int_{-\delta}^\delta \delta (A_0 \psi K \psi - B_0) d\psi dy, \\ &\simeq 8RK \int_0^\psi \frac{\psi^2}{\gamma(\psi)} d\psi \sim \frac{2}{3} R \delta^3, \quad \delta \ll 1. \end{aligned} \quad (4.63)$$

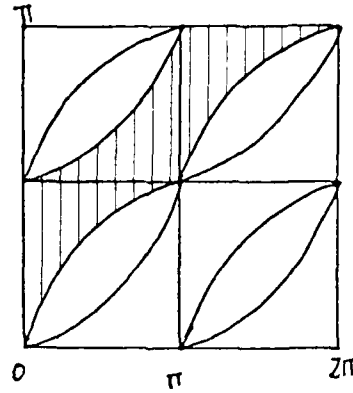


Figure 4.12

Thus

$$K^{-1}(\alpha_1 - \alpha_2) = R^{-1/2} \left[\frac{2}{3} \beta^3 + o(\beta^3) \right] \quad (4.64)$$

This yields a very strong α -effect, from a field perpendicular to the channels.

4.4 Another Modification

We can add a weak uniform flow to break the symmetry of the cellular flow,

$$\psi = \epsilon(\cos \theta y - \sin \theta x) + \sin x \sin y \quad (4.65)$$

In order to solve the problem, we must include an electric field

$$- \epsilon(\sin \theta, \cos \theta) \cdot \langle \mathbf{B} \rangle \quad (4.66)$$

i.e.

$$A = A + \epsilon(\sin \theta, \cos \theta) \cdot \langle \mathbf{B} \rangle t \quad (4.67)$$

So the induction equation should be

$$(\mathbf{u} \cdot \nabla) A - \frac{1}{R} \nabla^2 A = -(\sin \theta, \cos \theta) \cdot \langle \mathbf{B} \rangle \quad (4.68)$$

which is also solvable. If we let θ be proportional to z , with a small multiplier, then \mathbf{u} can be thought as superposition of three Beltrami waves: the added part is a slowly modulated Beltrami wave and the cellular flow is a superposition of two Beltrami waves. In the form (65) the particle paths are seen to be equivalent to a map, mod 2π in x and y .

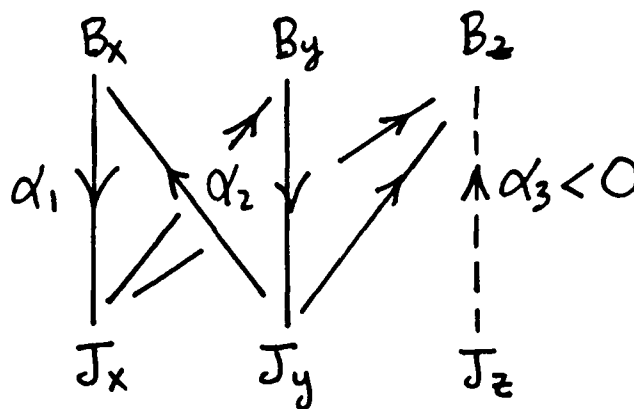


Figure 4.14

4.7 References

- Anufriyev, A.P. and Fishman, V.M., 1982. "Magnetic field structure in the two-dimensional motion of a conducting fluid", *Geomag. Aeron.*, 22, 245-248.
- Childress, S., 1979. "Alpha-effect in flux ropes and sheets", *Physics of Earth and Planetary Interior*, 20, 172-180.
- Gordon and Breach, pp. 91-97.
- Moffatt, H.K. and Kamkar, H., 1983. "The time-scale associated with flux expulsion", in *Stellar and Planetary Magnetism*, Ed. A.M. Soward.
- Rhines, P.B. and Young, W.R., 1983. "How rapidly is a passive scalar mixed within closed streamlines", *J. Fluid Mech.*, 133, 133-145.
- Roberts, G.O., 1972. "Dynamo action of fluid motions with two-dimensional periodicity", *Philos. Trans. R. Soc. Lond Ser. A.*, 271, 411-454.
- Roberts, G.O., 1970. "Spatially periodic dynamos", *Philos. Trans. R. Soc. Lond., Ser. A.*, 216, 535-558.
- Soward, A.M., 1987. "Fast dynamo action in a steady flow", *J. Fluid Mech.*, 180, 267-295.
- Weiss, N.O., 1966. "The expulsion of magnetic flux by eddies", *Proc. R. Soc Lond.*, A293, 310-328.

Notes submitted by Bin Bin Hu.

Lecture 5

The Genesis of the Fast Dynamos

5.1 Introduction

Definition: A fast dynamo is one in which dynamo action continues as $R \rightarrow \infty$ (R is the magnetic Reynolds number),
or more formally

$$\lim_{R \rightarrow \infty} (\inf p(R)) > 0 \quad (5.1)$$

where $\mathbf{B} = \mathbf{B}(\mathbf{r})e^{pt}$.

The motivation for considering such dynamos comes from astrophysics e.g. Vainshtein and Zel'dovich (1972). For stars, the generation of magnetic fields is thought to be due to a dynamo process, yet R in a typical star is very large. One way of calculating R is to consider the ratio of convective and diffusive timescales:

$$\tau_{diff} = \frac{L^2}{\eta}; \quad \tau_{conv} = \frac{L}{u} \Rightarrow R = \frac{\tau_{diff}}{\tau_{conv}} = \frac{UL}{\eta} \quad (5.2)$$

Our sun shows regular sunspot cycles (associated with a solar dynamo). A rough analysis gives:

$$\begin{aligned} L_{spot} &\approx 10^7 m, \quad U_{spot} \approx 10^3 ms^{-1}, \quad \eta_{spot} \approx 10^4 m^2 s^{-1} \\ \Rightarrow \tau_{diff} &\approx 10^{10} s^{-1} \text{ (very slow)}, \quad \tau_{conv} \approx 10^4 s^{-1} \text{ (fast)}, \quad R \approx 10^6 \gg 1 \end{aligned} \quad (5.3)$$

Thus the spot (and therefore \mathbf{B}) certainly seems to be evolving on a "fast" convective timescale (Priest, p. 101).

Before getting involved with analysis and models one might ask whether it is easy or difficult to find a fast dynamo mechanism. By the end of this and subsequent lectures, the reader should be in no doubt of the answer to this question.

Initially, we address the kinematic problem and seek uninterrupted growth rates. There are some ambiguities as to how growth rates should be measured and how large they have to be. For instance at large R , small scales will continue to grow for a long time before being diffused away. Also, U , L and ω can all be either steady or unsteady. Thus R must be clearly defined, and we demand that our definition of R results in $R \rightarrow \infty$ for the system. A dynamo box with a diffusivity knob gives a picture of what is envisaged. (See Figure 5.1.)

5.2 The Role of Diffusion

The way in which small diffusion acts in a fast dynamo is likely to be very important. Indeed, it is puzzling to note that finite diffusion enhances dynamo action for many slow

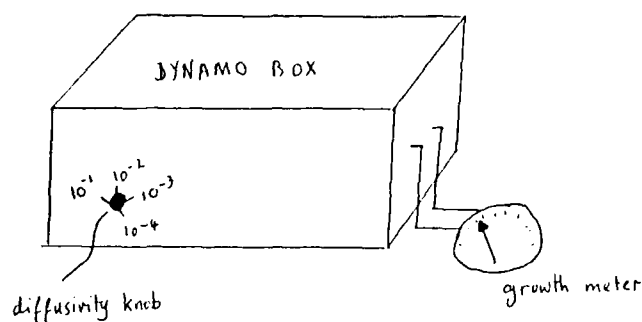


Figure 5.1: Dynamo box diagram

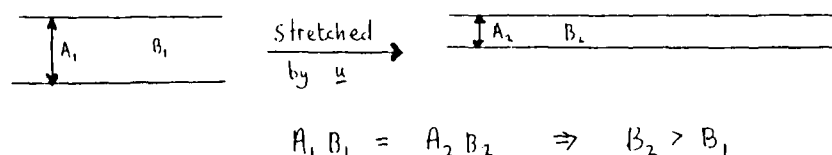


Figure 5.2

dynamos – some of which rely on $\eta > 0$ to give an alpha-effect (Moffatt).

One way of avoiding such small diffusivities is to argue that a large effective turbulent value of η is acting in a star. Molecular diffusivities are associated with friction between molecules, and this could be negligible compared to the friction between turbulent eddies. H. R. Strauss (1986) has put forward a dynamo model with an effective turbulent diffusivity. However, this approach does not indicate how molecular diffusion really operates.

With $\eta = 0$ any fluid movements translate directly to \mathbf{B} (frozen flux theorem). Magnetic flux is conserved, meaning that stretching implies field growth. (See Figure 5.2.)

Such large R systems are difficult to control, with every small turn in \mathbf{u} affecting \mathbf{B} . This gives a large build up of field on small scales (noise) which would have been filtered out if diffusion were larger.

5.3 Liapunov Exponents

Since stretching of field lines leads to field amplification, a measure of the separation of fluid particles with time in a flow could be useful.

Consider a line segment $\vec{\Delta x}$ of length $d(0)$. Let a flow $\mathbf{u}(\mathbf{x}, t)$ carry this segment into one of length $d(t)$ at time t .

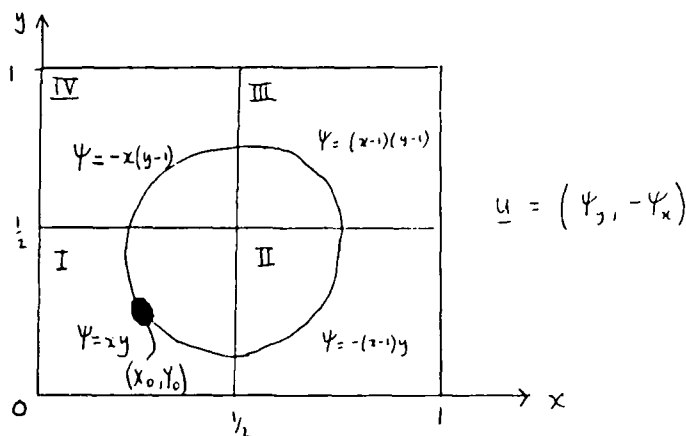


Figure 5.3

Define the exponent as follows:

$$\sigma = \lim_{t \rightarrow \infty} \frac{1}{t} \lim_{d(0) \rightarrow 0} \log_e \left(\frac{d(t)}{d(0)} \right); \quad \sigma > 0 \Rightarrow \text{growth} \quad (5.4)$$

For our flows ($R \rightarrow \infty$) we need only compute the Lagrangian Jacobian to find $d(t)$. Then by taking the proper basis for the Δx 's we get the set of exponents

$$\sigma_1 \geq \sigma_2 \geq \dots \geq \sigma_m (m = \text{dimension of flow space}) \quad (5.5)$$

5.3.1 Example: Square Cell Flow

This is a good example of how to construct a flow by smoothly joining different stream-functions. Consider the small blob of fluid drawn in Figure 5.3. The period for one orbit depends on the starting point (x_0, y_0) of a fluid particle in the blob (faster nearer the center). Suppose that particles on the streamline drawn have a period of \bar{T} .

$$\text{period} = \int_{\text{streamline}} \frac{ds}{q} = 4 \log_e \left(\frac{1}{4x_0y_0} \right) \quad (5.6)$$

At time $t = \bar{T}$, general particles in the blob will be at

$$x = x_0 e^{\bar{T} - T(x_0, y_0)}, \quad y = y_0 e^{-\bar{T} + T(x_0, y_0)} \quad (5.7)$$

The Jacobian associated with this distortion is

$$J = \frac{\partial(x, y)}{\partial(x_0, y_0)} = \begin{pmatrix} \frac{x}{x_0} - \frac{\partial T}{\partial x_0} x & -\frac{\partial T}{\partial y_0} x \\ \frac{\partial T}{\partial x_0} y & \frac{y}{y_0} + \frac{\partial T}{\partial y_0} y \end{pmatrix} \quad (5.8)$$

which has a determinant of +1 if $x = x_0$ and $y = y_0$. In 2-D a rotation of angle θ finds the proper basis for this matrix:

$$\begin{pmatrix} \cos \theta & \sin \theta \\ -\sin \theta & \cos \theta \end{pmatrix} \begin{pmatrix} 1 & 4(\frac{x_0}{y_0} + \frac{y_0}{x_0}) \\ 0 & 1 \end{pmatrix} \begin{pmatrix} \cos \theta & -\sin \theta \\ \sin \theta & \cos \theta \end{pmatrix} \quad (5.9)$$

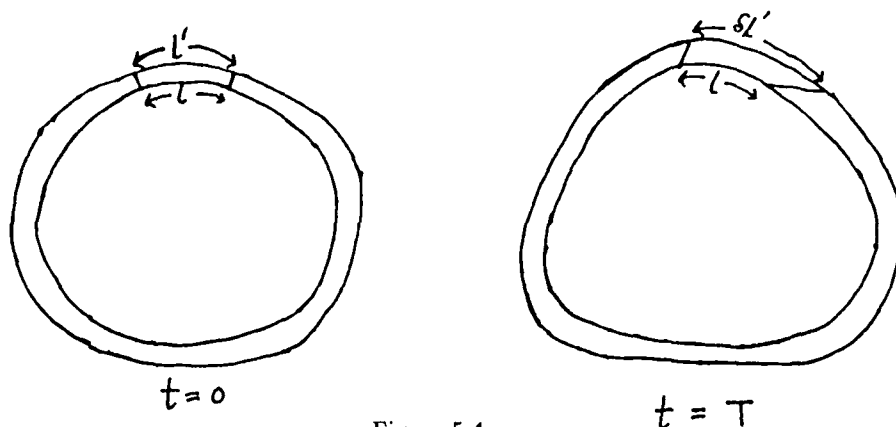


Figure 5.4

The resulting matrix represents a shear, but both its eigenvalues are unity showing that the area of the blob has been preserved. A zero Liapunov exponent is associated with this flow.

Another example is the 2-D flow defined by $u = (\psi_y, -\psi_x, k\psi)$, with $\psi = \sin x \sin y$ which has zero Liapunov exponents. To see this consider circulating particles on nearby streamlines. (See Figure 5.4.) After one orbit of the inner streamline the particles in the outer streamline are separated by $\delta l'$, after n orbits they will be separated by $n\delta l'$ i.e. growth in the direction of the flow is at most linear. Since areas are preserved (flow incompressible), growth perpendicular to the flow can be at most linear. Therefore, neither eigenvalue of J^n can grow as a power of n , giving zero Liapunov exponents.

5.4 Some Models of Fast Dynamos

5.4.1 The Baker's Dough Model ($\sigma = 3$)

Shears in a flow stretch field lines. In the Baker's dough model, an instantaneous folding takes place in which diffusion is ignored. This process is repeated on smaller and smaller scales as in Figure 5.5. Since $B(y, 0)$ is an odd function it can be represented as a sum of sines:

$$B(y, 0) = B_0 \frac{4}{\pi} \sum_{n=0}^{\infty} \frac{1}{(2n+1)} \sin(2n+1) \frac{\pi y}{L} \quad (5.10)$$

If $\eta^*(t) = g^{[t/\delta t]} \eta$ where $g^{[t/\delta t]}$ is a step function with jumps at $t = \delta t, 2\delta t, \dots$ a diffusion equation in the y -direction needs to be solved to get $B(y, t)$:

$$\frac{\partial B}{\partial t} = \eta^* \frac{\partial^2 B}{\partial y^2} \quad (5.11)$$

giving:

$$B(y, t) = 3^{[t/\delta t]} B_0 \frac{4}{\pi} \sum_{n=0}^{\infty} \frac{1}{(2n+1)} \left\{ e^{-\frac{\pi^2}{L^2(2n+1)^2} \int_0^t \eta^*(t) dt} \right\} \left[\sin(2n+1) \frac{\pi}{L} 3^{[t/\delta t]} y \right] \quad (5.12)$$

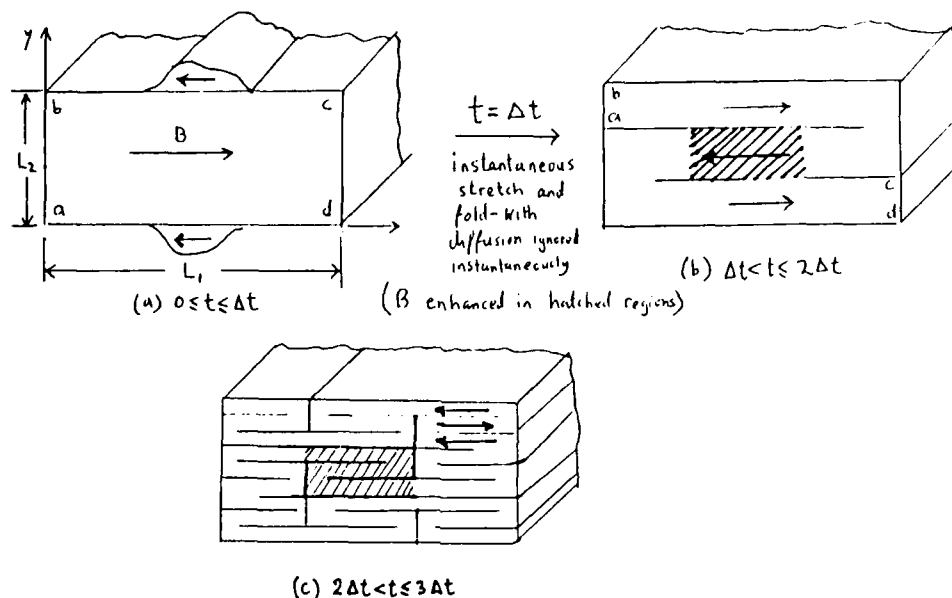


Figure 5.5

After the n th fold the averaged y value of B^2 satisfies:

$$\langle B^2 \rangle \leq g^{[t/\delta t]} B_0^2 \left[e^{-\frac{\pi^2}{L^2} g^{[t/\delta t]} \eta} \right] \quad (5.13)$$

which is of the form

$$\underbrace{k^n}_{\text{initial growth}} \underbrace{e^{-ck^n \eta}}_{\text{ultimate decay}}, \quad k > 1. \quad (5.14)$$

Thus, non zero diffusion prevents this model from acting as a dynamo, even though the Liapunov exponent $\sigma = 3$.

5.5 The Rope Dynamo

After the stretch stage (see Figure 5.6) there are two possible mechanisms: Alfvén considered cutting the stretched rope and stacking the two rings to double the field. Such cutting can be avoided by a fold and twist. Within the twisted part of the rope there will be complicated small scale structure which will be subject to diffusion. The rope dynamo is appealing since the process can be visualized as an ' $\alpha - \omega$ dynamo'. $\sigma = 2$ for this model.

A third model involves winding field around a line, then stretching this coiled field before rewinding the slack to give an increased field. (See Figure 5.7.) Unfortunately, this scheme has real difficulties due to the severe twisting on small scales which is bound to diffuse rapidly.

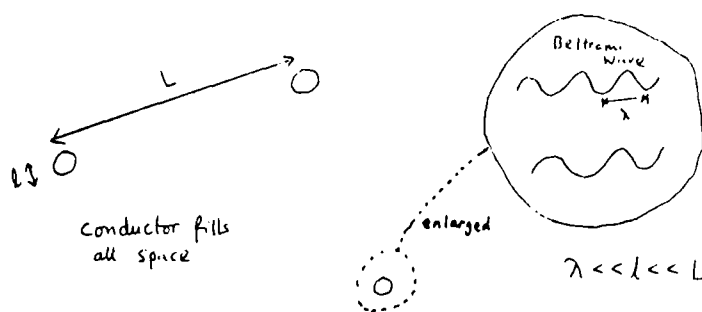


Figure 5.8

5.6 Problems Facing Fast Dynamos

5.6.1 Possible Breakdown of the α -effect

The α -effect is based on smoothing local disturbances in the presence of a large scale mean field and flow. In a fast dynamo, field will be acquiring structure on smaller and smaller scales so that the validity of the above smoothing techniques must be analyzed carefully. Measurements of about 1 Gauss for the Sun's mean field and about 10^3 Gauss for peak activity cast doubt on the applicability of smoothing to stellar dynamos too.

An idea of P.H. Roberts, developed by S. Childress (1983), in which a distribution of small packets of Beltrami waves were embedded in a conductor (analogous to the Herzenberg dynamo with only two rotors) was investigated to see what type of global α -effect resulted. A breakdown of a global α -effect was found to occur, because local packets began operating as α^2 - microdynamos. (See Figure 5.8.)

If K is a parameter measuring the density of the packets in the conductor and the intensity of the flow in the packets, it was found that for

$$\begin{aligned} K < K^*; & \quad \alpha - \text{effect on scale } \gg L \\ K > K^*; & \quad \alpha^2 - \text{microdynamos on scale } L \end{aligned} \quad (5.15)$$

5.6.2 Topological Problems

Moffatt and Proctor (1985) showed that setting $\eta \nabla^2 \mathbf{B} = 0$ makes a fast dynamo impossible in certain cases. Their argument uses the conservation of magnetic helicity property of \mathbf{B} :

$$\frac{d}{dt} \int_V \mathbf{A} \cdot \mathbf{B} dV = 0 \text{ where } \mathbf{B} = \nabla \wedge \mathbf{A} \quad (5.16)$$

This result is of topological importance. Consider a volume V , by uncurling the induction equation in V we get

$$p\mathbf{A} = \mathbf{u} \wedge \mathbf{B} + \nabla \phi \quad (5.17)$$

Applying the gauge shift $\mathbf{A} \rightarrow \mathbf{A} + \frac{1}{p} \nabla \phi$, then dotting both sides with \mathbf{B} gives $p\mathbf{A} \cdot \mathbf{B} = 0$ at all points in V . Clearly if $p > 0$, exponential growth of \mathbf{B} breaks the topological constraint outlined above. There is still the possibility that a field with zero helicity could grow exponentially (zero helicity \Rightarrow no linkage of field). However, the following analysis dismisses this.

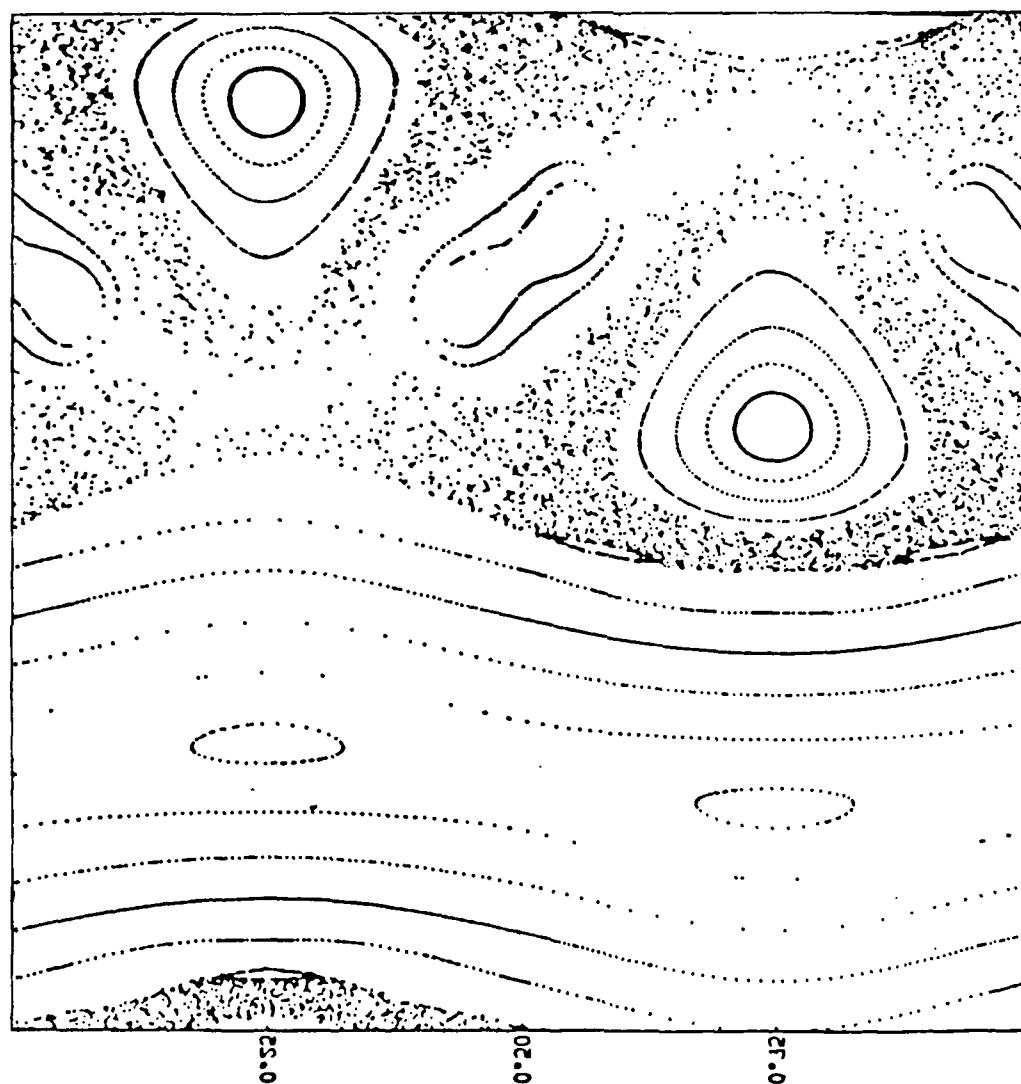


Figure 5.9: z-section of ABC flow of Dombre *et al.* 1985 and Hénon 1966. $A^2 = \frac{2}{3}$, $B^2 = \frac{1}{3}$, $C^2 = 1$.

Using the complex form of the Frobenius Theorem write $\mathbf{B} = \nabla f \wedge \nabla g$, for f, g complex scalar fields so $\mathbf{A} = f \nabla g$. Returning to the shifted version of 4.16 we have

$$pf \nabla g = (\mathbf{u} \cdot \nabla g) \nabla f - (\mathbf{u} \cdot \nabla f) \nabla g \quad (5.18)$$

$\nabla f \wedge$ throughout gives $(pf + \mathbf{u} \cdot \nabla f) \mathbf{B} = 0$ at each point in V . $\mathbf{B} = 0$ is trivial, so suppose that $pf + \mathbf{u} \cdot \nabla f = 0$, so that

$$p^* f^* + \mathbf{u} \cdot \nabla f^* = 0 \quad \text{where } * \text{ denotes complex conjugate.} \quad (5.19)$$

Integrating over V gives

$$(p + p^*) \int_V |f|^2 dV + \int_S |f|^2 \mathbf{u} \cdot d\mathbf{s} = 0 \quad (5.20)$$

using the divergence theorem.

$$\text{Now } \int_S |f|^2 \mathbf{u} \cdot d\mathbf{s} = 0 \quad (\text{since the boundaries are periodic or at infinity}) \quad (5.21)$$

Since $\int_V |f|^2 dV \neq 0$ we conclude that $\text{Re}(p) = 0$ which implies: NO FAST DYNAMO.

This result suggests that somehow $\eta \rightarrow 0$, but $\eta \nabla^2 \mathbf{B} \neq 0$ for a fast dynamo. Boundary layer structure such as magnetic ropes and sheets are associated with large spatial gradients and could certainly keep the term $\eta \nabla^2 \mathbf{B}$ bounded. Another possibility (very likely in reality) is that a fast dynamo could be unsteady (see lecture 8).

5.7 Conclusions

So far, the creation of a fast kinematic dynamo seems a difficult task. The precise way in which $R \rightarrow \infty$ is crucial, especially since fast dynamo action is sometimes impossible with $R = \infty$. Candidate flows are likely to be very complicated in order to carry out all the stretching, folding, twisting and shearing that is necessary in the models. However, the search for fast dynamos goes on!

To demonstrate the complexity that can be achieved with a well defined steady flow, a numerical simulation of an ABC flow (from Dombre et al., 1985) is shown. The picture shows a Poincaré map of a z -section for the flow at large time. (See Figure 5.9.) Non-axisymmetric vortices, a large wavy vortex passing perpendicular to the other ones and inclined slices of vortices are visible. Between the ordered flow regions particles are seen to wander without settling into any pattern. It is remarkable how orderly and disorderly flow can coexist like this.

5.8 References

- Childress, S., 1983. "Stationary Induction by Intermittent Velocity Fields" in *Stellar and Planetary Magnetism*. Ed. A. M. Soward. The Fluid Mechanics of Astrophysics and Geophysics, Vol. 2, pp 67-79, Gordon and Breach.
- Dombre et al. 1986. Chaotic Streamlines in the ABC flows. *J. Fluid Mech.* 167, 353-391.
- Herzenberg, A., 1958. *Phil. Trans. R. Soc. A* 250, 543-585.
- Moffatt, K., 1978. *Magnetic Field Generation in Fluids*, Cambridge Univ. Press.
- Moffatt, K., Proctor, M., 1985. Topological Constraints Associated with Fast Dynamo Action. *J. Fluid Mech.* 154, 493-507.
- Priest, E., 1982. *Solar Magnetohydrodynamics*, Reidel.

- Strauss, H.R., 1986. Resonant Fast Dynamo. *Physical Review Letters* 57, No. 17, 2231.
Vainshtein, S., Zel'dovich, Ya B, 1972. Origin of Magnetic Fields in Astrophysics. *Soviet Physics* 15, No. 2.

Notes submitted by Richard Jennings.

Lecture 6

Fast Dynamos I: Steady Flow

6.1 Introduction

At first glance steady flows might appear too simple to produce fast dynamos. This impression is a false one. In fact such flows can be surprisingly effective.

The Moffatt-Proctor results (1985) tell us the decomposition $\mathbf{B} = e^{\eta t} \tilde{\mathbf{B}}(\mathbf{x})$ may be too simple a decomposition. To see an example of the difficulties, consider the following flow. Let $(\psi_y(x, y, t), -\psi_x(x, y, t))$, $-\infty < t < +\infty$ be an arbitrary time-dependent 2-D flow. Following a suggestion of A. M. Soward, we consider the steady 3-D flow given by

$$\mathbf{u} = (u, v, w) = (\psi_y(x, y, \frac{z}{w_0}), -\psi_x(x, y, \frac{z}{w_0}), w_0), \quad w_0 = \text{constant} \quad (6.1)$$

We have $D\mathbf{B}/Dt = \mathbf{B} \cdot \nabla \mathbf{u} + \eta \nabla^2 \mathbf{B}$. Since the x and y components of the system form a 2-D flow, they satisfy the equation by themselves. This leaves an equation for the z -component given by

$$\frac{DB_z}{Dt} - \eta \nabla^2 B_z = 0 \quad (6.2)$$

(since $u_z = 0$). Assuming the boundary conditions are unforced we see that B_z will die away. Then if $(A_y, -A_x)$ is the magnetic field of the 2-D problem, $(A_y, -A_x, 0)$ is the magnetic field of the 3-D problem.

Uncurling the induction equation gives us

$$\frac{\partial A}{\partial t} + u \frac{\partial A}{\partial x} + v \frac{\partial A}{\partial y} + w_0 \frac{\partial A}{\partial z} - \eta \nabla^2 A = f(z, t) \quad (6.3)$$

Let $A = \tilde{A} + g(z, t)$ where

$$\frac{\partial g}{\partial t} + w_0 \frac{\partial g}{\partial z} - \eta \frac{\partial^2 g}{\partial z^2} = f(z, t) \quad (6.4)$$

Then

$$\begin{aligned} \frac{\partial \tilde{A}}{\partial t} + u \frac{\partial \tilde{A}}{\partial x} + v \frac{\partial \tilde{A}}{\partial y} + w_0 \frac{\partial \tilde{A}}{\partial z} - \eta \nabla^2 \tilde{A} &= 0 \\ \text{i.e.} \quad \frac{D\tilde{A}}{Dt} &= \eta \nabla^2 \tilde{A} \end{aligned} \quad (6.5)$$

Thus \tilde{A} decays if $\eta > 0$ and hence so does $B_x = \partial \tilde{A} / \partial y$, $B_y = -\partial \tilde{A} / \partial x$. If $\eta = 0$, then $D\tilde{A}/Dt = 0$ and field is frozen into the fluid.

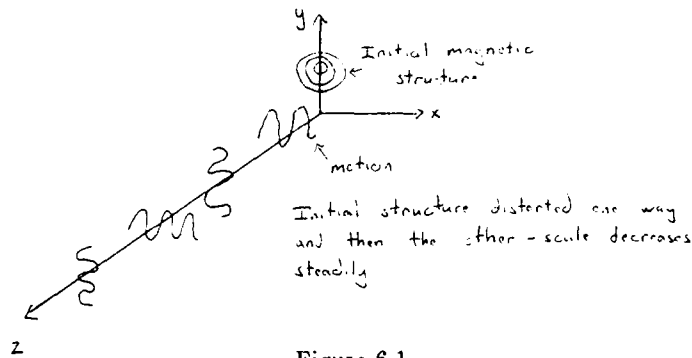


Figure 6.1

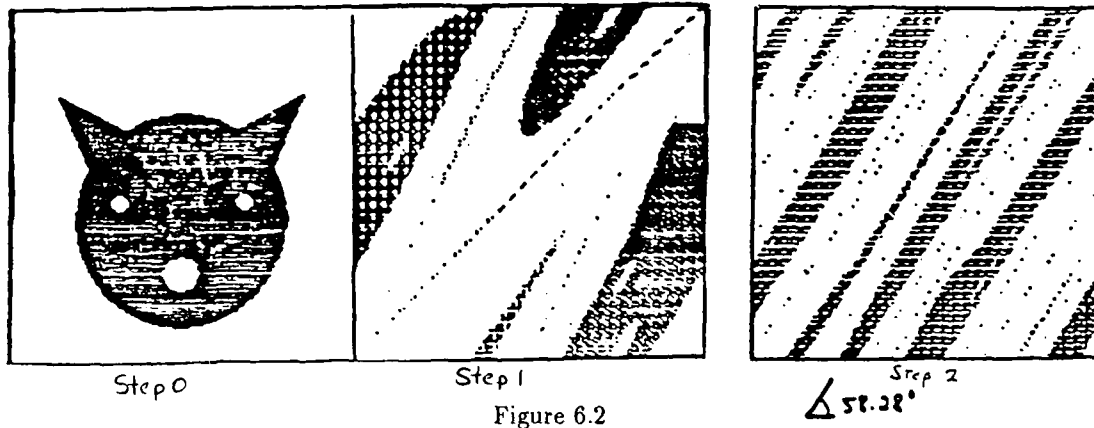


Figure 6.2

As an example consider the following situation (Figure 6.1). We have the "initial" magnetic field consisting of concentric rings on the x - y plane. Along the z -axis the motion alternates between a periodic wave in the x and y directions. As the initial structure gets carried in the z -direction it gets distorted, first one way and then another, into a horrible mess. Thus in this case no eigenfunctions exist. In the general case even if an eigenfunction exists it may be extremely complicated. However if $\eta > 0$ everything is OK, although decay will occur; we see that passing to the limit $\eta = 0$ can be dangerous.

As a model of a fast dynamo we now consider Arnold's cat (Arnold and Avez, 1967). We take as a flow map $(x, y) \rightarrow (x + y, x + 2y)$ on the unit square with periodic boundary conditions, which has the effect of stretching the fluid. A particular effect is to pull a cat's head out of recognition (Figure 6.2).

The Jacobian of this map is

$$J = \begin{pmatrix} 1 & 1 \\ 1 & 2 \end{pmatrix} \quad (1, (1 + \sqrt{5})/2) \quad (6.6)$$

which yields eigenvalues $\lambda_{1,2} = 3 \pm \sqrt{5}/2$ with corresponding eigenvectors $(1, 1 + \sqrt{5})/2$, $(-(1 + \sqrt{5})/2, 1)$. Then the inclination of the axis of stretching (i.e. direction of the principle eigenvector) is given by $\tan^{-1}((1 + \sqrt{5})/2) = 58.25^\circ$.

We can generate this map from a stagnation point flow iterated at unit time (figure 6.3).

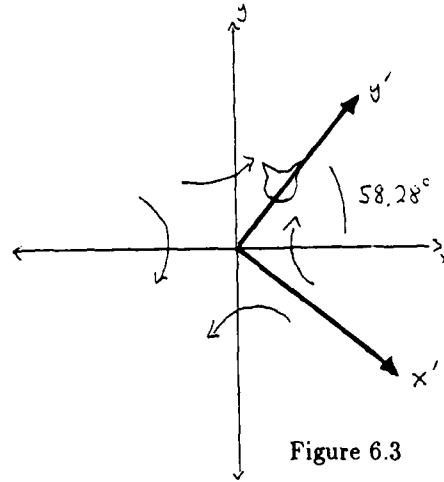


Figure 6.3

Changing to the prime coordinates (and then dropping the primes)

$$\mathbf{u} = (-\mu x, \mu y) \quad \mu = \ln\left(\frac{3+\sqrt{5}}{2}\right) = .9624 \quad (6.7)$$

We recover the cat-map by the unit time iteration $(x_0, y_0) \rightarrow (x_0 e^{-\mu}, y_0 e^{\mu}) = (\lambda_2 x_0, \lambda_1 y_0)$. (For an extensive investigation of flows of the form $\mathbf{u} = A(t) \cdot \mathbf{x}$ see Zel'dovich et al, 1984).

The Arnold, Zeldovich, Ruzmaikin, Sokoloff (AZRS) model (1981) utilizes the cat-map to establish a compact Riemannian manifold on which a dynamo exists for a simple flow. This complicated structure allows us to simplify the flow and also eliminates the difficulties inherent in any attempt to extend the flow periodically on the plane. As before we consider the velocity field

$$\mathbf{u} = (-\mu x, \mu y, 1) \quad \mu = \ln\left(\frac{3+\sqrt{5}}{2}\right) \quad (6.8)$$

with x, y pointing in the directions of principle strain. Then

$$\mathbf{u} \cdot \nabla = -\mu x \frac{\partial}{\partial x} + \mu y \frac{\partial}{\partial y} + \frac{\partial}{\partial z} \quad (6.9)$$

Introduce the new coordinates $\xi = e^{\mu z} x, \eta = e^{-\mu z} y, \zeta = z$ we get the simplification

$$\mathbf{u} \cdot \nabla = \frac{\partial}{\partial \zeta} \quad (6.10)$$

Also we get the new metric

$$ds^2 = e^{-2\mu\zeta} d\xi^2 + e^{2\mu\zeta} d\eta^2 + d\zeta^2 \quad (6.11)$$

If we take our flow in this metric to be $(0, 0, 1)$ then the induction equations transform to

$$\begin{aligned} \frac{\partial B_\xi}{\partial t} + \frac{\partial B_\xi}{\partial \zeta} &= -\mu B_\xi + \frac{1}{R} \left[(\Delta - \mu^2) B_\xi - 2\mu e^{\mu\zeta} \frac{\partial B_\zeta}{\partial \xi} \right] \\ \frac{\partial B_\eta}{\partial t} + \frac{\partial B_\eta}{\partial \zeta} &= \mu B_\eta + \frac{1}{R} \left[(\Delta - \mu^2) B_\eta + 2\mu e^{-\mu\zeta} \frac{\partial B_\zeta}{\partial \eta} \right] \\ \frac{\partial B_\zeta}{\partial t} + \frac{\partial B_\zeta}{\partial \zeta} &= \frac{1}{R} \left[(\Delta B_\zeta - 2\mu \frac{\partial B_\zeta}{\partial \zeta}) \right] \end{aligned} \quad (6.12)$$

Not surprisingly the straining augments diffusion of field dependent on ξ and η . B_η grows without bound in its mean component.

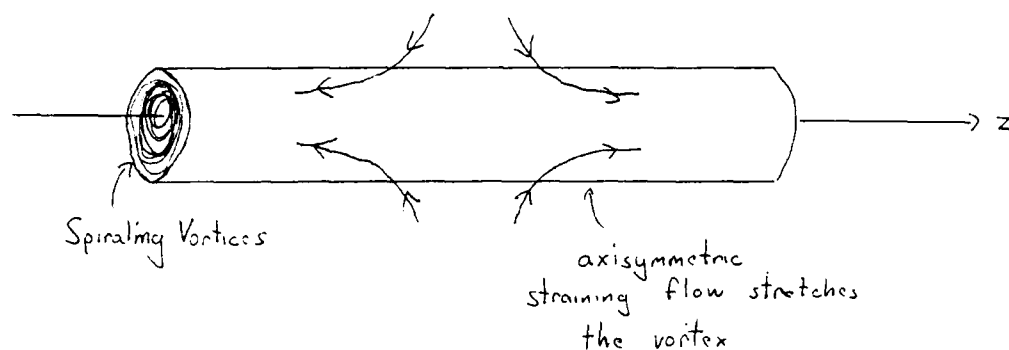


Figure 6.4

The value of this example lies in the emphasis on the escape of "noise" in a fast dynamo into a sink which operates irrespective of the value of diffusivity. The fact that diffusive effects can be treated explicitly in this example suggests that one seek a more realistic Riemannian manifold associated with a different flow.

As a final remark we note that T. S. Lundgren (1982) has applied a related model to his "spiralization" of two-dimensional vortex patches in axisymmetric straining flow (Figure 6.4). Here we see two negative eigenvalues and a positive one resulting in vortex stretching.

6.2 Numerical studies of Beltrami's Flow

Here we study the flow (ABC flow)

$$\begin{aligned} u &= A \sin z + C \cos y \\ v &= B \sin x + A \cos z \\ w &= C \sin y + B \cos x \end{aligned} \quad (6.13)$$

(See Arnold and Korkina 1983, Galloway and Frisch 1984, 1986; for a geometric treatment see Dombre et al., 1986.) This particular flow has a long and interesting history. Beltrami (1889) used it as a simple periodic example of a flow with $\nabla \times \mathbf{u} \parallel \mathbf{u}$ everywhere. Arnold (1965, 1966) was interested in its topology as a steady Euler flow:

$$\nabla H - \mathbf{u} \times \boldsymbol{\omega} = 0 \quad (6.14)$$

If $\nabla H \neq 0$ is smooth, then $\boldsymbol{\omega}$ and \mathbf{u} lie on surfaces of constant H . If $H \equiv 0$ then \mathbf{u} is a Beltrami flow with $\mathbf{u} = h(\mathbf{x})\boldsymbol{\omega}$. This implies that $\boldsymbol{\omega} \cdot \nabla h = 0$ and thus $\mathbf{u} \cdot \nabla h = 0$. Hence $\boldsymbol{\omega}$ and \mathbf{u} lie on surfaces of constant h . In both of these cases \mathbf{u} and $\boldsymbol{\omega}$ are organized by surfaces.

Recently Childress (1970) pointed out that the case $A = B = C = 1$ presents an isotropic $\alpha = \alpha_0 \mathbf{I}$ and forms an efficient first-order dynamo.

A question asked in turbulence theory is: Do patches of "Beltrami- stuff" get formed and carried about? (See Figure 6.5) Inside such "stuff" there is no transfer of kinetic energy down scales, i.e. the energy cascade (with associated dissipation at high wavenumber) is going on outside the patches. Inside the patches we get small dynamos. Note that the existence of Beltrami patches seems reasonable as inertial waves in a rotating system are Beltrami. Speziale (1987) notes, however, that helicity is not a Galilean invariant. Thus a

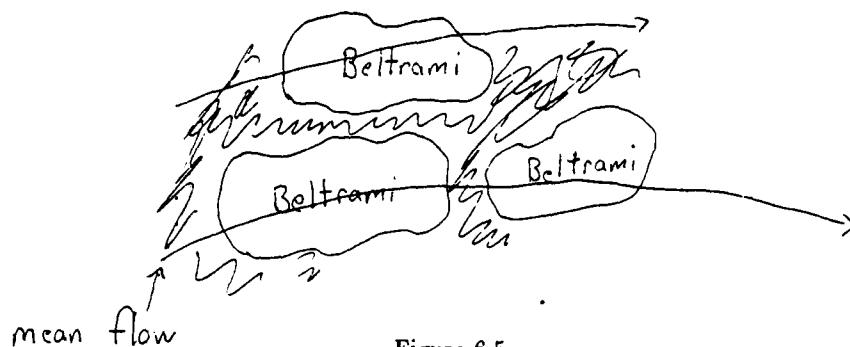


Figure 6.5

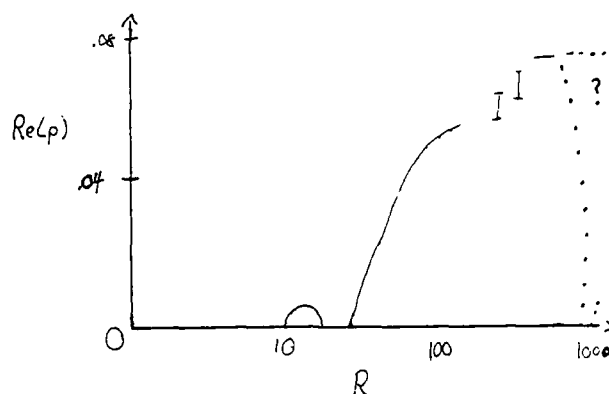


Figure 6.6

picture such as Figure 6.5 might be difficult to verify by experiment.

Arnold, Korkina, Galloway, and Frisch conducted numerical investigations of the Beltrami flow looking for a field B of the form

$$B(x, y, z, t) = e^{pt} \sum_{l, m, n = -\frac{N}{2} + 1}^{\frac{N}{2}} (X_{lmn}, Y_{lmn}, Z_{lmn}) e^{i(lx + my + nz)} \quad (6.15)$$

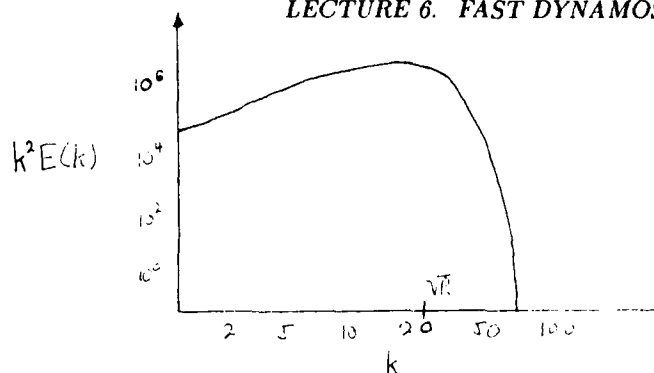
with $0 \leq x, y, z \leq 2\pi$. The mean field was set to zero. This representation is more restrictive than that allowed for the slow dynamo smoothing case, where the mean field is in fact a long-wavelength mode.

For $A = B = C = 1$, Arnold and Korkina found a mode $B \propto e^{pt}$, $Re(p) > 0$ that appears at $R \sim 8.9$ and disappears at $R \sim 17.5$. Galloway and Frisch verified this result and found a second "window" beginning at $R \sim 27$ (Figure 6.6).

The indication is of an exponentially growing ($Im(p) \sim 0$) solution $Re(p) \rightarrow .077$ at large R , but there are other possibilities:

1. No fast dynamo ultimately
2. A succession of "windows" which open and close.

The principal mode of instability was found to be associated with length scales of order $R^{-1/2}$ asymptotically. This result was supported by numerical evidence as, for example, we see above with $R = 450$ (Figure 6.7).



$$A=B=C=1, \quad R=450$$

Figure 6.7

Galloway and Frisch find that in the large window certain symmetries are broken resulting in a growing mode such that $\langle \mathbf{u} \times \mathbf{B} \rangle$ grows exponentially. On the other hand the old-fashioned large scale α -effect will still exist and may be $O(1)$ as $R \rightarrow \infty$. In any case it may be that in a real flow small-scale dynamos could be growing fastest, disrupting small-scale flow and causing "efficient" dynamos such as Beltrami flows to disappear.

6.3 Some Aspects of the Geometry of the ABC Flows

(See Dombre et al. 1986, Childress and Soward 1984)

Fortunately the ABC flow has certain symmetries:

1. $x \rightarrow -x, y \rightarrow \pi - y, z \rightarrow z, t \rightarrow -t$ and two other cyclic permutations (S_1, S_2, S_3)
2. The S_i commute mod 2π
3. If $A = B = C = 1$ then the flow is invariant under cyclic permutations of (x, y, z)

Also, although the flow is in general complicated, there are integrable cases; for example we set $C = 0$. Then

$$\dot{x} = B \sin y, \quad \dot{y} = A \cos x, \quad \dot{z} = A \sin x + B \cos y \quad (6.16)$$

Thus $A \sin x + B \cos y = V(x, y)$ is conserved, so $z = Vt + z_0$. (These are cat's eye flows, Figure 6.8.)

Now we take the case $A = B = C = 1$ and consider the geometry of streamlines connecting stagnation points. In particular we look at such streamlines that are straight (since $A = B = C = 1$ then any connecting streamline within a cell will be straight by symmetry). Taking cylindrical coordinates around these streamlines, then

$$(u_z, u_r, u_\theta) = [f(z), rG(z, \theta), rH(z, \theta)] + o(1, r, r) \quad (6.17)$$

nearby. We have $\nabla \cdot \mathbf{u} = 0$ and $\mathbf{i}_z \cdot [\nabla \times \mathbf{u} + \mathbf{u}] = 0$ (around the streamline). Thus

$$f_z + 2G + H_\theta = 0, \quad 2H - G_\theta = -f \quad (6.18)$$

Solving we get

$$\begin{aligned} (u_z, u_r, u_\theta) = & [f(z), -\frac{r}{2}f_z(z) + r(g(z) \cos 2\theta + h(z) \sin 2\theta), \\ & -\frac{rf(z)}{z} + r(h(z) \cos 2\theta - g(z) \sin 2\theta)] + o(1, r, r) \end{aligned} \quad (6.19)$$

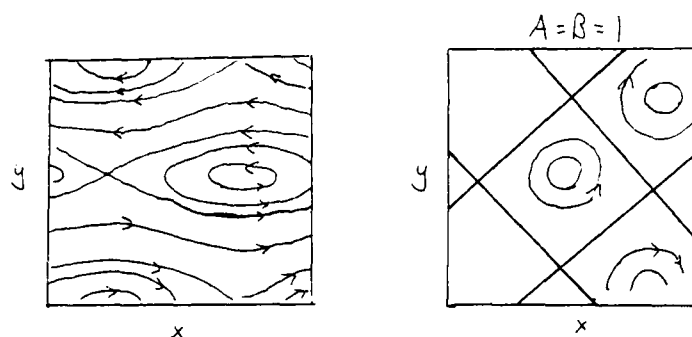


Figure 6.8

The geometry of streamlines connecting stagnation points is diagrammed in Figure 6.9.

The primary links join stagnation points within a single cell. A stable 2-D flow manifold feeds into the lower point and an unstable 2-D flow manifold feeds out of the upper point (these manifolds contain the secondary links). Note that although the manifolds are 2-D, they can be badly contorted (Figure 6.10).

The principle α -effect occurs on the unstable manifold. Here flux rings that wind around the primary link are rapidly stretched. Hopefully the interaction between the α -effects of various cells will produce a dynamo.

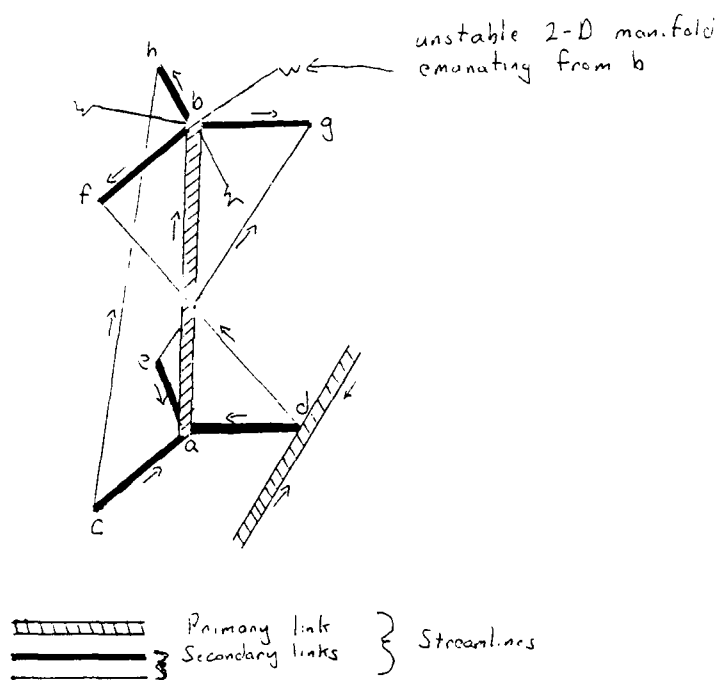
In order to estimate the α -effect one might try to compute the area of the unstable manifold perpendicular to the primary link in the limit $R \rightarrow \infty$. This could be done by following the history of a small disc on the unstable manifold (Figure 6.11). We see that there is no apparent limit. Possibly, it is necessary to watch the entire structure rather than one manifold. In any event no convincing computation of the α -effect has been made, but it is suspected to be $O(1)$. In general the flow lines on the stable and unstable manifolds are probably very complex, and nearby regions chaotic.

The ABC flow raises some interesting questions. Should we focus on the α -effect in the large R limit? It seems unnatural to carry over ideas of smoothing to flows dominated by noise. The key here seems to be that, instead of focusing on the α -effect, we should find a well-defined projection $P: \mathbf{B} \rightarrow \mathbf{B}_P$ and then track \mathbf{B}_P (fast growing $\mathbf{B}_P \Leftrightarrow$ fast dynamo).

Also chaos plays an interesting role here. It seems to be involved in the stretching out of the unstable manifolds. But it is difficult to draw any conclusions. Chaotic Lagrangian paths are usually found in smooth 3-D flows of any complexity. We cannot say they are a prerequisite to fast dynamos. At most it can be speculated that since such orbits are associated with stagnation points and fast dynamo action occurs in regions of stagnation points, that the two may be found together - i.e. to find the magnetic field, look for the chaos.

The ABC flow is exceedingly complicated. One might hope for a simpler fast dynamo. Such an example is provided by the flux rope sandwich (Soward and Childress, 1986). The flux rope sandwich consists of a set of sheets stacked consecutively at slight angles. Each sheet is made up of periodic array of flux rope boxes (Figure 6.12). A difficulty of this model is the discontinuity between sheets. This could possibly be remedied by placing conducting sheets of "cheese" between sandwich layers.

To show the possible effectiveness of this model let $\mathbf{A}(z) = (\cos \beta z, \sin \beta z, 0)$. Then by a plausible extension of axisymmetric results (cf. Section 4.5) to each rectangular flux rope



All vertices are equivalent stagnation points
 of type 1 (unstable 2-D manifold)
 or type 2 (stable 2-D manifold)

Figure 6.9

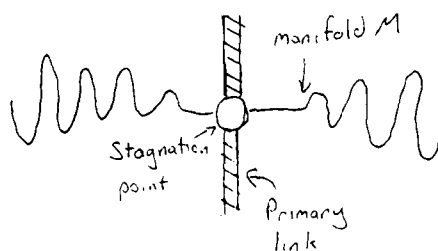


Figure 6.10

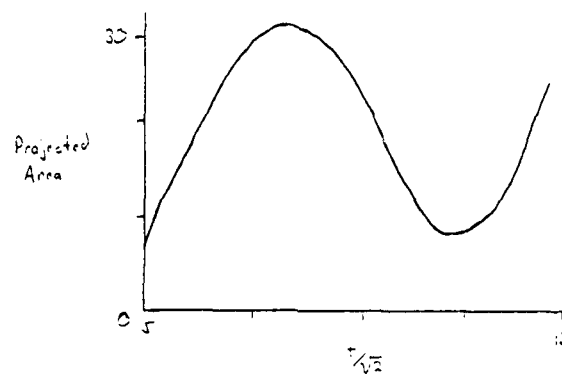


Figure 6.11

FLUX ROPE SANDWICH

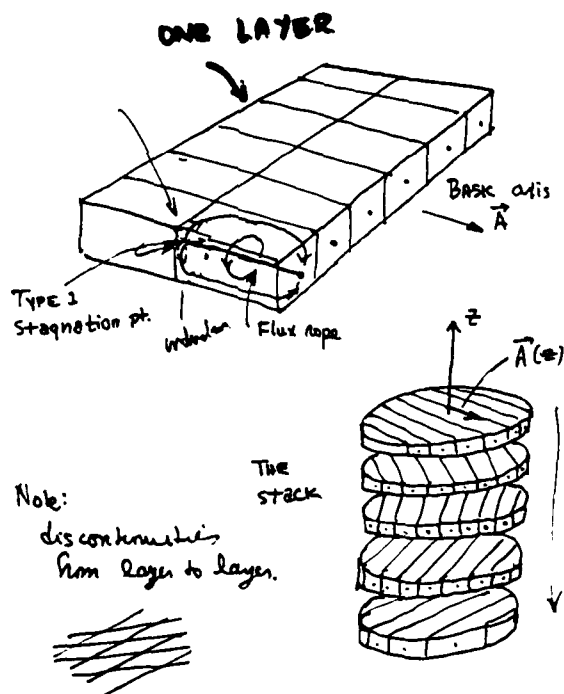


Figure 6.12

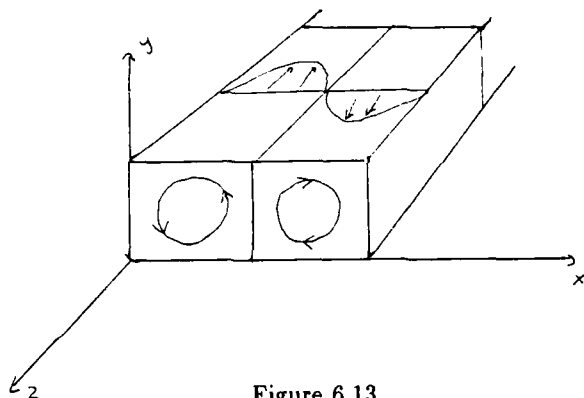


Figure 6.13

cell, we have

$$\langle \mathbf{u} \times \mathbf{B} \rangle = (\alpha_0 \langle \mathbf{B} \rangle \cdot \mathbf{A}) \mathbf{A} \quad (6.20)$$

Let $\langle \mathbf{B} \rangle = (B_x, B_y)(z, t)$ then

$$B_x + iB_y = (B_+ e^{ikz} + B_- e^{-ikz}) e^{pt+i\beta z} \quad (6.21)$$

where B_+, B_- are real. Then

$$\left[p + \frac{1}{R}(\beta \pm k)^2 + \frac{1}{2}\alpha_0(\beta \pm k) \right] B_{\pm} = -\frac{1}{2}\alpha_0(\beta \pm k) B_{\mp} \quad (6.22)$$

The maximum p occurs when $k = 0$. Then

$$p = -\alpha_0 \beta - \frac{1}{R} \beta^2, \quad (6.23)$$

So we get a fast dynamo if $\alpha_0 < 0$.

6.4 Soward's Analysis of Fast Dynamo Activity in Robert's Cellular Flow (1987)

The key idea here will be the exploitation of a well-defined mean magnetic field (in the x-y plane) that exists even when \mathbf{B} has z and t dependence. We set the z -dependence of $\langle \mathbf{B} \rangle$ to be $\sim e^{i\beta R^{1/2} z}$, $\beta \sim 0(1)$ (Figure 6.13). The rapid z -variation, coupled with fluid expulsion into the boundary layers makes the magnetic mode have a $R^{-1/2}$ scale in all directions. Note that this field structure conforms to the Moffatt-Proctor constraints since the eigenfunctions depend on R . Keep in mind however that flux expulsion takes a time $\sim R^{1/3}$.

Soward shows that the α -effect computation for a steady z -independent $\langle \mathbf{B} \rangle$ carries over to the new eigenvalue problem, and the growth rate may be computed from

$$p + \beta^2 = -\alpha_0 \beta \quad (\alpha_0 = -0.533) \quad (6.24)$$

provided that $K\beta\tau \ll 1$, where K is a constant multiplier in the stream function and $4\tau =$ time for a complete circuit on a streamline $\psi = 4\tau(\psi)$. In the boundary-layer (cf. lecture 3)

$$4\tau = \oint \frac{ds}{|u|} = 4 \int_0^{\cos^{-1}\psi} \frac{dx}{\sqrt{\cos^2 x - \psi^2}}, \quad (6.25)$$

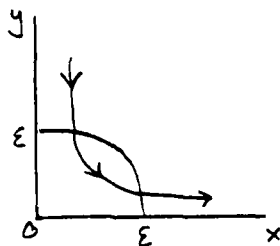


Figure 6.14

where also $\psi\sqrt{R} \sim 1$. Thus

$$\tau \sim -\ln\psi \sim \frac{1}{2}\ln R \quad (6.26)$$

This result, $p_{\max} \sim 0(1/\ln R)$, is the best we can get for free. The main difficulty is that streamlines get trapped near the corner stagnation points for long periods of time. However, we can modify u in the corners to make the circuit time shorter in the boundary layer in the $R \rightarrow \infty$ limit:

$$\begin{aligned} \psi &= a_\epsilon \sin x \sin y \\ a_\epsilon(r) &= 1 + [\ln(r/\epsilon)]^2 \quad r < \epsilon \ll 1 \end{aligned} \quad (6.27)$$

where r = distance to the stagnation point (Figure 6.14).

Now consider the time to move from 0 to ϵ along $y = 0$:

$$\Delta t = \int_0^\epsilon \frac{dx}{(1 + \ln \frac{x}{\epsilon})^2 \sin x} \simeq \int_0^\infty \frac{du}{(1 + u^2)} = \frac{\pi}{2} \quad (6.28)$$

This is independent of ϵ and R . Thus the time to go from ϵ to $\pi - \epsilon$ is $\sim -2\ln\epsilon$, and we see that $\tau \sim -2\ln\epsilon$, independent of R . This result (and our other studies of 3-D motion) suggests that the geometry of the flow near stagnation points is important for fast dynamo activity by a steady flow. Note also that although Soward's construction is very different from the dynamo of Galloway and Frisch, both concentrate on $O(R^{-1/2})$ structure.

6.5 References

- Arnold, V.I., 1965. "Sur la topologie des écoulements stationnaires des fluides parfaits", *C. R. Acad. Sci. Paris*, 261, 17-20.
- Arnold, V.I., 1966. "Sur la géométrie différentielle des groupes de Lie de dimension infinie et ses applications à l'hydrodynamique des fluides parfaits", *Ann. Inst. Fourier Grenoble*, 16, 319-361.
- Arnold, V.I. and Avez, A., 1967. *Problèmes Ergodiques de la Mécanique Classique* Gauthier-Villars, Paris.
- Arnold, V.I. and Korkina, E. I., 1987. "The growth of a magnetic field in a steady incompressible flow", *Vest. Mask. Un. Ta. Ser. 1. Matematika Mecanika*, 3, 43.
- Arnold, V.I., Zeldovich, Ya. B., Ruzmaikin, A.A., and Sokolov, D.D., 1981. "Magnetic field in a stationary flow with stretching in a Riemannian space", *Sov. Phys. JETP*, 54, (6).
- Beltrami, E., 1889. "Considerazioni idrodinamiche", *Percorsi de Reale Istituto Lambarda Serie II*, tomo XXII, 121-130 (see also *Opere Matematiche*, vol. IV, p. 304).

- Childress, S., 1970. "New solutions of the kinematic dynamo problem", *J. Math. Phys.*, 11, 3063-3076.
- Childress, S. and Soward, A.M., 1984. "On the rapid generation of magnetic fields", *Chaos in Astrophysics*, NATO Advanced Research Workshop, Palm Coast, Florida, USA.
- Dombre, T., Frisch, U., Greene, J.M., Hénon, M., Mehr, A., and Soward, A.M., 1986. "Chaotic streamlines in the ABC flows", *J. Fluid Mech.*, 167, 353-391.
- Galloway, D.J. and Frisch, U., 1984. "A numerical investigation of magnetic field generation in a flow with chaotic streamlines", *Geophys. Astrophys. Fluid Dyn.*, 29, 13.
- Galloway, D.J. and Frisch, U., 1986. "Dynamo action in a family of flows with chaotic streamlines", *Geophys. Astrophys. Fluid Dyn.*, 36, 53.
- Lundgren, T.S., 1982. "Strained spiral vortex model for turbulent fine structure", *Phys. Fluids*, 25, (12), 2193. * Moffatt, H.K. and Proctor, M.R.E., 1985. "Topological constraints associated with fast dynamo action", *J. Fluid Mech.*, 154, 493.
- Soward, A.M., 1987. "Fast dynamo action in a steady flow", *J. Fluid Mech.*, 180, 267-295.
- Soward, A.M. and Childress, S., 1986. "Analytic theory of dynamos", *Adv. Space Res.*, 6, 7.
- Speziale, C.G., 1987. "On helicity fluctuations in turbulence", *Quarterly of Applied Mathematics*, XLV (1).

Notes submitted by Isaac Klapper.

Lecture 7

Fast Dynamos II: Analysis of Complex Flows

7.1 Soward's Analysis of Cellular Flow in the Limit $R \rightarrow \infty$

Recall from Lecture 4 that we are studying mean field growth in cellular flows with:

$$\langle B \rangle \propto e^{i\beta R^{1/2} z}. \quad (7.1)$$

G. O. Roberts' (1972) flow, with a modification to the velocity field near the stagnation points, allows fast dynamo action when $K\beta\tau \ll 1$; this was established from a steady state z -independent alpha effect calculation (Soward 1987). It is much more difficult to study the action of the flow without the modification, for which $K\beta\tau \gtrsim 1$; however the maximum growth rate can be determined in the limit $R \rightarrow \infty$.

7.2 Heuristic Model

Despite these subtleties, there is a very robust physical basis for the dynamo activity, which Soward identifies as a variant of the rope dynamo mechanism: stretch-twist-fold. We shall refer to Soward's mechanism as the stretch-fold-shear (SFS) mechanism. (The full mechanism also involves a twist).

We study G. O. Roberts' (1972) flow without modifications:

$$\begin{aligned} \mathbf{u} &= (\psi_y, -\psi_x, K\psi) \\ \psi &= \sin x \sin y \end{aligned} \quad (7.2)$$

Given an x -directed mean field, taken to be of the form

$$\langle B_x \rangle \propto e^{i\beta R^{1/2} z} \quad (7.3)$$

we wish to create y -directed mean field. The effect of the x and y components of the flow is to draw out tongues of $\langle B_x \rangle$ flux in the z -direction, and create an alternating field B_y (Figure 7.1). This accomplishes the stretch and fold steps simultaneously. The effect of the z -component of the flow is to shear the distribution of B_y (Figure 7.2). Now $\langle B_y \rangle$ (averaged in the x -direction) has a mean component, which varies in the z -direction as $e^{i\beta R^{1/2} z}$. Note that there is also a component of B_x in the tongues, which is twisted into

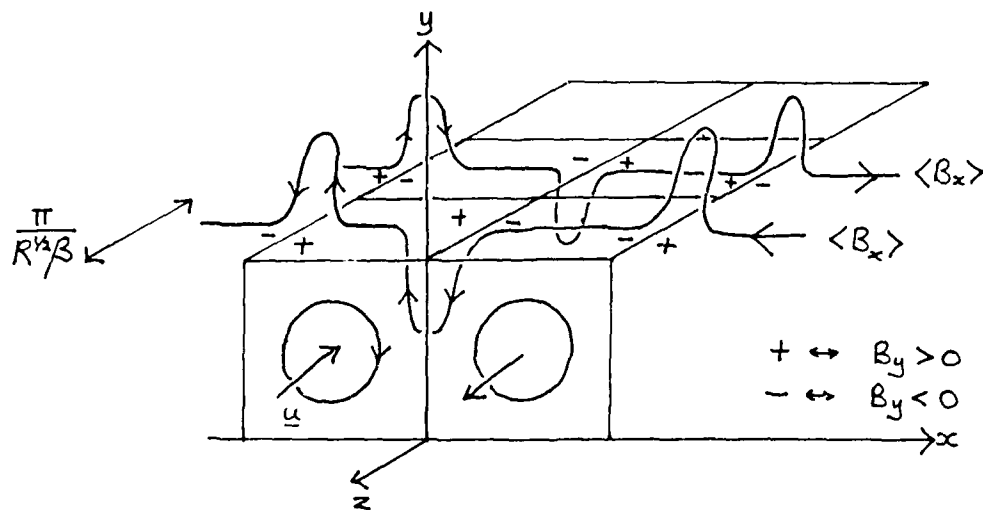


Figure 7.1

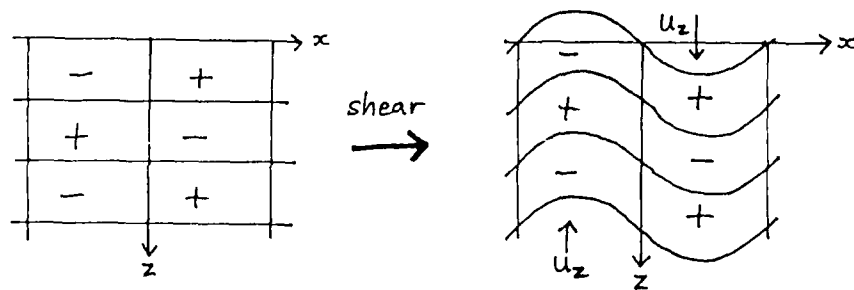


Figure 7.2

the z -direction by the shear. Mean field in the x -direction is generated from $\langle B_y \rangle$ by the same mechanism, and in this way the total magnetic field grows. Of course all these processes are happening simultaneously, since the flow is steady.

7.3 Boundary Layer Structure

We now sketch the analysis of dynamo action as $R \rightarrow \infty$ in G. O. Roberts' (1972) flow, without modification (Soward 1987). The essential ideas can be seen in the scalar equation:

$$\frac{\partial A}{\partial t} + \mathbf{u} \cdot \nabla A - R^{-1} \nabla^2 A = 0 \quad (7.4)$$

We set

$$A = e^{pt+i\beta R^{1/2}z} \tilde{A}(x, y) \quad (7.5)$$

and

$$\mathbf{u}_H = (u_x, u_y, 0) \quad (7.6)$$

then

$$(\mathbf{u}_H \cdot \nabla + \lambda) \tilde{A} = R^{-1} \nabla_H^2 \tilde{A} \quad (7.7)$$

with

$$\lambda = p + \beta^2 + i\beta R^{1/2} K \psi \quad (7.8)$$

The average time taken for fluid particles in the boundary layer to traverse the (unmodified) corners is $\tau \gg 1$. We shall assume $\beta \ll 1$, $\beta\tau \sim 1$, and take $\lambda = O(\beta)$ (to be verified).

In the boundary layers, of thickness $R^{-1/2}$:

$$\mathbf{u}_H \cdot \nabla \tilde{A} = R^{-1} \nabla_H^2 \tilde{A} \quad (7.9)$$

as in the previous ($\beta = 0$) case. In the corner layers, of thickness $R^{-1/4}$, $R^{-1} \nabla_H^2 \tilde{A}$ is negligible, and

$$\begin{aligned} (\mathbf{u}_H \cdot \nabla + \lambda) \tilde{A} &= 0 \\ \Rightarrow q \frac{\partial \tilde{A}}{\partial s} + \lambda \tilde{A} &= 0 \\ \tilde{A} = \tilde{A}_0 e^{-\lambda \int ds/q} &= \tilde{A}_0 e^{-\lambda \tau} \end{aligned} \quad (7.10)$$

(Note that $\lambda = O(\tau^{-1}) = O(\beta)$ from this.) A , instead of being continuous through the corners, now has a jump; this leads to an eigenvalue problem as follows. The equation for the growth rate involves α , which is calculated in the usual way from the boundary layer solution:

$$p = -\alpha\beta - \beta^2 \quad (7.11)$$

Then $\lambda = -\alpha\beta + i\beta K R^{1/2} \psi$ is substituted into $e^{-\tau\lambda}$ above, and so the matching conditions involve α . Define the order unity quantities: $\nu = -\alpha/K$, $\mu = K\beta\tau$, then the solution of the eigenvalue problem gives $\nu(\mu)$, and $p = \tau^{-1} \mu \nu - (K\tau)^{-2} \mu^2$, with $\tau = 1/2 \log R$. The growth rate, p , is of order $\beta \ll 1$.

Asymptotic analysis can be performed when μ is not of order unity; the limit $\mu \ll 1$ gives the $\beta = 0$ result, $\alpha_0 \simeq 0.533$. The maximum growth rate occurs for $\mu \sim \tau^{1/2} \gg 1$, when

$$\nu(\mu) = \sqrt{\frac{2}{\pi}} e^{-\mu\nu(\mu)} \quad (7.12)$$

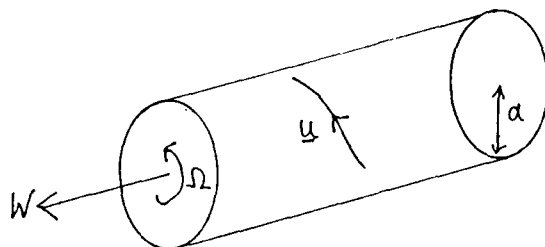


Figure 7.3

Thus

$$p = \sqrt{\frac{2}{\pi}} \beta K e^{-(p+\beta^2)\tau} - \beta^2 \quad (7.13)$$

The maximum growth rate is:

$$p_{\max} \sim \frac{\log \tau}{2\tau} \sim \frac{\log \log R}{\log R} \quad (7.14)$$

occurring when

$$\beta \sim (2\tau)^{-1/2} \sim (\log R)^{-1/2} \quad (7.15)$$

The maximum growth rate decreases as $R \rightarrow \infty$, but very slowly, so this is very nearly a fast dynamo.

7.3.1 Conclusions

1. With sufficient symmetry, steady two-dimensional flows can give fast dynamo action.
2. The process is controlled by the flow in the vicinity of the stagnation points.
3. In general, the latter also control the structure of the boundary layers.
4. The physical mechanism underlying the dynamo can be understood in terms of stretching and twisting of the field.

7.4 Ponomarenko's Helical Dynamo

Are stagnation points and square cells necessary for fast dynamo action? Let us reexamine the Ponomarenko (1973) dynamo. Recall that the dynamo consists of a solid rotor embedded in a conductor (Figure 7.3) with:

$$\mathbf{u} = \begin{cases} \Omega \rho \mathbf{i}_\theta + W \mathbf{i}_z & 0 \leq \rho < a \\ 0 & \rho > a \end{cases} \quad (7.16)$$

(in cylindrical polar coordinates (ρ, θ, z)) and provides a simple model of Parker's cyclonic events. The magnetic field satisfies:

$$\begin{aligned} (\partial_t + \Omega \partial_\theta^* + W \partial_z) \mathbf{B} &= \eta \nabla^2 \mathbf{B} & \rho < a \\ \partial_t \mathbf{B} &= \eta \nabla^2 \mathbf{B}, & \rho > a \end{aligned} \quad (7.17)$$

where $\partial_\theta^* \mathbf{B} = \mathbf{i}_\rho \partial_\theta B_\rho + \mathbf{i}_\theta \partial_\theta B_\theta + \mathbf{i}_z \partial_\theta B_z$. On the boundary, $\rho = a$, we require that B , E_θ and E_z be continuous. We put

$$\mathbf{B} = B_0(\rho) e^{im\theta + ikz + pt} \quad (7.18)$$

For large R , the process of flux expulsion will lead to a boundary layer of width $R^{-1/3}$ on $\rho = a$. This has been analyzed by P. H. Roberts (1987), who obtained the following asymptotic result:

$$q_0 + q = (i\Omega m/\eta a)(q_0 q)^{-1} \quad (7.19)$$

where:

$$\begin{aligned} q_0^2 &= k^2 + p/\eta \\ q^2 &= k^2 + (p + im\Omega + ikW)/\eta \end{aligned} \quad (7.20)$$

Let us examine the result more closely for the case:

$$m\Omega + kW = 0 \quad (7.21)$$

then:

$$p = \frac{e^{\pm i\pi/3}}{2^{2/3}} \cdot \left(\frac{\eta m^2 \Omega^2}{a^2} \right)^{1/3} - \eta k^2 \quad (7.22)$$

Set $R = \Omega a^2/\eta$, $\tilde{k} = ka$, which gives:

$$\frac{p}{\Omega} = \frac{e^{\pm i\pi/3}}{2^{2/3}} \cdot \frac{m^{2/3}}{R^{1/3}} - \frac{\tilde{k}^2}{R} \quad (7.23)$$

If we could set $m, ka \sim \sqrt{R}$, then $p/\Omega = 0(1)$ and we would have a fast dynamo; however the result is not actually valid in this limit, and further investigation is required. A. Gilbert discusses this problem in his Fellows' Project Report, this volume.

7.4.1 In Between Square and Circle

Consider rotational flow round a corner with angle α (see Figure 7.4a); the complex potential is

$$\phi + i\psi = z^{\pi/\alpha} \quad (7.24)$$

If $\alpha \leq \pi/2$, the time taken for particles to travel round the corner is unbounded, which is bad for fast dynamo action. However, if $\alpha > \pi/2$, the time taken is finite, which assists fast dynamo action; we can imagine cellular patterns which emphasize "good" corners – those with $\alpha > \pi/2$ (Figure 7.4b).

7.5 Dynamos from Non-Magnetic Instabilities

The preceding steady kinematic models are far from being natural systems. There are two distinct paths to more complicated systems. (See Figure 7.5.)

Systems involving inertial waves due to rotation, rotating convection and baroclinic instabilities have been studied in the slow context. However, little is known for fast dynamos. Some outstanding problems involve studying path 2 for both slow and fast dynamos at the dynamic level since wherever the dynamo mechanism is most intense the dynamics is likely to become important.

An observation that may be helpful is that, throughout the cosmos, rotating bodies (vorticity) and magnetic fields are usually found together, suggesting that:

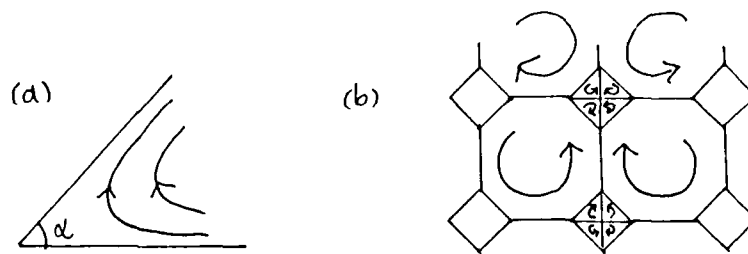


Figure 7.4

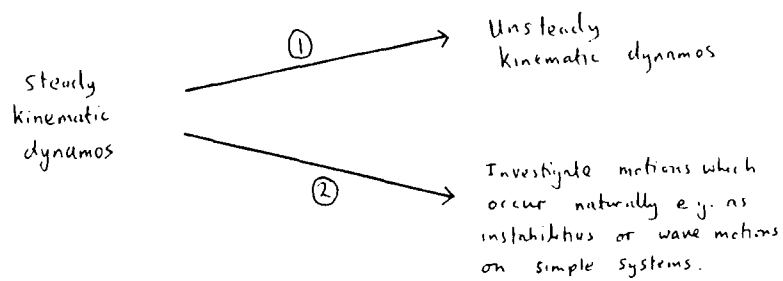


Figure 7.5

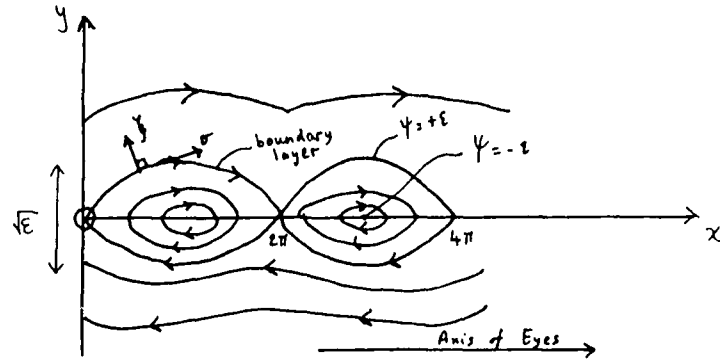


Figure 7.6

- Magnetic fields love vorticity (e.g. kinematic dynamos)
- Vorticity loves magnetic fields (e.g. magnetic destabilization).

7.6 Possible Approaches to Fast Dynamos via Instabilities at Zero Field Strength

7.6.1 Resonant Layers in Shear Flows

A parallel flow $\mathbf{u}(y) = (u(y), 0, 0)$ is perturbed proportional to e^{ikx} (e.g. $\mathbf{u}' = (0, e^{ikx}, 0)$ - divergence free). See Figure 7.6. Gradual enrichment of the geometry results by making the perturbation field \mathbf{u}' more complex e.g. (overlapping eyes, blinking eyes). Resonances occur where the fluid is stationary, i.e. at the nodes between the eyes. Braginsky (1964) considered resonant layers; in his model they represented layers of concentrated field generation.

Let resonance occur near $y = 0$ so that $U(y) = \Gamma y$, $\mathbf{u}' = \epsilon \sin kx \hat{y}$ making the stream-function ψ :

$$\psi = \frac{\Gamma y^2}{2} + \epsilon \cos x - \text{another cat's eyes flow!} \quad (7.25)$$

Field in the \hat{y} direction can be sheared by the basic flow in the \hat{x} direction, so we wish to determine whether an α -effect can reverse this process to give dynamo action. Analysis is done as $R \rightarrow \infty$ making boundary layer methods applicable.

The boundary of the eyes is the streamline $\psi = \epsilon$,

$$\Rightarrow \epsilon = \frac{\Gamma y^2}{2} + \epsilon \cos x \quad \Rightarrow y = \pm 2\sqrt{\frac{\epsilon}{\Gamma}} \sin(x/2) \quad (7.26)$$

Taking $\mathbf{u} = (\psi_y, -\psi_x, w(x, y))$, where the problem is independent of both z and time. Perturbations to the original uniform field ($\mathbf{B} = B_0 \hat{x}$) take the form $\mathbf{B}' = (A_y, A_x, b)$. Thus, the eyes generate a local α -effect:

$$\alpha_{\parallel} \text{ (parallel)} = \int \int (A_\psi w - b) \psi_x dx dy; \quad \alpha_{\perp} \text{ (perpendicular)} = \int \int (A_\psi w - b) \psi_y dx dy \quad (7.27)$$

We need to find $A(x, y)$ and $b(x, y)$ to calculate the α -effect. The induction equation gives:

$$(\mathbf{u} \cdot \nabla) A - \frac{1}{R} \nabla^2 A = 0 \quad (7.28)$$

As $R \rightarrow \infty$, $A \rightarrow A_o(\psi)$, and to find $A_o(\psi)$ above the eye say, we impose $dA_o/dx \rightarrow 1$ as $y \rightarrow \infty$ and then use the channel integral of Lecture 4.

$$\int_o^s q ds \frac{dA_o}{d\psi} = 2\pi \quad (7.29)$$

Setting $\Gamma = 1$, $A_o(\psi)$ can be found from $\psi = y^2/2 + \epsilon \cos x$. Note that if $\epsilon \ll 1$, we get a thin eye. The absolute velocity $q(n; \epsilon)$ can be written as

$$q(n; \epsilon) = (4\epsilon \sin^2(x/2) + \epsilon^2 \sin^2 x)^{1/2} \quad (7.30)$$

The arc length of a streamline $S(\psi)$ is given by the integral

$$S(x; \epsilon) = \int_o^x (1 + \epsilon \cos^2(x/2))^{1/2} dx \quad (7.31)$$

We now introduce the appropriate boundary layer coordinates (see lecture 4) in order to do the analysis on the boundary in the upper half plane.

$$\sigma(x) = \epsilon^{-1/2} \int_o^x q ds; \quad \xi(x, y) = \epsilon^{-1/4} R^{1/2} \psi \quad (7.32)$$

In these coordinates A satisfies $\partial A / \partial \sigma - \partial^2 A / \partial \xi^2 = 0$, and from 5.22 b satisfies

$$b_\sigma - b_{\xi\xi} = E^{-1/4} R^{1/2} W_\sigma(\sigma) A_\xi \quad \text{where } W(\sigma) = W(x, y_+(x)) \quad (7.33)$$

Observing that A_ξ satisfies the homogeneous equation for b , a solution is easily seen to be

$$\epsilon^{1/4} R^{-1/2} b = W(\sigma) A_\xi + b_o(\sigma, \xi) + o(1) \quad (7.34)$$

where b_o is the homogeneous solution. Assuming that $\lambda \equiv \epsilon^{-1/4} R^{1/2} \gg 1$, and all the terms in the above equation are $O(1)$, then B_o would give a contribution to b of order λ . A term this large would seem incompatible with the $O(1)$ forcing in the equation for b :

$$\frac{\partial(b, \psi)}{\partial(x, y)} - \eta \nabla^2 b = - \underbrace{\frac{\partial(a, W)}{\partial(x, y)}}_{\text{forcing}} \quad (7.35)$$

If this $O(1)$ forcing is indicative of the size of the solution, then b must match with $O(1)$ terms outside the boundary layer. Thus $O(\lambda)$ terms match with zero and leads us to homogeneous conditions for b_o i.e. b_o is zero.

Thus α_{\parallel} and α_{\perp} which are normally $O(1)$ effects vanish identically and we have no dynamo.

$$\alpha_{\parallel} = \int \int \underbrace{(b - w A_\xi)}_{\text{zero}} \psi_x dx dy, \quad \text{similarly for } \alpha_{\perp} \quad (7.36)$$

A deeper analysis shows that diffusion is playing no role here but a parallel interaction of velocity and field is taking place in the boundary layer. To resolve this one can take very thin eyes $\epsilon = O(R^{-2/3})$ making the boundary layers fill the eyes, and diffusion acting everywhere. This realizes an $O(R^{-1/3})\alpha$ -effect which communicates above and below $y=0$ between boundary layers.

A careful appraisal of the limits is required and is discussed in Childress (1986). Some of the boundary layer calculations involve classic Wiener-Hopf techniques as used by Benney and Bergeron (1969) who looked at resonance in viscous boundary layers.

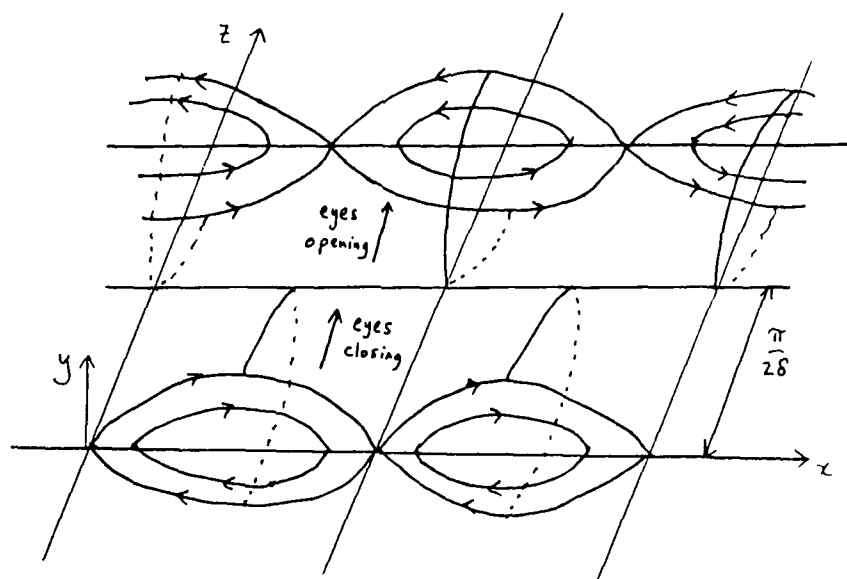


Figure 7.7

7.7 Overlapping Cat's Eyes

A difficult boundary layer analysis results from:

$$u' = (0, \epsilon[\sin(x + \delta z) + \sin(x - \delta z)], 0), \quad k \pm = i \pm \delta k, \quad \text{where } \delta \ll 1 \quad (7.37)$$

Take $U(y) = (u(y), 0, w(y))$ with $u(0) = 0, u'(0) = \Gamma \neq 0, w(0) = w_0 \neq 0$. By imposing resonance conditions and constructing a streamfunction the α -effect for the system can be calculated.

7.8 Blinking Eyes

From (7.37) we note that the eyes appear to open and close to an observer moving with velocity $(0, 0, w_0)$. Fluid particles can escape these eyes and it could be interesting to see what type of dynamo arises at large R . (See Figure 7.7.)

The idea of resonant magnetic layers is well known in the study of magnetic equilibria appropriate to plasma fusion. A rich literature on related Poincaré maps exists (e.g. see Lichtenberg and Lieberman).

7.9 Other Systems Worth Considering

Parker's cyclonic cells were viewed by him as a probable manifestation of convection in a rotating system. Convection dynamos have also been studied in simpler geometries by Busse, Soward, Fautrelle and Childress (see Soward 1979 for a review).

Convection in a rotating Bénard layer gives Bénard cells, which are thin for high rotation rates (Figure 7.8). The effect of the Coriolis force is to give a velocity in the y -direction,

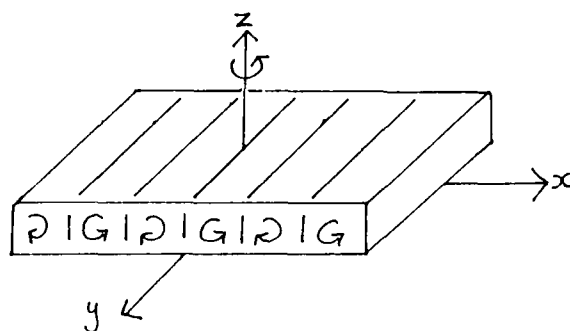


Figure 7.8

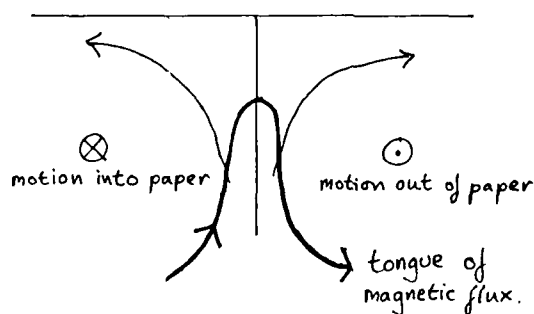


Figure 7.9

which we incorporated arbitrarily into the cellular flows we studied in the kinematic problem (Figure 7.9). Thus we have the ingredients for a dynamo; the motion draws out tongues of B_x flux and twists them to generate B_y flux. An interesting dynamical effect appears in Soward's analysis of a Bénard layer; if the induced magnetic field is not too strong, rolls tend to align perpendicular to the mean magnetic field in the x - y plane. The production of orthogonal field components by the alpha effect thus reorients the rolls, and they tend to rotate! However the Bénard dynamo is destabilized by a sufficiently large 'seed' field, and runs away, destroying the asymptotic ordering of scales.

As we have noted in Section 5.2, H. R. Strauss (1986) studied resonant fast dynamos with a very general perturbation:

$$\mathbf{u} = (u(y), 0, w(y)), \quad \mathbf{u}' = \sum_k \mathbf{u}_k(y) e^{i\mathbf{k} \cdot \mathbf{x} - i\Omega_k t + \gamma_k t} \quad (7.38)$$

He uses the Direct Interaction Approximation of Kraichnan to study turbulent diffusion and the α -effect. His dynamo hinges on the fact that turbulent diffusion produces an $Reff \sim 0(1)$ as $R \rightarrow \infty$.

Other systems which involve deviations from solid body rotation, give an interesting class of instabilities of a centrifugal nature which have no cut-off at large wavenumber (see

Widnall, Pierrehumbert, Bayly). One of these flows is an elliptical vortex, and it would be interesting to see how it fares as a fast dynamo.

7.10 References

- Bayly, B., 1986. "Fast magnetic dynamos in chaotic flows", *Phys. Rev. Letters*, 57, 2800-2803.
- Benny, Bergeron, 1969. "A new class of nonlinear waves in parallel flows", *Studies in App. Math.*, 48, 181-204.
- Braginsky, S. I., 1964. "Theory of the hydromagnetic dynamo", *J. Exp. Theor. Phys.*, 47, 2178-2193.
- Childress, S., 1986. "Alpha Effect in a 2-D Steady Cat's-Eye Flow" (unpublished note).
- Lichtenberg and Lieberman, 1985. *Regular and Stochastic Motion*. Springer-Verlag.
- Pierrehumbert, R.T. and Widnall, S.E., 1982. "The two- and three-dimensional instabilities in a spatially-periodic shear layer", *J. Fluid Mech.*, 114, 59-82.
- Pierrehumbert, R., 1986. "Universal short-wave instability of two-dimensional eddies in an inviscid fluid", *Phys. Rev. Letters*, 57, 2157.
- Ponomarenko, Y.B., 1973. "On the theory of hydromagnetic dynamos". *Zh. Prikl. Mech. Tech. Fiz. (USSR)*, 6, 775.
- Roberts, G.O., 1972. "Dynamo action of fluid motions with two-dimensional periodicity", *Phil. Trans. Roy. Soc.*, A271, 411.
- Roberts, P.H., 1987. "Dynamo Theory", preprint.
- Soward, A.M., 1979. "Convection driven dynamos" *Phys. Earth. Planet. Inter.*, 20, 131.
- Soward, A.M., 1987. "Fast dynamo action in a steady flow", *J. Fluid Mech.*, 180, 267-295.
- Strauss, H. R., 1986. "Resonant Fast Dynamo", *Phys. Rev. Letters*, 57, no. 17, 2231.

Notes submitted by Andrew Gilbert and Richard Jennings.

Lecture 8

Fast Dynamos III: Methods Based on Unsteady Maps and Flows

8.1 Introduction

Presently we wish to exploit Soward's "stretch" mechanism through mappings which can be studied numerically and (to some extent) analytically. Also, projections onto a well-defined mean field will be considered.

Recall that the "stretch" describes the effect of shear on the "flux tongues" created in the magnetic layers. The mechanism then operates steadily to yield an alpha effect: $\langle B_x \rangle \rightarrow \langle B_y \rangle \rightarrow \langle B_x \rangle$. We propose a similar mechanism to operate over a finite 3-dimensional domain. The phases are to be carried out rapidly but sequentially and time will be allotted for diffusion to occur.

The procedures are as follows:

1. Introduce a map on 3-D space which represents a rapid application of a flow for short time δ . The characteristic speed $U \sim L/\delta$ and the magnetic Reynolds number $R = L^2/\delta\eta \gg 1$ (R can effectively be taken as infinite here i.e., neglect diffusion during time δ).
2. Consider a periodic sequence: Apply the map, then allow the field to diffuse freely for a time $T - \delta \simeq T$ (i.e., $\delta/T \ll 1$). This is an approach used by Parker, Backus and others to study slow dynamos.
3. Define a suitable mean field and follow its growth as steps 1 and 2 are repeated indefinitely.
4. Try to realize the map in step 1 by a temporal sequence of Beltrami waves.

8.2 The Stretch-Fold-Shear (SFS) Map

Consider the unit cube $0 \leq x, y, z < 1$ in R^3 . We define the following map of the cube into itself:

$$(x, y, z) \rightarrow \begin{cases} (2x, y/2, z + \alpha(y - 1/2)), & 0 \leq x < 1/2 \\ (2 - 2x, 1 - y/2, z + \alpha(y - 1/2)), & 1/2 \leq x < 1 \end{cases} \quad (8.1)$$

Note that the mapping preserves the volume; $\text{Det } J = 1$ where $J = \text{Jacobian} \equiv \partial r' / \partial r$. (Volume conservation here is necessary as incompressibility of the fluid is assumed.) We

point out that the parameter α in (8.1) has no direct significance as an alpha effect. It represents the amplitude of a shearing component of the map.

This mapping consists of three steps, which are illustrated below. Also included is a mean magnetic field which is directed along the x-axis. The 'white' region denotes $B_x > 0$; the darkened region, $B_x < 0$. (B_x varies with z as shown.)

The map oversimplifies the fold, as the Jacobian is discontinuous at $x = 1/2$:

$$J = \begin{bmatrix} 2 & 0 & 0 \\ 0 & \frac{1}{2} & 0 \\ 0 & \alpha & 1 \end{bmatrix} \text{ for } 0 \leq x \leq \frac{1}{2} \text{ and } J = \begin{bmatrix} -2 & 0 & 0 \\ 0 & -\frac{1}{2} & 0 \\ 0 & \alpha & 1 \end{bmatrix} \text{ for } \frac{1}{2} \leq x < 1 \quad (8.2)$$

However, we have in mind fast reconnections at the folds with fields in neighboring cubes, so the discontinuity doesn't seem to be a problem.

Figure 8.1 illustrates the basic SFS map with $\mathbf{B} = [B_x(y, x), 0, 0]$. Shown here is the case $\alpha = 1$. Figure 8.1a shows a single application of the map on the field $\mathbf{B} = [\text{sgn}(z - 1/2), 0, 0]$. Here, black denotes positive field strength, white negative. The two cubes demonstrate how the fields can be extended to all space as periodic functions with period 2 in y .

Figures 8.1b, 8.1c, and 8.1d show the effect of multiple applications of the map onto the \mathbf{B} field just described. Let M = number of map applications. Figures 8.1b and 8.1c show the y - z plane for $M=2$ and 3, respectively. The field strength is $\pm 2^M$. In Figure 8.1d, the mean of B_x over y is plotted versus z for $M = 1, 2$, and 3.

8.3 Mapping the Magnetic Field

- A. We consider a field initially parallel to the x-axis; hence only B_x is nonzero for all iterates. Thus with each successive application, the field at given position (y, z) will be multiplied by ± 2 . The Liapunov exponents are thereby, if the applications are at $t = 1, 2, \dots, (\ln 2, -\ln 2, 0)$.
- B. The problem is separable in z and, for now, we can assume that the field is periodic in y with period 1. Thus $\mathbf{B} = (b(y)e^{2\pi iz}, 0, 0)$ where $b(y) = \sum_{k=-\infty}^{+\infty} b_k e^{2\pi iky}$.
- C. If we want to know the field at a point (y', z') after one application, then we look at the field at the pre-image (y, z) of (y', z') and multiply by ± 2 .

So we start with $B = B_x = \sum_{k=-\infty}^{+\infty} b_k e^{2\pi i(z+ky)}$. After one mapping the field becomes

$$B' = \begin{cases} 2 \sum_{k=-\infty}^{+\infty} b_k e^{2\pi i(z-\alpha(y-1/2)+2ky)} & 0 \leq y < \frac{1}{2} \\ -2 \sum_{k=-\infty}^{+\infty} b_k e^{2\pi i(z-\alpha(y-1/2)+2k(1-y))} & \frac{1}{2} \leq y < 1 \end{cases} \quad (8.3)$$

$$= \sum_k b'_k e^{2\pi i(z+ky)} \quad (8.4)$$

Inverting to find the b'_j 's, we have

$$b'_j = \sum_{k=-\infty}^{+\infty} b_k \int_0^1 e^{-2\pi i y j} \left\{ \begin{array}{ll} 2e^{2\pi i(\alpha/2 - \alpha y + 2ky)}; & 0 \leq y < \frac{1}{2} \\ -2e^{2\pi i(\alpha/2 - \alpha y + 2k - 2ky)}; & \frac{1}{2} \leq y < 1 \end{array} \right\} dy \quad (8.5)$$

or

$$b'_j = \sum_k b_k \left[e^{i\pi\alpha} \int_0^1 e^{i\pi u(2k - \alpha - j)} du - e^{-i\pi\alpha} \int_0^1 e^{i\pi u(2k + j + \alpha)} du \right] \quad (8.6)$$

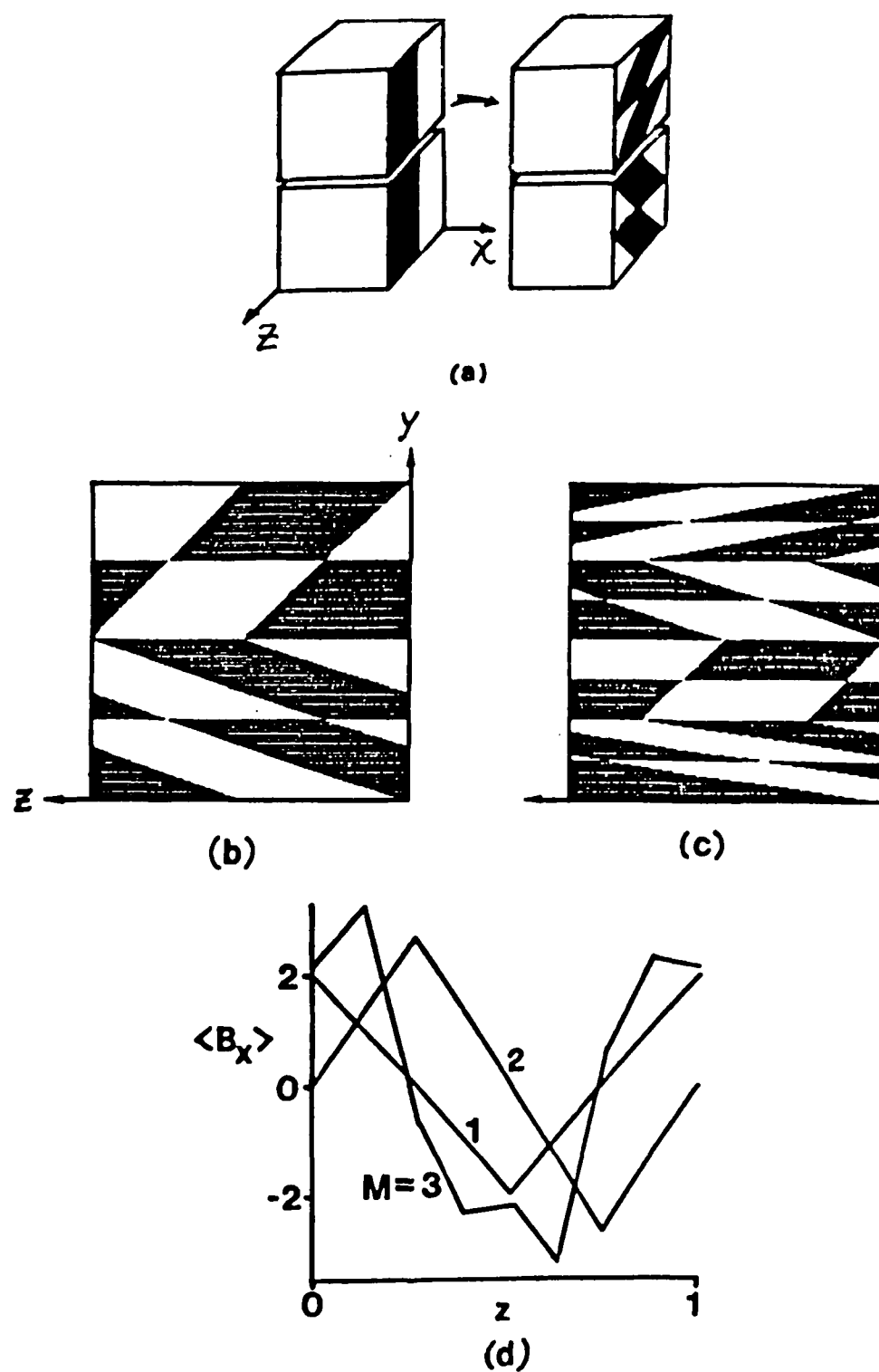


Figure 8.1

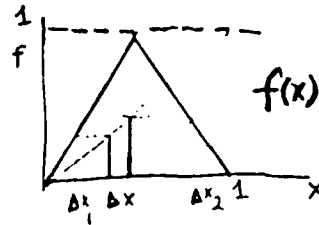


Figure 8.2

where $u = 2y$ in the former integral and $u = 2 - 2y$ in the latter. Also, this can be written as

$$b'_j = \sum_{k=-\infty}^{+\infty} G_{jk} b_k \text{ where } G_{jk} = e^{i\pi\alpha} \int_0^1 e^{i\pi u(2k-j-\alpha)} du - e^{-i\pi\alpha} \int_0^1 e^{i\pi u(2k+j+\alpha)} du \quad (8.7)$$

Now that the mapping is complete, allow diffusion to occur for a unit time (assuming dimensionless variables). Let $\epsilon = 4\pi^2/R$; then $b''_j = b_j e^{-\epsilon(j^2+1)}$.

Numerically we wish to iterate the transformation $T[B] \equiv T_j[b] = \sum_{k=-\infty}^{+\infty} e^{-\epsilon(j^2+1)} G_{jk} b_k$ on the space of doubly infinite complex sequences b . As in Soward's model, a major advantage is the existence of a 'clear' projection onto an unambiguous mean field, namely the average over the xy -plane. Here, no averaging on x is needed, so that we need only follow the Fourier coefficient b_0 to track the growth of the mean field. A growth rate is defined by:

$$p_{ave}(M) = \frac{1}{M} \ln |T^M(b)_0|$$

Also of interest is the *instantaneous* growth rate

$$p_{inst} = \ln |T^M(b)_0| - \ln |T^{M-1}(b)_0|$$

8.4 Digression on the "Tent Map"

Consider the function $\psi(x) = |2x - 2[x + 1/2]|$ where $[\cdot] = \text{integer part of } (\cdot)$ (i.e., the greatest integer less than the argument of $[\cdot]$). The Takagi function (Takagi, 1903) is defined as

$$\sum_{n=1}^{\infty} 2^{-n} \psi^n(x) \quad (8.8)$$

and is everywhere continuous but nowhere differentiable. Note that it is simpler to describe than Weierstrass' example. There are two interesting connections with the famous logistic map $x \rightarrow kx(1-x)$:

1. $\sum_{n=1}^{\infty} 4^{-n} \psi^n(x) = x(1-x)$
2. $4x(1-x)$ is transformed into $\psi(x')$ by $x' = 2/\pi \sin^{-1} \sqrt{x'}$

This has a simple invariant distribution $f(x) = 1$. This results from the fact that any interval Δx has two preimages Δx_1 and Δx_2 and $|\Delta x| = |\Delta x_1| + |\Delta x_2|$ (See Figure 8.2) $\mu(x) | \Delta x | = \mu(x_1) | \Delta x_1 | + \mu(x_2) | \Delta x_2 |$ or $\mu(x) = \mu(x_1)/f'(x_1) + \mu(x_2)/f'(x_2)$ where

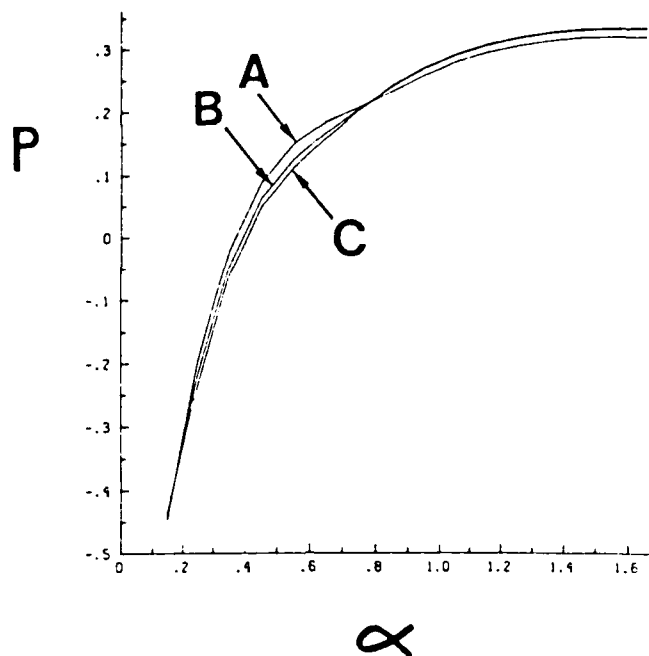


Figure 8.3

$\mu(x) = 1/2\{\mu(x_1) + \mu(x_2)\}$ Here $\mu = 1$. If we follow a small interval over many iterations, then the time averages are replaced by averages with respect to the invariant distribution.

Let x have a binary representation a_1, a_2, \dots where $a_1 = 0$ or 1 . If $0 \leq x < 1/2$ then $\psi(x) = a_2 a_3 \dots$ in binary. The reason for this is as follows: if $x < 1/2$, then $a_1 = 0$ and $x = a_2/2^2 + a_3/2^3 + \dots$, $2x = a_2/2^1 + a_3/2^2 + \dots$ and $[x + 1/2] = 0$, therefore $\psi(x) = a_2/2^1 + a_3/2^2 + \dots = a_2 a_3 \dots$ in the binary representation. Likewise, if $1/2 \leq x < 1$, then $\psi(x) = (1 - a_2)(1 - a_3)$ in binary.

Proof: if $1/2 \leq x < 1$, then $a_1 = 1$ and $x = 1/2 + a_2/2^2 + a_3/2^3 + \dots$, $2x = 1 + a_2/2 + a_3/2^2 + \dots$, $[x + 1/2] = 1$ here so $\psi(x) = |2x - 2| = 2 - 2x = 1 - a_2/2 - a_3/2^2 - \dots$. But $1 = 1/2 + 1/4 + 1/8 + \dots$ so this becomes $(1 - a_2)/2 + (1 - a_3)/2^2 + \dots$ so $\psi(x) = (1 - a_2)(1 - a_3) \dots$ in binary.

8.5 Some Graphical Results

Figure 8.2 displays a plot of the growth rate p versus α for various E , as computed from the Fourier representation and the equation $b_j = \sum_{k=-\infty}^{+\infty} D(j)g(j, k)b_k$ where $D(j) = e^{-(j^2+1)}$ and $G(j, k) = e^{i\pi\alpha} \int_0^1 e^{i\pi u(2k-j-\alpha)} du - e^{-i\pi\alpha} \int_0^1 e^{i\pi u(2k+j+\alpha)} du$. For A, $\epsilon = .01, N = 64$; for B $\epsilon = .001, N = 128$; and for C $\epsilon = .0001, N = 256$. The growth rates p are .258, .269, .271, respectively for A, B, and C.

Figure 8.4 presents the power spectra of b , normalized by b_0 , for $\alpha = .95$. Again A is for $(\epsilon, N) = (.01, 64)$, B is for $(.001, 128)$ and C is for $(.0001, 256)$.

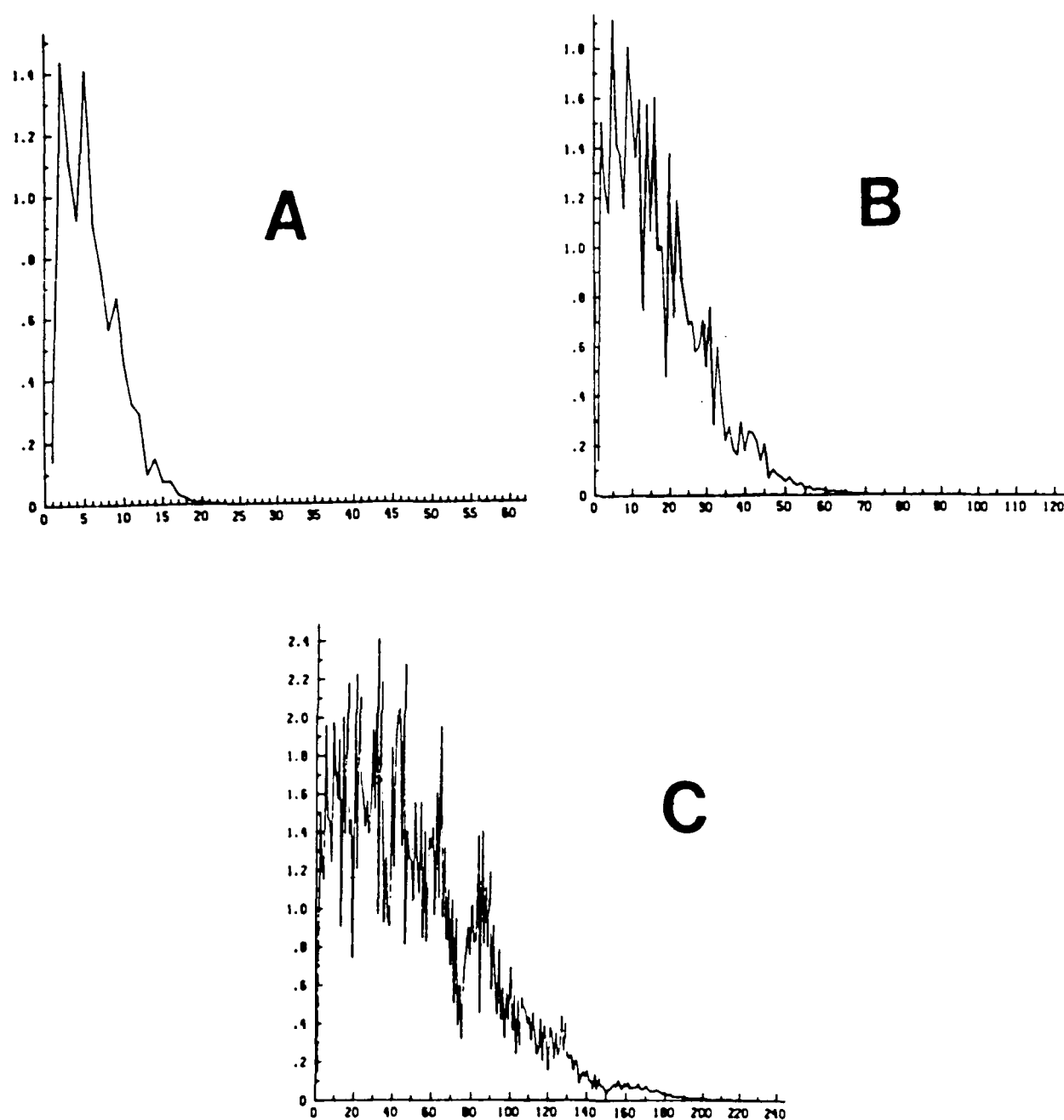


Figure 8.4

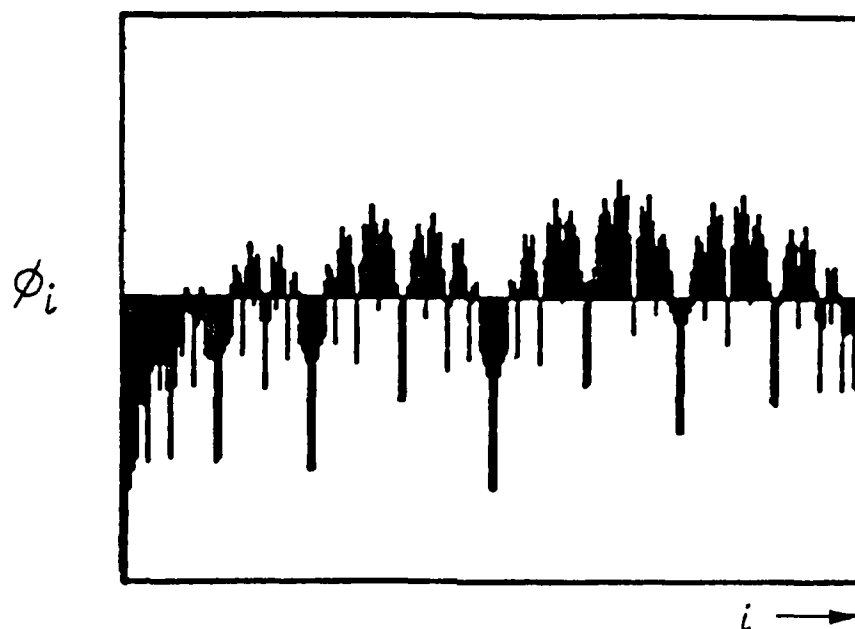


Figure 8.5: Exact expression for growth rate (at $\varepsilon = 0$) in terms of iterates ϕ_i .

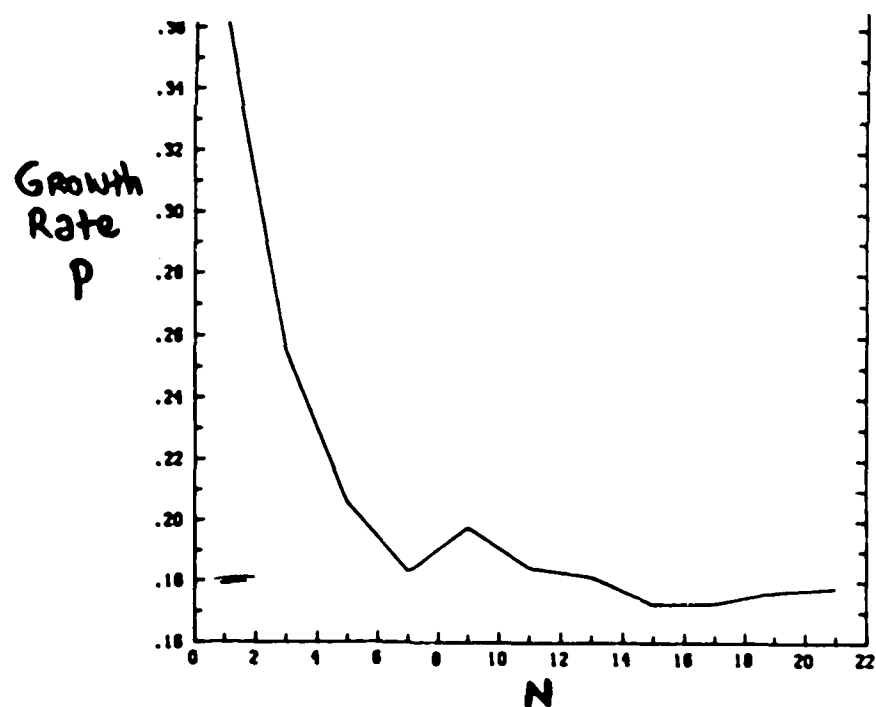


Figure 8.6: Truncation above 10 and diffusion give approximately same growth rates.

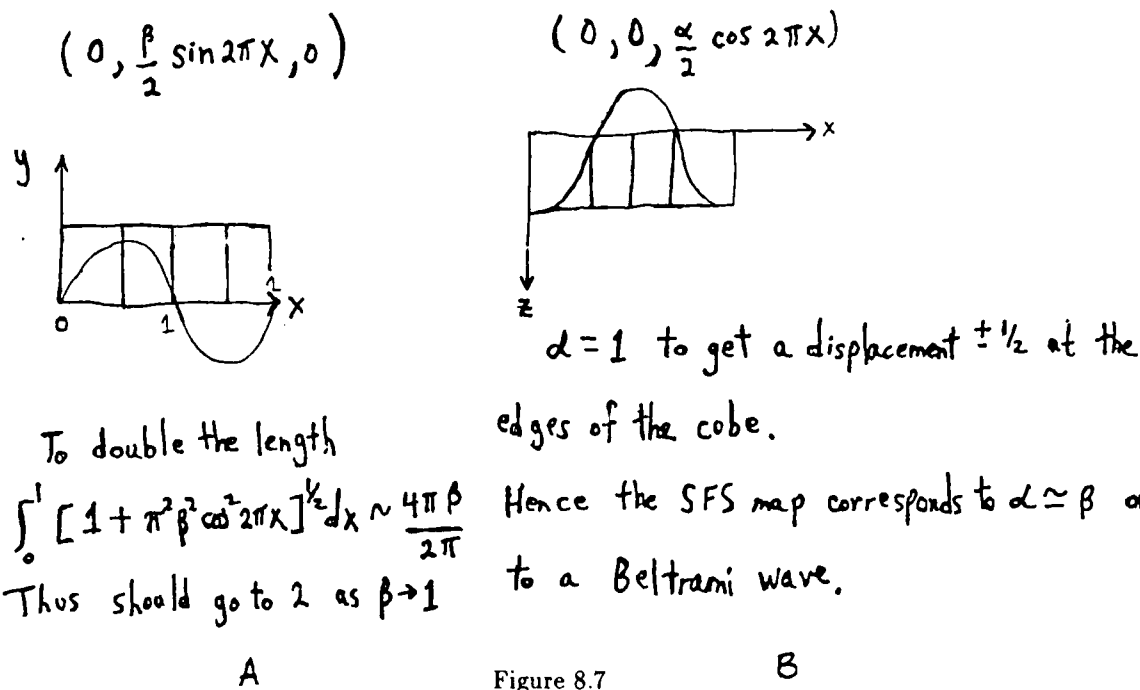


Figure 8.7

Figure 8.5 shows ϕ_i vs i and the exact expression for the growth rate p in terms of the iterates ϕ_i at $\epsilon = 0$:

$$e^{pN} = \frac{2^{N+1}}{\pi a} \sum_{i=1}^{2^{N-1}} e^{2\pi i \phi_i} \sin^2 \left(\frac{\pi a(2i-1)}{2^N} \right), 2^{N-1} = 512 \quad (8.9)$$

Figure 8.6 has plotted the growth rate p versus N . This calculation shows growth at $\epsilon = 0$ ($R = \infty, \alpha = .7$) of the mean field is essentially independent of coefficients b_N where $N \geq 10$, approximately. Note that truncations above $N \approx 10$ along with small diffusion give approximately the same growth rates.

The following figures compare the SFS map with a period 2 extension to pulsed Beltrami waves.

Figure 8.8 shows the power spectrum obtained from a pulsed Beltrami wave with $\alpha = \beta = 1$ using $(B_x, B_y) = \sum_{j=-N}^N \sum_{k=-N}^N (B_{xjk}, B_{yjk}) e^{2\pi i(jx+ky)}$. The coefficients B_{xjk}, B_{yjk} are obtained under the above transformation, by

$$\begin{aligned} B_{xjk}' &= \sum_{l=-N}^N [\pi \beta D(i, j) (H(l-k+1, j) + H(l-k-1, j)) B_{xlj} + D(j, k) H(l-k, j) B_{ylj}] \\ B_{yjk}' &= \sum_{l=-N}^N D(j, k) H(l-k, j) B_{xlj} \text{ where } H(k, j) = ie^{ik\phi_j} J_k(q_j) \\ \phi_j &= \tan^{-1}(j\beta/\alpha); q_j = 2\pi\sqrt{\alpha^2 + \beta^2 j^2}; D(j, k) = e^{-\epsilon(j^2+k^2+1)} \end{aligned} \quad (8.10)$$

and J_k is a Bessel function.

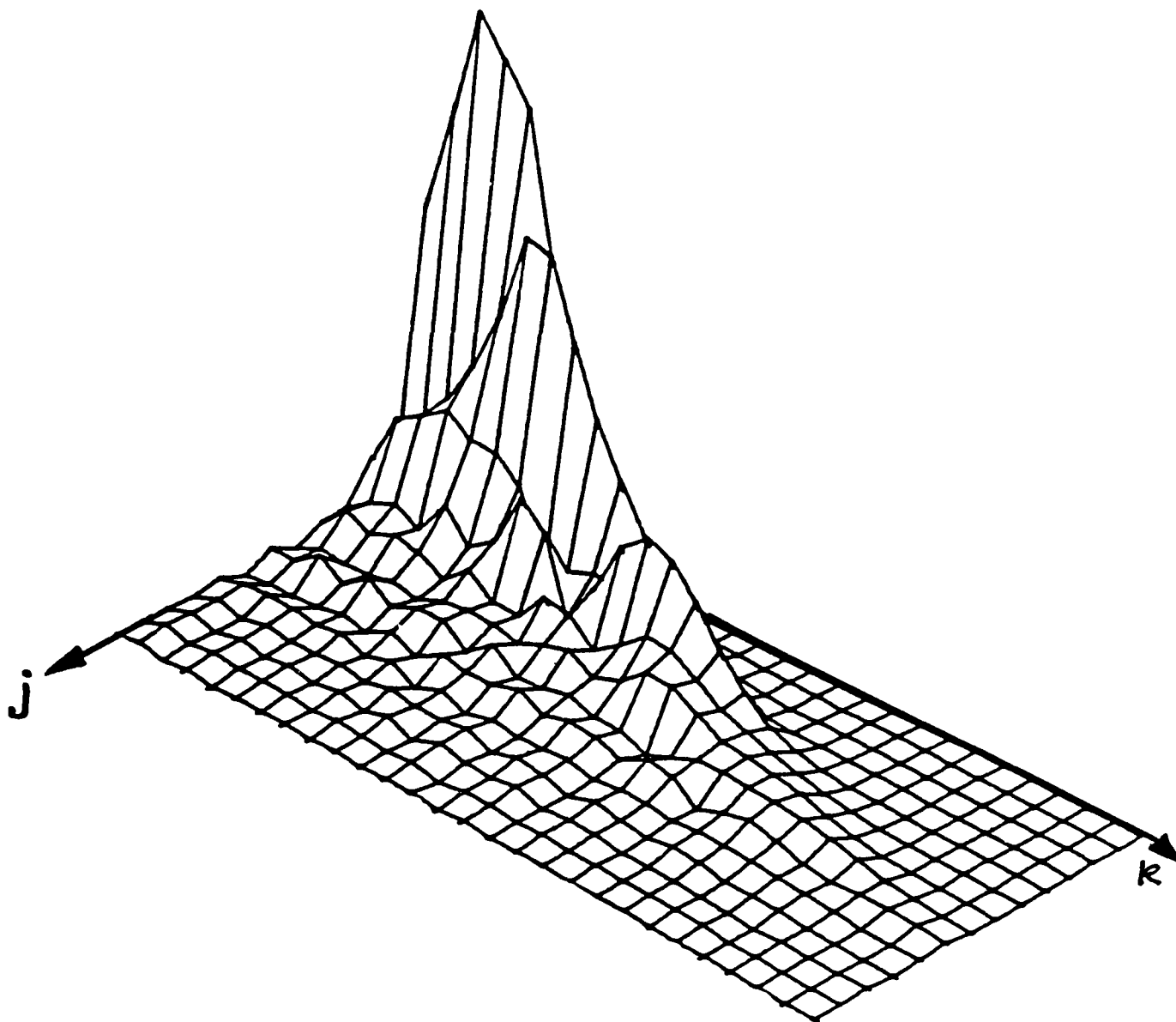


Figure 8.8: Power spectrum of a pulsed Beltrami wave. $\alpha = \beta = 1$, $N = 32$, $\epsilon = .004$ after $M = 40$ steps.

8.6 Some Analysis of the Model

For $\epsilon = 0$, the SFS map doubles the field strength. Let $T[b]$ denote a map on $\{b_k, -\infty < k < \infty\}$. Thus if $\|b\|^2 = \sum_k |b_k|^2$, then $\|T[b]\| = 2\|b\|$ or $1/2T$ preserves the length in Hilbert space (isometry). The implication of this is that any eigenvalue of $T/2$ (i.e., corresponding to an eigenfunction in L^2) must be unity. Since for small $\epsilon > 0$, we obtain eigenfunctions with much lower growth rates than $\ln 2 = 0.693$, we must conclude that corresponding $\epsilon = 0$ eigenfunctions are not in L^2 . A simple model of this is to let $b_k \in L^2$, $T[b] = \sqrt{2}e^{-\epsilon k^2}b(k/2)$. For $\epsilon = 0$, $T/2$ is an isometry on L^2 . But the 'mean field' $b(0)$ has a growth rate $1/2 \ln 2 = .34$. We can solve the eigenvalue problem for $\epsilon > 0$:

$$T[b] = \lambda b \Rightarrow \lambda = \sqrt{2}, \text{ thus } b = e^{4\epsilon k^2/3} \quad (8.11)$$

This b is not in L^2 if $\epsilon = 0$. We handle this by now introducing a new norm, so that the shift of magnetic energy to higher wave number is a "small" operation on b .

Alternatively, but equivalently, let $c_k = b_k / |k|^\alpha$, $k \neq 0$ and $c_0 \equiv b_0$

Then $\|c\|^2 = \sum_k |c_k|^2$. Also define a new operator \tilde{T} on c . We try to a "main" part of $P_c =$ projection of $c = (\dots, 0, 0, c_{-N}, c_{-N+1}, \dots, c_{N-1}, c_N, 0, 0, \dots)$ as distinct from the remaining 'noise' part. This idea goes back certainly to Parker (1955) and was used to advantage by Backus (1958).

\tilde{T} can be represented by a matrix:

$$N \begin{Bmatrix} \overbrace{\tilde{T}^{<<} \quad \tilde{T}^{<>}}^N \\ \tilde{T}^{><} \quad \tilde{T}^{>>} \end{Bmatrix} \quad (8.12)$$

and P can be decomposed into $P_\xi + P_\eta$, where $\xi =$ eigenvector of $\tilde{T}^{<<}$. We then would like to amplify the eigenfunction while keeping the noise under control. It is sufficient to show that, if $\|P_\xi c\| = 1$, and $\|(I - P)c\| < \|P_\eta c\| < \delta$, then $\|P_\xi \tilde{T}c\| \geq \lambda > 1$, $\|(I - P)\tilde{T}c\| < \Delta$, and $\|P_\eta c\| < \delta$. This is easier said than done! We will find this to occur if ξ corresponds to the maximal eigenvalue $\lambda > 1$, well separated from the next smallest part of the spectrum (by a gap which does not close as $N \rightarrow \infty$). Estimates of \tilde{T} go as expected (i.e., \tilde{T} looks "small" when operating on the 'noise'), provided that $0 < \alpha < 1$ and α is sufficiently close to 1. At present N has to be extremely large (≈ 5000) to satisfy all conditions. Numerical iterations do indicate fortunately that the needed spectral gap does exist. Nevertheless this does appear to be an awkward approach to fast dynamos.

8.7 References

- Bayly, B. and Childress, S., 1987. "Fast Dynamo Action in Unsteady Maps and Flows in Three Dimensions", *Phys. Rev. Letts.*, in press.
- Lichtenberg, A.J. and Lieberman, M.A., 1983. *Regular and Stochastic Motion*, Springer-Verlag.

Lecture 9

Dynamo Concepts Applied to Vortex Stretching

9.1 Preamble

The last two lectures of this series have, for the sake of an impending holiday, been stretched and folded into one. In fact, our object today is to treat four distinct subjects simultaneously (see Figure 9.1). All have some link to problems encountered in dynamo theory but they deal with questions of classical fluid dynamics.

9.2 General Introduction

In our analyses of kinematic dynamo action with prescribed velocity field \mathbf{u} , we have dealt with a linear equation for the magnetic field \mathbf{B} , whose solution has been sought subject to some initial configuration $\mathbf{B}(\mathbf{r}, 0)$. A formally similar but much more difficult problem involves the evolution of the vorticity field $\boldsymbol{\omega}$ of an incompressible Newtonian viscous fluid. The relevant vorticity equation is given by

$$\frac{\partial \boldsymbol{\omega}}{\partial t} + \mathbf{u} \cdot \nabla \boldsymbol{\omega} - \boldsymbol{\omega} \cdot \nabla \mathbf{u} - R^{-1} \nabla^2 \boldsymbol{\omega} = 0, \quad \boldsymbol{\omega} = \nabla \times \mathbf{u} \quad (9.1)$$

where $R = UL/\nu$ is the classical Reynolds number. The important thing about (9.1), in relation to the dynamo problem, is that $\boldsymbol{\omega}$ now determines \mathbf{u} , through the kinematic Biot-Savart law:

$$\mathbf{u} = -\frac{1}{4\pi} \int \int \int \frac{(\mathbf{r} - \mathbf{r}') \times \boldsymbol{\omega}(\mathbf{r}')}{|\mathbf{r} - \mathbf{r}'|^3} dV' \quad (9.2)$$

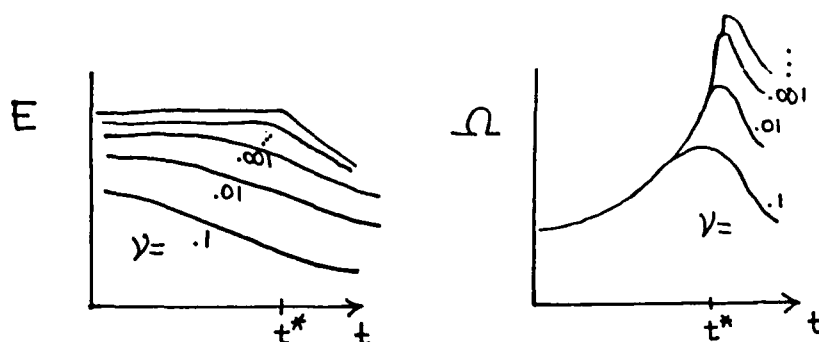
Here we have not exhibited dependence on t and have assumed that $\boldsymbol{\omega}$ is defined in all space but decays sufficiently rapidly at infinity. Thus, rather than simply observe a prescribed velocity field moving a prescribed set of material lines, we now deal with a flow determined instantaneously by these material lines. The implied nonlinearity is what makes the problem such a difficult one.

For an incompressible fluid, with $\nabla \cdot \mathbf{u} = 0$, the Navier-Stokes equations yield (9.1) under a curl operation. The "fast dynamo" theory now corresponds, because of the formal equivalence of (9.1) to the induction equation, to the inviscid limit $R \rightarrow \infty$; if the viscous term in (9.1) is formally neglected we obtain the *Euler equations*.

We may next contrast the invariants and the useful observables in the two problems. In the kinematic dynamo problem, our object is to increase the magnetic energy, usually

NOW PLAYING	
1 BIZARRE! STRANGE SINGULARITIES OF EULER FLOW "Is it a point? Is it a line? Oh my God, A FRACTAL! SEE IT IN 3-D" "WICKED" - LARRY TIER RATED: G	2 The incredible Hell in CASCADES OF ENERGY - A cast of thousands - Active and inactive daughter vortices and oh SHOWN: Andy Bear "PROVOCATIVE" - NY POST "HOMERUN RUN" - NY TIMES RATED: PG
3 THE ENGLISH CLASSIC: TAYLOR - GREEN New version - stretched contour - averaged, and conformed. A sensitive tale of vorticity Winner: PAUL EPHRAIM "A riveting breakdown" - NEW YORKER RATED: G	4 A World Overrun BY PERSONAL CREAM'S THE INVASION OF THE CELLULAR AUTOMATA THE PERSON NEXT TO YOU MAY BE INFECTED! "DON'T MISS THIS ONE" - PLAYBOY RATED: PG

Figure 9.1

Figure 9.2: Behavior of E and Ω

exponentially in periodic systems. In the flow problems, the analog of magnetic energy is the *enstrophy* $\iiint |\omega|^2 dV \equiv \Omega$. The important energy is kinetic and given by $E \equiv \rho/2 \iiint |\mathbf{u}|^2 dV$. If the fluid is inviscid and unforced by the boundaries, then E is a constant, while enstrophy may vary and perhaps grow without bound.

We have described in Lecture 5 a box experiment for fast dynamos, and it is of interest to examine now the corresponding experiment for a classical fluid. The box is equipped with a "viscosity knob" and the same, fairly complicated but extremely smooth (e.g. analytic) initial vorticity field is used in each run. Meters for both energy and enstrophy are monitored. One scenario is shown in Figure 9.2. Continual lowering of the viscosity (raising of R), leads to constant energy for some time t^* (in the figure, indicated as finite) after which time energy begins to decrease, irrespective of how large R may be. Corresponding to this event the enstrophy becomes unbounded. The evidence for this scenario, as yet unproven but believed by many to correctly describe the inviscid limit, is largely numerical; an example is discussed below. We shall also consider the general problem of establishing such a breakdown of regularity in the inviscid limit.

It is also of interest to consider the power spectrum for magnetic field and velocity in the two problems. As we have seen in the asymptotic constructions for large magnetic Reynolds number, the magnetic field is dominated by structures of size $R^{-1/2}$, cf Figure 9.3a. The

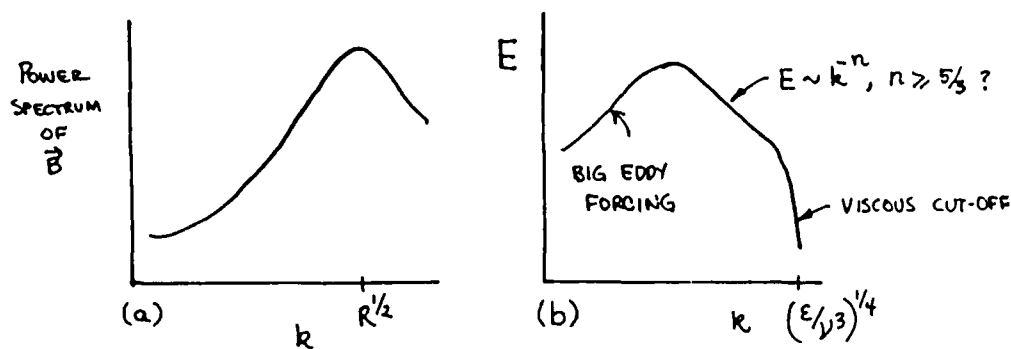


Figure 9.3: Power Spectra

kinetic energy of a forced turbulent flow, on the other hand, develops an inertial range as indicated in Figure 9.3b, terminating at a length scale $(\nu^3/\epsilon)^{1/4}$ where viscous stresses are effective, ϵ being the rate of energy dissipation (and the rate of working of the forcing).

The vorticity might behave as the magnetic field does, under the conditions of forcing at low wavenumber. However the problems differ greatly, to say the least, owing to the dynamics of the fluid.

Perhaps the most interesting aspect of magnetohydrodynamics is the intriguing combination of two vector fields having similar formal equations but quite different physics. Recently Moffatt (1986, 87) has shown how the MHD system can be used to derive considerable information concerning the existence of solutions of either subsystem having prescribed topology.

9.3 Possible Singularities of Euler and Navier-Stokes Flows

We discuss first an interesting question which has an essential connection with the rapid growth of enstrophy and the the transfer of kinetic energy to small geometrical scales, and no direct counterpart in dynamo theory. The assertion is that at the time t^* of the box experiment, the initial smoothness of the inviscid flow is lost, at least at a point. The question of singularities of the Navier-Stokes equations was studied by Leray in the 1930's but the attempts to investigate the appearance of singularities in Euler and Navier-Stokes problems through numerical simulation has been quite recent. One line of attack has focused on a specific initial value problem introduced by Taylor and Green in 1937 (see the next section). Another approach, pioneered by Chorin (1982, 85) utilizes approximations to the Biot-Savart integral in order to implement efficient algorithms for moving line vortices and following their stretching. The resulting simulations of Euler flows indeed yield an extremely rapid growth of enstrophy, consistent with the scenario outlined above.

A related but quite different investigation was initiated by Siggia (1985), see most recently Pumir and Siggia (1987). The focus here is on the interaction of paired, oppositely oriented finite-core line vortices. In addition to the lateral motion of paired vortices as an "oriented ribbon", extremely local interactions produce distortions leading toward a point singularity. An interesting feature of this study is the relative insensitivity of the latter process to the viscosity of the fluid. The singularities for the Navier-Stokes equations envisaged by Leray might therefore correspond to physically realizable flows. In any event it is important to separate the inviscid limit as in the box experiment from the behavior of a solution of Euler's equations.

One major difficulty with simulations of breakdown using finite-core vortices is the clear need to introduce some sort of basic irreducible element, e.g. a segment of vortex tube having a core of known geometry, which by scaling permits a representation of arbitrarily small structures. The natural question is whether the structures thus realized actually permit the irreducible elements to exist; will the vortex cores be disrupted by neighboring structures, for example? In Section 9.4 we will describe a kinematic model of a vortex hierarchy with arbitrarily small scales.

Among the considerable mathematical literature dealing with the Navier-Stokes and Euler equations, the possible size of singular sets, etc. we mention only two results. First, Kato (1967) has proved that no finite-time singularities develop in two-dimensional Euler flows in bounded domains. In this case (9.1) reduces to

$$\frac{\partial \omega}{\partial t} + \mathbf{u} \cdot \nabla \omega = 0, \quad \omega = \omega \cdot \mathbf{i}_z \quad (9.3)$$

While the material invariance of ω establishes immediately that vorticity stays bounded, this observation alone cannot guarantee that derivatives of vorticity or other combinations of first derivatives do not become infinite in finite time. The regularity of the flow can nevertheless be identified with the absence of vortex stretching, so that the attempts to construct singular Euler solutions in three dimensions have in one way or another sought to reduce the cross-sectional area of a vortex tube to zero in finite time, either by stretching and other distortions. We remark in passing that there are other two-dimensional problems where the singularities have not been ruled out in the absence of dissipation. Two examples are the MHD flow of an incompressible perfectly conducting fluid, and the flow of an unstably-stratified Boussinesq fluid.

The second result is a characterization by Beale, Kato, and Majda (1983) of the possible form of a singularity. They establish that if an Euler flow does break down then necessarily

$$\int_0^t \max |\omega| dt \rightarrow \infty \text{ as } t \rightarrow t^*, \quad (9.4)$$

where the maximum is taken over the domain of the flow.

In particular the vorticity, because of stretching and distortion, must become infinite somewhere. Of course all of the questions we have raised here could presumably be answered by exhibiting an analytical solution of the Navier-Stokes equations in a bounded domain exhibiting finite-time breakdown in the inviscid limit. In the absence of an example of this kind we can only point to suggestive partial results. The simplest solutions have the form $u_i = A_{ij}(t)x_j$, $p = B_{ij}x_i x_j$. For Euler's equations finite time singularities are easily seen to occur; indeed this can happen for an irrotational velocity field! A somewhat more interesting class resolves the flow structure in one space dimension, leaving unboundedness in the other two. A two-dimensional example has the velocity field $\mathbf{u} = (f(x, t), -yf'(x, t))$, where $0 < x < L$, $y > 0$. This substitution generalizes that introduced classically to study the viscous flow near a stagnation point. A variant of this approach can be applied to Boussinesq stratified flow. In either case it can be shown that breakdown occurs. Note that in the Euler case Kato's result insures that the breakdown is a result of the unbounded domain. An important next step would be to resolve a flow in two dimensions, leaving say a linear variation in the third, and follow the structure to breakdown.

In the kinematic dynamo problem we have seen examples of fast dynamo action which are associated with exponential decrease of scales down to a diffusion length. Finite time breakdown must be associated with the accelerated accumulation of new, shorter length scales within the advecting velocity. Physical processes analogous to the ω and α effects might have vortex counterparts but they must be accompanied by a continual refinement of scale in order to realize singularities of the kind envisaged.

9.4 The Taylor-Green Problem

We consider now the classical initial-value problem studied by Taylor and Green (1937), as an example of computations of the process of vortex stretching. The latter-day extensions of the Taylor-Green (TG) problem (Goldstein 1940, Orszag 1971, Van Dyke 1975, Morf *et al.* 1980, and especially Brachet *et al.* 1983, cf. references in Van Dyke, 1975 and Brachet, 1983) have provided what is essentially an implementation of the box experiment of Figure 9.2. Our summary here will be based upon the results of Brachet *et al.* (1983).

The initial velocity field in its most general form is

$$\begin{aligned} u &= \frac{2}{\sqrt{3}} \sin\left(\theta + \frac{2\pi}{3}\right) \sin x \cos y \cos z, \\ v &= \frac{2}{\sqrt{3}} \sin\left(\theta - \frac{2\pi}{3}\right) \cos x \sin y \cos z, \\ w &= \frac{2}{\sqrt{3}} \sin \theta \cos x \cos y \cos z. \end{aligned} \quad (9.5)$$

The case $\theta = 0$ has been frequently studied. In this case the streamlines are initially confined to planes $z = \text{constant}$ with streamfunction $\psi = \sin x \sin y \cos z$. The initial vorticity field is however three-dimensional. In the present discussion this initial-value problem is the analog of the cellular kinematic dynamo.

9.5 Discussion

Malkus: "Why did Taylor and Green consider this problem?"

Childress: "Most probably, their intention was to study the nonlinear processes by which eddies of different scales evolve in an unbounded fluid. The particular choice of initial conditions is motivated by, among other things, the symmetry."

Zalesky: "Recently S. Kida performed a numerical computation using an initial condition having more symmetry than the Taylor-Green condition." (See S. Kida and Y. Murakami, *J. Phys. Soc. Japan*, 55, 9-12, 1986.)

Childress: "Certainly the question of the 'best' initial condition deserves more attention. Spiegel and I were once interested in $(\sin(y) + \sin(z), \sin(z) + \sin(x), \sin(x) + \sin(y))$, which is almost as nice as the T-G condition and has a pleasing similarity to a Beltrami flow. Moreover the initial vorticity is two-dimensional."

We now summarize certain results of Brachet *et al.*:

1. There is an initial phase of compression of vorticity onto thin sheets on the planes $z = \pi/2 \bmod \pi$.
2. For the inviscid case, calculations out to $t \sim 4$ yield an energy spectrum function $E(k) \sim k^{-n(t)}$, where $n(t)$ decreases to 4 as t increases.
3. For positive viscosity, Reynolds numbers out to 3000 were reached. Here vortex sheets become unstable and rapid reconnection occurs. A short inertial range is established with n in the range 1.6 - 2.2. Energy dissipation is found to be spatially intermittent.
4. The flow does exhibit a rapid growth of enstrophy which is not inconsistent with finite time breakdown and singular behavior of the vorticity.

The effect of viscosity is therefore dramatic, emphasizing the distinction between an inviscid flow and the inviscid limit of viscous flows. The possible action of dissipation on

the topology of vorticity is analogous to its role in the alpha effect in many slow dynamos. Only the initial compression phase seems to be insensitive to viscosity.

This initial phase is also of interest because it is susceptible to asymptotic analysis (Childress 1987). The procedure is in some ways similar to Braginskii's asymptotic method (see lecture 2). If we adopt a "stretched" version of the TG initial condition with $\theta = 0$, as given by

$$\psi = \sin x \sin y \cos \epsilon z, \quad 0 < \epsilon \ll 1, \quad (9.6)$$

we can seek to evolve the streamfunction approximately in terms of slow variables $\zeta = \epsilon z$, $\tau = \epsilon t$:

$$\dot{x} = \psi_y, \quad \dot{y} = -\psi_x, \quad \psi = \psi(x, y; \tau, \zeta), \quad \nabla^2 \psi = H_\psi(\psi; \tau, \zeta) \quad (9.7)$$

The results of this analysis are as follows:

1. If the equations of an *axisymmetric* version of the TG problem are written in terms of the Bernoulli function H and the circulation Γ , then in terms of the slow variables, to first order, the same system applies to the TG problem, with one essential exception. The axisymmetric connection between circulation and velocity, $\Gamma = 2\pi r u_\theta$, is no longer relevant. Instead, the radial variable must be redefined as $\pi r^2 = A(\psi)$, the local area enclosed by a contour $\psi = \text{constant}$, and a local swirl component by an integration of the tangential flow around a contour. The desired connection is then obtained by solving (9.7) for the streamlines at given values of the slow variables.
2. The stretched, axisymmetric version of the TG problem appears to break down in finite time. This breakdown is in the stretched variable, and is associated with the compression of vortex lines which penetrate the boundary of the TG cell. It is not known whether or not the unstretched axisymmetric version of the TG problem actually breaks down as strongly as does the square cell.

9.6 Vortex Tube Models of the Energy Cascade

The inertial range of fully-developed turbulence is characterized by nearly inviscid transfer of kinetic energy, presumably dominated by transfers from larger to smaller length scales. If the process is represented by vortex tubes, we may contemplate a model which is analogous to the rope model of fast dynamo action (lecture 5). While the rope dynamo is supposed to produce intense, small-scale magnetic structures while it causes an average field to grow exponentially, the inertial-range transfers are required to conserve total kinetic energy, approximately. On the other hand the small viscosity might, by fast reconnection processes, be crucial in determining the topological configuration of tubes.

This approach leads to essentially "kinematic" models of the inertial range, with the dynamics reflected only in the conservation of a few invariant scalars. The simplest assumption is to require a hierarchy of exactly self-similar vortex structures (no stochasticity in the cascade). In addition we deal with a cartoon geometry: for example, consider a vortex ring of size L carrying a circulation Γ . A characteristic speed is then $U = \Gamma/L$, and the integrated kinetic energy is $E = U^2 L^3 = \Gamma^2 L$. Suppose that this vortex ring is split into two rings of size L' , simply by cutting the tube at two points and reattachment of the two sets of ends. Since we have assumed self-similarity the conservation of volume requires $2L'^3 = L^3$. On the other hand, the circulation Γ is conserved. Thus the energy after the cutting is $E' = 2\Gamma^2 L' = 2^{2/3} E$, which is larger than E . Thus energy is not conserved in this model, and many repetitions of the process would produce a very unrealistic cascade of vortex structure to small scales. Note that the preceding argument neglected the interactions

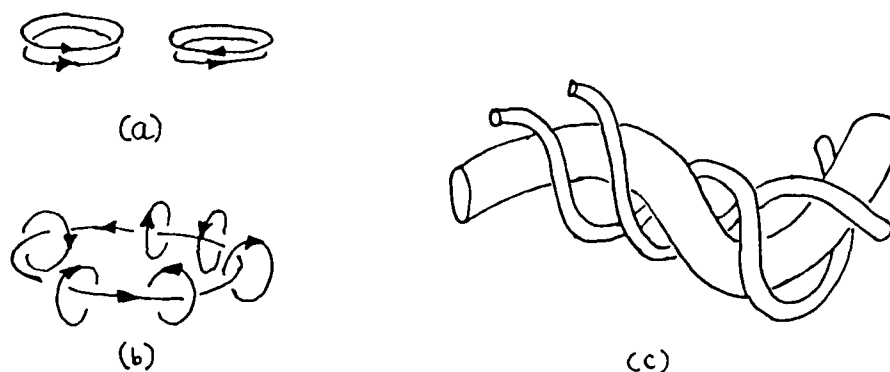


Figure 9.4: (a) Possible orientations of ring vortices yielding different energies. (b) Rings upon rings (c) Helical gamma model with $M = 2$.

between the two daughter rings in assessing their energy. The pair of rings can be placed in various orientations (Figure 9.4a) until energy is made equal to E . The problem is then to repeat the process and still be able to carry out the computation. One possible way to organize this is to build a structure consisting of “rings upon rings upon rings ...”, (Figure 9.4b). Here self-similarity is crucial to computation of the energy transfer in one step. But self-similarity is likely to be unrealistic in fully-developed turbulence. Under rescaling, self-similarity is a fixed point or equilibrium. The scaling parameters of real cascades can drift about on periodic or even chaotic attractors.

The ring model involves unrealistic cutting and fusing of tubes. A related model based upon helical structures is more satisfactory although it is still very much a cartoon of the process. The conservation of energy turns out to be difficult to satisfy with vortices of fixed circulation. One way out of this is to introduce “splitting” of vortices, as if the vortex were composed of strands of smaller tubes which could be separated. Thus the “gamma model” in Childress (1982) uses a two-step process: first an active parent vortex (one turn of a helical vortex tube) splits into M active daughter tubes and an inactive tube, the activity being determined by the core structure. The active daughter tubes, now carrying smaller circulation than the parent, form N self-similar but smaller copies of the parent. Applied to the helical geometry this process produces “inactive” structures, which contain all scales, in the sense that a helical winding of scale L' is actually wound into a helix of large scale L , and so on up the cascade (figure 9.4c).

The splitting process is envisaged as a vortex instability. In Figure 5 we show, as an example, the result of instability of a finite vortex core in a rigid cylinder. Here the computation, which was done in helical coordinates, would be interpreted as producing three daughter vortices and an inactive central core.

We now ask: How many such models can satisfy the physical constraints which must be imposed? The latter must certainly include

1. conservation of energy,
2. conservation of volume,
3. physical realizability in three dimensions (i.e. no overlap of tubes).

The constraints introduced by the last of these come from the growth of the structure as the cascade is repeated endlessly. We shall also want to conserve total helicity (but will not conserve all constraints on knottedness). It turns out that there are still an infinite number

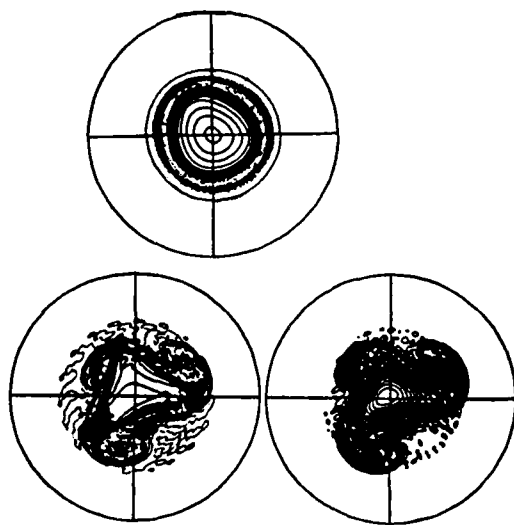


Figure 9.5

of models which are compatible, as the number of daughters M and the number of copies N are varied. Large values of M and N are unrealistic, however, as are the fractal dimensions of some of the sets obtained at the termination of the cascade. There is, however, a simplest model with minimal M and minimal stretching, which is compatible with all constraints. It is characterized by the following properties:

1. $M = 2$.
2. The scaling factor L'/L is $2^{-5/4}$.
3. Each tube is stretched by a factor 2 during a step.
4. The self-similar dimension of the terminating singularity is 2.6.
5. There is equipartition of energy between inactive and active elements, during a step of the cascade.
6. The total energy has the property that

$$\lim_{\nu \rightarrow 0} \frac{dE}{dt} = 0 \quad 0 < t < t^*, \quad < 0, t = t^* \quad (9.8)$$

The number 2.6 is a quite reasonable one, but models of this kind are not in agreement with measurements of intermittency of higher moments of the velocity. But vortex constructions can be applied to cascade models other than the beta model. More fluid dynamics in the vortex interactions might lead to models with natural stochasticity and more reasonable intermittency predictions.

9.7 Vortical Automata

Recently the prospect of using massively parallel computers to study fluid problems has led to considerable interest in formulations using cellular automata. The basic idea is to

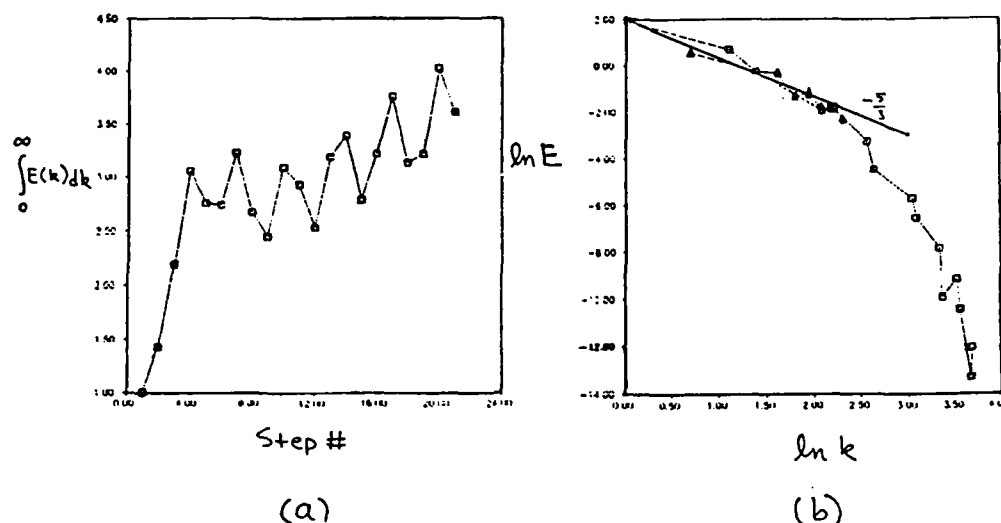


Figure 9.6: SFS map applied 20 times with $\epsilon = 4\pi^2/R = .01$, $N = 128$, period 2 symmetry. (a) Total energy vs. step number. (b) E vs. k yields an approximate $5/3$ law with viscous cutoff.

represent the fluid by a large number of equivalent components which are meant to simulate some simple, repetitive event in the flow (e.g. a molecular collision). This event should be computable independently of all other simultaneous events, simply from a knowledge of the current state of the system. We shall consider now the possibility of applying this idea to vortex structures containing a hierarchy of scales.

Chorin (1985) has proposed one means of representing the vorticity field on a square lattice, which discretizes the Biot-Savart law and allows vortex mechanics to be converted to a set of transition rules on the lattice. The evolution of a vortex filament can then be reduced to a large number of elementary transformations of a connected path on the lattice. Our aim here is to try something similar utilizing maps acting on rather small regions of space. In this way the problem is made to resemble our use of time-dependent maps in the construction of fast dynamos in the last lecture.

Consider first a simple application of the SFS map to the mean vorticity field e^{i2} . As in our fast dynamo study, the map is iterated M times at constant shear α ; however we now choose α so that the kinetic energy of the initial flow is maintained at a roughly constant value. Since this procedure generates very small scales, we should be able to recover an "inertial range" law for the three-dimensional energy spectrum function $E(k)$. A sample calculation, with $\alpha = .3$, is shown in Figure 9.6. We chose this α to give something close to a $5/3$ law; the exponent depends upon α and is actually closer to 2, but it is interesting that we can model the observed law for a reasonable value, i.e. one which nearly conserves energy. Here $E(k)$ is computed by integrating the one-dimensional spectrum over the unit sphere in k -space.

We try now to use an assemblage of cubes, which might be made to represent dynamical structures responsible for the predominant vortex stretching in a turbulent flow filling an

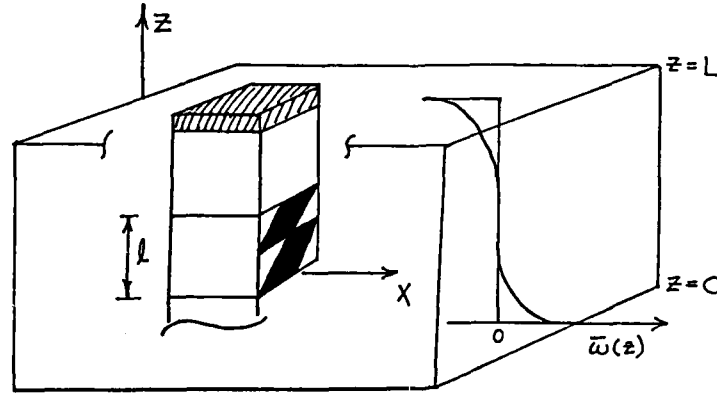


Figure 9.7: Turbulent channel flow. The cross-hatched region is the upper laminar sublayer. The orientation of the SFS maps, within the line of cubes from top to bottom, is shown.

extensive region. To focus on a specific problem, let us take turbulent channel flow as an example. The mean vorticity $\langle \omega \rangle$, the average being over the x - y plane and t (see Figure 9.7, is given by $\bar{\omega}(z)\mathbf{i}_y$. The x -momentum equation then yields

$$\frac{d}{dz} \langle uw \rangle + \Gamma = \nu \frac{d\bar{\omega}}{dz} \quad (9.9)$$

where Γ is the mean pressure gradient down the channel divided by the density.

In the laminar sublayer at either wall, $\langle uw \rangle \sim 0$ and (9.8) yields a flux of $\bar{\omega}$ into the layer,

$$\nu \frac{d\bar{\omega}}{dz} = \Gamma \quad (9.10)$$

Such a flux introduces vorticity into the region occupied by the cubes, adjacent to the sublayers. Suppose that, at each step, the requisite vorticity influx is introduced into the two cubes adjacent to the laminar sublayers, and then all cubes are acted upon by the same SFS map thereby exchanging vorticity because of the vertical shear. We could then determine both the mean vorticity and the total kinetic energy after each step, in the process producing finer and finer vortex structures down to the viscous cut-off.

The shear parameter α of the SFS map must be adjusted to insure that exponential growth of $\bar{\omega}$ does not occur, quite the opposite situation from the fast dynamo problem. If $\bar{\omega}(z)$ is represented in the form

$$\bar{\omega} \sim \sum_{n=0}^N A_n \sin(2n+1) \frac{\pi z}{L} \quad (9.11)$$

then the calculations of lecture 8 suggest that none of these modes will be excited provided that

$$\alpha(2N + 1)\pi l/L < k \sim 2 \quad (9.12)$$

We might then find that the Fourier modes saturate at a level determined by the forcing and the decay rates associated with the map. Note that the shear within the two end cubes must be modified to reflect the absence of any significant vertical motion into the sublayers.

Physically, the vorticity, once introduced into the channel by the forcing, gets chewed up by the maps in a way which is wavenumber sensitive. If equilibrium occurs there is a well-determined mean profile $\bar{\omega}$, hence a definite mean flux (given Γ). It is not clear how the process would depend upon the choice of acceptable α . These suggestions have not as yet been tried and so we don't know if reasonable profiles can be obtained this way.

There are a number of basic difficulties with making vortical automata acceptable dynamically. A few which come to mind are:

1. There is no provision in the SFS map for a change of scale of the *folding process*. Thus, small scales are developed through advection by a larger-scale motion. This is an extremely non-local transfer of energy. Real dynamical processes could evoke on the scales associated with the eddies breaking down. It would be necessary to invoke renormalization methods, involving rescalings, to allow for the local transfers within the present model.
2. To operate in parallel a cube (or small set of cubes) must be large enough to incorporate all spatially-correlated structures which occur during one step of the system. This may rule out maps which are simple enough to implement numerically.
3. Ideally, the map (M say) should be allowed to depend on a vector of parameters α , with α chosen internally to maintain invariants in the small. For example, we might want to define a local kinetic energy whose change must be zero. If a choice of α allows this, the cube is regarded as "turbulent" and M is applied. Otherwise it is "laminar" and M is not applied.
4. It may be impossible to deal with less than a full three dimensional vorticity field within each cube.

Nevertheless, mapping techniques seem naturally suited to high Reynolds numbers, magnetic or viscous, and the relative ease with which they can be adapted to the fast dynamo theory suggests that it may be worth pursuing some aspects of this approach, even though at present it is very speculative and incomplete.

9.8 References

- Beale, J.T., Kato, T., and Majda, A., 1983. "Remarks on the breakdown of smooth solutions for the 3-D Euler equations", PAM-158, CPAM, Berkeley.
- Brachet, M.E. *et al.*, 1983. "Small-scale structure of the Taylor-Green vortex", *J. Fluid Mech.*, **130**, 411-452.
- Childress, S., 1987. "Nearly two-dimensional solutions of Euler's equations", *Phys. Fluids*, **30**, 944-953.
- Childress, S., 1982. "A vortex-tube model of eddies in the inertial range", *Geophys. Astrophys. Fluid Dyn.*, **29**, 29-64.
- Chorin, S.J., 1982. "The evolution of a turbulent vortex", *Commun. Math. Phys.*, **83**, 517-535.
- Chorin, A.J., 1985. *Turbulence and vortex stretching on a lattice*, Report No. PAM-306, Center for Pure and Applied Mathematics, University of California, Berkeley.

- Kato, T., 1967. "On the classical solution of the two-dimensional, non-stationary Euler equation", *Arch. Rat. Mech. Analysis*, **25**, 188-200.
- Moffatt, H.K., 1985. "Magnetostatic equilibrium and analogous Euler flows of arbitrarily complex topology. Part 1. Fundamentals", *J. Fluid Mech.*, **159**, 359-378.
- Moffatt, H.K., 1986. "Magnetostatic equilibria and analogous Euler flows of arbitrarily complex topology. Part 2. Stability considerations", *J. Fluid Mech.*, **166**, 359-378.
- Pumir, A. and Siggia, E. D., 1987. "Vortex dynamics and the existence of solutions of the Navier-Stokes equations", *Phys. Fluids*, **30**, 1606- 26.
- Siggia, E. D., 1985. "Collapse and amplification of a vortex filament", *Phys. Fluids*, **28**, 794-805.
- Van Dyke, M., 1975. "Computer extension of perturbation series in fluid mechanics", *SIAM J. Appl. Math.*, **28**, 720-734.

1987 Summer Study Program

in

Geophysical Fluid Dynamics

ABSTRACTS OF PARTICIPANTS

FAST DYNAMOS IN CHAOTIC FLOW

Bruce Bayly

Courant Institute of Mathematical Sciences

251 Mercer Street

New York, NY 10012

This seminar was intended to introduce a way of looking at magnetic fields in chaotic flows of highly conducting fluid. The main idea is that, since the magnetic field lines behave like material lines in a perfectly conducting fluid, the exponential line-element stretching associated with the positive Liapunov exponent of the chaos could translate into a mechanism for robust fast dynamo action. The flows of interest are almost always incompressible, and hence generate measure-preserving transformations on the (usually assumed) finite domain occupied by the fluid. The classical ergodic theorems of Poincaré, Birkhoff, and Oseledec apply to such flows, and establish that the concepts of long-time averages, Liapunov exponents, etc., can be freely applied.

One of the most important properties of a chaotic flow with positive Liapunov exponent is that there exists a direction field (function of position) called the *dilating direction*. If a material line element is initially aligned with the dilating direction at its starting point, then it remains so aligned forever, and its length increases exponentially at a rapid rate. Furthermore, an arbitrarily aligned field element will approach alignment with the dilating direction exponentially rapidly. It seems reasonable to seek a fast dynamo mode whose field vector is everywhere approximately aligned with the dilating field.

To show this explicitly, we consider an idealized class of flows that are chaotic, ergodic (every trajectory fills the entire domain), and whose dilating direction is *orientable*. The last condition is highly nontrivial (see I. Klapper's Fellowship lecture); it means that we can choose a continuous field of unit vectors $\mathbf{e}_d(\mathbf{x})$ which are aligned everywhere with the dilating direction, and which are preserved under the flow. If the dilating direction is orientable, then the dilating vector field satisfies

$$\mathbf{u} \cdot \nabla \mathbf{e}_d = \mathbf{e}_d \cdot \nabla \mathbf{u} - \Lambda(\mathbf{x}) \mathbf{e}_d \quad (1)$$

$$\Lambda(\mathbf{x}) = \mathbf{e}_d \cdot (\mathbf{e}_d \cdot \nabla \mathbf{u})$$

$$\int_D \Lambda = \lambda > 0$$

where D is the flow domain and λ is the Liapunov exponent of the chaotic flow. The field \mathbf{e}_d is typically continuous, but rarely differentiable; at best we can expect that \mathbf{e}_d is a $C^{1/3}$ function of position. For the purpose of constructing a dynamo in a fluid with dimensionless diffusivity ϵ , we first obtain a smooth function $\mathbf{e}(\mathbf{x})$ by convoluting \mathbf{e}_d with a smooth function of unit mass, whose width equals the dissipation length $\epsilon^{1/2}$. This smoothing leads to errors of order $\epsilon^{1/6}$ in the following leading order analysis.

The above remarks suggest seeking a magnetic field whose leading order structure is a scalar function $\beta(\mathbf{x}, t)$ times $\mathbf{e}(\mathbf{x})$. The scalar β then satisfies

$$(\partial_t + \mathbf{u} \cdot \nabla)\beta = \Lambda\beta + \epsilon \nabla^2 \beta \quad (2)$$

Equation (2) has solutions that are everywhere positive for all time, so we can let $\beta = e^s$ and consider the evolution of s :

$$(\partial_t + \mathbf{u} \cdot \nabla)s = \Lambda + \epsilon |\nabla s|^2 + \epsilon \nabla^2 s \quad (3)$$

Integrating (3) first over space and then over time yields

$$\int_D s(t) > \int_D s(t=0) + \lambda t \quad (4)$$

and so

$$\int_D \beta(t) > \int_D \beta(t=0) e^{\lambda t} \quad (5)$$

by Jensen's inequality. (5) implies that, in the limit of zero diffusivity, the Liapunov exponent is a *lower bound* on the growth rate of a magnetic field of the above form.

Essentially, we have shown that the orientability of the dilating direction field for a chaotic flow with positive Liapunov exponent is sufficient to give fast dynamo action. The catch is that very little is known about the dilating direction and its topological properties for general flows. Through studies like I. Klapper's Fellowship report, we hope to gain further insight into these problems and their implications for magnetic fields in highly conducting flows.

References

Bayly, B.J., 1986. *Phys. Rev. Lett.*, 57, No. 22, 2800.

OBSERVATIONAL CONSTRAINTS ON THEORIES OF THE GEODYNAMO

Jeremy Bloxham
Department of Earth & Planetary Sciences
Harvard University
Cambridge, MA 02138

Interactions between dynamo theory and studies of the Earth's magnetic field have been few: dynamo theories aim to explain the predominantly dipolar nature of the field and its irregular reversals. The observational record, however, which spans over 300 years, may potentially contain very useful information on the nature of the dynamo process in the core, and provide useful constraints on the process.

We have mapped the magnetic field at the core-mantle boundary at selected epochs from 1715 to 1980. Although these models are necessarily nonunique in that a range of models exists with adequate fits to the data and, in particular, they almost certainly represent but a low-pass filtered version of the true field at the core-mantle boundary, useful inferences can be drawn.

The most remarkable inference from the models is that the field is changing very slowly with time over a large region of the core-mantle boundary, specifically near both poles and throughout the Pacific hemisphere (the region from 90° E eastwards to 270° E). Westward drift, previously thought to be a global phenomenon, is absent from this region. In other regions, especially beneath southern Africa and the south Atlantic Ocean, rapid changes in the field with time are observed. During the period 1905-1925 we observe the rapid emergence of a core spot pair: two small intense adjacent regions of opposite signed flux. Numerical simulations suggest that expulsion of toroidal field by an upwelling motion in the core is a possible explanation of this feature.

The very slowly changing part of the field is roughly antisymmetric about the geographic equator. We observe low field near each pole of extent corresponding to the cylindrical extension of the inner core along the rotation axis, and concentrations of field arranged symmetrically around this cylinder. Such an arrangement is highly suggestive of the importance of rotational effects within the core, with different regimes inside the cylinder enclosing the inner core and outside the cylinder.

Comparison of the arrangement of these flux concentrations with maps of variations in seismic P-wave velocity in the lowermost mantle (which one interpreted in terms of lateral temperature variations in the mantle) lends support to the hypothesis that the pattern of convection in the core is modified by the very large lateral variations in temperature in the mantle just above the core-mantle boundary.

References

- Backus, G. E., 1987. "Bayesian inference in geomagnetism", *Geophys. J. Roy. Astr. Soc.*, in press.
- Bloxham, J., 1986. "The expulsion of magnetic flux from the Earth's core", *Geophys. J. Roy. Astr. Soc.*, **87**, 669-678.
- Bloxham, J. and Gubbins, D., 1985. "The secular variation of Earth's magnetic field", *Nature*, **317**, 777-781.
- Bloxham, J. and Gubbins, D., 1987. "Thermal core-mantle interactions", *Nature*, **325**, 511-513.
- Gubbins, D. and Bloxham, J., 1987. "Morphology of the geomagnetic field and implications for the geodynamo", *Nature*, **325**, 509-511.

NONLINEAR CONVECTION IN A SPHERICAL SHELL

Edward W. Bolton
Department of Geology & Geophysics
Yale University
New Haven, CT 06511

Motion created by buoyancy in rotating spherical shells is of obvious relevance to the fluid dynamics of the Earth's liquid outer core. Although the energy source for such fluid motion is debatable, either thermal convection or compositional convection driven by latent heat release and deposition of heavier elements on the solid inner core is most likely occurring in the outer core. We focus here on an idealized model of such convection and will look at the initial bifurcation of the flow which has the form of thermal Rossby waves (Busse, 1970). (An alternate approach of looking at a turbulent dynamo has been examined by Gilman and Miller (1981) and Glatzmaier (1984).) Here the problem is formulated so one can numerically solve for the full nonlinear solution of the drifting columnar waves. The magnetic field is also included in this formulation, such that a magnetohydrodynamic dynamo may be investigated.

We consider the model problem of a rotating spherical fluid shell of arbitrary radius ratio. We assume that the fluid is self-gravitating, internally heated, Boussinesq and that the centrifugal force is negligible. The governing equations (momentum, conservation of mass, heat and magnetic induction) are nondimensionalized in the traditional manner which yields five nondimensional parameters: Rayleigh (heating), Taylor (rotation), Prandtl (fluid properties), magnetic Prandtl (conductivity and fluid properties) numbers and the radius ratio. The temperature perturbation from the static state and the poloidal and toroidal components for the velocity and the magnetic fields remain as the five unknown scalars. These are expanded in terms of spherical harmonics and radial functions which satisfy the boundary conditions. This extends the work of Cuong and Busse (1981) to higher zonal wave numbers.

At the inner and outer boundaries we assume free-slip, isothermal and electrically insulating conditions. Substituting the expansions into the governing equations and projecting onto the space of the assumed functions yields an infinite set of equations. Once truncated, this set may be solved by a Newton-Raphson method if one starts with a reasonable seed solution.

Results for thermal convection solutions without magnetic fields reveal some similarities to previous experiments on convection in rotating annuli (Azouni, Bolton and Busse (1986)). These include prograde drift of the thermal Rossby waves for rapid rotation rates and increasing amplitudes and wave speeds with decreasing Prandtl number. Also the amplitude often achieves a maximum then decreases with increasing Rayleigh number. Onset at a (Taylor and Prandtl number dependent) critical Rayleigh number appears similar to a supercritical Hopf bifurcation.

It would be of interest to examine the character of the drifting columns for the case of inhomogeneous outer shell thermal boundary conditions. Hot spots in the lower mantle have been implicated as influencing the Earth's magnetic field (Bloxham, 1987). This effect could be studied in an extension of the present model.

This work has been done with F.H. Busse at UCLA and much of the formulation and the results were drawn from Bolton (1985). This work is continuing by the author and with another code by Zhang and Busse (1987).

References

- Azouni, M.A., E.W. Bolton and F.H. Busse, 1986. "Convection driven by centrifugal buoyancy in a rotating annulus", *Geophys. Astrophys. Fluid Dyn.*, **34**, 301-317.
- Bloxham, J., 1987. "Observational constraints on the geodynamo", 1987 Summer Program in Geophysical Fluid Dynamics, Woods Hole Oceanographic Institution, this volume.
- Bolton, E.W., 1985. "Problems in nonlinear convection in planar and spherical geometries", Ph.D. Dissertation, Univ. of California, Los Angeles.
- Busse, F.H., 1970. "Thermal instabilities in rapidly rotating systems", *J. Fluid Mech.*, **44**, 441-460.
- Gilman, P.A., and J. Miller, 1981. "Dynamically consistent nonlinear dynamos driven by convection in a rotating spherical shell", *Ap. J.*, **46**, 221f.
- Glatzmaier, G.A., 1984. "Numerical simulations of stellar convective dynamos: I. The model and method", *J. Comp. Phys.*, **55**.
- Zhang, K.K. and F.H. Busse, 1987. "On the onset of convection in rotating shells", Submitted to *Geophys. Astrophys. Fluid Dyn.*.

LOW ORDER MODEL OF THE SOLAR DYNAMO

Fausto Cattaneo

Joint Institute for Laboratory Astrophysics

University of Colorado

Boulder, Colorado 80309

Two of the most striking features of the solar magnetic cycle are its statistically well defined period of approximately eleven years and the recurrent episodes of reduced activity the most famous of which is the Maunder minimum. If we assume that the solar dynamo, complex though it is, has only a small number of dynamically active degrees of freedom it is then reasonable to seek a description in terms of low order models. One such model can be constructed (Cattaneo *et al.*, 1983; Weiss *et al.*, 1984) which includes, in a highly parametrized form, the generation of toroidal field by differential rotation and the generation of poloidal field by the α -effect. Nonlinear interactions are introduced by the dependence of the differential rotation on Lorentz torques which are quadratic in the field strength.

The natural stability parameter for this model is the dynamo number D which is a dimensionless measure of the ratio of regenerative processes (differential rotation and the α -effect) to dissipative ones (Ohmic and viscous dissipation). As the dynamo number becomes large the sixth order family of ordinary differential equations which describes this model displays interesting dynamical behaviour (Jones *et al.*, 1985). For values of D just greater than unity the system possesses an exact periodic solution which describes nonlinear stable dynamo waves. As D is increased a series of bifurcations occurs which gives rise to doubly and triply periodic solutions and eventually to a strange attractor (see, for example, Sparrow, 1982).

In the strange attractor régime measures of magnetic activity like, for instance, the amplitude of the toroidal ingredient as a function of time show a behavior suggestive of the solar cycle, namely they possess aperiodicity interspersed with intervals of reduced activity. Within the framework of this simple model both the aperiodicity and the Maunder-like minima can be understood in terms of the interaction between a limit cycle and the unstable fixed point at the origin. The success of low order models like the one outlined here in describing features of the magnetic cycle suggest the possibility of a geometrical description of complicated systems like the solar dynamo.

References

- Cattaneo, F., Jones, C. A. and Weiss, N. O., 1983. "Periodic and aperiodic behaviour in stellar dynamos," in *Solar and Stellar Magnetic Fields* (ed. J. Stenflo), pp. 307-310, Reidel, Dordrecht.
- Jones, C. A., Weiss, N. O. and Cattaneo, F., 1985. "Nonlinear dynamos: a complex generalization of the Lorenz equations," *Physica D*, *14*, 161-176.
- Sparrow, C. T., 1982. *The Lorenz Equations: Bifurcations, Chaos and Strange Attractors*, Springer-Verlag, New York.
- Weiss, N. O., Cattaneo, F. and Jones, C. A., 1984. "Periodic and aperiodic dynamo waves," *Geophys. Astrophys. Fluid Dyn.*, *30*, 305-341.

CURRENT SHEETS IN FORCE-FREE MAGNETIC FIELDS

George Field
 Smithsonian Center for Astrophysics
 60 Garden Street
 Cambridge, MA 02138

In a classic paper Parker (1972) posed a problem in MHD that is important for understanding the solar corona (Parker, 1987). Despite a number of papers over the years (Parker, 1986a, b), the solution to the problem is still not completely understood.

Parker modelled the magnetized plasma of the solar corona by a perfectly conducting fluid bounded by two plates at $z = 0$ and L , supposed to represent two regions of the photosphere having opposite magnetic polarity. The photospheric plasma on the end plates, being much denser than that of the corona, flows in a prescribed manner because underlying thermal convection displaces the foot points of the field. If the excursion in x and $y = 0(\lambda)$, the time scale for this motion is $t_v = \lambda/v$. The time for an Alfvén wave to cross the system is $t_A = L/v_A$, and the sound crossing time is $t_s = L/v_s$. In practice, $t_v > t_s$, so that $\mathbf{B} \cdot \nabla|_p \approx 0$, and $t_v \gg t_A$, so the response of the coronal plasma can be regarded as quasistatic. I also assume that the coronal pressure $p \ll B^2/8\pi$, so only magnetic forces are effective, and must be in balance, so

$$(\nabla \times \mathbf{B}) \times \mathbf{B} = 0, \text{ or } \nabla \times \mathbf{B} = \alpha \mathbf{B} \quad (1)$$

with

$$\mathbf{B} \cdot \nabla \alpha = 0 \quad (2)$$

The evolution starts at $t = 0$ with $\mathbf{B} = B_0 \mathbf{u}_z$ everywhere.

Parker argued that in general for most types of motion on the boundary there are no equilibrium solutions available. He further argued that the resulting motions in the coronal plasma would inevitably lead to the formation of current sheets, at which the direction of \mathbf{B} changes discontinuously. This conclusion, if correct, could help to explain why the solar corona is so hot ($\sim 10^6 K$), because ohmic dissipation would be large at the current sheets, even though the rest of the flow is characterized by high magnetic Reynolds number.

In a forthcoming paper (Field, 1988) I argue that if one includes configurations with discontinuous \mathbf{B} (current sheets), there are equilibrium states for all possible boundary motions. Normally the system evolves quasistatically in an equilibrium state that is a global energy minimum (the ground state), but from time to time local minima of higher energy (excited states) form. When such a state becomes unstable, there is a rapid transition (on the time-scale t_A) to the ground state, accompanied by release of magnetic energy. The resulting kinetic energy can be dissipated by viscosity, heating the coronal plasma. In a contribution to the Summer Program,

H. F. Strauss and N. F. Otani (1987) show that a localized twist of the field leads to instability, large current density, and enhanced ohmic dissipation that may also be important in heating the corona. The dynamical evolution found by Strauss and Otani may be an example of the rapid transitions discussed by Field (1988).

It is not clear whether the large current densities found by Strauss and Otani would suffice for coronal heating or whether the infinite current densities advocated by Parker are required. According to van Ballegooijen (1987), assuming the existence of a current sheet in an equilibrium force-free field leads to a contradiction in the problem posed by Parker.

I have considered the evolution of the current during periods of quasistatic evolution between rapid transitions. The quantity α (= current \div field) defined by (1) satisfies

$$\rho \frac{\partial}{\partial t} \left(\frac{\alpha}{\rho} \right) = \frac{\partial \Omega_z}{\partial z} - \frac{1}{B_0} (\mathbf{B} \times \nabla)_z \left(\frac{1}{\rho} \frac{\partial \rho}{\partial t} \right) \quad (3)$$

This equation applies at $z = 0$ (where Parker assumed that $\mathbf{v} = 0$); $\Omega = \nabla \times \mathbf{v}$ and ρ is the density.

If the plasma is isothermal, $\mathbf{B} \cdot \nabla p \sim 0 \Rightarrow \mathbf{B} \cdot \nabla \rho \sim 0$, and I show (Field, 1988) that ρ remains of order ρ_0 at all times. For current sheets to form in a finite time, $\alpha \rightarrow \infty$ and hence $\partial \alpha / \partial t \rightarrow \infty$. As ρ is bounded, current sheets require (3) to become infinite. It can do so in two ways: (i) Although $(1/\rho) \partial \rho / \partial t$ is bounded, the horizontal gradients implied by $(\mathbf{B} \times \nabla)_z = B_x \partial_y - B_y \partial_x$ could become infinite. (Previous authors have usually considered the incompressible case, and have therefore overlooked this possibility.) (ii) The other, more plausible way for (3) to become infinite is through the term $\partial \Omega_z / \partial z$. Although Ω_z itself vanishes at $z = 0$, its value at $z = L$ is determined by the boundary flow. The problem posed by Parker is equivalent to one with plates at $z = L$ and $-L$, and $\mathbf{v}(x, y, -z) = -\mathbf{v}(x, y, z)$, consistent with an imposed flow at the bottom boundary, $\mathbf{v}(-L) = -\mathbf{v}(L)$. For this problem Ω_z is an odd function of z , vanishing at $z = 0$ as required. In general, $\partial \Omega_z / \partial z$ does not vanish at $z = 0$, and because the only scales in the problem are L , the distance between the plates, λ , the excursion of a particle in the boundary flow, and $d = |v / \Omega_z|$, the horizontal distance over which there is significant shear in the boundary flow, we conjecture that

$$\left| \frac{\partial \Omega_z}{\partial z} \right| (z = 0) < |\Omega_z(z = L)| \min(L, \lambda, d) \quad (4)$$

In practice, $\lambda \sim 10^{-2} L$, so $\min(L, \lambda) = \lambda$. Hence the contribution of vorticity to (3) is less than $|\Omega_z(L)/\lambda|$ or $|\Omega_z^2/v|$, whichever is bigger. I conjecture that (3) can become infinite via vorticity only if $|\Omega_z|$ itself is infinite. This conjecture is unproven. We note that some of the solutions having current sheets described qualitatively by Parker since 1972 involve bodily transport of flux tubes relative to surrounding fluid in the boundary flow, which would involve $\Omega_z \rightarrow \infty$ at the surface of such tubes.

I conclude that Parker's problem always has equilibrium solutions, that they apply during the periods between rapid transitions from excited states to the ground

state, that both viscous and ohmic dissipation of the energy released in rapid transitions may be important for coronal heating, and that it is reasonable to conjecture that current sheets normally form from vorticity in the boundary flow only if $\Omega_z \rightarrow \infty$. The role of the horizontal derivative of $\rho^{-1} \partial \rho / \partial t$ in forming current sheets is unknown; however, I conjecture that it is not significant.

This work has benefited from discussions with Aad van Ballegooijen, Cedric Lacey, George Rybicki and Ellen Zweibel, and, at the Woods Hole Oceanographic Institution Summer Program in Geophysical Fluid Dynamics, Steve Childress, Willem Malkus, Mike Proctor, Ed Spiegel, and Hank Strauss. It was supported in part by NASA grant NAGW-931 to the Smithsonian Astrophysical Observatory, and by the Summer Program in Geophysical Fluid Dynamics.

References

- Field G.B., 1988 in preparation *Ap. J.*
- Parker, E.N., 1972. *Ap. J.*, 174, 499.
- Parker, E.N., 1986a, b. *Geophys. Astrophys. Fluid Dyn.*, 34, 243 and 35, 277.
- Parker, E.N., 1987. *Physics Today*, 40, 36.
- Strauss, H.F. and Otani, N.F., 1987. Lecture presented at Summer Program in Geophysical Fluid Dynamics (see enclosed abstract).
- van Ballegooijen, A., 1987. Submitted to *Geophys. Astrophys. Fluid Dyn.*

WIND-DRIVEN CIRCULATION AND FREE EQUILIBRIUM STATES IN A CLOSED BASIN

Annalisa Griffa

E.N.E.A. and Scripps Institution of Oceanography
La Jolla, CA 92093

Some aspects of the inertial circulation in a simple wind-driven ocean model are considered. The model is quasigeostrophic, barotropic, with flat bottom and simple square geometry. Our approach is suggested by the theory of equilibrium statistical mechanics, which applies to the truncated (i.e., finite-difference) quasigeostrophic system in the absence of forcing and dissipation. The theory predicts the "absolute equilibrium" state (i.e., the state towards which nonlinear interactions, acting alone, would drive the flow) based on the conservation of three integral invariants, the total energy E , the total potential vorticity Q , and the total potential enstrophy Q_2 . The predicted mean flow satisfies Fofonoff's (1954) equation,

$$\langle q \rangle = C_0 \langle \psi \rangle + C_1 \quad (1)$$

where $\langle \psi \rangle$ is the average streamfunction, $\langle q \rangle$ the average potential vorticity and C_0, C_1 are constants that depend on E , Q and Q_2 . Numerical experiments confirm that free (i.e. unforced, nondissipated) solutions of the quasigeostrophic equation approach the mean state predicted by the above equation and reveal interesting details about the mechanism of equilibration.

We approach the wind-driven problem by trying to extend the main assumptions of equilibrium statistical mechanics to forced-dissipative systems. We enquire whether the forced-dissipated system is strongly determined by a few global integral constraints (the equations for E , Q and Q_2) and if the role of nonlinear advection can still be understood as *tending* to drive the system towards the free equilibrium state (based upon instantaneous values of E , Q and Q_2). If this is the case, the complete forced and dissipative solution is expected to be a rough balance between nonlinear advection, which pushes the system toward the Fofonoff state, and power integral constraints involving the forcing and dissipation. If the wind stress is in the same general direction as the Fofonoff mean flow, then the wind-driven solution is expected to resemble the free equilibrium state, characterized by a strong inertial mean flow with a linear relationship between $\langle \psi \rangle$ and $\langle q \rangle$. If, on the contrary, the wind opposes the Fofonoff flow, the expected solution has a weaker mean flow directly driven by the wind, and a strong eddy field opposing it. Numerical experiments with various wind stresses confirm the general picture outlined above.

In order to test more closely the hypothesis that the forced-dissipated equilibrium state is largely determined by global constraints, a *stochastic* model is introduced. The stochastic model is obtained by replacing the nonlinear advection term in the quasigeostrophic equation by a stochastic term that is constrained not to be a source of E , Q or Q_2 . The good agreement between average solutions of the quasigeostrophic equation and of the stochastic model is a strong indication that the main characteristics of the flow are indeed determined by the global constraints.

THE DETERMINATION OF TOPOGRAPHIC CORE-MANTLE COUPLING FROM GEOPHYSICAL DATA

Raymond Hide
Geophysical Fluid Dynamics Laboratory
Meteorological Office
London Road, Bracknell, U.K.

Geophysicists accept that the irregular "decade variations" in the length of the day of up to about 5×10^{-3} are a manifestation of angular momentum exchange between the core and mantle. Concomitant fluctuating torques at the core-mantle interface are due to time-varying fluid motions in the liquid metallic core. The implied stresses at the core-mantle interface arise as a result of the action of (a) tangential viscous stresses in the Ekman-Hartmann boundary layer, (b) tangential Lorentz forces associated with the interaction of electric currents in the weakly-conducting lower mantle with the magnetic field there, and (c) the action of normal pressure forces on bumps (i.e., departures in shape from axial symmetry) on the core-mantle boundary. The investigation of the relative effectiveness of these three agencies is clearly a matter of importance in the study of the structure and dynamics of the Earth's core and lower mantle.

The contribution of viscous stresses is unlikely to be significant except under extreme assumptions about the coefficient of viscosity of the core. For this reason, Bullard proposed in the 1950's that electromagnetic coupling must be the principal agency. Recent refinements in theoretical models of electromagnetic coupling have strengthened the original case for invoking that mechanism (for references see Paulus and Stix, 1986), but both qualitative and quantitative difficulties remain, the latter being associated with assumptions concerning the strength of the toroidal part of the geomagnetic field in the outer reaches of the core and the distribution of electrical conductivity in the lower mantle.

The idea of topographic coupling was proposed by Hide (1969), who argued that the magnitude of the stresses implied by the amplitude and timescale of the decade variations in the length of the day might easily be accounted for if there are bumps on the core mantle boundary of height h no greater than about a kilometer and possibly less. Such bumps could easily be caused by viscous stresses associated with deep convection in the mantle (not a popular idea in the 1960's and 1970's, when mantle convection was generally regarded as being confined to the top 700 km; but now accepted by many geophysicists). How bumps and horizontal temperature variations at the core-mantle interface due to deep mantle convection influence core motions, thereby distorting the Earth's magnetic field, poses important questions in geophysical fluid dynamics, the investigation of which should be of considerable theoretical and practical significance. But it is also of interest to consider whether direct estimates of topographic coupling can be obtained more or less directly from geophysical data.

A method for doing this has recently been proposed (Hide, 1986) and its practical applicability is now being studied by a group consisting of R. Clayton, B. Hager and M.A. Spieth of Cal Tech, C. Voorhies of the Goddard Space Flight Center, and the author. From geomagnetic secular variation data, fields of horizontal motion just below the core-mantle interface are obtained on the basis of a method that exploits Alfvén's frozen magnetic flux theorem plus additional reasonable hypotheses concerning the dynamics of the flow. Horizontal pressure gradients are obtained from these hypothetical velocity fields on the basis of the geostrophic relationship, which should apply in the outer reaches of the core, where the largest a geostrophic term (the Lorentz force) is probably no more than about 10^{-2} times the Coriolis force in magnitude. Gravity and seismic data incorporated in various rheological models of the mantle provide hypothetical topographic maps of the core-mantle interface. The "decade" contribution to changes in the length of day and corresponding changes in the *direction* of the Earth's rotation axis (polar motion) are obtained from astronomical observations of the Earth's rotation when allowance has been made for tidal effects and short-term contributions due to the atmosphere. First results are encouraging, for they show that for the one epoch studied to date topographic coupling could account for the observed changes in the Earth's rotation both qualitatively and quantitatively, without having to invoke extreme models of core-mantle interface topography and fields of core motions. A full report is now being prepared for publication.

References

- Hide, R., 1969. *Nature*, 222, 1055-1056.
- Hide, R., 1986. *Q.J.R. Astron. Soc.*, 27, 3-20.
- Paulus, M. and Stix, M., 1986. in *Earth Rotation: Solved and Unsolved Problems*, (ed. A. Cazenave), D. Reidel Publishing Co., Dordrecht, Holland.

THE NONLINEAR BREAKUP OF A MAGNETIC LAYER

David W. Hughes

D.A.M.T.P., University of Cambridge,
Silver Street, Cambridge, CB3 9EW, U.K.

Although the convection zone is, in some respects, the obvious place for the solar dynamo to operate (since it is a region of both differential rotation and helical motions), there are two serious problems associated with this picture. One is the difficulty of keeping strong magnetic flux tubes within the convection zone for timescales comparable to the solar cycle: convective motions will tend to expel magnetic fields by some sort of flux expulsion (see the review by Proctor & Weiss 1982, for example) and, independently, the intrinsic buoyancy of magnetic flux tubes will cause them to rise (Parker 1955). The second problem results from numerical simulations of convection-zone dynamos by Gilman and Glatzmaier (described in the review by Gilman 1983) which predict migration of magnetic features towards the poles, contrary to observations. To circumvent these problems it has been postulated by several authors that the dynamo may be operating not in the convection zone proper but in the convectively stable overshoot region situated at the boundary of the convective and radiative zones. It should however be stressed that no satisfactory model of such a dynamo has, as yet, been constructed.

Motivated by the possibility of a strong toroidal magnetic field being generated in the overshoot zone Fausto Cattaneo and I have considered the stability of such a field, one of our aims being to discover whether a large-scale diffuse field could give rise to the isolated flux tubes observed bursting through the solar photosphere. The model we have studied has, as its initial state, a uniform horizontal magnetic field embedded in a convectively stable atmosphere. The total (gas + magnetic) pressure and the temperature are assumed continuous and thus the density at the interfaces of the magnetic field is discontinuous. In particular, at the upper interface, heavier (non-magnetic) gas is being supported by lighter (magnetic) gas and Rayleigh-Taylor type instabilities can ensue. To date we have restricted our attention to two-dimensional motions. Unfortunately, the undulatory modes, with motion in the vertical and in the direction of the initial field, were found always to be stable and thus it is only the interchange modes, for which the magnetic field lines remain straight and the motion is perpendicular to the field, which are of interest.

We have solved, numerically, the full nonlinear compressible MHD equations for a perfect gas and have followed the complete evolution of the instability. We find that the upper magnetic interface rapidly deforms from the sinusoidal shape predicted by linear theory into the mushroom-shaped structures characteristic of certain Rayleigh-Taylor instabilities (see Daly 1967 for instance). Our most interesting result is that associated with the wings of the mushrooms are regions of intense vorticity which, once most of the available potential energy has been released, play a key role in the subsequent evolution of the layer. Indeed, somewhat surprisingly,

certain vortex-vortex interactions are of sufficient strength to prevent the escape of pockets of high magnetic field even though such regions are lighter than their surroundings.

As yet we are unable to say for sure whether isolated flux tubes may result from the instability of a large-scale diffuse field although bulbous structures suggestive of tubes are indeed formed. Improvements of our model to incorporate the effects of an overlying convectively unstable region and also, eventually, to study the three-dimensional instabilities, should further clarify matters.

References

- Daly, B.J., 1967. "Numerical study of two-fluid Rayleigh-Taylor instability." *Phys. Fluids*, **12**, 1340-1354.
- Gilman, P.A., 1983. "Dynamo of the sun and stars and associated convection zone dynamics." In *Solar and Stellar Magnetic Fields* (ed. J.O. Stenflo) Reidel, Dordrecht, 247-270.
- Parker, E.N., 1955. "The formation of sunspots from the solar toroidal field." *Astrophys. J.*, **121**, 491-507.
- Proctor, M.R.E. and Weiss, N.O., 1982. "Magnetconvection." *Rep. Prog. Phys.*, **45**, 1317-1379.

MACRODYNAMIC EQUILIBRATION AND EIGENFLOWS

Glenn Ierley
 Department of Mathematical Sciences
 Michigan Technological University
 Houghton, MI 49931

The Taylor constraint states that there can be no net torque on geostrophic contours in the limit of vanishing viscosity. A simple physical model for the equilibration process is the torque balance achieved by rigid, magnetically coupled, spherical shells. This latter model is one ingredient in the complex recipe of torques acting between mantle and core which leads to westward drift (if it exists) and the jerks, bumps, and grinds which we observe as changes in the length of day.

Central to models of the geodynamo is an extension of this problem - are there magnetic fields compatible with the Taylor constraint with an amplitude independent of viscosity? This latter problem, I contend, remains largely unresolved.

In the context of dynamo models, there are two approaches in the literature. One is to average over presumed small scale motions, parameterizing their effect in terms of the mean field electrodynamic " α -effect". This partially kinematic treatment of the problem is formally justified only for irrelevant circumstances, but may be informally justified if the results for α^2 -dynamoes (or $\alpha\omega$ -dynamoes) turn out not to depend sensitively on the choice of parameterization. The alternative is to require a self-consistent generation process. This latter route implicitly or explicitly involves some added assumptions about the (magnetic and/or convective) stability of the realized mean, but these at least, one may hope, might be derivable as a formal consequence (which as yet eludes us) of the dynamical equations.

Realizability of the Taylor state, i.e., the existence of a torque-free solution, is not self-evident and so a further dichotomy in modeling involves a choice either of retaining finite viscosity and attempting to approach the limit, or setting the viscosity directly to zero. Whether the limit is singular is uncertain in general.

A number of partial results appearing in the literature are reviewed, the bulk of which suggest that further progress requires that one be clever, and probably numerically inclined as well. Examination of Braginskii's proposed "Z-model" dynamo suggests a torque-free interior is primarily a property of the kinematic eigensolution obtained by restricting the class of permissible α 's. Whether a torque-free interior with sharp current boundary layer obtains more generally is debatable. Results from Ierley (1985) suggest that amplitude of the magnetic field for α^2 -dynamoes remains viscously limited.

References

- Braginskii, S.I. 1975. "Nearly axially symmetric model of the hydromagnetic dynamo of the Earth. I", *Geomag. Aeron.*, 15, 149.
- Braginskii, S.I. 1976. "On the nearly axially-symmetric model of the hydromagnetic dynamo of the Earth", *Phys. Earth Planet. Inter.*, 11, 191.
- Braginskii, S.I. 1978. "Nearly axially symmetric model of the hydromagnetic dynamo of the Earth", *Geomag. Aeron.*, 18, 340.
- Fearn, D.R. and Proctor, M.R.E. 1984. "Self-consistent dynamo models driven by hydromagnetic instabilities", *Phys. Earth Planet Inter.*, 36, 78.
- Fearn, D.R. and Proctor, M.R.E. 1986a. "Kinematic dynamos satisfying Taylor's constraint", *J. Fluid Mech.*, to appear.
- Fearn, D.R. and Proctor, M.R.E. 1986b. "Self-consistent hydromagnetic dynamos", *Geophys. Astrophys. Fluid Dyn.*, to appear
- Greenspan, H.P. 1974. "On α -dynamos", *Stud. Appl. Math.*, 34, 35.
- Ierley, G.R. 1985. "Macrodynamics of α^2 -dynamos", *Geophys. Astrophys. Fluid Dyn.* 34, 143.
- Malkus, W.V.R. and Proctor, M.R.E. 1975. "The macrodynamics of α -effect dynamos in rotating fluids", *J. Fluid Mech.* 67, 417.
- Proctor, M.R.E. 1975. "Non-linear mean field dynamo models and related topics", Ph.D. thesis, University of Cambridge.
- Soward, A.M. 1986. "Non-linear marginal convection in a rotating magnetic system", *Geophys. Astrophys. Fluid Dyn.* 35, 329.
- Soward, A.M. and Jones, C.A. 1983. " α^2 -dynamos and Taylor's constraint", *Geophys. Astrophys. Fluid Dyn.* 27, 87.

COMPUTATION OF VORTEX SHEET ROLL-UP

Robert Krasny

Courant Institute of Mathematical Sciences

251 Mercer Street

New York, NY 10012

A vortex sheet is an asymptotic model of a free shear layer in which the transition region between the two fluid streams is approximated by a surface across which the tangential velocity component is discontinuous. A common theme in fluid dynamics is that the vortex sheet model can be useful in understanding the dynamics of coherent vortex structures observed in turbulent flows. The goal of this research is to learn how to compute vortex sheet evolution.

Singularity Formation in a Periodic Vortex Sheet

The initial value problem for perturbations of a flat, constant-strength vortex sheet is linearly ill posed in the sense of Hadamard, owing to Kelvin-Helmholtz instability (Birkhoff, et al., 1962). In this situation, an analytic vortex sheet exists locally in time and a singularity can form in a finite time (Moore 1979, Meiron et al., 1982, and Caffisch and Orellana 1986). Previous numerical studies of this problem using Rosenhead's point vortex approximation have experienced difficulty in converging when the number of point vortices was increased. Explaining the course of this difficulty and providing a remedy for it have been longstanding issues.

Using discrete Fourier analysis, it was shown that perturbations introduced spuriously by computer roundoff error are responsible for the irregular point vortex motion that occurs at a smaller time as the number of points is increased (Krasny, 1986). This source of computational error can be controlled by using either higher precision arithmetic or a new filtering technique. The results indicate the formation of a singularity in the vortex sheet at a finite time as found by Moore and Meiron, Baker and Orszag using different techniques of analysis. At the critical time, the vortex sheet strength has a cusp and the curvature has an infinite jump discontinuity, although the sheet's slope remains bounded and its tangent vector is continuous. Numerical evidence suggests that the point vortex approximation converges up to but not beyond the time of singularity formation in the vortex sheet.

Roll-Up of a Periodic Vortex Sheet Past the Critical Time

One approach to extending the vortex sheet solution past the critical time is based on desingularizing the Cauchy principal value integral which defines the sheet's velocity (Chorin and Bernard 1973, Krasny 1986). Linear stability analysis shows that this diminishes the vortex sheet's short wavelength instability, yielding a numerically more tractable set of equations. Computational evidence indicates that this approximation converges, beyond the vortex sheet's critical time, if the mesh is refined and the smoothing parameter is reduced in the proper order. The results (e.g., figure 1) suggest that the vortex sheet rolls up into a double-branched spiral past the critical time.

Vortex Sheet Roll-Up in the Trefftz Plane

The desingularization approach has been applied to the vortex sheet shed by a finite span wing (Krasny, 1987). An initial value problem in the two-dimensional Trefftz plane is studied under the assumption that the wake's streamwise variation is small. The loading on the wing's trailing edge is incorporated into the vortex sheet's initial circulation distribution. The two problems studied are for elliptical loading and a simulated fuselage-flap loading (figure 2).

References

- Birkhoff, G., 1962. "Helmholtz and Taylor instability", *Proc. Symp. Appl. Math. XIII A.M.S.*, 55.
- Caffisch, R.E. and Orellana, O.F., 1986. "Long time existence for a slightly perturbed vortex sheet", *Comm. Pure Appl. Math.* 39, 807.
- Chorin, A.J. and Bernard, P.S., 1973. "Discretization of a vortex sheet, with an example of roll-up", *J. Comp. Phys.* 13, 423.
- Krasny, R., 1986. "A study of singularity formation in a vortex sheet by the point vortex approximation", *J. Fluid Mech.* 167, 65.
- Krasny, R., 1986. "Desingularization of periodic vortex sheet roll-up". *J. Comp. Phys.* 65, 292.
- Krasny, R., 1987. "Computation of vortex sheet roll-up in the Trefftz plane", *J. Fluid Mech.*, to appear.
- Meiron, D.I., Baker, G.R. and Orszag, S.A., 1982. "Analytic structure of vortex sheet dynamics. I. Kelvin-Helmholtz instability", *J. Fluid Mech.* 114, 283.
- Moore, D. W., 1979. "The spontaneous appearance of a singularity in the shape of an evolving vortex sheet", *Proc. Roy. Soc. Lond. A* 365, 105.

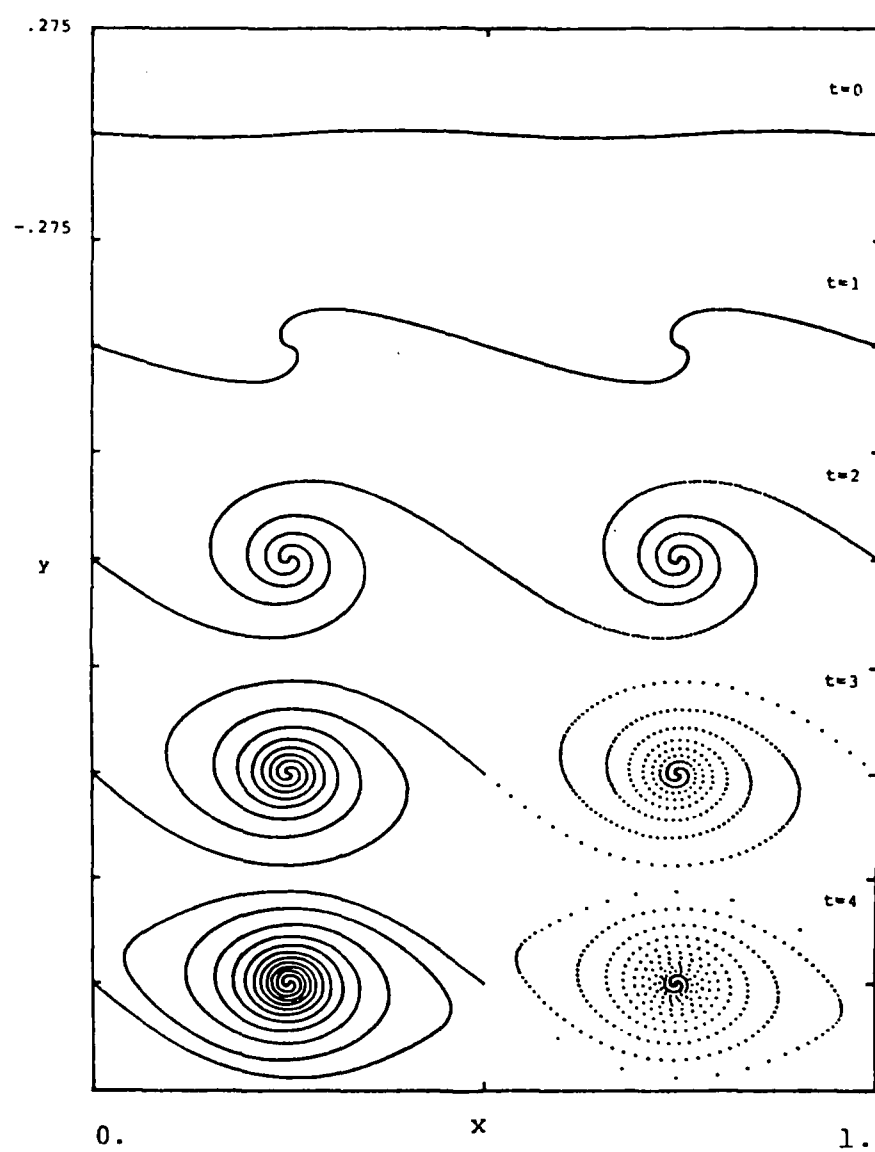


Figure 1

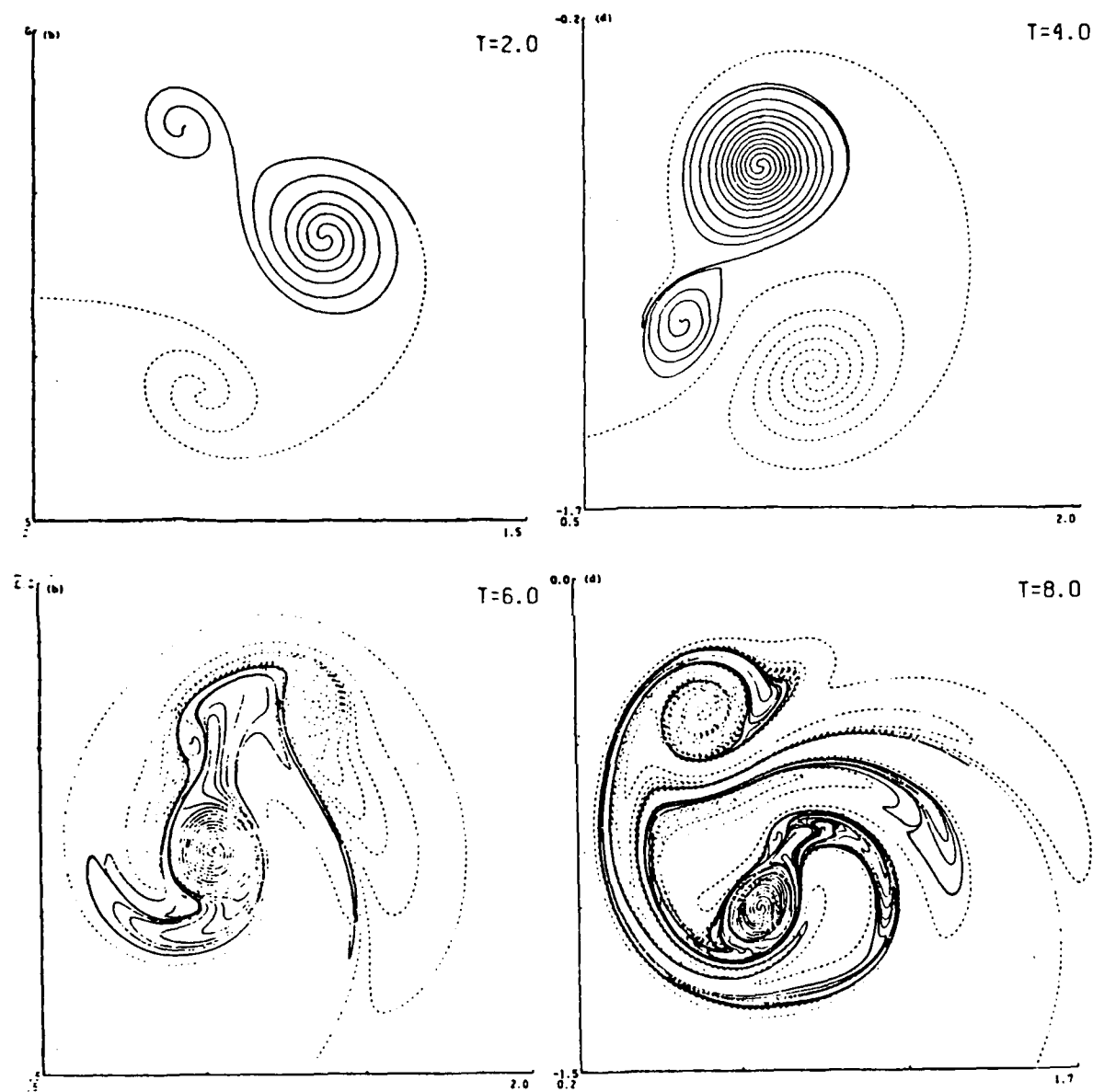


Figure 2

SHUNTED HOMOPOLAR DYNAMO – ANALYTIC APPROACH TO A POINCARÉ MAP

Ya Yan Lu

Department of Mathematics
Massachusetts Institute of Technology
Cambridge, MA 02139

The dynamo theories (Childress, 1987) are based on the idea that the motion of a conducting fluid is possible to sustain a magnetic field like in the sun and the earth. Bullard (1955) introduced the homopolar disk dynamo to illustrate this fundamental issue. Although dynamo action is sustained in his model, it does not permit reversals of the magnetic field. A shunted homopolar dynamo is proposed by Malkus (1972) to make reversals possible. The equations describing Malkus' model are

$$\begin{aligned}\frac{da}{dt} &= bc - a \\ \frac{db}{dt} &= R - b - ac, \\ \sigma_1 \frac{dc}{dt} &= a - c + \sigma_1^{-1} \frac{da}{dt}.\end{aligned}$$

where a, b, c are proportional to the current in the disk, the angular velocity of the disk, and the current in the coil respectively. R is the parameter proportional to external torque applied to the axis, and σ, σ_1 are two other parameters.

This set of equations is equivalent to the famous Lorenz set when the parameter σ_1 goes to infinity. The Lorenz set has been studied extensively (Sparrow, 1982). One excitement about it is the strange attractor found in certain parameter range. An important description for strange attractors is their Poincaré maps which maps any point in a plane (or a suitable surface in 3-D phase space here) to its first return to that plane. For the Lorenz set, the Poincaré map can only be obtained numerically in the parameter range of stable strange attractor. But for our system here, it is possible to obtain an analytic expression of the map. The reason is that when σ_1 is finite, the strange attractor of Lorenz type persists for arbitrary large R , while the Lorenz set has stable period orbit in that limit and does not have the interesting strange attractor anymore.

We study this set for larger R by a suitable scaling for a, b, c and t . The set of equations becomes a perturbation around an integral system. The Poincaré map for large R is therefore found through perturbation method. Based on this map, it is easy to study certain features of the strange attractor. For example, we can easily predict a reversal of the magnetic field one period of oscillation before it actually occurs. These results are confirmed by direct numerical calculations.

References

- Bullard, E. C., 1955. *Proc. Camb. Phil. Soc.*, 51, 744-760.
- Childress, S., 1987. this volume.
- Lorenz, E. N., 1963. *J. Atmos. Sci.*, 20, 130-141.
- Malkus, V.W.R., 1972. *EOS, Trans. Am. Geophys. Union*, 53, 617.
- Sparrow, C., 1982. *The Lorenz Equation*, Springer-Verlag.

INERTIAL MODES IN LABORATORY SPHEROIDS

Willem V.R. Malkus
 Department of Mathematics
 Massachusetts Institute of Technology
 Cambridge, MA 02139

Recent studies by Orszag and Patera, Bayly, Pierrehumbert, Craik and Criminale, and others, indicate that smooth, two-dimensional, elliptical flow can be inertially unstable to disturbances across a broad band of wavenumbers. Such elliptical streamlines occurs in Orr-Sommerfeld instability in Ekman layers and other shearing flow. The observed secondary instabilities appear to be inertial and broadband.

A more elementary elliptical flow is the Poincaré solution for a precessing fluid in an oblate spheroidal container. Poincaré observed that, in a coordinate system rotating with the precessional angular frequency, an exact solution for the velocity of the fluid was one of constant vorticity with the same shape elliptical streamlines everywhere. Only in a thin film at the boundary of the container were viscous corrections required. This solution can be realized in a laboratory flow, at least for low precession rates. It will be demonstrated that such flow is initially stable, first unstable to waves on a shear flow induced by boundary friction, and finally fully turbulent. Our spheroid has only the small ellipticity of 1.05. The transition to full turbulence is violent and subcritical (e.g., a large hysteresis in torque). However, the possibility that the turbulence has its origin in viscous boundary layer instabilities has not been ruled out. Fellowship studies of this summer (L. Brazell) suggest that a finite ellipticity may be required to initiate the internal inertial instabilities. We plan to construct a spheroid of ellipticity 1.5 and study its sequence of precessional instabilities. If internal modes are the first to appear, it is plausible that a large liquid metal version would exhibit dynamo action.

References

- Bayly, B., 1987. *Phys. Fluids*, in press.
- Brazell, L., 1987. "The instability of an elliptical flow in the presence of a magnetic field", 1987 Summer Program in Geophysical Fluid Dynamics, Woods Hole Oceanographic Institution, in press.
- Craik, A. and Criminale, W., 1986. *Proc. Roy. Soc. Lond., A* 406, 13.
- Orszag, S. and Patera, A., 1980. *Phys. Rev. Lett.*, 45, 989.
- Pierrehumbert, R., 1986. *Phys. Rev. Lett.*, 57, 2157.
- Poincaré, H., 1910. *Bull. Astron.*, 27, 321.

22
 23
 24
 25
 26
 27
 28
 29
 30
 31
 32
 33
 34
 35
 36
 37
 38
 39
 40
 41
 42
 43
 44
 45
 46
 47
 48
 49
 50
 51
 52
 53
 54
 55
 56
 57
 58
 59
 60
 61
 62
 63
 64
 65
 66
 67
 68
 69
 70
 71
 72
 73
 74
 75
 76
 77
 78
 79
 80
 81
 82
 83
 84
 85
 86
 87
 88
 89
 90
 91
 92
 93
 94
 95
 96
 97
 98
 99
 100
 101
 102
 103
 104
 105
 106
 107
 108
 109
 110
 111
 112
 113
 114
 115
 116
 117
 118
 119
 120
 121
 122
 123
 124
 125
 126
 127
 128
 129
 130
 131
 132
 133
 134
 135
 136
 137
 138
 139
 140
 141
 142
 143
 144
 145
 146
 147
 148
 149
 150
 151
 152
 153
 154
 155
 156
 157
 158
 159
 160
 161
 162
 163
 164
 165
 166
 167
 168
 169
 170
 171
 172
 173
 174
 175
 176
 177
 178
 179
 180
 181
 182
 183
 184
 185
 186
 187
 188
 189
 190
 191
 192
 193
 194
 195
 196
 197
 198
 199
 200
 201
 202
 203
 204
 205
 206
 207
 208
 209
 210
 211
 212
 213
 214
 215
 216
 217
 218
 219
 220
 221
 222
 223
 224
 225
 226
 227
 228
 229
 230
 231
 232
 233
 234
 235
 236
 237
 238
 239
 240
 241
 242
 243
 244
 245
 246
 247
 248
 249
 250
 251
 252
 253
 254
 255
 256
 257
 258
 259
 260
 261
 262
 263
 264
 265
 266
 267
 268
 269
 270
 271
 272
 273
 274
 275
 276
 277
 278
 279
 280
 281
 282
 283
 284
 285
 286
 287
 288
 289
 290
 291
 292
 293
 294
 295
 296
 297
 298
 299
 300
 301
 302
 303
 304
 305
 306
 307
 308
 309
 310
 311
 312
 313
 314
 315
 316
 317
 318
 319
 320
 321
 322
 323
 324
 325
 326
 327
 328
 329
 330
 331
 332
 333
 334
 335
 336
 337
 338
 339
 340
 341
 342
 343
 344
 345
 346
 347
 348
 349
 350
 351
 352
 353
 354
 355
 356
 357
 358
 359
 360
 361
 362
 363
 364
 365
 366
 367
 368
 369
 370
 371
 372
 373
 374
 375
 376
 377
 378
 379
 380
 381
 382
 383
 384
 385
 386
 387
 388
 389
 390
 391
 392
 393
 394
 395
 396
 397
 398
 399
 400
 401
 402
 403
 404
 405
 406
 407
 408
 409
 410
 411
 412
 413
 414
 415
 416
 417
 418
 419
 420
 421
 422
 423
 424
 425
 426
 427
 428
 429
 430
 431
 432
 433
 434
 435
 436
 437
 438
 439
 440
 441
 442
 443
 444
 445
 446
 447
 448
 449
 450
 451
 452
 453
 454
 455
 456
 457
 458
 459
 460
 461
 462
 463
 464
 465
 466
 467
 468
 469
 470
 471
 472
 473
 474
 475
 476
 477
 478
 479
 480
 481
 482
 483
 484
 485
 486
 487
 488
 489
 490
 491
 492
 493
 494
 495
 496
 497
 498
 499
 500
 501
 502
 503
 504
 505
 506
 507
 508
 509
 510
 511
 512
 513
 514
 515
 516
 517
 518
 519
 520
 521
 522
 523
 524
 525
 526
 527
 528
 529
 530
 531
 532
 533
 534
 535
 536
 537
 538
 539
 540
 541
 542
 543
 544
 545
 546
 547
 548
 549
 550
 551
 552
 553
 554
 555
 556
 557
 558
 559
 560
 561
 562
 563
 564
 565
 566
 567
 568
 569
 570
 571
 572
 573
 574
 575
 576
 577
 578
 579
 580
 581
 582
 583
 584
 585
 586
 587
 588
 589
 590
 591
 592
 593
 594
 595
 596
 597
 598
 599
 600
 601
 602
 603
 604
 605
 606
 607
 608
 609
 610
 611
 612
 613
 614
 615
 616
 617
 618
 619
 620
 621
 622
 623
 624
 625
 626
 627
 628
 629
 630
 631
 632
 633
 634
 635
 636
 637
 638
 639
 640
 641
 642
 643
 644
 645
 646
 647
 648
 649
 650
 651
 652
 653
 654
 655
 656
 657
 658
 659
 660
 661
 662
 663
 664
 665
 666
 667
 668
 669
 670
 671
 672
 673
 674
 675
 676
 677
 678
 679
 680
 681
 682
 683
 684
 685
 686
 687
 688
 689
 690
 691
 692
 693
 694
 695
 696
 697
 698
 699
 700
 701
 702
 703
 704
 705
 706
 707
 708
 709
 710
 711
 712
 713
 714
 715
 716
 717
 718
 719
 720
 721
 722
 723
 724
 725
 726
 727
 728
 729
 730
 731
 732
 733
 734
 735
 736
 737
 738
 739
 740
 741
 742
 743
 744
 745
 746
 747
 748
 749
 750
 751
 752
 753
 754
 755
 756
 757
 758
 759
 760
 761
 762
 763
 764
 765
 766
 767
 768
 769
 770
 771
 772
 773
 774
 775
 776
 777
 778
 779
 780
 781
 782
 783
 784
 785
 786
 787
 788
 789
 790
 791
 792
 793
 794
 795
 796
 797
 798
 799
 800
 801
 802
 803
 804
 805
 806
 807
 808
 809
 810
 811
 812
 813
 814
 815
 816
 817
 818
 819
 820
 821
 822
 823
 824
 825
 826
 827
 828
 829
 830
 831
 832
 833
 834
 835
 836
 837
 838
 839
 840
 841
 842
 843
 844
 845
 846
 847
 848
 849
 850
 851
 852
 853
 854
 855
 856
 857
 858
 859
 860
 861
 862
 863
 864
 865
 866
 867
 868
 869
 870
 871
 872
 873
 874
 875
 876
 877
 878
 879
 880
 881
 882
 883
 884
 885
 886
 887
 888
 889
 890
 891
 892
 893
 894
 895
 896
 897
 898
 899
 900
 901
 902
 903
 904
 905
 906
 907
 908
 909
 910
 911
 912
 913
 914
 915
 916
 917
 918
 919
 920
 921
 922
 923
 924
 925
 926
 927
 928
 929
 930
 931
 932
 933
 934
 935
 936
 937
 938
 939
 940
 941
 942
 943
 944
 945
 946
 947
 948
 949
 950
 951
 952
 953
 954
 955
 956
 957
 958
 959
 960
 961
 962
 963
 964
 965
 966
 967
 968
 969
 970
 971
 972
 973
 974
 975
 976
 977
 978
 979
 980
 981
 982
 983
 984
 985
 986
 987
 988
 989
 990
 991
 992
 993
 994
 995
 996
 997
 998
 999
 1000
 1001
 1002
 1003
 1004
 1005
 1006
 1007
 1008
 1009
 1010
 1011
 1012
 1013
 1014
 1015
 1016
 1017
 1018
 1019
 1020
 1021
 1022
 1023
 1024
 1025
 1026
 1027
 1028
 1029
 1030
 1031
 1032
 1033
 1034
 1035
 1036
 1037
 1038
 1039
 1040
 1041
 1042
 1043
 1044
 1045
 1046
 1047
 1048
 1049
 1050
 1051
 1052
 1053
 1054
 1055
 1056
 1057
 1058
 1059
 1060
 1061
 1062
 1063
 1064
 1065
 1066
 1067
 1068
 1069
 1070
 1071
 1072
 1073
 1074
 1075
 1076
 1077
 1078
 1079
 1080
 1081
 1082
 1083
 1084
 1085
 1086
 1087
 1088
 1089
 1090
 1091
 1092
 1093
 1094
 1095
 1096
 1097
 1098
 1099
 1100
 1101
 1102
 1103
 1104
 1105
 1106
 1107
 1108
 1109
 1110
 1111
 1112
 1113
 1114
 1115
 1116
 1117
 1118
 1119
 1120
 1121
 1122
 1123
 1124
 1125
 1126
 1127
 1128
 1129
 1130
 1131
 1132
 1133
 1134
 1135
 1136
 1137
 1138
 1139
 1140
 1141
 1142
 1143
 1144
 1145
 1146
 1147
 1148
 1149
 1150
 1151
 1152
 1153
 1154
 1155
 1156
 1157
 1158
 1159
 1160
 1161
 1162
 1163
 1164
 1165
 1166
 1167
 1168
 1169
 1170
 1171
 1172
 1173
 1174
 1175
 1176
 1177
 1178
 1179
 1180
 1181
 1182
 1183
 1184
 1185
 1186
 1187
 1188
 1189
 1190
 1191
 1192
 1193
 1194
 1195
 1196
 1197
 1198
 1199
 1200
 1201
 1202
 1203
 1204
 1205
 1206
 1207
 1208
 1209
 1210
 1211
 1212
 1213
 1214
 1215
 1216
 1217
 1218
 1219
 1220
 1221
 1222
 1223
 1224
 1225
 1226
 1227
 1228
 1229
 1230
 1231
 1232
 1233
 1234
 1235
 1236
 1237
 1238
 1239
 1240
 1241
 1242
 1243
 1244
 1245
 1246
 1247
 1248
 1249
 1250
 1251
 1252
 1253
 1254
 1255
 1256
 1257
 1258
 1259
 1260
 1261
 1262
 1263
 1264
 1265
 1266
 1267
 1268
 1269
 1270
 1271
 1272
 1273
 1274
 1275
 1276
 1277
 1278
 1279
 1280
 1281
 1282
 1283
 1284
 1285
 1286
 1287
 1288
 1289
 1290
 1291
 1292
 1293
 1294
 1295
 1296
 1297
 1298
 1299
 1300
 1301
 1302
 1303
 1304
 1305
 1306
 1307
 1308
 1309
 1310
 1311
 1312
 1313
 1314
 1315
 1316
 1317
 1318
 1319
 1320
 1321
 1322
 1323
 1324
 1325
 1326
 1327
 1328
 1329
 1330
 1331
 1332
 1333
 1334
 1335
 1336
 1337
 1338
 1339
 1340
 1341
 1342
 1343
 1344
 1345
 1346
 1347
 1348
 1349
 1350
 1351
 1352
 1353
 1354
 1355
 1356
 1357
 1358
 1359
 1360
 1361
 1362
 1363
 1364
 1365
 1366
 1367
 1368
 1369
 1370
 1371
 1372
 1373
 1374
 1375
 1376
 1377
 1378
 1379
 1380
 1381
 1382
 1383
 1384
 1385
 1386
 1387
 1388
 1389
 1390
 1391
 1392
 1393
 1394
 1395
 1396
 1397
 1398
 1399
 1400
 1401
 1402
 1403
 1404
 1405
 1406
 1407
 1408
 1409
 1410
 1411
 1412
 1413
 1414
 1415
 1416
 1417
 1418
 1419
 1420
 1421
 1422
 1423
 1424
 1425
 1426
 1427
 1428
 1429
 1430
 1431
 1432
 1433
 1434
 1435
 1436
 1437
 1438
 1439
 1440
 1441
 1442
 1443
 1444
 1445
 1446
 1447
 1448
 1449
 1450
 1451
 1452
 1453
 1454
 1455
 1456
 1457
 1458
 1459
 1460
 1461
 1462
 1463
 1464
 1465
 1466
 1467
 1468
 1469
 1470
 1471
 1472
 1473
 1474
 1475
 1476
 1477
 1478
 1479
 1480
 1481
 1482
 1483
 1484
 1485
 1486
 1487
 1488
 1489
 1490
 1491
 1492
 1493
 1494
 1495
 1496
 1497
 1498
 1499
 1500
 1501
 1502
 1503
 1504
 1505
 1506
 1507
 15

STRONG SPATIAL RESONANCE AND TRAVELLING WAVES IN BÉNARD CONVECTION

M. R. E. Proctor

D.A.M.T.P., University of Cambridge
Silver Street, Cambridge, CB3 9EW, U.K.

The role of multiple bifurcations in the production of time dependence by convective instability has been greatly elucidated recently. Segel (1962) and Knobloch and Guckenheimer (1982) have investigated the consequences of the simultaneous onset of two modes of different horizontal wavenumber in Bénard convection with symmetric boundary conditions. They found that the complex amplitudes A_1, A_2 of the two modes obey evolution equations of the form

$$\begin{aligned}\dot{A}_1 &= \mu_1 A_1 - A_1 \{a_1 |A_1| + b_1 |A_2|\} + O(|A|^5) \\ \dot{A}_2 &= \mu_2 A_2 - A_2 \{a_2 |A_2| + b_2 |A_1|\} + O(|A|^5)\end{aligned}\quad (1)$$

Though a variety of mixed mode solutions can be found, as well as 'pure mode' solutions in which either of A_1, A_2 is zero, the equations are not complete because information on the relative *phases* of A_1, A_2 is lacking, only the amplitudes being given unambiguously by (1). Although there are higher order terms that do couple the relative phases when the bifurcating wavenumbers are in a rational ratio (and when this ratio is 2:1 these terms are of fifth order in $|A|$) these do not affect the initial bifurcation; and no new stable phenomena apparently appear.

The situation is quite different, however, when either the up-down symmetry inherent in the Boussinesq approximation is relaxed (by acknowledging the effects of compressibility and finite scale heights), or the boundary conditions are asymmetrical. Then in the case of 2:1 resonance, *quadratic* terms can appear in the normal form equations: the latter then take the leading order form

$$\begin{aligned}\dot{A}_1 &= \mu_1 A_1 + \alpha A_2 \bar{A}_1 - A_1 \{a_1 |A_1|^2 + b_1 |A_2|^2\} \\ \dot{A}_2 &+ \mu_2 A_2 \pm \alpha A_1^2 - A_2 \{a_2 |A_2|^2 + b_2 |A_1|^2\}\end{aligned}\quad (2)$$

where the sign of the α term in 2(b) depends on the nature of the physical problem. For a Boussinesq fluid with asymmetric boundary conditions the minus sign always appears: this is because of the energy preserving character of the nonlinear term and the self-adjointness of the underlying linear stability problem. If the linear and cubic terms are ignored, the resulting system

$$\begin{aligned}\dot{A}_1 &= \alpha A_2 \bar{A}_1 \\ \dot{A}_2 &= -\alpha A_1^2\end{aligned}\quad (3)$$

possesses the two invariants

$$|A_1|^2 + |A_2|^2, \quad A_1^2 A_2 - \bar{A}_1^2 A_2 \quad (4)$$

The system (3) is thus completely integrable, and the solutions (obtainable in terms of elliptic functions) represent *travelling waves*, of constant or periodically modulated amplitude. When the linear and cubic terms are restored, we find that, indeed, there are for certain merges of parameters stable solutions of both these types, as well as steady convection modes similar to those found in the non-resonant problem. This is remarkable because the initial bifurcations are *simple*, unlike the related binary mixture problem where initial Hopf bifurcations lead in many cases to travelling waves with a well defined phase velocity at onset. Here the phase speed of the waves arises from the resonant interaction, and tends to zero as the polycritical point $\mu_1 = \mu_2 = 0$ is approached.

There is a further fascinating phenomenon that can occur, in the form of a homoclinic orbit (characterized by short pulses of nonzero A_1 , with $|A_2|$ more or less constant except during pulses, and the interval between the latter increasing geometrically with time. This orbit exists for a wide range of parameter values because it lies entirely in planes in the phase space that are invariant under even $O(1)$ changes to the parameters. Armbruster (1987) who have also looked at this system in a different context conjecture that such homoclinic orbits play an important part in the phenomenon of intermittency in turbulent shear flows. These orbits can be destroyed by introducing imperfections (e.g. a small constant term into 2(a)); they then become attracting periodic orbits of long period, the latter tending to infinity as the logarithm of the size of the imperfection.

Such rich behavior is remarkable in such a simple system of o.d.e.'s. Apart from the intrinsic interest of the problem, there is the exciting possibility that bifurcation leading to travelling waves may occur in many large fluid systems far from threshold, and play an important part in the transition to disorder for such systems.

This abstract partially summarizes work done by Dangelmayt (1986), Jones and Proctor (1987), and Proctor and Jones (1987).

References

- Armbruster, D., Guckenheimer, J., and Holmes, P., 1987. *Physica D*, in press.
- Dangelmayt, G., 1986. *Dyn. Stab. Sys.*, 1, 159.
- Jones, C.A. and Proctor, M.R.E., 1987. *Phys. Lett. A*, 121, 224.
- Knobloch, E. and Guckenheimer, J., 1982. *Phys. Rev. A*, 27, 408.
- Proctor, M.R.E. and Jones, C.A., 1987. *J. Fluid Mech.*, in press.
- Segel, L.A., 1962. *J. Fluid Mech.*, 14, 97.

A REVIEW OF HAMILTONIAN FLUID MECHANICS

Rick Salmon
Scripps Institution of Oceanography
La Jolla, CA 92093

The Lagrangian for a perfect fluid is closely analogous to the corresponding Lagrangian for interacting point particles. However, the fluid Lagrangian has an important symmetry property corresponding to the continuous relabeling of fluid particles with the same density and entropy. This symmetry property is responsible for the *existence* of a closed Eulerian description, and it gives rise (by Noether's theorem) to the most general statement of vorticity conservation. The general vorticity law cannot be stated without referring to the locations of marked fluid particles, but the well-known theorems on potential vorticity, circulation, and helicity follow immediately from it. The corresponding Lagrangian for magnetohydrodynamics seems to lack the particle-relabeling symmetry property, suggesting that no analog of potential vorticity exists for MHD.

The "particle-mechanics" form of Hamilton's principle for a fluid is considerably simpler than the various "velocity-potential" forms of the principle, which can be obtained, roughly speaking, by interchanging the roles of dependent and independent variables. The velocity potentials are analogous to electromagnetic potentials in the familiar Lagrangian for interacting charged particles. However, Feynman and Wheeler have shown that the latter system also has a "particle-mechanics" Lagrangian in which no fields of any kind appear. This Lagrangian resembles the Lagrangians for a superfluid and for an ordinary fluid composed of two hydrostatic layers, suggesting the possibility of an eventual synthesis.

NONLINEAR STABILITY AND SOME OF ITS IMPLICATIONS

T. G. Shepherd

D.A.M.T.P., University of Cambridge
Silver Street, CB3 9EW, U.K.

We use the methods of Arnol'd (1965, 1966) to derive a finite-amplitude generalized Rayleigh stability theorem for disturbances to a parallel flow having a monotonic profile of absolute vorticity. This theorem, (7) below, bounds the possible growth of disturbances of arbitrary initial magnitude. It thus has profound implications concerning the possible ergodicity of the flow dynamics, because trajectories beginning in a neighborhood of any stable flow must remain close to that neighborhood for all time. In addition, the ultimate growth of disturbances to an unstable flow can be bounded if the latter is sufficiently close to a stable flow; in this case the unstable flow can be considered as a finite-amplitude disturbance to the stable flow, and is thereby constrained by the generalized Rayleigh theorem.

The system we consider is that of inviscid two-dimensional flow in a rotating coordinate system, which is governed by conservation of the absolute vorticity $P \equiv \nabla^2 \Phi + f(y)$, where Φ is the flow streamfunction and $f(y)$ the Coriolis term, viz.

$$\frac{DP}{Dt} \equiv P_t + \partial(\Phi, P) \equiv P_t + \Phi_x P_y - \Phi_y P_x = 0 \quad (1)$$

If there are solid boundaries, then there must be no flow normal to the boundaries, and the circulation around each connected portion of the boundary must be constant in time. If the geometry has zonal (x) symmetry, then this system has the following integral invariants:

1. Energy $\int \int \frac{1}{2} |\nabla \Phi|^2 dx dy$, from the temporal symmetry;
2. Impulse $\int \int y P dx dy$, from the spatial (x) symmetry; and
3. Casimirs $\int \int C(P) dx dy$, for any function $C(P)$, from the "particle-relabeling" symmetry (see McIntyre and Shepherd, 1987; Salmon, 1988).

Note that the impulse is related to the zonal momentum via integration by parts, and that a well-known special case of a Casimir is the enstrophy $P^2/2$.

Now consider a parallel "basic state" $Q(y) = \Psi_{yy} + f(y)$, itself a steady solution to (1); for a given total flow (Φ, P) the disturbance (ψ, q) is defined by

$$P \equiv Q + q, \quad \Phi \equiv \Phi + \psi \quad (2)$$

The method of Arnol'd (1965, 1966) for finding nonlinear stability theorems is to construct conserved disturbance quantities which are quadratic in the limit of small

disturbance amplitude a . Since the impulse of the total flow, yP , and of the basic flow, yQ , are both conserved, so is their difference, the "impulse increment"

$$\Delta I \equiv yq \quad (3)$$

However ΔI is $O(a)$ in the limit $a \ll 1$. Fortunately, we are free to add a "Casimir increment",

$$\Delta C \equiv C(Q + q) - C(Q) \quad (4)$$

to ΔI , for any C , and it is evident that if C is chosen such that $C'(Q) = -y$ then the $O(a)$ component of $\Delta I + \Delta C$ will vanish. The resulting invariant may be written

$$\Delta I + \Delta C \equiv J = - \int_0^q [Y_0(Q + q') - Y_0(Q)] dq' \quad (5)$$

where $Y_0(Q)$ is defined such that $y = Y_0(Q(y))$. In the applications discussed here $Q(y)$ will be monotonic so its inverse $Y_0(Q)$ will be well-defined. For discussion of the case of multivalued $Q(y)$, and for more details of the method outlined above, see §§5 and 7 respectively of McIntyre and Shepherd (1987).

If $Q(y)$ is monotonic and Q_y is bounded away from zero and infinity, then it is straightforward to see that, with a disturbance norm given by

$$\|q\| \equiv \left\{ \int \int q^2 dx dy \right\}^{1/2} \quad (6)$$

the disturbance amplitude at any time $t > 0$ is bounded in terms of its initial amplitude at $t = 0$ according to

$$\|q(t)\|^2 \leq \frac{|Q_y|_{\max}}{|Q_y|_{\min}} \|q(0)\|^2 \quad (7)$$

Equation (7) is a statement of Liapunov stability, and may be considered a generalized Rayleigh stability theorem.

As already mentioned, because (7) applies to initial disturbances of any amplitude whatever, it has implications concerning the possible ergodicity of the flow dynamics. For example, in the theory of two-dimensional turbulence it is frequently hypothesized (e.g., Kraichnan, 1975) that the statistical evolution of the flow is governed only by the quadratic invariants of total energy and enstrophy. Two-dimensional flow on a beta-plane (with $f(y) = \beta y$ in (1)) possesses the same quadratic invariants, but for a wave steepness $\epsilon \equiv 2\sqrt{2}Z/\beta u < 1$ (where Z is the total enstrophy and u the r.m.s. velocity) it can be shown via the stability theorem (Shepherd, 1987) that flows which are sufficiently close to certain stable parallel flows can never become isotropic. Since the quadratic invariants are isotropic, this shows that the dynamics is not ergodic on the phase-space surface of constant energy and enstrophy for $\epsilon < 1$. Rather, the dynamics is then constrained in certain regions by the higher-order (non-quadratic) invariants associated with the material conservation of P .

For a given flow, the (integral of the) quantity J defined by (5) is conserved for any choice of the basic flow (Ψ, Q) whatever. This means that one is at liberty to choose as a basic flow anything that is convenient for the problem at hand. In the case of an unstable initial flow, for example, one may choose a basic state which is stable, and then apply (7) to constrain the evolution of the (finite-amplitude) disturbance and bound the equilibration of the instability. To make things concrete, we give two examples here.

The first is that of the "point-jet" instability in a beta-plane channel of width L . We consider an initially infinitesimal disturbance to the zonal flow

$$\bar{u}(y) = \Gamma \left| y - \frac{L}{2} \right| - \Gamma \frac{L}{2} \quad \text{for } 0 \leq y \leq L \quad (8)$$

with associated absolute vorticity

$$\bar{P}(y) = \begin{cases} \beta y + \Gamma & \text{for } 0 \leq y \leq L/2 \\ \beta y - \Gamma & \text{for } L/2 \leq y \leq L \end{cases} \quad (9)$$

where the overbar represents a zonal average. Now construct a one-parameter family of stable basic flows

$$Q(y) = \begin{cases} \beta y + \Gamma & \text{for } 0 \leq y \leq L/2 - y_c \\ \eta y & \text{for } L/2 - y_c \leq y \leq L/2 + y_c \\ \beta y - \Gamma & \text{for } L/2 + y_c \leq y \leq L \end{cases} \quad (10)$$

with $y_c = \Gamma/(B - \eta)$. The enstrophy of the wavy part of the flow is bounded by the enstrophy of the disturbance to (10), which in turn is bounded by the Rayleigh theorem (7), namely

$$\left\langle \frac{1}{2} \overline{q'^2} \right\rangle \equiv \frac{1}{L} \int \frac{1}{2} \overline{q'^2} \leq \left\langle \frac{1}{2} \overline{q^2} \right\rangle \leq \frac{\beta}{\eta} \left\langle \frac{1}{2} \overline{q^2(0)} \right\rangle = \frac{\beta \Gamma^3}{3L} \frac{1}{\eta(\beta - \eta)} \quad (11)$$

The right-hand side of (11) is minimized for the choice $\eta = B/2$, yielding the rigorous (least upper) bound

$$\left\langle \frac{1}{2} \overline{q'^2} \right\rangle \leq \frac{4\Gamma^3}{3\beta L} \quad (12)$$

Schoeberl and Lindzen (1984) propose a "saturation limit" for the wavy enstrophy in this problem, based on the ad hoc assumption that the wave will grow until it neutralizes the zonal-mean vorticity gradient; they obtain $\Gamma^3/3\beta L$. Numerical calculations by Schoeberl and Lindzen (1984, figure 8) show $\left\langle \frac{1}{2} \overline{q'^2} \right\rangle$ overshooting this "saturation limit" by a factor of two, coming within a factor of two of the rigorous nonlinear bound (12). This and other examples of equilibration of barotropic instabilities are discussed in Shepherd (1988a).

A second example is that of the Phillips model of baroclinic instability in a two-layer quasi-geostrophic fluid. Here (1) holds in each of the two layers, but P is now the potential vorticity

$$P_i = \nabla^2 \Phi_i + \beta y + (-1)^i F(\Phi_1 - \Phi_2), \quad [i = 1, 2] \quad (13)$$

where F is a stratification parameter. Given an initially infinitesimal disturbance to a supercritical (unstable) zonal flow

$$\bar{u} \equiv \bar{u}_1 - \bar{u}_2 = \frac{B}{F}(1 + \epsilon) \quad (14)$$

we consider this as a finite-amplitude disturbance to a subcritical (stable) basic flow

$$u = \frac{\beta}{F}(1 - \delta) \quad (15)$$

The Rayleigh theorem (7) in this case gives

$$\int_0^1 \frac{1}{2}(\bar{q}_1^2 + \bar{q}_2^2)(t)dy \leq \frac{2 - \delta}{\delta} \int_0^1 \frac{1}{2}(\bar{q}_1^2 + \bar{q}_2^2)(0) = \left(\frac{2 - \delta}{\delta}\right) \frac{1}{3}\beta^2(\epsilon + \delta)^2 \quad (16)$$

and the right-hand side of (16) is (nearly) minimized for $\delta = \epsilon$ if $\epsilon \leq 0.2$, and for $\delta = 1$ if $\epsilon \geq 0.2$. This can be summarized in the bound

$$\int_0^1 \frac{1}{2}(\bar{q}_1^2 + \bar{q}_2^2)dy \leq \frac{1}{3}\beta^2 f(\epsilon) \quad (17)$$

where

$$f(\epsilon) \equiv \begin{cases} 4\epsilon(2 - \epsilon) & \text{for } \epsilon \leq 0.2 \\ (1 + \epsilon)^2 & \text{for } \epsilon \geq 0.2 \end{cases} \quad (18)$$

This problem is discussed further, and the bound (17) compared with the results of weakly-nonlinear theory for single-wave equilibration, in Shepherd (1988b).

The results up to this point have relied on the generalized Rayleigh stability theorem, which has its origin in the conservation of impulse. An entirely analogous procedure can be carried through using energy, in which case one chooses the Casimir C such that $\Delta E + \Delta C$ is $O(a^2)$ in the limit $a \ll 1$. See McIntyre and Shepherd (1987) for further details, and in particular §7 of that paper for a discussion of how the various conserved quantities are related to the symmetries in the Hamiltonian structure of the problem.

Finally, we examine the nonlinear stability of a circular patch of constant vorticity

$$\nabla^2 \Psi = \begin{cases} 1 & \text{for } r < 1, \\ 0 & \text{for } r > 1. \end{cases} \quad (19)$$

In such a system results of the type (7) break down. Two invariants for this system are the angular momentum and the area, which may be written respectively as

$$\int \int (1 + \eta)^3 d\eta d\theta \quad \text{and} \quad \int \int (1 + \eta) d\eta d\theta \quad (20)$$

integrating over the patch, where $r \equiv 1 + \eta$. Taking the difference of these two invariants yields the invariant

$$J_A \equiv \oint \frac{1}{4} \eta^2 (\eta + 2)^2 d\theta \quad (21)$$

integrating around the contour. Because of the circular geometry, it does not seem possible to use the invariance of (21) to prove Liapunov stability in any conventional sense. However, if one takes the norm

$$\|\eta\| \equiv \left\{ \oint \eta^2 d\theta \right\}^{1/2} \quad (22)$$

then it is easy to show that

$$\|\eta(t)\|^2 \leq J^A(t) = J_A(0) \leq \frac{1}{4}(c+2)^2 \|\eta(0)\|^2 \quad (23)$$

where $\leq = \sup_{\theta} |\eta(0)|$. Hence any given initial disturbance can still be usefully constrained. For further details, see Dritschel and Shepherd (1988).

References

- Arnol'd, V.I., 1965. "Conditions for nonlinear stability of stationary plane curvilinear flows of an ideal fluid". *Dokl. Akad. Nauk. SSSR*, 162, 975-978. (English translation: *Soviet Math.*, 6, 773-777, 1965.)
- Arnol'd, V.I., 1966. "On an a priori estimate in the theory of hydrodynamical stability". *Izv. Vyssh. Uchebn. Zaved. Matematika*, 54, no. 5, 3-5. (English translation: *Amer. Math. Soc. Transl., Series 2*, 79, 267-269, 1969).
- Dritschel, D.G. and Shepherd, T.G., 1988. "On the nonlinear stability of the circular vortex patch". *Proc. Roy. Soc. Lond. A*, to be submitted.
- Kraichnan, R.H., 1975. "Statistical dynamics of two-dimensional flow". *J. Fluid Mech.*, 67, 155-175.
- McIntyre, M.E. and Shepherd, T.G., 1987. "An exact local conservation theorem for finite-amplitude disturbances to non-parallel shear flows, with remarks on Hamiltonian structure and on Arnol'd's stability theorems". *J. Fluid Mech.*, 181, 527-565.
- Salmon, R., 1988. "Hamiltonian fluid mechanics". *Ann. Rev. Fluid Mech.*, to appear.
- Schoeberl, M.R. and Lindzen, R.S., 1984. "A numerical simulation of barotropic instability. Part I: Wave-mean flow interaction". *J. Atmos. Sci.*, 41, 1368-1379.
- Shepherd, T.G., 1987. "Non-ergodicity of inviscid two-dimensional flow on a beta-plane and on the surface of a rotating sphere". *J. Fluid Mech.*, in the press.
- Shepherd, T.G., 1988a. "Nonlinear equilibration of barotropic instability on the beta-plane". *J. Fluid Mech.*, to be submitted.
- Shepherd, T.G., 1988b. "Nonlinear equilibration of baroclinic instability". *J. Atmos. Sci.*, submitted.

VORTICES IN A TURBULENT SHEAR: A MODEL OF THE GREAT RED SPOT OF JUPITER

Joël Sommeria
University of Grenoble
Grenoble, France

The Great Red Spot of Jupiter is a huge vortex known to have existed for at least 300 years. Understanding its great stability in the presence of a strong (quasi two-dimensional) turbulent shear is a challenge for geophysical fluid dynamics. Beyond the case of Jupiter, the interaction between coherent structures and turbulence has probably an important influence in the long-term predictability of the Earth's atmosphere.

There is good evidence that Jupiter's atmosphere is very inertial: the forcing and friction mechanisms have little influence during a period of a few eddy turnover times. Furthermore the eddies are most probably shallow features (but the zonal flow could be much deeper). A simple model for these inertial effects is two-dimensional turbulence in a strong zonal shear, where the Coriolis force is taken into account with the beta-plane approximation.

We have reproduced these effects in an annular rotating tank (diameter 0.8 m, spinning frequency 1-4 Hz) with a radially sloping bottom. The apparatus was designed to minimize the friction effects at small Rossby number (0.1). An azimuthal eastward (prograde) or westward (retrograde) jet is produced by a set of water sources and sinks at the bottom of the tank. The eastward jet (Sommeria, et al., 1987a) has always a coherent sinuous shape, while the westward jet (Sommeria, et al., 1987b) is very turbulent. A permanent vortex of the same sign as the shear is generated in this turbulence. New smaller vortices of the same sign are permanently produced by the sinks. These vortices merge together and with the main vortex. The interaction of the main vortex with turbulence, far from destroying it, contributes to feeding it with vorticity and energy. Vortices of the opposite sign are also produced but are very unstable and short-lived. The coexistence between a coherent vortex and turbulence is clearly illustrated by the transport properties: while dye is quickly mixed in the turbulent domain, there is little transport between the vortex core and the surrounding.

When the forcing is sufficiently strong, the width and shape of the jet depend on the total production of momentum, but not on the detail of the forcing. The mean velocity profile tends to reach a state of uniform potential vorticity as a result of turbulent mixing. The corresponding parabolic profile fits well the tip of the westward jet. The potential vorticity can be only uniformized on the edges of the eastward jet, and must have a strong gradient at the jet center, allowing Rossby wave propagation. By contrast waves cannot be sustained in the uniform potential vorticity of the westward jet: the effect of the shear on a weak perturbation is balanced by the beta-effect. We can understand then that the dynamics must be

strongly non-linear, like two-dimensional turbulence, and this turbulence maintains the uniform potential vorticity by a feedback effect.

The vortex dynamics that we observe seems to be indeed a general property of a zonal shear with uniform potential vorticity, as was shown by P. Marcus (1987) (in fact the laboratory experiment was inspired by these computations). We can predict that coherent spots on Jupiter should be located where a shear maximum is in a region of quasi-uniform potential vorticity. The beta-effect can be due both to the planetary curvature and to a sloping bottom (in reality a tilt of the iso-density surfaces), associated with the existence of a deep zonal flow. This slope can be estimated from observations at the cloud level by measuring the variations of the vorticity of fluid particles followed in their motion, and assuming the conservation of potential vorticity. The potential vorticity of the zonal flow near the Great Red Spot and White Oval BC obtained by this method (Dowling and Ingersoll, 1987), appears to be indeed fairly uniform.

References

- Dowling, T.E. and Ingersoll, A.P., 1987. "Potential vorticity and topography of the flow around Jupiter's Great Red Spot and White Oval BC", submitted to *J. Atm. Sci.*
- Marcus, P.S., 1987. "Isolated spots in turbulent zonal flows: a model for Jupiter's Great Red Spot", submitted to *Nature*.
- Sommeria, J., Meyers, S.D., Swinney, H.L., 1987a. "Laboratory model of a planetary eastward jet", submitted to *Science*.
- Sommeria J., Meyers, S.D., Swinney, H.L., 1987b. "A laboratory simulation of the Great Red Spot of Jupiter", submitted to *Nature*.

ASPECTS OF FAST DYNAMO THEORY

Andrew Soward

School of Mathematics, University of Newcastle-Upon-Tyne
Newcastle-Upon-Tyne, NE1 7RU, U.K.

Various aspects of fast dynamos are discussed with particular reference to exact solutions of the magnetic induction equation for specific steady flows when the magnetic Reynolds number, R , is large. The nature of the solution for perfectly conducting fluids ($R^{-1} = 0$) is distinguished from those with R large but finite.

The transient behavior of magnetic field in steady two-dimensional straining motion provides an illuminating example of basic inductive mechanisms. The case of spatially periodic field with zero mean is considered first. When $R^{-1} = 0$, an important distinction can be made between stagnation point flows and linear shear. The former exhibits the fast dynamo property of exponential growth of the magnetic field, whereas the latter is not fast because the magnetic field only grows linearly like the separation of fluid particles. The result, used in conjunction with the exact Cauchy solution, illustrates the point that, for general flows, the growth rate is a local rather than a global property of the particular dynamo model. On the other hand, when R is finite, the growth on the convective time scale is halted when the induced "local" length scale is reduced sufficiently for the "local" magnetic Reynolds number to be of order unity. The magnetic field then decays rapidly. The case of non-zero mean fields is also important. The magnetic flux of the mean field is conserved but concentrated into flux ropes or sheets which we again characterize by "local" magnetic Reynolds numbers of order unity.

The concentration of magnetic flux into sheets and ropes is fundamental to any fast dynamo with $1 << R < \infty$. In that limit the perturbation magnetic field, \mathbf{B}' , is necessarily large compared with the mean field, \mathbf{B} . Typically $|\mathbf{B}'|/|\mathbf{B}|$ is large of order $R^{1/2}$ in flux sheets and of order R in flux ropes. Here the usual approximations used in mean field MHD, which assume that $|\mathbf{B}'| \ll |\mathbf{B}|$, fail. Nevertheless valid mean field equations can be derived as Childress (1979) has shown and explained in his Lectures 4 and 6. The two prototype problems to which he applied his ideas are the two-dimensional spatially periodic motion, $\mathbf{u} = \nabla \times \psi \mathbf{i}_z + w(\psi) \mathbf{i}_z$, where for example $\psi = \sin x \sin y$ and $w = K\psi$ ($K = \text{constant}$) and axially symmetric swirling flow, $\mathbf{u} = \nabla \times s^{-1} \psi \mathbf{i}_\phi + s^{-1} h(\psi) \mathbf{i}_\phi$, where the angular momentum h is assumed constant on streamlines. (On the symmetry axis, $s = 0$, we have $h(0) = 0$.) In the former case, the mean magnetic field lies in horizontal planes, $z = \text{constant}$, while in the latter case the mean field is axial.

The nature of the boundary layers for axisymmetric motion was discussed in detail using boundary layer coordinates. The development in these coordinates is particularly simple and illuminating. The details are outlined by Soward (1987). One feature which the approach helps to explain is the reason why magnetic flux is concentrated as a rope on the axis rather than a sheet on the outer cylindrical

boundary of the flow (periodic in z). The explanation relies on the fact that the mass flux along the axial boundary layer is small compared with the return flow in the sheet boundary layers. This leads to an effective magnetic diffusivity which is small on the axis. The dynamo mechanism itself relies on the ω -effect which induces strong azimuthal magnetic field in the axial boundary layer. In turn that field is intensified by an order of magnitude when it emerges on stream surfaces, $\psi = 0$. It leads to a mean EMF in the axial direction. The α -effect, which ensues, is proportional to the total helicity, $\int_{-\infty}^{+\infty} \mathbf{u} \cdot \nabla \times \mathbf{u} dt$, integrated with respect to time t for a fluid particle moving between two neighboring stagnation points on the axis. The remarkable property of the dynamo mechanism is that the magnitude of the α -effect linked with the mean magnetic field is independent of the magnetic diffusivity, whereas the local structure is dependent inasmuch as the boundary layer widths are functions of R .

References

- Childress, S. 1979, "Alpha-effect in flux ropes and sheets." *Phys. Earth Planet. Inter.*, 20, 172.
- Soward, A.M., 1987. "Fast dynamos with flux expulsion" in *NATO Advanced Research Workshop: Secular Solar and Geomagnetic Variations in the last 10,000 years*, Eds. F. R. Stephenson and A. F. Wolfendale, Durham, U.K. Reidel.

APPLICATION OF THE WIENER-HOPF METHOD TO FAST DYNAMOS

Andrew Soward

School of Mathematics, University of Newcastle-Upon-Tyne
Newcastle-Upon-Tyne NE1 7RU, U.K.

Ongoing research with Professor Childress is reported in which the Wiener-Hopf method is used to calculate the α -effect appropriate to fast dynamos in spatially periodic two-dimensional flows. The motion considered was

$$\mathbf{u} = \nabla \times \psi \mathbf{i}_z + K \psi \mathbf{i}_z \text{ where } \psi = \sin x \sin y + \delta \cos x \cos y \quad (1)$$

and K and δ are constants. When $\delta = 0$, motion consists of spiralling vortices whose boundaries are the streamlines, $\psi = 0$, which connect the stagnation points at $x = n\pi, y = m\pi$ (n, m integers). When $\delta > 0$, the bounding streamlines are either $\psi = \delta$ or $\psi = -\delta$. They form rows of cats' eyes with junction streamlines (see Dombre et al., 1986) at $x = n\pi, y = (N + n)\pi$, (n, N are integers). Each row is distinguished by a distinct value of N , the regions between adjacent rows of cats' eyes in which the streamlines are open and no longer closed.

The objective, which is explained by Professor Childress in his lectures 4 and 6, is to determine the steady magnetic field,

$$\mathbf{B} = \nabla \times A \mathbf{i}_z + K B \mathbf{i}_z \quad (2)$$

which results when there is an applied magnetic field,

$$\bar{\mathbf{B}} = \nabla \times \bar{A} \mathbf{i}_z, \quad \bar{A} = (\bar{\mathbf{B}} \times \mathbf{x}) \cdot \mathbf{i}_z \quad (3)$$

The results are used to calculate the mean EMF,

$$E = \overline{\mathbf{u} \times \mathbf{B}} = K \overline{(\psi \nabla A - B \nabla \psi)} = K R^{-1/2} \boldsymbol{\alpha} \cdot \mathbf{B} \quad (4)$$

Magnetic field is expelled from the cats' eyes. Inside them A takes a constant value which differs from one cat's eye to another. Magnetic boundary layers carry fluid flux of order $R^{-1/2}$, while the channel fluid flux is $O(\delta)$. Their ratio is of order

$$\beta = R^{1/2} \delta \quad (5)$$

When β is of order unity the boundary layer fills the channel and the solution must be found numerically. When β is large, the magnetic boundary layers are triggered at the junction streamlines and are confined to thin layers close to the cat's eye boundaries $\psi = \pm\delta$. In that case a mainstream solution can be found and matched to the cat's eye boundary layers. Since the cats eye boundaries can be treated in isolation, their solution can be found using the Wiener-Hopf method.

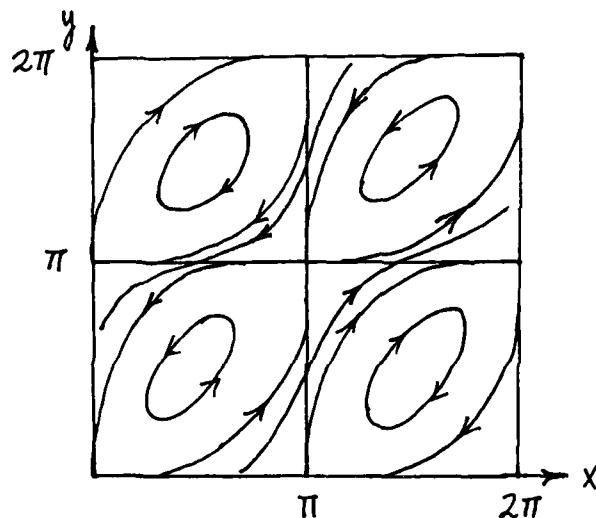


Figure 1

The symmetries of our problem imply that the α -tensor has the form,

$$\alpha = \begin{bmatrix} \alpha_1 & \alpha_2 \\ \alpha_2 & \alpha_1 \end{bmatrix} \quad (6)$$

For the case $\beta \gg 1$, analytic solutions are found. With the two choices $\mathbf{B} = (-1, 1)$, $\mathbf{B} = (1, 1)$ for the mean magnetic field, the mean EMF, \mathbf{E} , yields respectively the results,

$$\begin{aligned} \alpha_1 - \alpha_2 &= -\frac{2}{3}\beta^3 + O(\beta^2) \\ \alpha_1 - \alpha_2 &= -\frac{2\Gamma}{\beta^2} + O(\beta^{-3}) \end{aligned} \quad (7)$$

where Γ is a known constant. In the former case the mean magnetic field is transverse to the channel flows. The channel flows produce long tongues of magnetic field of high field strength which in turn leads to an intense EMF of order β^3 . On the other hand, in the latter case the field is almost aligned with the flow in the channel. Very little induction takes place in the channel. It is confined almost entirely to the boundary layers and is small, of order β^{-2} .

The mean magnetic field has solutions proportional to e^{pt+ikz} . The dispersion relation for such modes is

$$p = -KR^{-1/2}\sqrt{\alpha_1^2 - \alpha_2^2 k} - R^{-1}k^2 \quad (8)$$

The theory is limited by the fact that the vertical length scale is at least comparable with the channel width, δ . Otherwise, vertical diffusion neglected in the α -effect

calculation is not valid. The restriction gives a maximum growth rate whose order of magnitude is

$$K \left(\frac{\beta}{R} \right)^{1/2} k \sim \frac{K}{\beta^{1/2}}, \text{ since } \left(k \sim \frac{1}{\delta} \right), \sim \left(\frac{K}{\delta^{1/2}} \right) R^{-1/4} \quad (9)$$

For fixed β , fast dynamo action may be possible as $R \rightarrow \infty$. For fixed δ , on the other hand, the growth rate tends to zero.

The Wiener-Hopf method can also be used to obtain the solution when $\beta = 0$ (i.e. $\delta = 0$) (See Soward, 1987).

References

- Dombre, T., Frisch, V., Greene, J.M., Henon, M., Mehr, A. and Soward, A.M., 1986. "Chaotic streamlines and Lagrangian turbulence: the ABC flows," *J. Fluid Mech.* 167, 353.
- Soward, A.M., 1987. "Fast dynamo action in a steady flow," *J. Fluid Mech.* 180, 267.

THE LOSS OF INTEGRABILITY

E. A. Spiegel
Department of Astronomy
Columbia University
New York, NY 10027

This abstract is based on work in progress with J. D. Fournier and O. Thual. We are trying to understand the way integrability is lost as we pass through a sequence of p.d.e.s. For definiteness, consider equations of the form

$$\partial_t u + u \partial_x u = \mu_n \partial_x^n u + \mu_{n-2} \partial_x^{n-2} u + \dots, \quad (1)$$

where u depends only on x and t and the μ_k ($k = n, n-2, \dots$ down to three or two) are constants. The idea is abroad (see Ablowitz and Segur for references and explanation) that integrability of an equation like (1) is connected with the Painlevé property. Just how close this connection is, remains a subject for investigation.

To test (1) for the Painlevé property, convert it to an O.D.E. by means of a wave or similarity ansatz. Then look at the movable singularities (see Ince). If they are simple poles, the equation has the Painlevé property.

For a p.d.e., a singularity moves in time along some path $x = X(t)$. In the approach of Weiss, Tabor and Carnavale, one writes this in the form $\phi(x, t) = 0$, which is the equation defining a manifold in which the singularity is found. Then you can look at an expansion like

$$u(x, t) = \phi^{-\alpha}(x, t) \sum_{k=0}^{\infty} u_k(x, t) \phi^k(x, t) \quad (2)$$

where the $u_k(x, t)$ are analytic. The α is found easily. When Weiss, Tabor and Carnavale tried this on the Burgers equation, they found an autoBäcklund transformation that forces you to discover the Hopf-Cole transformation.

We tried this on the Kuramoto-Sivashinsky equation, a paradigm of spatio-temporal chaos, and were led to the transformation that leads exact solutions. That is, in

$$\partial_t u + u \partial_x u = \mu_4 \partial_x^4 u + \mu_2 \partial_x^2 u \quad (3)$$

a truncation of (2) (suggested by the procedure), with $\alpha = 3$, leads to the form (Fournier and Spiegel)

$$u(x, t) = 60 \partial_x^3 \ln \phi + \frac{60}{19} \partial_x \ln \phi \quad (4)$$

and to some exact solutions, including the shock

$$u(x, t) = 6.6 \tanh^3 .38x - 5.4 \tanh .38x, \quad (5)$$

This steady solution, close to one perceived by Kuramoto and Tsuzuki, is equivalent to a traveling wave, by virtue of Galilean invariance.

The finding of a few such solutions, seemingly isolated in a sea of chaotic solutions has perplexed us. It suggests to us that integrability does not disappear abruptly with increasing n , but fades gradually. Is there a last equation with a simple analytic solution like (5), as there is a last KAM surface, or a smile on a cheshire cat? That is what we are brooding on.

Let $\eta = 3 + \epsilon$. Let us look for a steady solution of (1). Then we can at once perform an integral and we are led to study equations like

$$D^{2+\epsilon}X + aD^2X + bDX + cX = X^2 \quad (6)$$

where $X = X(t)$ and $D = d/dt$. For $\epsilon = 0$, we surely have an integrable system. For suitable a, b, c , with $\epsilon = 1$, we get chaos. How does the transition look as ϵ goes from 0 to 1?

To give an idea of what we are up to, let me describe the case

$$D^\alpha X = X^2 \quad (7)$$

In the spirit of Painlevé tests, we try to find the order of the singularity with

$$x(t) = t^{-\alpha}(X_0 + X_\rho t^\rho) \quad (8)$$

(see Ablowitz and Segur for details on such things). We find in leading order that

$$X_0 = \Gamma(-\alpha + 1)/\Gamma(-2\alpha + 1) \quad (9)$$

In next order we get the resonance condition that fixes ρ . With some rearranging, this becomes

$$\frac{\Gamma(\rho + 1 - \alpha)}{\Gamma(\rho + 1 - 2\alpha)} = \frac{\Gamma(-\alpha)}{\Gamma(-2\alpha)} \quad (10)$$

For $\alpha = 2$, this has the roots $\rho = -1$ and $\rho = 6$. For $\alpha = 3$, the roots are -1 and $13/2 \pm i\sqrt{71}/2$. In between we descry various landmarks in this equation whose meaning we have only partly comprehended. But it is clear that the map of the route to nonintegrability will be some time in the making, including the placement of the natural frontiers for general ϵ .

References

- Ablowitz, M.J. and Segur, H., 1981. "Solitons and the Inverse Scattering Transform", *S.I.A.M.*, Philadelphia.
- Ince, E.L., 1981. "Ordinary Differential Equations", *Dover*.
- Weiss, Tabor and Carnevale, 1983. *J. Math. Phys.*, 24, 522.

EVOLUTION OF A LOCALLY UNSTABLE SHEAR FLOW NEAR A WALL OR A COAST

Melvin E. Stern
Department of Oceanography
Florida State University
Tallahassee, Florida 32306-3048

All the Kelvin-Helmholtz waves in an inflected shear layer are stabilized by the presence of a wall or coastal boundary at a certain critical distance from the inflected layer. A given non-parallel flow is said to be "locally stable" if, at all downstream positions, it satisfies this formal stability condition. The nonlinear temporal evolution of such initial states is discussed using a piecewise uniform vorticity model. Numerical integrations of the contour dynamical equations show that sufficiently wide inflectional patches in a locally stable initial state evolve into "locally unstable" states. Large Reynolds stresses are then produced as a vortex forms, and as the unstable patch is ejected above the wall region. The parametric regime in which this finite amplitude instability occurs is sketched on the basis of several numerical runs. It is suggested that this relatively simple model captures a key phase of turbulence production, viz. that which occurs *after* a local spanwise circulation creates an inflected streamwise flow above the wall. "Local instability" is also relevant to the formation of isolated ocean vortices observed in quasi-barotropic coastal currents.

TURBULENT FAST DYNAMOS

Henry Strauss

Courant Institute of Mathematical Sciences
251 Mercer Street
New York, NY 10012

We consider fast kinematic dynamos produced by incompressible, non-parallel shear flows with resonant perturbations. The mean flow depends on a coordinate x and has components in the $y - z$ plane. The perturbations are periodic in y, z . A velocity perturbation consisting of a single Fourier mode produces cats' eyes or islands in the flow. When there are many modes, the islands overlap and the flow becomes chaotic.

We first calculate the mean electric field using first order smoothing. The magnetic perturbations are obtained near the resonances. The resonances have a width which varies as the $1/3$ power of the resistivity. The mean electric field consists of α and β terms, which involve sums containing resonance functions. For this to be valid, the resonance width has to be greater than the island width, which in turn requires that α, β , vanish with the resistivity.

To attempt to remedy this situation, the cross terms in the equations for the magnetic field perturbations, which are quadratic in the perturbations, are taken into account. In an averaged sense, these terms can be modelled by a turbulent resistivity obtained using procedures equivalent to the direct interaction approximation. Using the renormalized, turbulent resistivity, the mean α, β contain broadened resonances whose width is independent of the molecular resistivity, so that the dynamo effect is independent of resistivity.

Some preliminary numerical work was done with a simplified model, in which the z -component of the magnetic field was constant. In the case of a single resonant Fourier mode, the induced magnetic field was localized around the edges of the cat's eye. In the case of many, overlapping cats' eyes, a mean magnetic field in the y -direction is generated in a few turnover times. Short wavelength noise is also generated, which decays in a time which scales as a negative fractional power of the resistivity.

References

Strauss, H., 1986. *Phys. Rev. Lett.* 57, 2231.

Plus other references cited therein.

CURRENT SHEETS IN THE SOLAR CORONA

Henry Strauss and N. Otani
Courant Institute of Mathematical Sciences
251 Mercer Street
New York, NY 10012

Coronal magnetic fields are twisted up by motion of their footpoints in the photosphere. Parker has argued that in general the magnetic field in the corona does not have a smooth equilibrium, but instead current sheets form. This permits relatively rapid dissipation of magnetic energy and heats the corona. On the other hand, Van Ballegooijen has shown that smooth equilibria can exist.

We investigate the problem numerically. We first find two-dimensional smooth equilibria, which are produced by twisting the magnetic field. The amount of twist, and the current, grow linearly in time. Once a threshold is exceeded, the equilibrium becomes unstable to a kind of kink mode. Nonlinearly, the instability appears to produce current sheets, as found in the helically symmetric case by Rosenbluth et al.

References

- H. Strauss and N. Otani, 1987. submitted to *Ap. J.*.
Rosenbluth, M.N., Dagoyian, R.Y. and Rutherford, P.H., 1973. *Phys. Fluids*, 16, 1894.

OCEAN CIRCULATION DRIVEN BY WIND AND BUOYANCY

George Veronis
Kline Geological Laboratory
Box 6666
Yale University
New Haven, CT 06511

The subtropical, anti-cyclonic gyre in the North Atlantic exhibits a north-south asymmetry (an eastward jet in the north and a slower, westward flow in the south) which is much more pronounced than any such structure in the driving wind-stress. Associated with the asymmetry is a deep thermocline just south of the Gulf Stream. Measurements of air-sea exchanges indicate maximum cooling of the surface water in that region.

A three-layer model with the bottom layer at rest has been constructed to study the combined driving by wind-stress and surface cooling in the N. Atlantic, and in particular, to determine whether buoyancy driving can account for the asymmetric behavior described above. The model requires that the layer thicknesses be known on the eastern boundary. The wind stress is zonal, a sinusoidal function of latitude, and independent of longitude. The buoyancy driving is parameterized as a vertical velocity across the bottom of the upper layer which is written as $w = k(h_m - h_1)$, where k is a constant decay-time, h_m is a constant depth ($= 200m$), and h_1 is the thickness of the upper layer. The rationale for this choice is that a deep upper layer corresponds to a warm surface temperature, so as the upper layer becomes deeper, the cooling (manifested here as a flux of water from upper to middle layer across the interface) increases.

The model is geostrophic (except for the wind-stress) and hydrostatic. The motion is assumed to be steady. There is no stress across either interface. No limitation is imposed on the variation of the layer thicknesses. In particular, a layer thickness may vanish.

The equations for the interior can be reduced to a combination of two equations involving h_1 and h (where $h = h_1 + h_2$ and h_2 is the middle layer thickness). The calculation reduces essentially to a characteristic integration of a first-order, hyperbolic partial differential equation. Characteristics from the eastern boundary penetrate only the eastern and southern parts of the subtropical basin and leave bare a northwestern region, which we identify with the recirculation region south of the Gulf Stream. A method has been devised to determine values of the thicknesses needed to extend the calculation throughout the recirculation region.

The analysis is extended to the subpolar basin where the wind stress is cyclonic. Upper-layer water covers only an eastern strip of the subpolar basin.

A western boundary current is added to the upper layer so that mass conservation is satisfied. This current is dynamically required to separate from the western

boundary at about 33°N and to cross the subtropical basin eastward and northward into the subpolar basin. The final picture shows a circulation with a separated Gulf Stream, to the south of which lies the recirculation region. Thus, it exhibits the observed north-south asymmetry. An added consequence of cooling is an increase of the Gulf Stream transport by about 50% at the point where it separates from the western boundary. Thus, an enhanced transport is obtained but it is clear that other processes, such as inertial effects and eddies, must be responsible for the much larger transport that is observed.

TOY SYSTEMS AND STELLAR DYNAMOS

Nigel Weiss

D.A.M.T.P., University of Cambridge
Cambridge CB3 9EW, U.K.

Magnetic activity can be detected in many lower main-sequence stars like the sun, which have deep outer convective zones. Solar activity is comparatively weak: sunspots cover only a small fraction of the surface of the sun and produce variations of order 0.1% in its luminosity. The most active stars have fields comparable to those in sunspots over half their surface area and starspots can lead to variations of order 50% in luminosity as a star rotates. X-ray observations confirm that these stars have hot coronae, which are magnetically heated and responsible for stellar winds. Systematic observations of Ca^+ emission from late-type stars show that the degree of activity depends both on the mass and the age of a star (Baliunas and Vaughan, 1985). Stars of given mass have a wide range of activity. The youngest, most rapidly rotating stars are the most active, while older stars rotate more slowly and are magnetically feeble. The rate at which they lose angular momentum depends on the strength of the magnetic field that is carried outwards by the stellar wind. Thus a star rotates rapidly when it arrives on the main sequence and is quickly spun down by magnetic braking; as its angular velocity Ω decreases it becomes less active and the rate of magnetic braking is correspondingly decreased. Cyclic variations of activity with periods of order 10 years seem to be a normal feature of slow rotators like the sun and the cycle period P_c apparently increases as Ω decreases. The available data are consistent with a power law of the form $P_c \propto \Omega^{-n}$ with $n = 1.3 \pm 0.5$ (Noyes et al., 1984).

Solar activity has been studied in detail for 380 years. Magnetic flux erupts to form active regions within which sunspots are located and the zones of activity migrate towards the solar equator. Activity varies aperiodically with a mean period of 11 years but the sense of the magnetic field alternates so that the magnetic cycle has a 22 year period. Activity is modulated on a longer timescale by grand minima, such as the Maunder minimum of the 17th century. These episodes affect the rate of production of ^{14}C in the earth's atmosphere and so the envelope of the activity cycle can be determined over the last 9000 years (Stuiver et al., 1986). Grand minima recur irregularly with a characteristic spacing of about 200 years and solar activity appears to be an example of deterministic chaos.

Hydromagnetic dynamos provide the only plausible explanation for the magnetic fields in stars like the sun, which oscillate with a period much shorter than the diffusive timescale ($\sim 10^{10}$ years) for a star. Self-consistent magnetohydrodynamic calculations confirm that nonlinear dynamo waves can be maintained by convection in a rotating system (e.g., Gilman, 1983). Much attention has been devoted to mean field dynamo models, where dynamo action occurs when a dimensionless parameter D (the dynamo number) exceeds some critical value. Now $D \propto (\Omega\tau_c)^2$ where τ_c is

an appropriate convective timescale, and it is significant that stellar activity appears to be a function of the inverse Rossby number $\Omega\tau_c$ only. Moreover, observations of torsional oscillations with a period of 11 years on the sun suggest that the effect of the Lorentz force on the angular velocity may be an important nonlinear equilibration mechanism.

An alternative approach to dynamo theory is to construct low order model systems and to investigate their bifurcation structures. Such systems may be derived by some asymptotic procedure or by truncating a modal expansion or they may describe a realizable configuration (e.g., disc dynamos). Alternatively, toy systems may be designed to capture the essential physics of a nonlinear problem (c.f. Kennett, 1976). One such procedure, followed by F. Cattaneo, C. A. Jones and myself, is to generalize Parker's (1979) linear dynamo waves by adding suitable nonlinear terms to the equations and comparing the behavior of these low order systems with observations of solar and stellar magnetic fields (Weiss et al., 1984; Noyes et al., 1984).

In these toy models the magnetic field B is complex and has a toroidal component $B(t)$ and a poloidal component described by a vector potential $A(t)$. The simplest system has the form

$$\begin{aligned}\dot{A} &= 2D(1 + \kappa |B|^2)^{-1}B - A \\ \dot{B} &= iA - (1 + \lambda |B|^2)B\end{aligned}\quad (1)$$

where κ, λ are positive constants. This system has a trivial (field-free) solution $A = B = 0$. If $\kappa = \lambda = 0$ the system is linear and the trivial solution undergoes a Hopf bifurcation at $D = 1$; for $D > 1$ these are unstable dynamo waves with a frequency $p_0 = D^{1/2}$ in the linear problem. If $\lambda = 0$, so the only nonlinearity involves quenching of the α -effect by the magnetic field, the effective dynamo number $D_e = (1 + \kappa |B|^2)^{-1}D$ and the frequency of the oscillations remains constant in the nonlinear regime, which contradicts the observations. On the other hand, if $\kappa = 0$, so equilibration relies on enhanced diffusion through magnetic buoyancy, then the cycle frequency increases with increasing D . More precisely, the system (1) possesses nonlinear solutions of the form

$$\begin{aligned}B &= be^{ipt} \\ A &= 2Dabe^{i(pt+\phi)}\end{aligned}\quad (2)$$

where a, b, p and ϕ are real. Substitution from (2) into (1) yields the relations

$$\begin{aligned}p^2 &= 1 + \lambda b^2 \\ p(1 + \kappa b^2)(2 + \lambda b^2) - 2D &= 0\end{aligned}\quad (3)$$

It follows that when $\lambda = 0$, $p = 1$, $\phi = -\pi/4$ and $b^2 = (D - 1)/\kappa$. When $\kappa = 0$, $p^3 + p - 2D = 0$ so $p \sim (2D)^{1/3} \propto \Omega^{2/3}$ and $b \sim (2D)^{1/3}/\lambda^{1/2}$, which is compatible with observations. Moreover these solutions are all stable.

A more interesting system is obtained by considering the effect of the Lorentz force on the velocity shear. Since $\mathbf{j} \times \mathbf{B}$ is quadratic in \mathbf{B} the shear has a real spatially uniform component ω_o and a (complex) component ω with twice the spatial frequency of the dynamo waves. The resulting seventh order system has the form

$$\begin{aligned}\dot{A} &= 2DB - A \\ \dot{B} &= i(l + \omega_o)A - \frac{1}{2}iA^* \omega - B \\ \dot{\omega}_o &= \frac{1}{2}i(A^* B - AB^*) - \nu_o \omega_o \\ \dot{\omega} &= -iAB - \nu \omega\end{aligned}\tag{4}$$

where ν_o, ν are positive constants representing viscous braking. By letting $\nu \rightarrow \infty$ we obtain a fifth order system with ω_o only, which again possesses a solution of the form (2), with ω_o a constant. Once again this solution is stable for all $D > 1$ but it has the properties $p = 1, b^2 = \nu_o(D - 1)/D^2$: as D increases, the cycle frequency remains constant while the toroidal field actually decreases for $D > 2$. So this model is incompatible with the observed behavior of stellar magnetic fields.

The most interesting model is the sixth order system obtained by letting $\nu \rightarrow \infty$ so that only ω is present. There is again a periodic solution with $\omega \propto \exp(2ipt)$; for $\nu = 2, p = D$ and $b^2 \sim D^2$, which is just compatible with observations. This nonlinear solution is, however, unstable when $\nu < 1$. For $\nu = 1/2$ there are two further Hopf bifurcations, leading to quasiperiodic behavior, followed by frequency locking and a transition to chaos via a cascade of period-doubling bifurcations (Jones et al., 1985), as described by Cattaneo in these proceedings. The chaotic solutions exhibit modulation, with episodes of reduced activity, that resembles grand minima in solar activity. This suggests that the envelope of the solar cycle, as preserved in the ^{14}C record, bears the signature of a transition from quasiperiodicity to chaos with a "ghost attractor" affecting solutions in the chaotic regime.

References

- Bakunas, S. L. and Vaughan, A. H., 1985. *Ann. Rev. Astron. Astrophys.*, **23**, 3.
 Gilman, P. A., 1983. *Astrophys. J. Suppl. Ser.*, **53**, 243.
 Jones, C. A., Weiss, N. O. and Cattaneo, F., 1985. *Physica*, **14D**, 161.
 Kennett, R. G., 1976. *Stud. Appl. Math.*, **55**, 65.
 Noyes, R. W., Weiss, N. O. and Vaughan, A. H., 1984. *Astrophys. J.*, **287**, 769.
 Parker, E. N., 1979. *Cosmical Magnetic Fields*, Clarendon Press, Oxford.
 Stuiver, M., Pearson, G. W. and Braziunas, I., 1986. *Radiocarbon*, **28**, 980.
 Weiss, N. O., Cattaneo, F. and Jones, C. A., 1984. *Geophys. Astrophys. Fluid Dyn.*, **30**, 305.

NONLINEAR CORNER FLOWS ON A β -PLANE

William R. Young

Department of Earth, Atmospheric, & Planetary Sciences

Massachusetts Institute of Technology

Cambridge, MA 02139

A sub-basin scale recirculation can be driven by imposing low values of potential vorticity in the northwest corner of a β -plane box. Mesoscale eddies, parametrized by lateral potential vorticity diffusion, carry this anomaly into the interior and establish the mean flow. While the structure of the flow is not sensitive to details of the boundary forcing or to the size of the diffusion coefficient, κ , the amplitude and length scale are. For instance, as κ is reduced, the maximum transport scales as $\kappa^{1/2}$ and the Reynolds number as $\kappa^{-1/2}$.

References

- Ierley, G.R., and Young, W.R., 1987. Nonlinear corner flows on a β -plane, *J. Phys. Oceanogr.*, submitted.

1987 Summer Study Program

in

Geophysical Fluid Dynamics

REPORTS OF FELLOWS

THE INSTABILITY OF AN ELLIPTICAL FLOW IN THE PRESENCE OF A MAGNETIC FIELD

Lorna Brazell
University of Cambridge

Introduction

The existence of growing instabilities in an inviscid two-dimensional elliptical flow was studied by Bayly (1986), who found them to take their fundamental modes to be plane waves, of which the wavevector rotates elliptically about the vertical axis. The behavior of waves in conducting fluids such as the solar plasma or the outer core of the Earth is of interest in order better to understand their observed magnetic fields. The waves which arise in an ordinary flow, whose wavevector is not time-dependent, are well understood and the effects on them of magnetic and Coriolis forces are known, since in this case the governing equations can be solved analytically (e.g. Priest, 1982). As a large part of the analysis applies equally to the elliptical problem, I give it here - and also for comparison later.

The system considered is an inviscid, incompressible fluid of constant density and zero magnetic diffusivity. Cartesian coordinates are used, of which the z axis is also the rotation axis; the basic fluid flow is elliptical in the x - y plane with no variation in the z direction, and there is also a steady, uniform magnetic field present. This is shown in Figure 1.1

In the rotating frame, the equations are in standard notation:

$$(i) \quad \partial_t \underline{B} = \nabla \wedge (\underline{u} \wedge \underline{B}) \quad \text{- the induction equation}$$

$$\rho (\partial_t + \underline{u} \cdot \nabla) \underline{u} = -\nabla p + \frac{1}{\mu} (\nabla \wedge \underline{B}) \wedge \underline{B} - 2\rho \underline{\Omega} \wedge \underline{u}$$

- the momentum equation

$$\nabla \cdot \underline{u} = 0$$

$$\text{and } \nabla \cdot \underline{B} = 0$$

It is convenient to divide through the momentum equation by the density and to normalize the pressure and magnetic induction by

$$p \rightarrow \frac{p}{\rho} \quad \underline{B} \rightarrow \frac{\underline{B}}{\sqrt{\mu \rho}}$$

Then

$$(ii) \quad (\partial_t + \underline{u} \cdot \nabla) \underline{u} = -\nabla p + (\nabla \wedge \underline{B}) \wedge \underline{B} - 2\underline{\Omega} \wedge \underline{u}$$

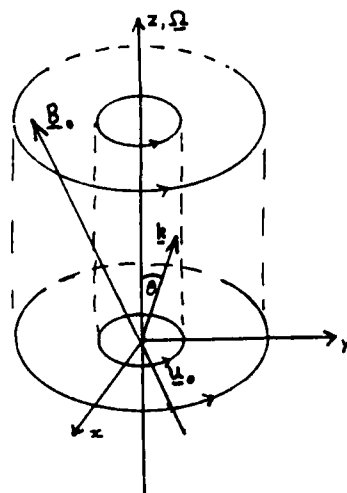


Figure F1.1: The geometry of the system.

The new B has the dimensions of velocity and is the Alfvén speed at which Alfvén waves would travel in a fluid not subject to other forces.

To investigate departures from equilibrium, the velocity, pressure and magnetic field can be written in terms of mean quantities and small perturbations (denoted by $'$):

$$\begin{aligned}\underline{u} &= \underline{u}' \\ \rho &= \rho_0 + \rho' \\ \underline{B} &= \underline{B}_0 + \underline{B}'\end{aligned}$$

Substituting these expressions into the equation (i) and (ii) and neglecting products of small quantities gives, for the perturbations:

$$(iii) \quad \partial_t \underline{u}' = -\underline{\nabla} \rho' + (\underline{\nabla} \wedge \underline{B}') \wedge \underline{B}_0 - 2\Omega \wedge \underline{u}'$$

$$(iv) \quad \partial_t \underline{B}' = \underline{\nabla} \wedge (\underline{u}' \wedge \underline{B}_0)$$

$$\text{Also } \underline{\nabla} \cdot \underline{u}' = \underline{\nabla} \cdot \underline{B}' = 0$$

Differentiating (iii) again with respect to time and substituting (iv) in leaves

$$(v) \quad \partial_t^2 \underline{u}' = \underline{\nabla} \wedge (\underline{\nabla} \wedge (\underline{u}' \wedge \underline{B}_0)) \wedge \underline{B}_0 - 2\Omega \wedge \partial_t \underline{u}'$$

Plane wave solutions would have the forms

$$(\underline{u}', \underline{B}') = (\underline{v}, \underline{b}) e^{i(\underline{k} \cdot \underline{x} - \omega t)}$$

where \underline{v} and \underline{b} are independent of time. With these forms the operations ∂_t and ∇ become $-i\omega$ and $i\mathbf{k}$ respectively. So the equation (v) becomes

$$\omega^2 \underline{v} = -2i\omega \underline{\Omega} \wedge \underline{v} + [\mathbf{k} \wedge (\mathbf{k} \wedge (\underline{v} \wedge \underline{B}_0))] \wedge \underline{B}_0$$

Taking the vector product of \mathbf{k} with this equation gives the dispersion relation

$$(vi) \quad \omega^2 \mp \frac{2\mathbf{k} \cdot \underline{\Omega}}{k} - (\mathbf{k} \cdot \underline{B}_0)^2 = 0$$

which may also be written in terms of the frequencies ω_I and ω_A obtained in the purely inertial and purely magnetic limits, as

$$\omega^2 \mp \omega_I \omega - \omega_A^2 = 0$$

If ω_A is much larger than ω_I , the Coriolis force produces a small frequency splitting of the Alfvén waves, when \mathbf{k} , $\underline{\Omega}$ and \underline{B}_0 are roughly parallel. If ω_I is larger, inertial waves and slow hydromagnetic inertial waves are produced.

In the elliptic flow case without rotation or magnetic field, Bayly (1986) found that the waves were destabilized; the instabilities were independent of length scale and were found in a well-defined band of angles of \mathbf{k} to the vertical axis. This range increased with increasing ellipticity of the flow, as did the maximum growth rate of the instability. The critical angle θ_c , from which the band opened at ellipticities slightly larger than 1, was in this case $\pi/3$. These results are shown in Figure 1.2.

Theory

Equations (i) and (ii) apply also to the elliptical case, but the mean part of the velocity is no longer zero; the expression for velocity is

$$\underline{u} = \underline{u}_0 + \underline{u}'$$

F1.4

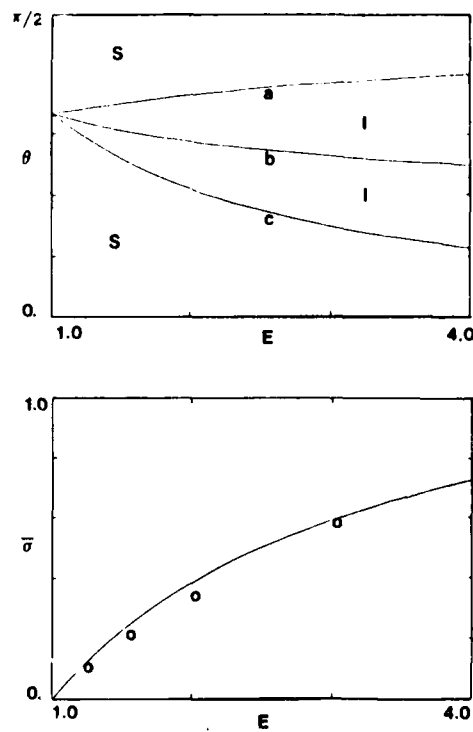


Figure F1.2: From Bayly (1986)

where $\underline{u}_0 = \Omega, A \underline{x}$ and $A = \begin{pmatrix} 0 & -E & 0 \\ E & 0 & 0 \\ 0 & 0 & 0 \end{pmatrix}$

that is, represents a flow with ellipticity E in the x-y plane that is zero in the z-direction. Then the linearized equations for the perturbation quantities become

$$\partial_t \underline{u}' + \underline{u}_0 \cdot \nabla \underline{u}' + \underline{u}' \cdot \nabla \underline{u}_0 = -\nabla p' + [(\underline{B}_0 \cdot \nabla) \underline{B}' + (\underline{B}' \cdot \nabla) \underline{B}_0 - \nabla (\underline{B}_0 \cdot \underline{B}')] - 2\Omega \wedge \underline{u}'$$

after expanding the Lorentz force term;

$$\partial_t \underline{B}' + \underline{u}_0 \cdot \nabla \underline{B}' + \underline{u}' \cdot \nabla \underline{B}_0 = \underline{B}_0 \cdot \nabla \underline{u}' + \underline{B}' \cdot \nabla \underline{u}_0$$

$$\nabla \cdot \underline{B}' = \nabla \cdot \underline{u}' = 0$$

or, taking account of the form of \underline{u}_0 ,

$$\partial_t \underline{u}' + \Omega_c A \underline{x} \cdot \nabla \underline{u}' + \Omega_c A \underline{u}' = -\nabla(p' + \underline{B}_0 \cdot \underline{B}') + \underline{B}_0 \cdot \nabla \underline{B}' - 2\Omega_c \underline{n} \underline{u}'$$

combining the magnetic and fluid pressures into one term;

$$\partial_t \underline{B}' + \Omega_c A \underline{x} \cdot \nabla \underline{B}' = \underline{B}_0 \cdot \nabla \underline{u}' + \Omega_c A \underline{B}'$$

Again assume the small quantities have the form of plane waves, but now the wavevector \underline{k} is time-dependent, i.e.

$$(\underline{u}', \underline{B}', p') = (\underline{v}(t), \underline{b}(t), \phi(t)) e^{i\underline{k}(t) \cdot \underline{x}}$$

Then

$$\begin{aligned} \dot{\underline{v}} + i\dot{\underline{k}} \cdot \underline{x} \underline{v} + i\Omega_c A \underline{x} \cdot \underline{k} \underline{v} + \Omega_c A \underline{v} &= i\dot{\underline{k}}(\phi + \underline{B}_0 \cdot \underline{b}) + i\dot{\underline{k}} \cdot \underline{B}_0 \underline{b} - 2\Omega_c \underline{n} \underline{v} \\ \dot{\underline{b}} + i\dot{\underline{k}} \cdot \underline{x} \underline{b} + i\Omega_c A \underline{x} \cdot \underline{k} \underline{b} &= i\dot{\underline{k}} \cdot \underline{B}_0 \underline{b} + \Omega_c A \underline{b} \\ \underline{k} \cdot \underline{b} &= \underline{k} \cdot \underline{v} = 0 \end{aligned}$$

The terms proportional to \underline{x} must cancel, so

$$\dot{\underline{k}} + \Omega_c A \underline{k} = 0$$

which has general solution

$$\underline{k}(t) = \underline{k}_0 (\sin \Theta \cos \Omega_c(t-t_0), \mp \sin \Theta \sin \Omega_c(t-t_0), \cos \Theta)$$

The remaining equations are then, in component form

$$\begin{aligned}\dot{v}_j + \Omega_i A_{jk} v_k &= -ik_j (\phi + B_0 b) + ik_i B_{0j} b_j - 2\Omega_{ij} v_j \\ b_r &= ik_i B_{0r} v_r + \Omega_i A_{rs} b_s\end{aligned}$$

Contracting the velocity equation with the tensor $(\delta_{ij} - k^i k^j / k^2)$ projects out the pressure term. Noting that

$$\underline{k} \cdot \underline{v} = \underline{k} \cdot \underline{\dot{v}}$$

then

$$\begin{aligned}\dot{v}_i &= i\gamma b_i + (2\frac{k_i k_j}{k^2} - \delta_{ij})(A_{jk} + \frac{\Omega_{jk}}{\Omega_i}) v_k - \frac{\Omega_{ik}}{\Omega_i} v_i \\ b_r &= i\gamma v_r + A_{rs} b_s\end{aligned}$$

The dimensionless parameter γ , which is the scalar product of \underline{k} and \underline{B}_0 now expresses the effect of the main field on the disturbances; it is the ratio of the frequency of the Alfvén waves to that of the basic flow. It can also be seen as the projection of the magnetic field \underline{B}_0 onto the wavevector – an important consequence being that it is impossible to investigate the effect of varying the direction of \underline{B}_0 explicitly. Instead, changing γ can be viewed as changing the wavelength of the perturbations for fixed component of \underline{B}_0 parallel to them, or as changing the field strength for fixed wavelength and angle of field to the wavevector.

The equations obtained are four coupled linear ordinary differential equations with periodic coefficients, so that a natural approach to solving them is to use Floquet theory.

The fundamental solution matrix $(u_{ij}(t))$ of such a system satisfies:

$$u_{ij} = A_{ik}(t) u_{kj} \quad \text{and} \quad u_{ij}(0) = \delta_{ij}$$

where

$$\dot{x}_i = A_{ij}(t) x_j \quad \text{and} \quad x_i(0) = x_i^0$$

are the original equations. Then the general solution is

$$\begin{aligned} x_i(t) &= U_{ij}(t) x_j^0 \\ &= e^{\pi i} f_i(x_i(t, t)) \quad \text{— a superposition of Floquet modes} \end{aligned}$$

where $f(a)$ is periodic with period 2π . The exponent $e^{\sigma T}$ is an eigenvalue of $U_{ij}(T)$. Since $U_{ij}(t)$ also solves matrix equations where

$$\dot{V}_{ij}(t) = A_{im}(t) V_{mj}(t) \quad \text{and} \quad V_{ij}(0) = V_{ij}^0$$

with

$$\dot{V}_{ij}(t) = U_{im}(t) V_{mj}^0$$

then if $A(t+T) = A(t)$ for all t ,

$$V(t) = U(t+T) \quad \text{if} \quad V(0) = U(T)$$

$$\Rightarrow V(t) = U(t)U(T)$$

$$\Rightarrow U(2T) = U^2(T)$$

or in general,

$$U(nT) = U^n(T)$$

Then as t tends to infinity such a matrix and its eigenvalues simply reemultiplied. In order to find out if the superposition of Floquet modes solving the original equations grow exponentially, it is only necessary to find if there are eigenvalues of $U(T)$ that

are real and greater than one. The growth rate is given by

$$\sigma(\alpha) = \frac{1}{T} \log \mu(\alpha)$$

where $\mu(\alpha)$ are the eigenvalues.

Method

The matrix $U(T)$ was found by integrating the equation coefficients over a period of 2π – which was in fact twice the period of the coefficient since these only include trigonometric quantities in quadratic form. This led to some spurious apparently real eigenvalues being found where the actual ones were purely imaginary; however these had negative real parts and so stood out. Isaac's fourth order Runge-Kutta routine was used for the integration. A range of values of γ and Ω were studied, both separately and in combination.

Tests

The program was checked by running the non-elliptical and elliptical non-magnetic cases and comparing the output with the results of theory and those in Bayly (1986). Some eigenvalues for magnetoinertial waves in the rigid rotating case were also found and compared with the predicted $e^{2\pi i \omega}$, where ω is given by the dispersion relation, equation (vi) of the Introduction. At all times Ω_1 was taken to be 1. The program stepped through θ and so could not produce the smooth curves of Figure 1.2; for comparison Figure 1.3 shows the equivalent 'curve' it produces for the elliptical, non-rotating and non-magnetic case. In all subsequent figures the stepped, smoothed form is due to this and to the plotting program.

Results

(a) *Non-rotating case.* For values of γ less than about 1.0, the relation of E to σ , θ are virtually the same as the purely inertial case (Figure 1.4.). For all γ the width of the band of instabilities increases as E increases. In almost all cases; that is until near the extinction point, the maximum growth rate increases monotonically with E .

Near γ equal to one, the point of onset of instabilities begins to move away from ellipticity one (Figure 1.5), and the change in this onset ellipticity increases more rapidly for γ above root 3. The rate of increase of maximum growth rate with E decreases for γ greater than one and the curve flattens out to look like a line of progressively decreasing slope, at and above γ equal to root 3 (Figure 1.6). The exception to this decreasing slope is that the line is slightly steeper when γ is 2 than when γ is root 3. Finally, somewhere between 2.6 and 3.0 the instabilities are

GAMMA=0.00

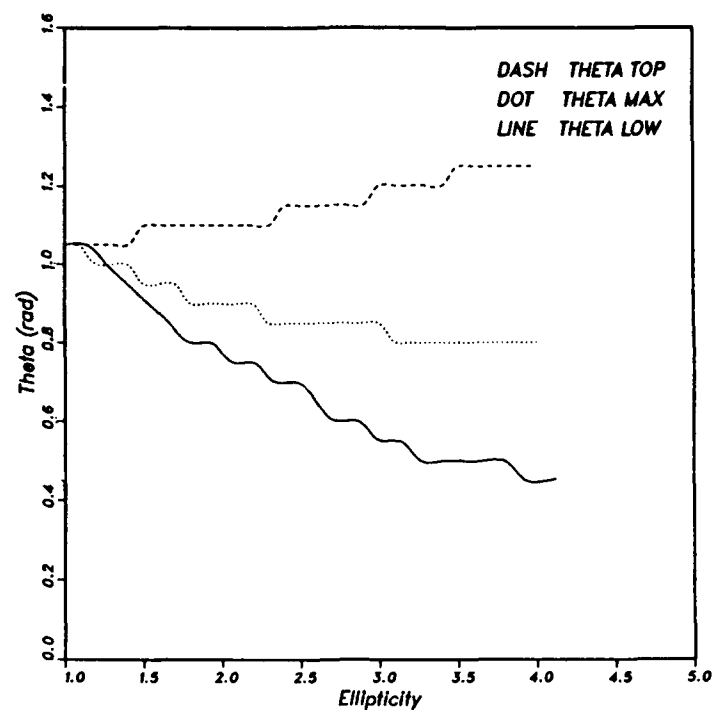


Figure F1.3

GAMMA=0.50

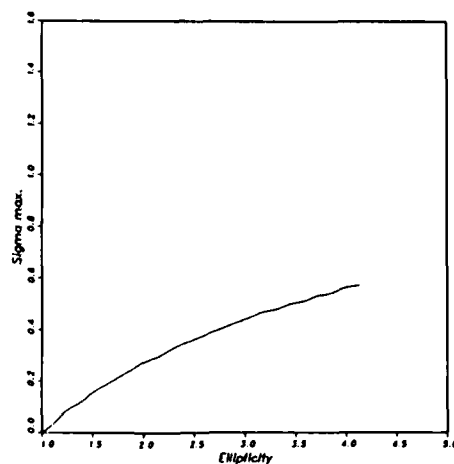


Figure F1.4

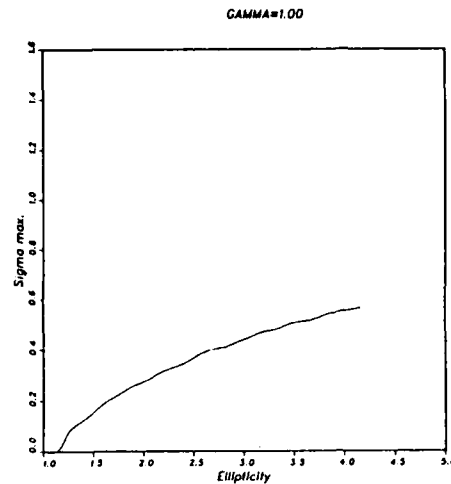


Figure F1.5

completely suppressed. Near this point the neat band structure become confused: when γ is 2.6 there is a small range of ellipticities for which the waves are unstable, but then they become briefly stable again before the 'usual' band opens. This is shown in Figure 1.7.

The band of angles in which instability arose tended to decrease as γ increased, but there were exceptions where γ was 1.5 and 2.5 (Figure 1.8). Also, in the case where γ was unit, a second very narrow band of marginally unstable waves seemed to be present below the main one (Figure 1.9). Apart from the presence of this line, the 'critical' angle increased steadily with increasing γ until it reached $\pi/2$, when it jumped back to 0.85 radians and began increasing again.

At a few points only two of the four eigenvalues were real, which means either the fluid on the magnetic waves were unstable but not, as elsewhere, both. It is not clear why nor which remained stable.

(b) *Non-magnetic case.* A rotation rate of 0.1 barely affected the results of the non-rotating case, but for an Ω of 0.5 the onset ellipticity for the instabilities was no longer 1. For a rotation rate of 1, surprisingly the instabilities again began at ellipticity 1, although with reduced maximum growth rate. For higher rotation rates, the onset ellipticity was roughly 1.5 and constant and the maximum growth meter decreased only slightly for Ω up to 3; their trace never became linear.

As before, the band of angles broadened as ellipticity increased and decreased as Ω increased. The critical angle increased continuously but slowly as Ω increased and never reached $\pi/2$. All points which had real eigenvalues had only two of them real.

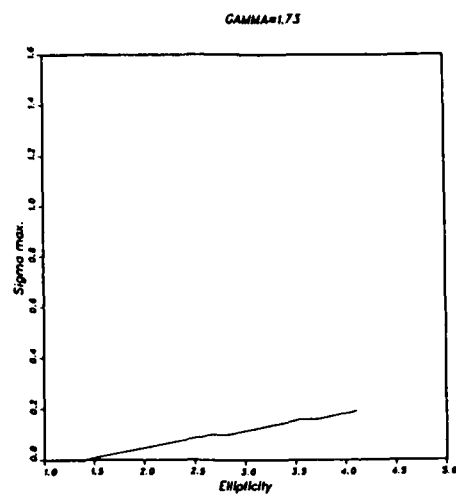


Figure F1.6

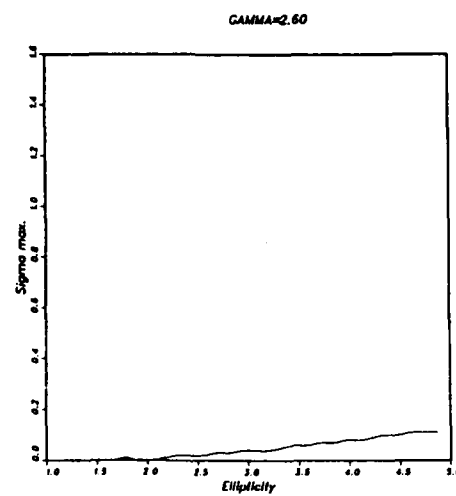


Figure F1.7

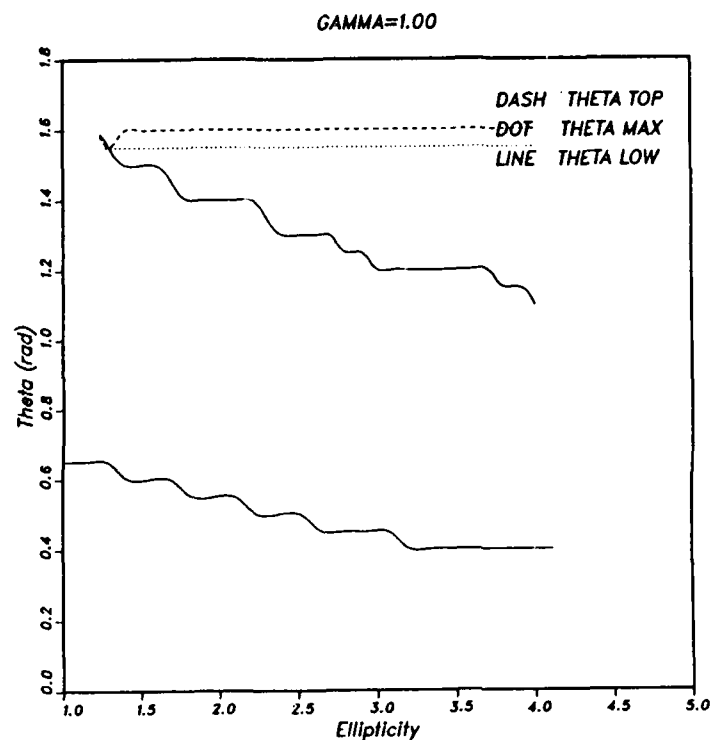


Figure F1.8

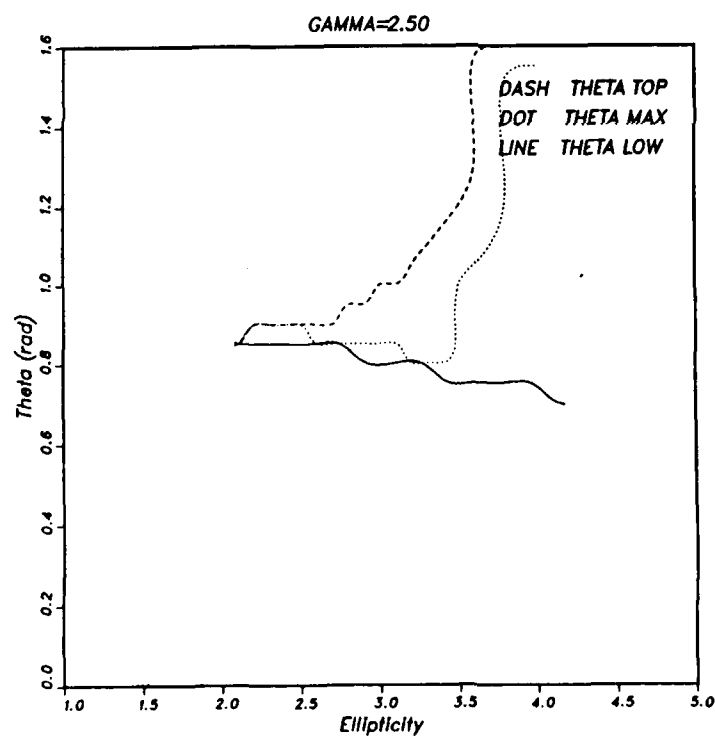


Figure F1.9

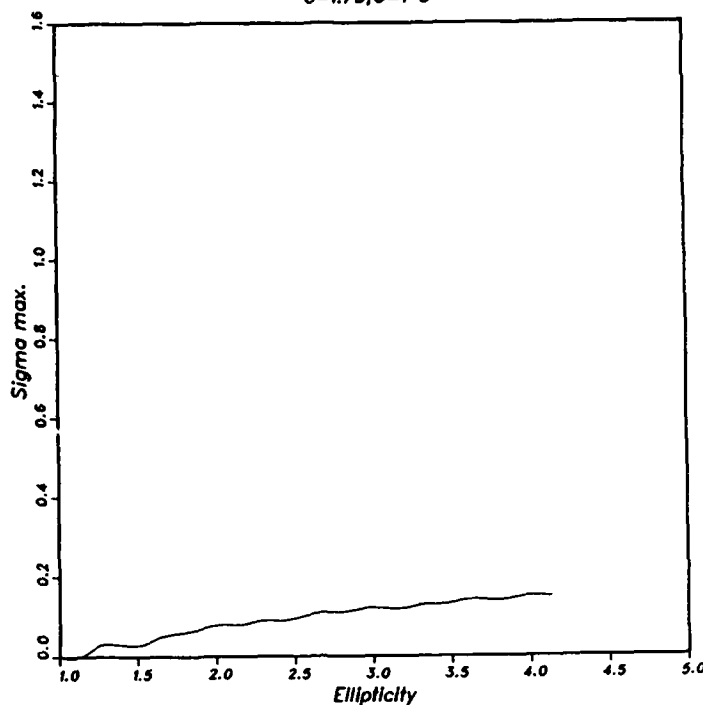


Figure F1.10

(c) *Rotating, magnetic case.* The results obtained with both γ and Ω non-zero look in most cases similar to those with Ω zero – but there are many small differences and a few large ones.

Where γ is small a small rotation rate has little effect but a larger one (Ω greater than one) delays the onset of instability to a higher ellipticity, where the curve of maximum growth rate is initially steeper but then as with zero Ω .

When γ is medium sized (1.73) the interaction is most complicated. A small rotation leads to instability in less elliptical flow but a rate greater than 1 delays the onset. The case where Ω is one gives a higher maximum growth rate at any ellipticity than any other rotation rate except zero – and higher even than that for ellipticities up to about 3.0 (compare Figures 1.6 and 1.10). Only one other case (γ 2.5 and Ω 0.1) gave a higher rate than the non-rotating equivalent, and there the increase is comparable to the numerical error.

At high γ , any rotation destabilized the waves compared to the non-rotating case, so that when γ is 3.0 instabilities are seen intermittently at rotation rate 1 and the usual continuous band appeared by Ω equal to 2.

At a given rotation rate, the variation in maximum growth rate with γ was much the same as the non-rotating case.

For small and large (but not intermediate) γ , the appearance of the band of angles where instabilities occur was like the non-rotating versions; the lower limit moved steadily up with increasing rotation rate, as did the critical angle, giving a

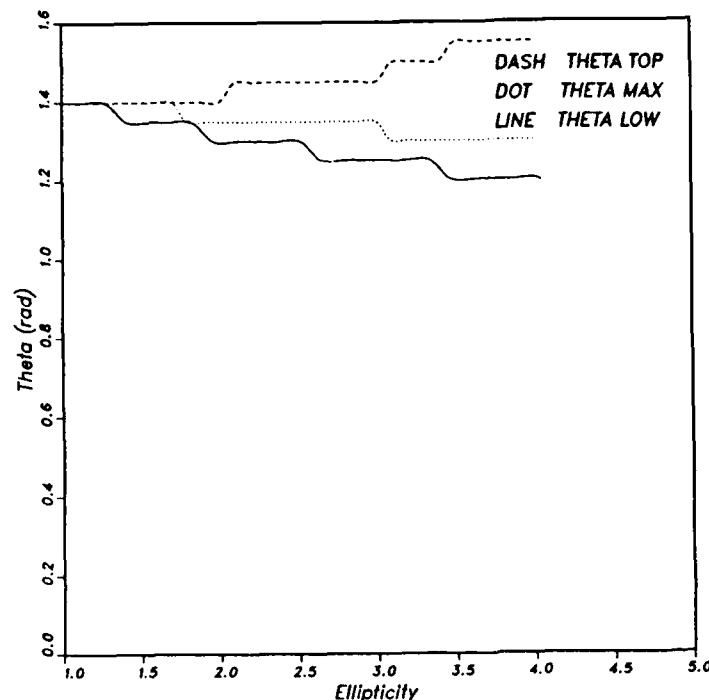


Figure F1.11

band whose width increased as the ellipticity did as in the previous case – but the critical angle never reached $\pi/2$ and did not jump down again. Figures 1.11 and 1.12 show examples where γ is small. Usually θ_{max} trends downwards. The case where γ is 2.5 is again exceptional with a broad band whose upper limit falls at one point, and θ_{max} increases (Figure 1.13). For higher γ a thin, wholly downward trending band whose width did not increase was seen (Figure 1.14).

The intermediate value of γ studied, 1.73 or square root of 3, showed a double band for all rotation rates above 0.1. The second band appeared at a higher critical angle than the first and at a higher ellipticity of the main flow. For small rotation rates it was broader than the lower band and the angle at which maximum growth rate occurred moved to this band when it appeared (Figure 1.15). Both bands showed higher critical angles at higher rotation rates so that eventually the upper band was squeezed thinner than the lower and the maximum growth angle remained in the lower one (Figure 1.16).

In some cases instability was present for ellipticities near 1 but then there was a break where all was stable: the plotting program could not cope with this so it is not shown. Another observation is that in general when rotation is present only two eigenvalues are real where there is instability; if all four velocity and magnetic components are destabilized it is in a narrow band of angles usually just above the lower limit shown.

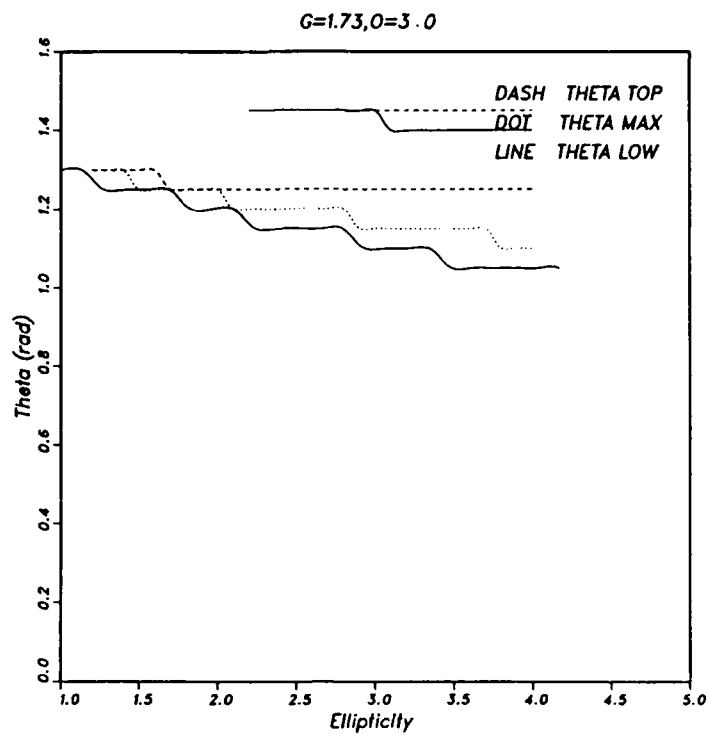


Figure F1.12

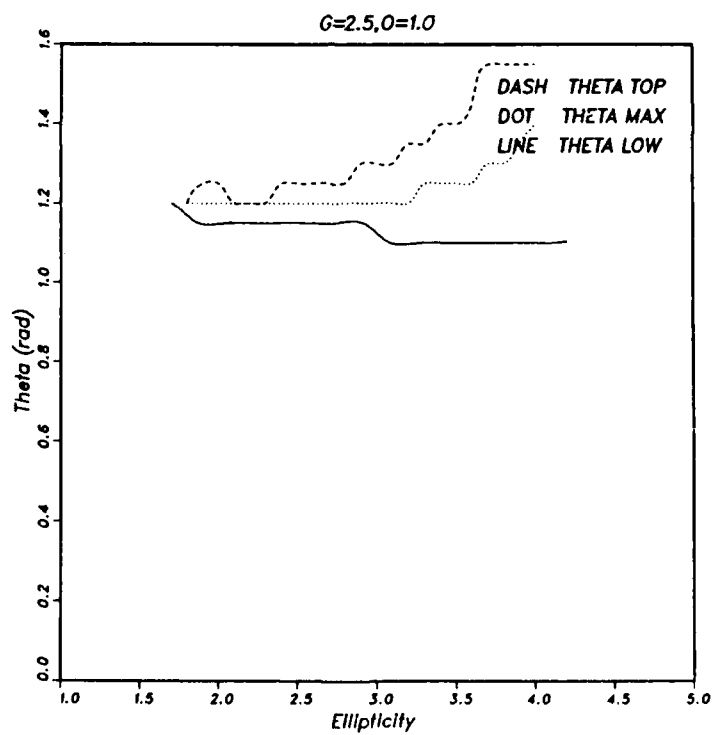


Figure F1.13

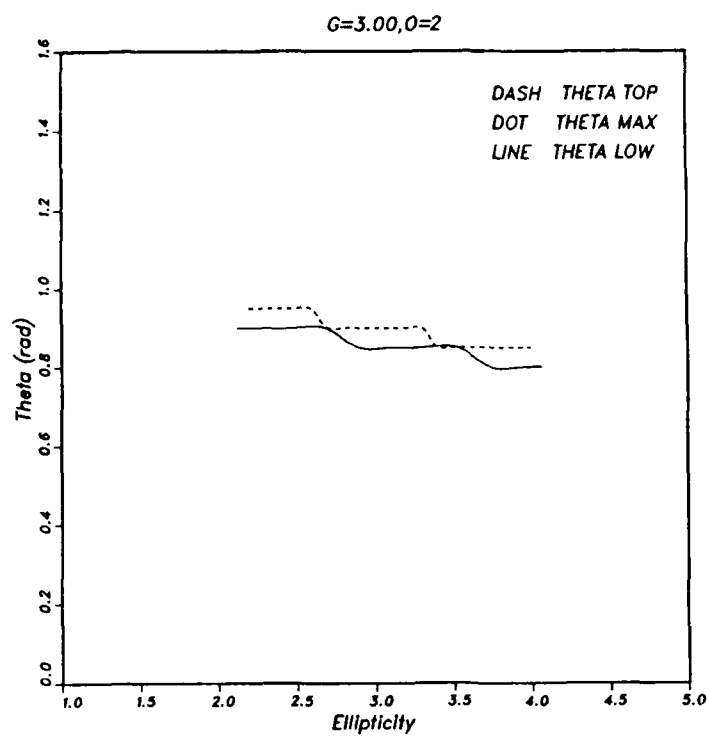


Figure F1.14

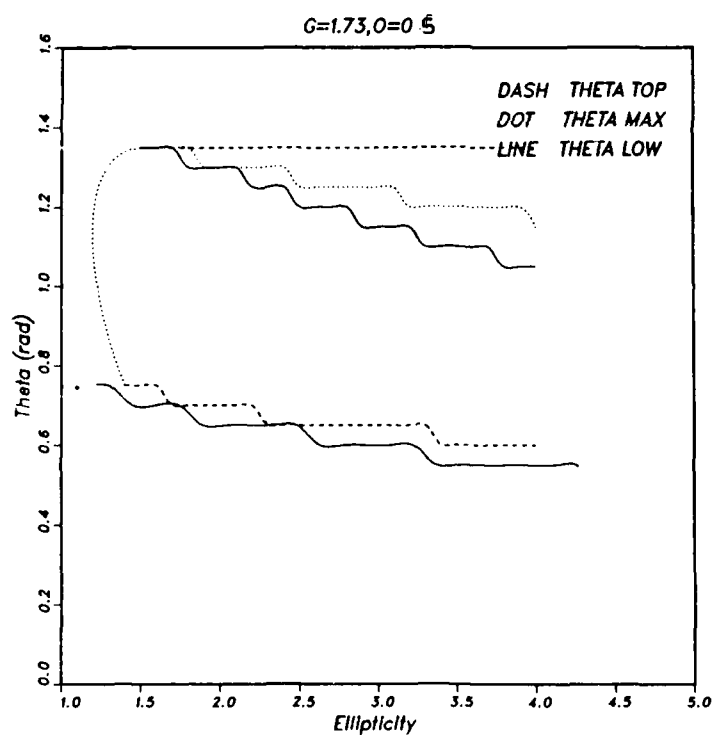


Figure F1.15

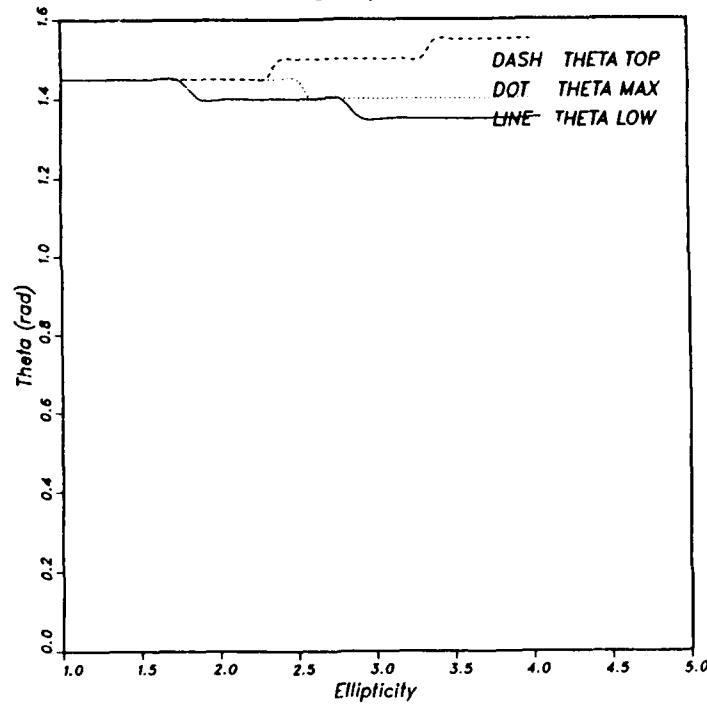


Figure F1.16

Discussion

Non-rotating case. Since γ can be interpreted in terms of varying wavenumber or of varying Alfvén speed, the damping of the instabilities observed arises due to a combination of these effects in general. For a given Alfvén speed, the shorter wavelengths are more heavily damped than the longer ones: the independence of length scale which was observed in the non-magnetic case is lost. From the same observation, an increase in Alfvén speed increases the damping of the instability of a given wavenumber, although the growth rates remain substantial at high ellipticities until γ approaches the extinction value. The effect of a magnetic field may be highlighted by pointing out that for any field strength greater than zero there are some wavelength waves which will never become unstable – unless the field is exactly perpendicular to the wavevector, in which case γ is always zero so the field has no effect whatsoever.

Non-magnetic case. A rotation rate less than 1 stabilizes the fluid waves, by reducing the growth rate of instabilities, delaying their onset, or both. The destabilizing effect of having the frame rotating at the same rate as the fluid particles was not expected. Higher rotation rates postpone the onset of instabilities much less than an increase in γ of the same amount; the highest rate tried (5.5) had a similar maximum growth rate to that at an Ω of 1: above a certain stabilizing rate of rotation, the Coriolis force has minimal further effect.

Magnetic, rotating case. The interaction of the Lorentz and Coriolis force effects is quite complex, since they oppose each other in some parameter combinations

and enhance in others. The small rotational stabilizing effect becomes destabilizing when γ is non-zero, and the short wavelengths are destabilized in the presence of any magnitude of rotation. Similarly in the presence of a large field, rotation always destabilizes the waves at a given wavenumber. The long wavelengths, on the other hand, are stabilized by a large rotation rate, as are waves when the Alfvén velocity is small. In terms of growth rates the effect of rotation is to stabilize except in the case $\Omega = 1$; also, two out of the four velocity and magnetic perturbation components are usually stable when both rotation and magnetic field are present.

Conclusions

A two-dimensional elliptical flow in an inviscid, incompressible fluid under frozen-flux is usually subject to destabilizable perturbations of long enough wavelengths are considered, in the presence of any degree of rotation and size of magnetic field. Unless the rotation rates of the reference frame and basic flow are the same, the instabilities will grow faster without rotation being present; no magnetic field enhances the maximum growth rate but a field perpendicular to the wavevector will not hinder the growth as all other fields will.

Acknowledgements

Much thanks to Bruce Bayly for suggesting this project and for his endless enthusiasm, optimism, patience and guidance throughout. Glenn Lerley's advice on computing was useful, as was Andrew Gilbert's willingness to listen while I sorted out the matter. I am grateful to the organizers for my fellowship, Dr. Malkus for his continual interest, and Dave Gubbins for suggesting I come in the first place. Finally Mary Berry anchored GFD, conquered our lectures and benefitted the summer's work considerably with her calm and cheerfulness: thanks!

References

- Bayly, B., 1986. "Three-dimensional instability of elliptical flow", *Phys. Rev. Lett.*, 57, 2160.
- Priest, E., 1982. *Solar Magnetohydrodynamics*, Reidel.

THE PONOMARENKO DYNAMO

Andrew D. Gilbert,
Cambridge University.

Introduction

One of the simplest kinematic dynamos was proposed by Ponomarenko (1973). In cylindrical polar coordinates, (r, θ, z) , the velocity field is given by:

$$\mathbf{u} = \begin{cases} r\omega\mathbf{e}_\theta + U\mathbf{e}_z & r < a \\ 0 & r > a \end{cases} \quad (1)$$

where a, ω and U are positive constants (figure 1). Inside the cylinder, $r = a$,

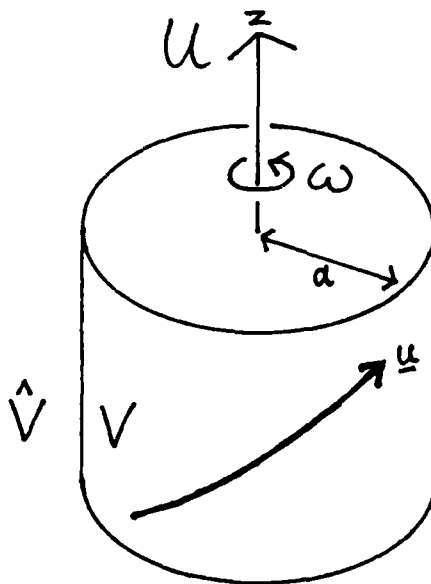


Figure F2.1: The geometry of the Ponomarenko dynamo.

particles describe helices, moving with uniform angular velocity and uniform axial velocity; so the motion here is that of a solid body. The velocity field is discontinuous across the cylinder, where there is an infinite helical shear. There is no motion outside the cylinder. The model is clearly somewhat idealised, as it involves a motion unbounded in space and a discontinuous velocity field. However its simplicity means that it is amenable to detailed analysis and worthy of study.

Ponomarenko (1973) proved that this velocity field gives dynamo action (see also Roberts 1987 & Zeldovich et al. 1983). He considered a class of normal modes of the magnetic field which grow exponentially with time. In the limit of large

magnetic Reynolds number, R , the growth rate of these modes falls off as $R^{-1/3}$ and the Ponomarenko dynamo would appear to be slow (Zeldovich et al. 1983). However the growth rate increases as the scale of the magnetic field decreases; so we shall consider magnetic modes with finer structure, varying on spatial scales of order $R^{-1/2}$. Certain of these small-scale modes have a growth rate of order unity, independent of the magnetic Reynolds number, as it tends to infinity. Thus the Ponomarenko dynamo is a *fast* dynamo. The dynamo contrasts with other known or conjectured examples of fast dynamos. It does not have chaotic streamlines, nor stagnation points; so there is no exponential stretching of material elements. However the velocity field is singular, possessing a discontinuity, which is vital for fast dynamo action. The essential mechanism behind the Ponomarenko dynamo is the stretching of field lines by the infinite helical shear across the cylinder, combined with diffusion in curved geometry.

In §2 we shall develop the mathematical model and discuss previous work. We shall perform a boundary layer analysis for a magnetic field confined close to the cylinder in §3 and identify the physical mechanism of the dynamo. We show in §4 that fast dynamo action occurs and offer further discussion and conclusions in §5.

Formulation and Discussion

We are interested in solving the magnetic induction equation:

$$\partial_t \mathbf{b} + \mathbf{u} \cdot \nabla \mathbf{b} = \mathbf{b} \cdot \nabla \mathbf{u} + \eta \Delta \mathbf{b} \quad (2)$$

together with

$$\nabla \cdot \mathbf{b} = 0 \quad (3)$$

for the velocity field (1). The boundary conditions appropriate for the discontinuity in the velocity are that the magnetic field and tangential electric field be continuous across the cylinder $r = a$:

$$[\mathbf{B}]_+^- = 0 \quad (4)$$

$$[E_\theta]_+^- = 0 \quad (5)$$

$$[E_z]_+^- = 0. \quad (6)$$

Here $[X]_+^- \equiv X|_{r=a-} - X|_{r=a+}$ is the jump in a quantity, X , across the cylinder. These conditions follow from Maxwell's equations provided that the magnetic diffusivity is non-zero and the magnetic field is unsteady; note that of these five scalar conditions only four are independent.

We seek normal modes with growth rate, λ , by setting:

$$\mathbf{b} = \mathbf{B}(r)e^{im\theta + ikz + \lambda t} \quad (7)$$

where the azimuthal wave-number, m , is an integer and the axial wave-number, k , is real. The physical magnetic field is to be understood as the real part of the above complex quantity. We shall write quantities with circumflexes, such as $\hat{\mathbf{B}}$, to denote

values on the outside, \hat{V} , of the cylinder, and quantities without circumflexes for their values on the inside, V , of the cylinder (figure 1).

With this notation the induction equation becomes:

$$q^2 \mathbf{B} = \Delta_H \mathbf{B} \quad (8)$$

$$\hat{q}^2 \hat{\mathbf{B}} = \Delta_H \hat{\mathbf{B}}, \quad (9)$$

where

$$q^2 \equiv k^2 + (\lambda + im\omega + ikU)/\eta \quad (10)$$

$$\hat{q}^2 \equiv k^2 + \lambda/\eta \quad (11)$$

$$\Delta_H \equiv \Delta - \partial_s^2. \quad (12)$$

We are interested in the limit of large magnetic Reynolds number, defined here as $R = a^2\omega/\eta$, and we take $U/a\omega = O(1)$. We shall think of a, ω, U and \mathbf{B} as being of order unity in some system of units, so that we may write orders of magnitude loosely, such as:

$$\eta \sim R^{-1}; \quad (13)$$

this is, of course, equivalent to non-dimensionalising all quantities using characteristic length- and time-scales of the flow. We are free to choose the orders of the wave-numbers, m and k , to investigate the evolution of magnetic fields of different scales. Ponomarenko (1973) (see also Roberts 1987 & Zeldovich et al. 1983) examined the case when m and k are of order unity (independent of R as $R \rightarrow \infty$) and showed that modes satisfying

$$m\omega + kU \ll 1 \quad (14)$$

grow exponentially with time. In this case the dominant field has no radial component and is approximately aligned with the infinite shear across the cylinder. The field is concentrated in a thin layer, of radial thickness $O(R^{-1/3})$, about the cylinder.

The growth rate for the above normal modes, with m and k of order unity, is

$$\lambda \simeq \frac{\eta^{1/3}}{2} \left(\frac{|m|\omega}{2a} \right)^{2/3} \quad (15)$$

which, for fixed m , decreases with increasing magnetic Reynolds number as $R^{-1/3}$. However, for fixed R , the growth-rate increases with m and motivates examination of magnetic fields varying on smaller scales. For fast dynamo action we should like $\lambda = O(1)$ as $R \rightarrow \infty$, which suggests that we consider the class of normal modes for which $m \sim R^{1/2}$.

Boundary Layer Analysis

In pursuit of fast dynamo action, and following the above discussion, let us consider magnetic fields with:

$$m, k \sim R^{1/2}, \quad (16)$$

approximately aligned with the infinite shear:

$$m\omega + kU \equiv \omega l = O(1). \quad (17)$$

For convenience we also define

$$n = -kU/\omega \sim R^{1/2} \quad (18)$$

so that

$$m = n + l. \quad (19)$$

If the lines of constant magnetic field were exactly aligned with the shear, n would be the azimuthal wave-number corresponding to the axial wave-number, k . The quantity l is a measure of the small deviation from this situation; the difference in pitch between the helices of the field and the helical shear across the cylinder being of order $R^{-1/2}$. From (11,12), we take

$$q, \hat{q} \sim R^{1/2}. \quad (20)$$

It is not difficult to write down the general solution to the vector diffusion equations (9,10) together with boundary conditions; however the resulting relation between q and \hat{q} (Ponomarenko 1973) is rather unilluminating. Instead we shall perform an asymptotic analysis of a magnetic field confined to a thin boundary layer about $r = a$, following Roberts' (1987) discussion of this dynamo. The width of the boundary layer suggested by (9,10) is of order $R^{-1/2}$; so we take

$$\partial_r \sim R^{1/2} \quad (21)$$

and define

$$s = r - a \sim R^{-1/2} \quad (22)$$

within the magnetic boundary layer.

We shall expand everything in powers of $R^{-1/2}$; the magnetic field is

$$\mathbf{B}(r) = \mathbf{B}^{(0)}(s) + R^{-1/2}\mathbf{B}^{(1)}(s) + \dots \quad (23)$$

and similarly for $\hat{\mathbf{B}}$. Let

$$\mathbf{c}(r, \theta, z) \equiv \mathbf{C}(s)e^{im\theta + ikz} \quad (24)$$

be an arbitrary vector function; then we shall need $\nabla \cdot \mathbf{c}$ and $\Delta_H \mathbf{c}$ expanded in powers of $R^{-1/2}$. We use the orderings we have defined to write:

$$\Delta_H \mathbf{c} \equiv (\partial_r^2 + r^{-1}\partial_r + r^{-2}\partial_\theta^2)\mathbf{c} + r^{-2}(-2\partial_\theta c_\theta - c_r, 2\partial_\theta c_r - c_\theta, 0) \quad (25)$$

$$= \Delta_H^{(0)}\mathbf{c} + \Delta_H^{(1)}\mathbf{c} + \dots \quad (26)$$

where

$$\Delta_H^{(0)}\mathbf{c} = (\partial_r^2 - n^2/a^2)\mathbf{c} \quad (27)$$

$$\Delta_H^{(1)}\mathbf{c} = (\partial_r/a + 2sn^2/a^3 - 2nl/a^2)\mathbf{c} + (-2inc_\theta/a^2, 2inc_r/a^2, 0). \quad (28)$$

Similarly

$$\nabla \cdot \mathbf{c} \equiv \partial_r c_r + c_r/r + \partial_\theta c_\theta/r + \partial_z c_z \quad (29)$$

$$= \nabla^{(0)} \cdot \mathbf{c} + \nabla^{(1)} \cdot \mathbf{c} + \dots \quad (30)$$

where

$$\nabla^{(0)} \cdot \mathbf{c} = \partial_r c_r + i n c_\theta / a + i k c_z \quad (31)$$

$$\nabla^{(1)} \cdot \mathbf{c} = c_r/a - i s n c_\theta / a^2 + i l c_\theta / a. \quad (32)$$

The continuity of magnetic field across the cylinder will apply at each order, as will the continuity of the tangential electric field. Since

$$\mathbf{E} = \eta \nabla \times \mathbf{B} - \mathbf{u} \times \mathbf{B} \quad (33)$$

and the velocity field is discontinuous, there will, in general, be discontinuities in the radial derivatives of the magnetic field. Using the continuity of the magnetic field, the condition that the tangential electric field be continuous gives the following relations:

$$- [E_\theta]_+ = \eta [\partial_r B_z]_+ + U B_r = 0 \quad (34)$$

$$[E_z]_+ = \eta [\partial_r B_\theta]_+ + a \omega B_r = 0. \quad (35)$$

Note that $\eta \partial_r \sim R^{-1/2}$ whereas $a \omega, U \sim O(1)$; thus these boundary conditions relate magnetic fields of different orders.

We commence by solving the zero order induction equation inside the cylinder, $s < 0$:

$$q^2 \mathbf{B}^{(0)} = \Delta_H^{(0)} \mathbf{B}^{(0)} = (\partial_r^2 - n^2/a^2) \mathbf{B}^{(0)} \quad (36)$$

yielding a decaying solution:

$$\mathbf{B}^{(0)} = (R^{(0)}, T^{(0)}, Z^{(0)}) e^{Qs} \quad (37)$$

where $R^{(0)}, T^{(0)}, Z^{(0)}$ are constants, and Q is the root of

$$Q^2 = q^2 + n^2/a^2 = k^2 + n^2/a^2 + (\lambda + i m \omega + i k U)/\eta \quad (38)$$

with positive real part (assumed to be non-zero). The induction equation is solved similarly outside the cylinder:

$$\hat{\mathbf{B}}^{(0)} = (R^{(0)}, T^{(0)}, Z^{(0)}) e^{-\hat{Q}s} \quad (39)$$

where we have used the continuity of $\mathbf{B}^{(0)}$ across the cylinder, and \hat{Q} is the root of the equation:

$$\hat{Q}^2 = \hat{q}^2 + n^2/a^2 = k^2 + n^2/a^2 + \lambda/\eta \quad (40)$$

with positive real part.

The continuity of the electric field gives:

$$a\omega R^{(0)} = UR^{(0)} = 0; \quad (41)$$

thus there is no radial magnetic field at this order. The condition that \mathbf{B} be solenoidal, at this order,

$$\nabla^{(0)} \cdot \mathbf{B}^{(0)} = \nabla^{(0)} \cdot \hat{\mathbf{B}}^{(0)} = 0 \quad (42)$$

applied on the inside, or the outside of the cylinder, yields just one relation:

$$inT^{(0)}/a + ikZ^{(0)} = 0. \quad (43)$$

The dominant magnetic field is azimuthal and axial, and is approximately aligned with the shear across the cylinder (figure 2). This suggests an element of the physical mechanism of the dynamo. A weak radial field would be stretched by the shear across $r = a$ into a helical magnetic field aligned with the shear; this is essentially an omega effect. What is now required is some mechanism to create such a radial field.

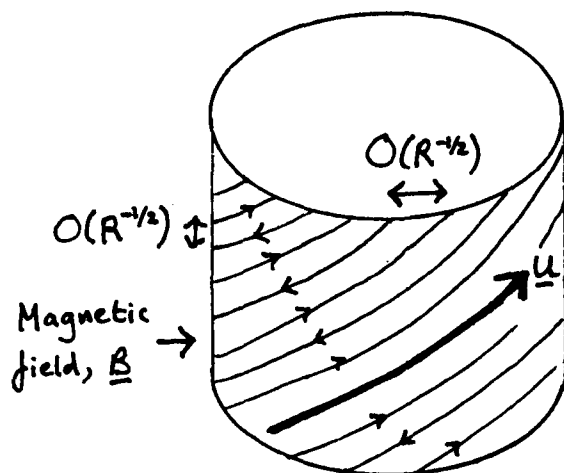


Figure F2.2: The structure of the magnetic field in the case $m, k \sim R^{1/2}$ and $m\omega + kU \sim 1$, when it is approximately aligned with the shear across the cylinder.

We proceed to next order; the induction equation is

$$q^2 \mathbf{B}^{(1)} = \Delta_H^{(0)} \mathbf{B}^{(1)} + \Delta_H^{(1)} \mathbf{B}^{(0)} \quad (44)$$

on the inside of the cylinder, which gives

$$(Q^2 - \partial_r^2)B_r^{(1)} = -2ina^{-2}T^{(0)}e^{Qs} \quad (45)$$

$$(Q^2 - \partial_r^2)B_\theta^{(1)} = (Q/a + 2sn^2/a^3 - 2nl/a^2)T^{(0)}e^{Qs} \quad (46)$$

$$(Q^2 - \partial_r^2)B_z^{(1)} = (Q/a + 2sn^2/a^3 - 2nl/a^2)Z^{(0)}e^{Qs}. \quad (47)$$

Note that the first order radial field is coupled to the zero order azimuthal field through the laplacian. When vector diffusion takes place in a cylindrical geometry, the radial and azimuthal components do not diffuse independently; we shall see that this mechanism regenerates radial field.

These equations may be integrated to obtain:

$$B_r^{(1)} = R^{(1)}e^{Qs} + \frac{ins}{Qa^2}T^{(0)}e^{Qs} \quad (48)$$

$$B_\theta^{(1)} = T^{(1)}e^{Qs} + \left[\left(\frac{n^2}{Q^2a^2} + \frac{2nl}{Qa} - 1 \right) \frac{s}{2a} - \frac{n^2s^2}{2Qa^3} \right] T^{(0)}e^{Qs} \quad (49)$$

$$B_z^{(1)} = Z^{(1)}e^{Qs} + \left[\left(\frac{n^2}{Q^2a^2} + \frac{2nl}{Qa} - 1 \right) \frac{s}{2a} - \frac{n^2s^2}{2Qa^3} \right] Z^{(0)}e^{Qs}. \quad (50)$$

The form of the magnetic field on the outside of the cylinder is the same, with Q replaced by $-\hat{Q}$; the constants $R^{(1)}, T^{(1)}, Z^{(1)}$ are the same, using the continuity of the field across the cylinder. We apply the condition that the divergence of the magnetic field vanish at first order:

$$\nabla^{(0)} \cdot \mathbf{B}^{(1)} + \nabla^{(1)} \cdot \mathbf{B}^{(0)} = \nabla^{(0)} \cdot \hat{\mathbf{B}}^{(1)} + \nabla^{(1)} \cdot \hat{\mathbf{B}}^{(0)} = 0 \quad (51)$$

which results in the conditions

$$QR^{(1)} + (in/Qa^2 + il/a)T^{(0)} + inT^{(1)}/a + ikZ^{(0)} = 0 \quad (52)$$

$$-\hat{Q}R^{(1)} + (-in/\hat{Q}a^2 + il/a)T^{(0)} + inT^{(1)}/a + ikZ^{(0)} = 0. \quad (53)$$

These may be combined to give

$$Q\hat{Q}R^{(1)} + inT^{(0)}/a^2 = 0. \quad (54)$$

Thus there is indeed a first order radial field created by the diffusion of azimuthal field and we can identify the complete dynamo mechanism. The action of the infinite helical shear across the boundary stretches weak radial field into azimuthal and axial field aligned with the shear. Diffusion of the azimuthal field in the curved geometry replenishes the radial field. The dynamo could thus be called a *stretch-diffuse* dynamo. Note that diffusion plays a vital rôle in renewing the field. This is in contrast with dynamos that employ chaotic flows, where diffusion is often invoked to smooth the magnetic field on small scales, but is not important for its generation by the exponential stretching of field lines.

Finally we use the continuity of the tangential electric field at this order

$$\eta \left[\partial_r B_\theta^{(0)} \right]_+^- + a\omega B_r^{(1)} = \eta \left[\partial_r B_z^{(0)} \right]_+^- + U B_r^{(1)} = 0 \quad (55)$$

which gives:

$$\eta(Q + \hat{Q})T^{(0)} + a\omega B_r^{(1)} = 0 \quad (56)$$

$$\eta(Q + \hat{Q})Z^{(0)} + UB_r^{(1)} = 0. \quad (57)$$

These conditions are the same, by virtue of (19,44). From (55,57) we obtain a relation between Q and \hat{Q} :

$$Q + \hat{Q} = \frac{i n \omega}{\eta a} \frac{1}{Q \hat{Q}}; \quad (58)$$

this may be solved in conjunction with

$$Q^2 = \hat{Q}^2 + i l \omega / \eta \quad (59)$$

which arises from the definitions of Q and \hat{Q} . The growth rate is given by

$$\lambda = \eta \hat{Q}^2 - \eta n^2 (1 + a^2 \omega^2 / U^2) / a^2 \quad (60)$$

from (19,41).

Fast Dynamo Action

The simultaneous equations (59,60) for Q and \hat{Q} are most easily solved when $l = 0$, so that the zero order field is exactly aligned with the shear across the cylinder. In this case the only solution for which both Q and \hat{Q} have positive real parts is

$$Q = \hat{Q} = e^{i \pi \text{sgn}(m)/6} (\omega |m| / 2 \eta a)^{1/3} \quad (61)$$

and the real part of the growth rate is

$$\text{Re } \lambda = \frac{\eta^{1/3}}{2} \left(\frac{|m| \omega}{2a} \right)^{2/3} - \frac{\eta m^2}{a^2} \left(1 + \frac{a^2 \omega^2}{U^2} \right). \quad (62)$$

Since we are studying the asymptotic regime for which $m \sim R^{1/2}$, the growth rate is of order unity, and may be positive. Its maximum real part is

$$(\text{Re } \lambda)_{\max} = \frac{\omega}{6^{3/2}} \left(1 + \frac{a^2 \omega^2}{U^2} \right)^{-1/2} \quad (63)$$

which is achieved when

$$|m| = \left(\frac{a^2}{6(1 + a^2 \omega^2 / U^2)} \right)^{3/4} \left(\frac{\omega}{2a\eta} \right)^{1/2}. \quad (64)$$

Thus we have established that the Ponomarenko dynamo is fast; there are modes of the magnetic field with a growth rate of order unity, in the limit of high magnetic Reynolds number.

It is reassuring that this result may be obtained from the exact solution (Ponomarenko 1973) as well as from our boundary layer analysis. The vector diffusion

equations (9,10) may be solved in terms of modified Bessel functions (Abramowitz & Stegun (1964) §9). The equation for q in this case, $l = 0$, is given by:

$$I_{m+1}(qa)K_{m+1}(qa) - I_{m-1}(qa)K_{m-1}(qa) = 2i\eta/\omega a^2. \quad (65)$$

In our case $q, m \sim R^{1/2}$ and so it is appropriate to use the uniform asymptotic expansions of the modified Bessel functions for large order (Abramowitz & Stegun (1964) §9.7.7-8). A little algebra yields the result

$$Q = \left(q^2 + \frac{m^2}{a^2}\right)^{1/2} = \left(\frac{im\omega}{2\eta a}\right)^{1/3} (1 + O(m^{-1})) \quad (66)$$

as in equation (62) of the boundary layer analysis.

Now let us consider normal modes for which the magnetic field is only approximately aligned with the shear across the cylinder. We are interested in $l \neq 0$, but we are taking $|l| \sim 1 \ll |n| \sim R^{1/2}$. We expect dynamo action to be less effective in the light of the physical mechanism discussed above. It is sufficient to restrict our attention to the case $n > 0$, and it is convenient to define order unity quantities, N, L, P, \hat{P} by

$$Na\eta^{-1/2} = n\omega = -kU = m\omega + O(1) \quad (67)$$

$$L = l\omega N^{-2/3} \quad (68)$$

$$P = Q\eta^{1/2} N^{-1/3} \quad (69)$$

$$\hat{P} = \hat{Q}\eta^{1/2} N^{-1/3}. \quad (70)$$

Then the simultaneous equations (59,60) for Q and \hat{Q} become

$$P + \hat{P} = i(P\hat{P})^{-1} \quad (71)$$

$$P^2 = \hat{P}^2 + iL \quad (72)$$

and the problem now contains only one parameter, L , rather than two. These equations have two useful symmetries:

$$P \rightarrow -\hat{P}^*, \hat{P} \rightarrow -P^* \quad (73)$$

and

$$L \rightarrow -L, P \rightarrow \hat{P}, \hat{P} \rightarrow P \quad (74)$$

which implies, using (61,71,73), that the real part of the growth rate depends on L solely through $|L|$; thus we lose no generality in taking $L \geq 0$ in the following. The equations may be reduced to the following quartic equation for \hat{P} , by writing $P = \hat{P}(1 + \gamma)$, solving for γ from (73) and substituting in (72):

$$iL\hat{P}^4 - 2i\hat{P}^3 - L^2\hat{P}^2 + 2L\hat{P} - 1 = 0. \quad (75)$$

The roots of this equation give values of \hat{P} ; P may then be calculated from (73), the sign of the square root being chosen to ensure that (72) is satisfied.

The solutions may be found perturbatively when $L \ll 1$. We require that the real parts of P and \hat{P} be positive, so that the magnetic field decays away from the cylinder, $r = a$. Of the four solutions only one satisfies this condition, namely

$$P = p + iL/4p + iL^2/24 + O(L^3) \quad (76)$$

$$\hat{P} = p - iL/4p + iL^2/24 + O(L^3) \quad (77)$$

with $p = e^{i\pi/6}/2^{1/3}$. The real part of the growth rate is given by

$$\text{Re } \lambda = N^{2/3}(2^{-5/3} - 5L^2/(2^{1/3}48) + O(L^3)) - N^2(1 + a^2\omega^2/U^2). \quad (78)$$

As anticipated, a mode for which the field is not exactly aligned with the shear, so that $L \neq 0$, has a reduced growth rate, for a given value of N . The asymptotic solutions may also be found in the limit $L \gg 1$, but less than some power of R , which further analysis shows to be $R^{1/6}$. The one solution for which both P and \hat{P} have positive real parts, is given by

$$P = e^{i\pi/4}L^{1/2}(1 - iL^{-3}/2 + O(L^{-9/2})) \quad (79)$$

$$\hat{P} = L^{-1}(1 + e^{3i\pi/4}L^{-3/2} + O(L^{-3})). \quad (80)$$

The corresponding growth rate is

$$\text{Re } \lambda = -N^2(1 + a^2\omega^2/U^2)/\omega^2 + O(N^{2/3}L^{-2}); \quad (81)$$

there is no dynamo action in this regime.

In order to check these asymptotic results and bridge them to find the marginal stability curve, $\lambda = 0$, the equations for P and \hat{P} may be solved numerically. For all values of L it is found that of the four solutions there is only one for which the real parts of both P and \hat{P} are positive. Although P and \hat{P} depend only on L , the growth rate depends on N , and also on U, a and ω . The real part of the growth rate is plotted in figure 3 as a contour graph against N and L for the simplest case, in which $a = U = \omega = 1$. In this case the maximum growth rate is $\lambda \simeq 0.048$ which occurs when $L = 0$ and $N \simeq 0.11$. Modes with large N or large L are not sustained by dynamo action. As N is decreased the range of L for which dynamo action occurs, broadens; however the growth rate of these modes decreases.

Discussion and Conclusions

We have seen that the Ponomarenko dynamo is a fast dynamo. The essential mechanism is the stretching of radial field by helical shear to form axial and azimuthal field, combined with diffusion of azimuthal field in the cylindrical geometry to regenerate radial field. The unstable modes have a boundary layer structure, being concentrated in a layer of width $O(R^{-1/2})$ about the cylinder; this is in agreement with the assertion of Moffatt and Proctor (1985) that in a fast dynamo the unstable modes possess spatial structure on this scale.

The Ponomarenko dynamo has the unphysical feature of a discontinuous velocity field; it is of interest to explore to what extent this is necessary for the dynamo

action to be fast. We have also considered smooth axisymmetric velocity fields; dynamo action still occurs by the same stretch-diffuse mechanism. However now the most unstable modes vary on spatial scales of order $R^{-1/3}$, and the maximum growth rate falls off as $R^{-1/3}$, in the limit $R \rightarrow \infty$. Thus if we imagine a more physically realistic dynamo than Ponomarenko's, in which the discontinuity is only approximate, having a width $\delta \ll a$, we might expect that the maximum growth rate would be independent of R , while $R^{-1/2} \gg \delta/a$, since then the magnetic boundary layer would be much wider than the scale of the approximate discontinuity and our calculation above would apply. However when $R^{-1/3} \ll \delta/a$, the magnetic field would resolve a smooth profile, the growth rate would fall off as $R^{-1/3}$, and the dynamo would reveal itself to be slow. It thus seems likely that a singular velocity field is necessary for fast dynamo action in such axisymmetric flows. Other possible lines for further research include incorporating dynamical effects, generalising the geometry, and examining possible experimental realisations of the Ponomarenko dynamo.

Acknowledgements

I wish to record my thanks to Stephen Childress who suggested this fruitful line of research and guided me through my summer project. I am grateful to him, as well as Andrew Soward, for interesting discussions and ideas. I should like to thank the GFD Programme, its organiser, Willem Malkus, and all the other participants, for a very enjoyable and stimulating summer.

References

- Abramowitz, M. & Stegun, I.A. 1964, "Handbook of mathematical functions with formulas, graphs and tables", United States Department of Commerce.
- Moffatt, H.K. & Proctor, M.R.E. 1985, "Topological constraints associated with fast dynamo action", *J. Fluid Mech.*, **154**, 493.
- Ponomarenko, Y.B. 1973, "On the theory of hydromagnetic dynamos", *Zh. Prikl. Mech. Tech. Fiz. (USSR)*, **6**, 775.
- Roberts, P.H. 1987, "Dynamo theory", preprint.
- Zeldovich, Ya.B., Ruzmaikin, A.A. & Sokoloff, D.D. 1983, "Magnetic fields in astrophysics", Gordon and Breach.

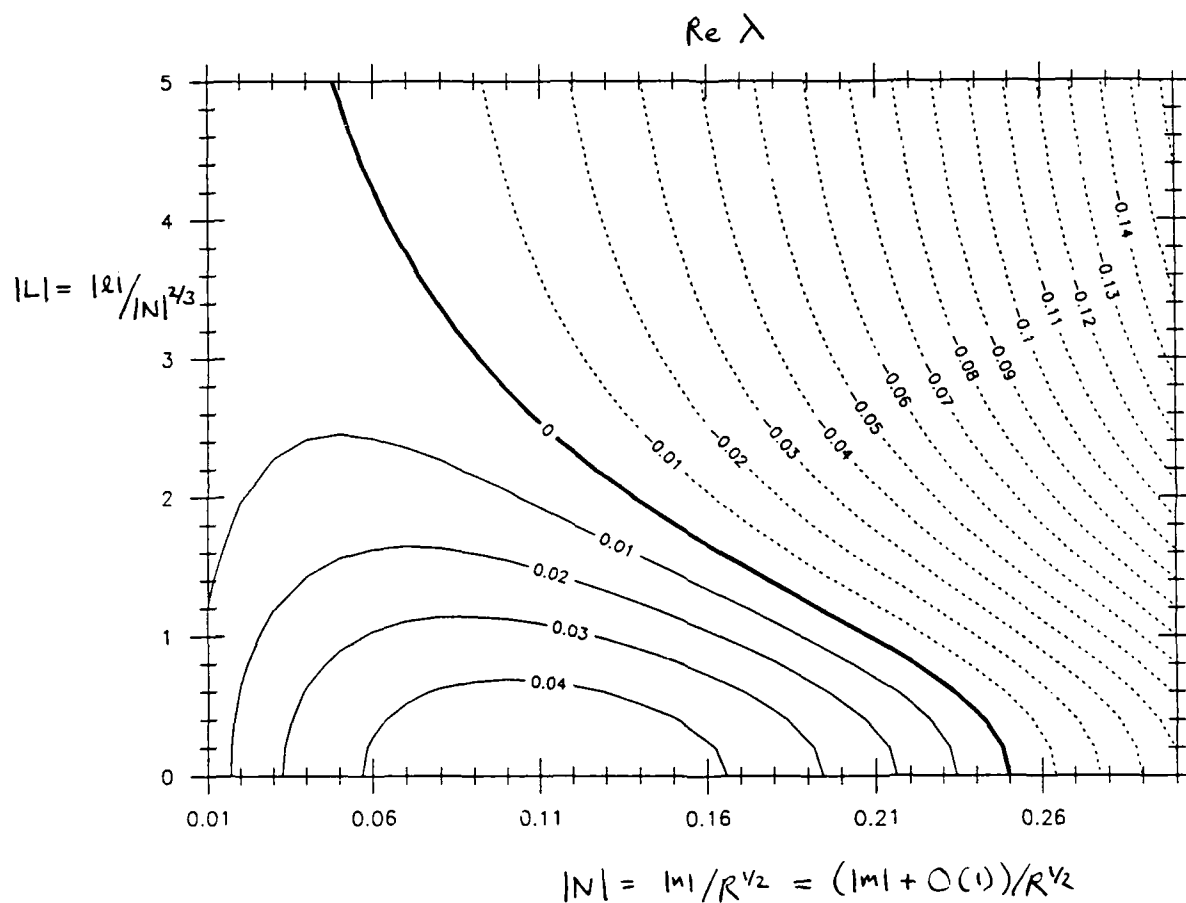


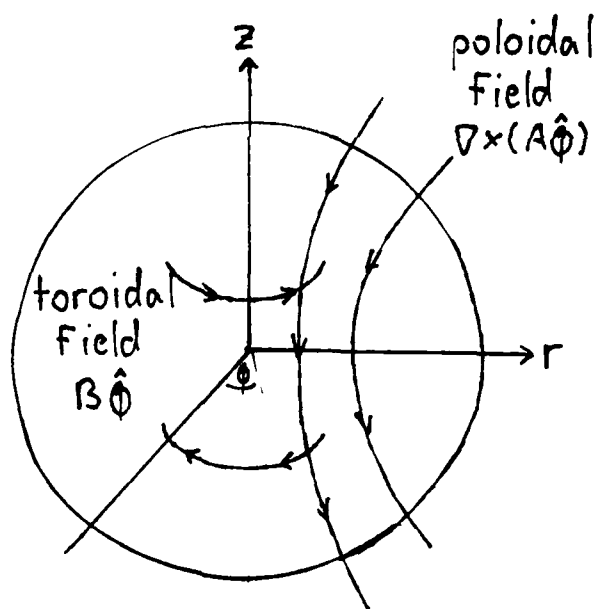
Figure F2.3: Contour plot of the real part of the growth rate against scaled wave-numbers, N and L , for the case $U = a = \omega = 1$.

A NUMERICAL MODEL OF α^2 AND $\alpha\omega$ DYNAMOS IN THE LIMIT OF ASYMPTOTICALLY SMALL VISCOSITY

Rainer Hollerbach
Scripps Institution of Oceanography

Introduction

The purpose of this project is a numerical investigation of α^2 and $\alpha\omega$ dynamos in the limit of asymptotically small viscosity. The basic philosophy is that the underlying field generation mechanism is parameterized rather arbitrarily by a choice of α and ω , where α is a measure of small-scale helical motions and ω is some kinematically prescribed differential rotation. The subsequent equilibration of the field is treated dynamically, however, by considering the reaction of the Lorentz forces back onto the fluid motions. Thus, one must solve the induction and momentum equations simultaneously. In this work these equations are solved in a spherical dynamo, with no-slip boundary conditions on the fluid and with attention restricted to the class of dipole solutions (so A is symmetric about the equator, whereas B is antisymmetric.)



Having solved the equations, they are finite differenced at the lowest order that still retains the basic physics, so that the resulting system will be of very low order and can be numerically investigated for asymptotically small viscosities.

Basic Equations

Scaling the mean-field equations according to Malkus and Proctor (1975), we get

$$\textcircled{1} \quad E_m \frac{D\vec{u}}{Dt} + 2\vec{k} \times \vec{u} = -\nabla p + (\nabla \times \vec{B}) \times \vec{B} + E \nabla^2 \vec{u}$$

$$\textcircled{2} \quad \frac{\partial \vec{B}}{\partial t} = \nabla \times (\vec{u} \times \vec{B} + \alpha \vec{B}) + \nabla^2 \vec{B}$$

$$\textcircled{3} \quad \nabla \cdot \vec{B} = \nabla \cdot \vec{u} = 0$$

where $E_m = \text{magnetic diffusivity}/\Omega L^2 = \text{Inertia Force/Lorentz Force}$ and $E = \text{diffusivity}/\Omega L^2 = \text{Viscous Force/Lorentz Force}$ are both small. In fact, the term $E_m \frac{D\vec{u}}{Dt}$ will be neglected henceforth, so the fluid's inertia is ignored and it is assumed to adjust itself instantaneously to the magnetic field. Then, since we're looking for axisymmetric solutions we take

$$\textcircled{4} \quad \vec{u} = u \hat{\phi} + \nabla \times (\psi \hat{\phi}) = (-\psi_z, u, \frac{1}{r}(r\psi)_r)$$

$$\textcircled{5} \quad \vec{B} = B \hat{\phi} + \nabla \times (A \hat{\phi}) = (-A_z, B, \frac{1}{r}(rA)_r)$$

The reason we work in cylindrical coordinates despite the spherical symmetry of our model is that by the Taylor-Proudman Theorem the interior flow to leading order will consist of vertical cylindrical shells rotating like rigid bodies. Also, for our α we take

$$\alpha = \begin{vmatrix} \alpha^* & 0 & 0 \\ 0 & \alpha & 0 \\ 0 & 0 & \alpha^* \end{vmatrix}$$

where α will turn out to regenerate the poloidal field and α^* the toroidal field.

Making these substitutions, Eq. (2) yields after a little algebra

$$(6) \quad A_+ = \alpha B + D^2 A + \frac{1}{r} (\Psi_z (rA)_r - (r\Psi)_r A_z)$$

$$(7) \quad B_+ = -\alpha^* D^2 A - \alpha_z^* A_z - \alpha_r^* \frac{1}{r} (rA)_r + D^2 B \\ + V_z \frac{1}{r} (rA)_r - \left(\frac{V}{r}\right)_r r A_z + \Psi_z r \left(\frac{B}{r}\right)_r - \frac{1}{r} (r\Psi)_r B_z$$

where the operator $D^2 = \nabla^2 - \frac{1}{r^2}$. Next, the curl of Eq. (1) yields after some more algebra

$$(8) \quad 2\Psi_z + E D^2 V = \frac{1}{r} (A_z (rB)_r - B_z (rA)_r)$$

$$(9) \quad 2V_z - E D^4 \Psi = \frac{2}{r} B B_z + A_r D^2 A_z - A_z D^2 A_r \\ + \frac{1}{r} (A D^2 A_z + A_z D^2 A)$$

(Ierley, 1985) It is these last four equations that we wish to solve.

Boundary Layer Analysis

We begin by solving Eqs. (8) and (9) for ψ and v in terms of A and B . At first order the interior solution is clearly

$$(10) \quad \Psi = \frac{1}{2} \int_0^z \frac{1}{r} (A_z (rB)_r - B_z (rA)_r) dz$$

$$(11) \quad V = \frac{1}{\sqrt{E}} V_0(r) + \frac{1}{2} \frac{B^2}{r} \\ + \frac{1}{2} \int_0^z \left[\frac{1}{r} (A D^2 A_z + A_z D^2 A) + A_r D^2 A_z - A_z D^2 A_r \right] dz$$

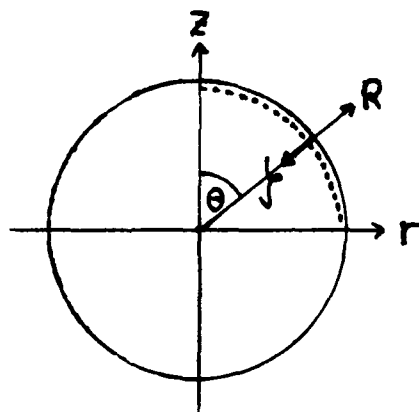
where the geostrophic velocity $E^{-1/2} V_0$ is as yet undetermined. This solution is just fine except that in general ψ won't be zero at the top boundary, and so we need

a boundary layer. So, we expand

$$V = \frac{1}{\sqrt{E}} [V_0(r) + V_1(y, \theta)]$$

$$\Psi = \Psi_0(r, z) + \Psi_1(y, \theta)$$

where $y = \frac{1-R}{\sqrt{E}}$ is the stretched distance measured inward from the boundary.



Then,

$$\frac{\partial}{\partial z} = \cos \theta \frac{\partial}{\partial R} - \frac{\sin \theta}{R} \frac{\partial}{\partial \theta} \approx -\frac{1}{\sqrt{E}} \cos \theta \frac{\partial}{\partial y}$$

$$\frac{\partial}{\partial r} = \sin \theta \frac{\partial}{\partial R} + \frac{\cos \theta}{R} \frac{\partial}{\partial \theta} \approx -\frac{1}{\sqrt{E}} \sin \theta \frac{\partial}{\partial y}$$

$$\nabla^2 = \frac{\partial^2}{\partial z^2} + \frac{\partial^2}{\partial r^2} + \frac{1}{r} \frac{\partial}{\partial r} - \frac{1}{r^2} \approx \frac{1}{E} \frac{\partial^2}{\partial y^2}$$

so to leading order Eqs. (8) and (9) become

$$2\left(-\frac{1}{\sqrt{E}} \cos \theta\right) \frac{\partial \Psi_1}{\partial y} + E \frac{1}{E} \frac{1}{\sqrt{E}} \frac{\partial^2 V_1}{\partial y^2} = 0$$

$$2\left(-\frac{1}{\sqrt{E}} \cos \theta\right) \frac{1}{\sqrt{E}} \frac{\partial V_1}{\partial y} - E \frac{1}{E^2} \frac{\partial^4 \Psi_1}{\partial y^4} = 0$$

Notice, incidentally, that by setting the right-hand sides equal to zero we are neglecting any possible boundary layers in the magnetic field at this order, including any caused by the boundary layer in the velocity acting back on the magnetic field. Thus, this boundary layer is a perfectly ordinary Ekman layer whose only purpose

is to match an interior flow to no-slip boundary conditions; it doesn't interact in any way with the magnetic field.

Returning now to the above equations, a suitably decaying (as $y \rightarrow \infty$) solution is

$$\psi_1 = e^{-cy} [C_s \sin cy + C_c \cos cy] \quad , \quad c = \sqrt{1 - r^2}$$

$$v_1 = \frac{\cos \theta}{c} e^{-cy} [(C_c - C_s) \sin cy - (C_c + C_s) \cos cy]$$

Also, to leading order the no-slip boundary conditions become

$$\psi_0 + \psi_1 = \frac{\partial \psi_1}{\partial y} = v_0 + v_1 = 0 \quad \text{at } y = 0$$

so in fact $C_s = C_c = C$. To fix C we integrate Eq. (8) from 0 to $\sqrt{1-r^2}$, so

$$\int_0^{\sqrt{1-r^2}} (2\psi_2 + ED^2 v) dz = \int_0^{\sqrt{1-r^2}} \frac{1}{r} (A_2(rB)_r - B_2(rA)_r) dz$$

which becomes to leading order

$$\int_0^{\infty} \frac{\partial^2 v_1}{\partial y^2} \frac{dy}{\cos \theta} = \int \frac{1}{r} (A_2(rB)_r - B_2(rA)_r) dz$$

and yields after a little algebra

$$C = -\frac{1}{2} \int \frac{1}{r} (A_2(rB)_r - B_2(rA)_r) dz$$

so finally

$$v_0(r) = -v_1(0, \theta) = -\frac{(1-r^2)^{1/2}}{r} \int_0^{\sqrt{1-r^2}} (A_2(rB)_r - B_2(rA)_r) dz$$

which determines the geostrophic velocity. Then, we note that the factor $(1-r^2)^{1/2}$ is a purely geometric factor due to the curvature of the boundary, which this model can't resolve anyway, and so we neglect it. And of course the same goes for the upper limit of integration, which becomes simply a constant in this model. Then, after integrating by parts once, we get

$$(12) \quad v_0(r) = -\frac{1}{r^2} \frac{d}{dr} \left[r^2 \int_0^{\infty} B A_2 dz \right]$$

which incidentally conserves the total angular momentum of the system, since

$$\int_0^1 r v_0(r) 2\pi r dr = 0$$

Energetics

Having now derived the velocity in terms of the magnetic field, we wish to examine its effect on the total energy. Dotting Eq. (1) with \mathbf{u} and Eq. (2) with \mathbf{B} and adding, we get

$$\frac{1}{2} \frac{\partial}{\partial t} |\mathbf{B}|^2 = \nabla \cdot [(\dot{\mathbf{u}} \times \hat{\mathbf{B}}) \times \hat{\mathbf{B}} - \dot{\mathbf{u}} \rho] + \hat{\mathbf{B}} \cdot \nabla \times (\alpha \hat{\mathbf{B}}) + \hat{\mathbf{B}} \cdot \nabla^2 \hat{\mathbf{B}} + E \dot{\mathbf{u}} \cdot \nabla^2 \dot{\mathbf{u}}$$

and since $\mathbf{u} = 0$ on the boundary the divergence terms vanish when integrated over the whole domain. Thus, the non-linear coupling terms between the velocity and the magnetic field merely transfer energy between kinetic and magnetic; they're not net energy sources. In fact, by distorting the field and thus enhancing diffusion they tend to increase energy losses. (This is in fact precisely how the dynamo equilibrates; the field grows until the increased energy losses just balance the energy sources.) In particular, the geostrophic velocity term always increases energy losses, since its contribution to the energy equation is

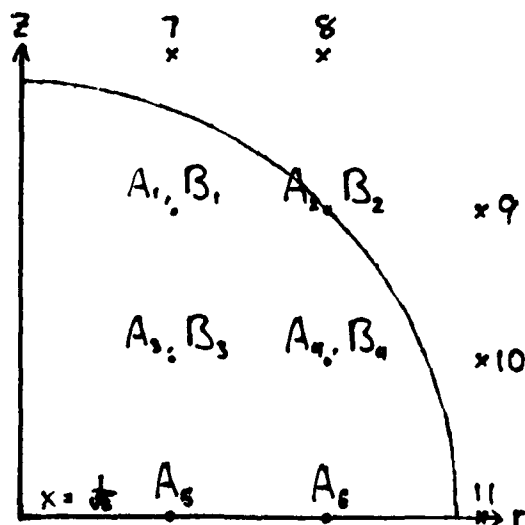
$$\begin{aligned} & \int B \frac{\partial B}{\partial t} r dr dz \\ &= - \int B \left(\left(\frac{\nabla}{r} \right)_r r A_z \right) r dr dz \\ &= \int_0^1 \int_0^{2\pi} r^2 B A_z \frac{d}{dr} \left[\frac{1}{J_E} \frac{1}{r^2} \frac{d}{dr} \left[r^2 \int_0^{2\pi} B A_z dz \right] \right] dz dr \\ &= - \frac{1}{J_E} \int_0^1 \left[\frac{1}{r^2} \frac{d}{dr} \left[r^2 \int_0^{2\pi} B A_z dz \right] \right]^2 r dr \leq 0 \end{aligned}$$

It is obviously important that the numerical implementation of these equations retain this feature.

Numerical Solution

We now wish to numerically solve Eqs. (6) and (7), with ψ and v given by Eqs. (10), (11), and (12). (Actually, in the implementation of v the rather messy integral involving A is neglected for convenience. That shouldn't matter much as long as the ageostrophic velocity terms that are included are capable of equilibrating the field, which they turn out to be. It would of course have been nice to include this term anyway, but time constraints simply didn't permit that.)

The first step in solving these equations is deciding where one wants to represent the solution. The following representation was chosen,



with A extended symmetrically below the equator and B antisymmetrically, which is of course why there is no B_5 or B_6 . Two levels were chosen in r because two is the minimum number one needs to represent a differential rotation, and three levels were chosen in z because three is the minimum number one needs to decide whether the Taylor constraint ($v_o = 0$) is being satisfied point-wise or only integral-wise. Thus, this system is the minimal system that still incorporate enough of the physics we want to study.

Having chosen this representation, one is faced with the immediate difficulty of choosing a finite difference representation of, say, $D^2 A$ at points 1, 2, 4, and 6. The problem, of course, is that A is unknown at points 7, 8, 9, 10, and 11. The solution is to make use of the fact that A must match to a potential field outside, so it must be of the form

$$\sum_{n=1}^{\infty} C_n R^{-2n} P'_{2n-1}(\cos \theta)$$

Truncating this series at $n = 4$ and evaluating it at the proper R 's and θ 's lets one express A_1 , A_2 , A_4 , and A_6 in terms of C_1 through C_4 , or conversely C_1 through C_4 in terms of A_1 , A_2 , A_4 , and A_6 . And of course A_7 through A_{11} are easily expressed in terms of C_1 through C_4 and therefore in terms of A_1 , A_2 , A_4 , and A_6 , which completes the potential match. Evidence that this match is reasonable comes from the fact that in the linearized ($u = 0$), unforced ($\alpha = 0$) problem A decays like $\exp(-8.75t)$, in good agreement with the exact, analytically derivable result $\exp(-\pi^2 t)$.

The only other subtlety in the numerical implementation is the evaluation of the geostrophic velocity, where care must be taken to ensure that it always increases the energy loss. The following procedure was used:

$$\begin{array}{l}
 A_1 \\
 r=0 \quad \left| \quad r^2 \int_0^{2\tau} B A_z dz = 0 \right. \\
 r=x \quad \left| \quad r^2 \int_0^{2\tau} B A_z dz = x^2 \left[B_1 \frac{A_1 - A_5}{2x} \cdot x + B_2 \frac{A_2 - A_3}{2x} \cdot x \right] \equiv x^2 I_1 \right. \\
 r=2x \quad \left| \quad r^2 \int_0^{2\tau} B A_z dz = 4x^2 \left[B_1 \frac{A_1 - A_5}{2x} \cdot x + B_2 \frac{A_2 - A_4}{2x} \cdot x \right] \equiv 4x^2 I_2 \right. \\
 r=3x \quad \left| \quad r^2 \int_0^{2\tau} B A_z dz = 0 \right.
 \end{array}$$

so finite differencing these in r yields

$$\omega(\frac{1}{2}x) = -\frac{1}{J_E} \frac{8}{x^2} (I_1)$$

$$\omega(\frac{3}{2}x) = -\frac{1}{J_E} \frac{8}{27x^2} (4I_2 - I_1)$$

$$\omega(\frac{5}{2}x) = -\frac{1}{J_E} \frac{32}{125x^2} (-I_2)$$

(Note, incidentally, that since $(x/2)^3 \omega(x/2) + (3x/2)^3 \omega(3x/2) + (5x/2)^3 \omega(5x/2) = 0$ total angular momentum is again conserved.) Finally, finite differencing these one more time yields

$$\omega_r(x) = \frac{1}{J_E} \frac{1}{x^3} (8.3 I_1 - 1.2 I_2)$$

$$\omega_r(2x) = \frac{1}{J_E} \frac{1}{x^3} (1.4 I_2 - 0.3 I_1)$$

which has the right energy properties, since its contribution to the energy equation is

$$\begin{aligned}
 & \int B \frac{\partial B}{\partial t} r dr dz \\
 &= -[x^3 \omega_r(x) I_1 + 4x^3 \omega_r(2x) I_2] \\
 &= -\frac{1}{J_E} [7.1 I_1^2 + 4.4 I_2^2 + 1.2 (I_1 - I_2)^2] \leq 0
 \end{aligned}$$

And note that this was by no means guaranteed to work out so nicely; other equally reasonable approximations to $\int \mathbf{B} \cdot \mathbf{A}_2 d\mathbf{z}$ don't necessarily have the right energy properties, leading to great consternation and dismay.

Other than that the numerical implementation is quite straightforward. What one gets ultimately is a system of ten ODE's of the general form

$$\frac{dy_i}{dt} = \sum_{j,k} \left(\frac{1}{\sqrt{E}} C_{ijk} + C'_{ijk} \right) y_j y_k y_i + \sum_j C''_{ij} y_j$$

which is solved using Gear's method (IMSL routine DIVPAG). For order one amplitudes the system is unfortunately very stiff, causing the integration to be quite time-consuming.

Results For α^2 Dynamo

Two choices of α were investigated:

$$\text{Case I: } \alpha = \alpha_0 z^3 r \quad \alpha'' = z^3 r$$

$$\text{Case II: } \alpha = \alpha_0 z \quad \alpha'' = z$$

The results in both cases are similar and in agreement with the original findings of Malkus and Proctor (1975): above a certain critical dynamo number ($D = \max(\alpha\alpha'')$) dynamo action sets in ($D_c \approx 32$ in Case I, and $D_c \approx 25$ in Case II), but the field remains viscously controlled, of order $E^{1/4}$, until a second critical dynamo number is reached ($D_T \approx 35.5$ in Case I, and $D_T \approx 34$ in Case II), at which point Taylor's constraint ($v_o = 0$) is satisfied and the field increases dramatically and becomes independent of E in Case I. In Case II a weak dependence on E remains, to be discussed further below. Also, in the Taylor regime the geostrophic velocity alone is incapable of equilibrating the field; Figure 1 shows the exponential growth of the energy in Case II if only the geostrophic velocity is included, and Case I is similar. There is one notable difference between the two cases though: in Case I the transition from the viscously controlled solution to the Taylor solution is a smooth progression, whereas in Case II it seems to require a finite amplitude jump.

Case I

Figure 2 shows the logarithm of the energy as a function of the dynamo number for several different values of E . Note the clear transition from the viscously controlled regime to the Taylor regime. (Note also that $E = 10^{-4}$ is not quite in the asymptotic regime yet.) Perhaps even more remarkable, however, is how small a change in the structure of the field is required to achieve this transition. Figure 3a shows the viscously controlled solution, whereas Figure 3b shows the Taylor solution; the difference between the two is almost imperceptible, and yet it is sufficient to satisfy Taylor's constraint and increase the field by three orders of magnitude.

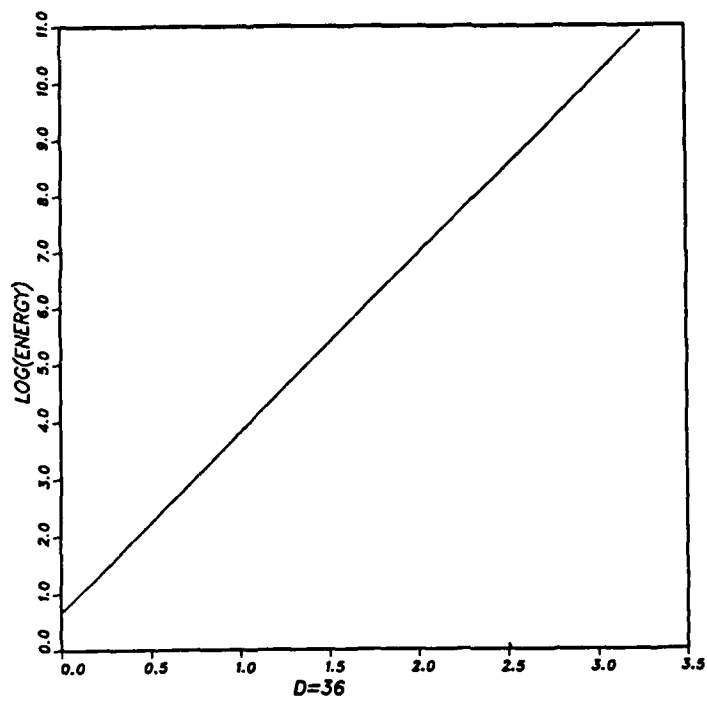


Figure F3.1.

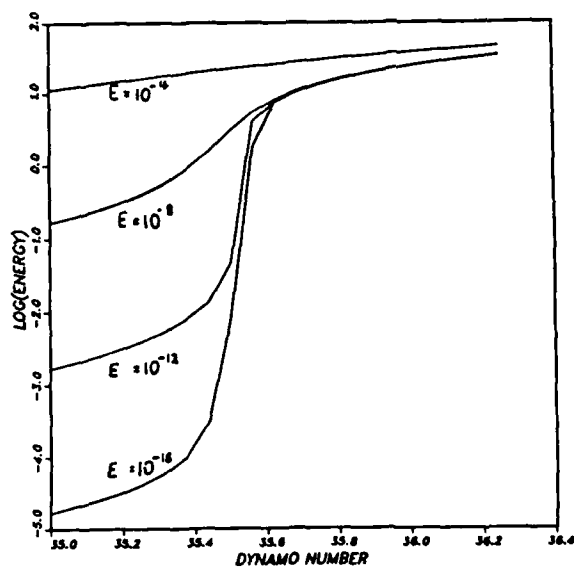


Figure F3.2

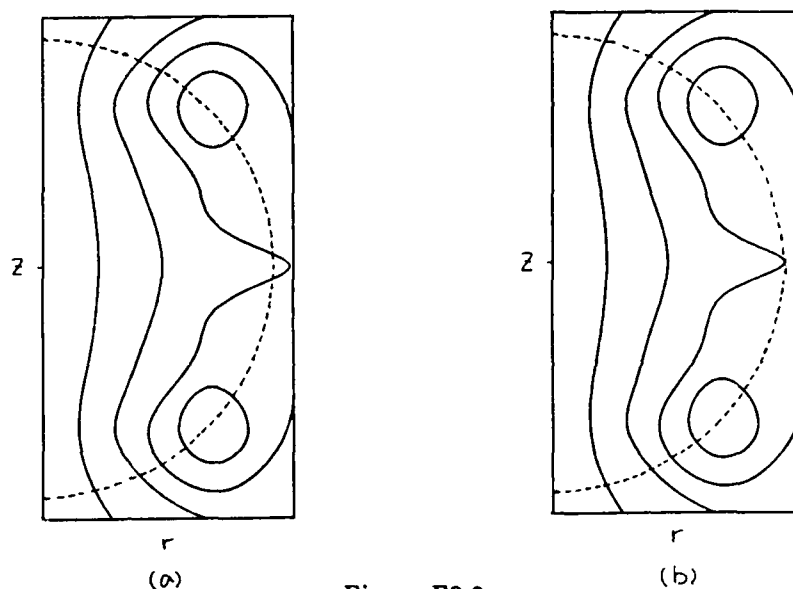


Figure F3.3

Case II

The new feature that emerges in Case II is that the solutions are no longer necessarily steady, as they were in Case I. (Actually, not all solutions of Case I are steady. For $D \gtrsim 37$ fluctuations of the type discussed below emerge, but time constraints did not permit a thorough investigation of these.) Figure 4 shows the energy as a function of time for several different dynamo numbers in the viscously controlled regime: $D = 26$ stabilizes quite rapidly, $D = 28$ fluctuates quite a bit before stabilizing, and $D = 30$ seems to fluctuate indefinitely. Note that these are not true oscillatory dynamos, however, in the sense that the field never reverses direction; it merely fluctuates in amplitude. These fluctuations suggest that perhaps the transition from the viscously controlled regime to the Taylor regime occurs as a finite amplitude instability, in agreement with Soward and Jones (1983), who find that for certain choices of α the viscously controlled solution is not connected to the Taylor solution.

These fluctuations persist even after one has made the transition to the Taylor regime, but the dependence on E changes markedly. In the viscously controlled regime the amplitude scales as $E^{1/4}$, but the period of the fluctuation remains unchanged, whereas in the Taylor regime the amplitude remains unchanged but the period increases gradually with decreasing E , scaling as $\ln(E^{-1})$. Figure 5 shows the logarithm of the energy as a function of time for different values of E , showing clearly the constant peak amplitude and gradually increasing period. Figure 6 shows the period scaling as $\ln(E^{-1})$. Figure 7, which shows the geostrophic velocity as a function of time for different values of E , makes clear why the period scales as it does: once the Taylor state becomes unstable and starts to decay exponentially, the geostrophic velocity must decrease below a fixed value before the field can start to

F3.12

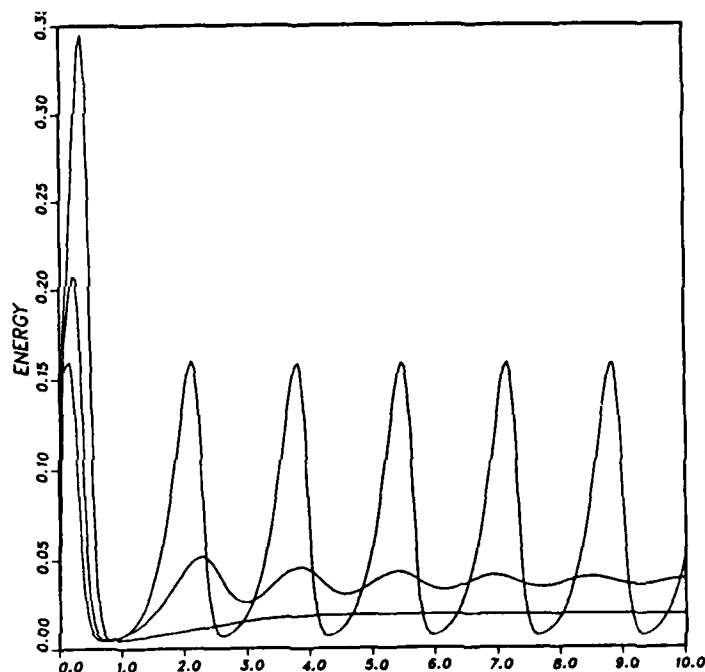
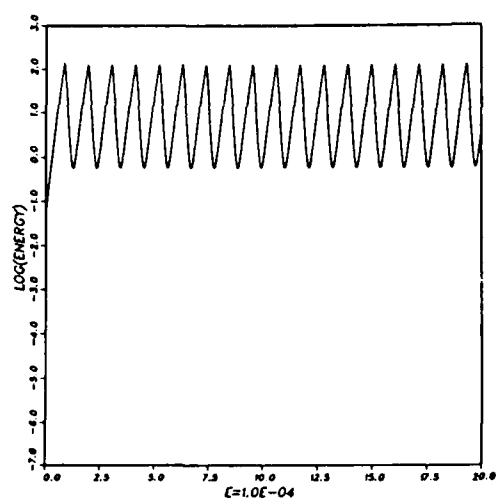


Figure F3.4

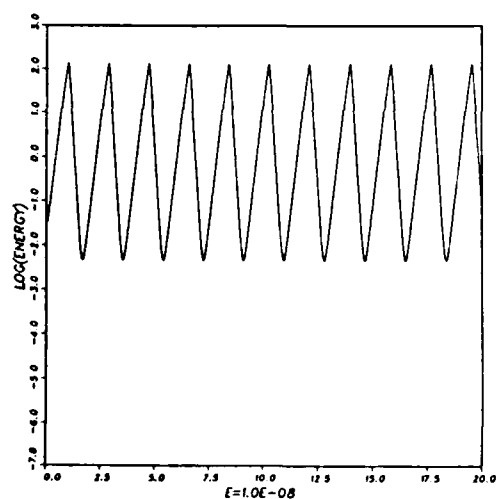
grow again, and so for smaller E the field must decay to a smaller amplitude, which takes longer.

Results For $\alpha\omega$ Dynamo

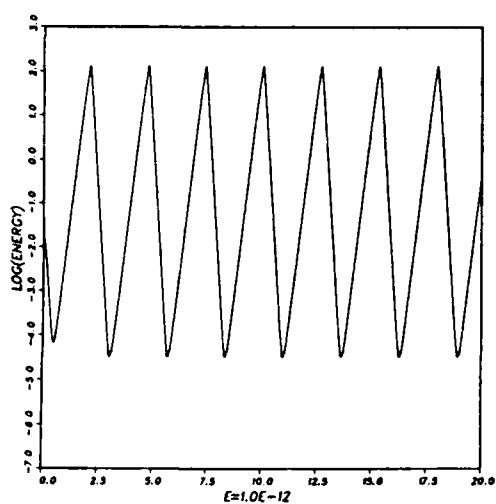
For the $\alpha\omega$ dynamo we set α^* equal to zero and instead regenerate the toroidal field by a prescribed differential rotation ω' that simply gets added to ω_r in Eq. (7). We took $\alpha = \alpha_0 z$ and $\omega' = 100$. As for the α^2 dynamo, above a certain critical dynamo number ($D_c = \max(\alpha\omega') \approx 3860$) dynamo action sets in, although the dynamo is oscillatory now. (The period, about 0.2, doesn't seem to have any special significance, and doesn't change much with D .) However, in sharp contrast to the α^2 dynamo, there doesn't seem to be any Taylor state. Figure 8 shows the logarithm of the energy (averaged over the period) as a function of time, where E is reduced periodically every 5.0 time units, showing that the amplitude scales as $E^{1/4}$ even for $D = 100 \cdot D_c$. Furthermore, there is no evidence of any finite amplitude instability; even if one increases the energy by a factor of 100 or so it always settles back to the value given by the $E^{1/4}$ scaling. Also, if we take $\alpha = \alpha_0 z^3 r$ and $\omega' = 100r$ we get the same result. Thus, the $\alpha\omega$ dynamo seems to be viscously controlled over its entire range.



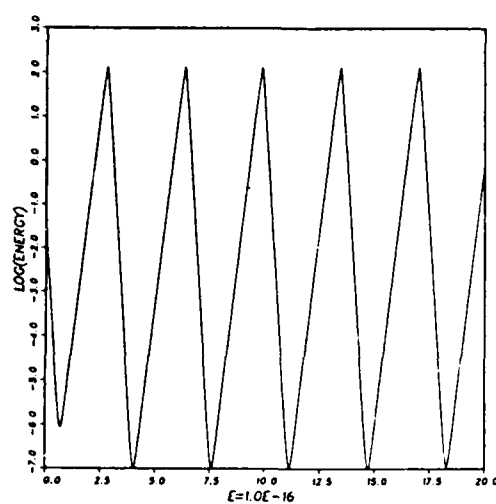
(a)



(b)



(c)



(d)

Figure F3.5

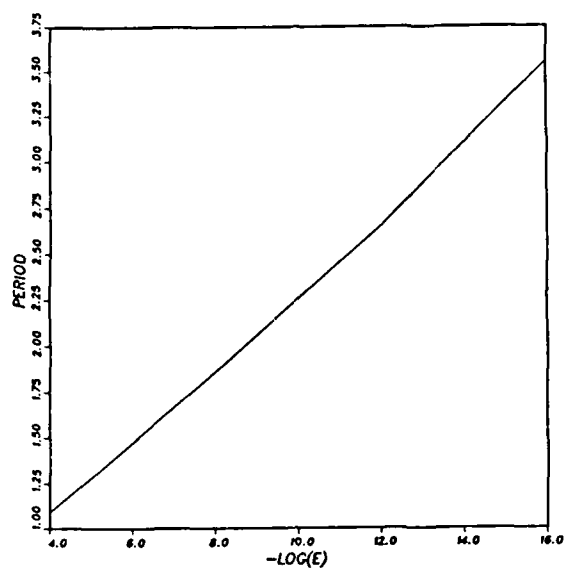
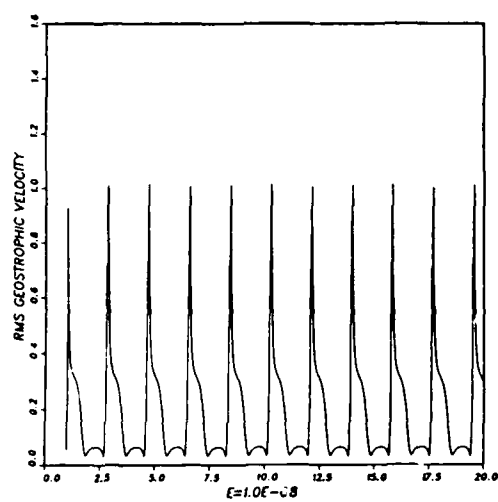
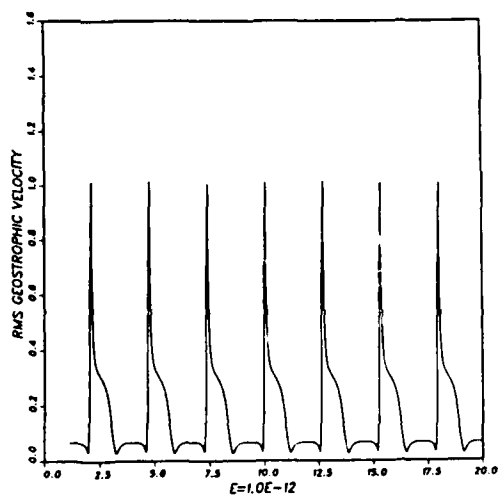


Figure F3.6

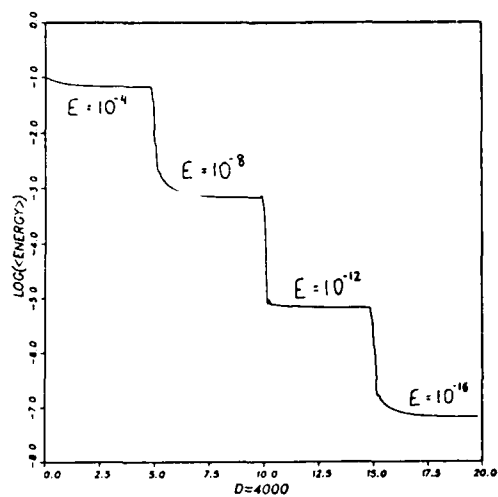


(a)

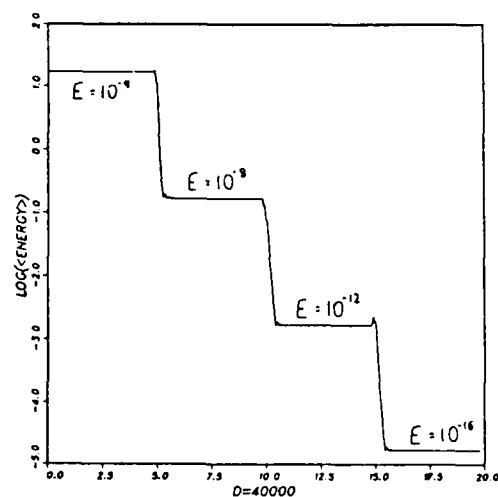


(b)

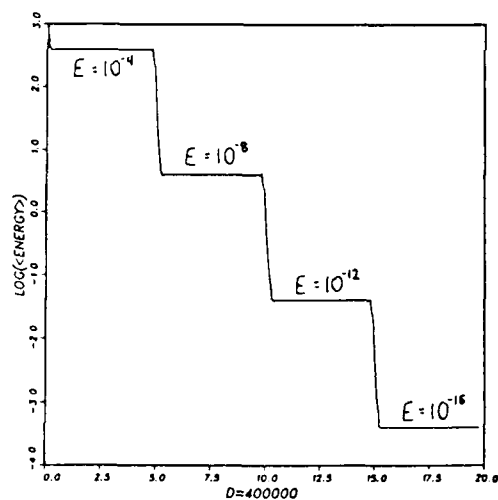
Figure F3.7



(a)



(b)



(c)

Figure F3.8

Acknowledgements

I would like to thank Glenn Ierley not only for having suggested this problem, but also for all the help he gave me along the way. I would also like to thank the rest of the GFD staff for a very enjoyable and stimulating summer.

References

- Ierley, G.R., 1985. "Macrodynamics of α^2 dynamos," *Geophys. Astrophys. Fluid Dynam.*, **34**, 143-173.
- Malkus, W.V.R. and Proctor, M.R.E., 1975. "The macrodynamics of α - effect dynamos in rotating fluids", *J. Fluid Mech.*, **67**, 417- 443.
- Soward, A.M. and Jones, C.A., 1983. " α^2 -Dynamos and Taylor's constraint," *Geophys. Astrophys. Fluid Dynam.*, **27**, 87-122.
- Taylor, J.B., 1963. "The magneto-hydrodynamics of a rotating fluid and the earth's dynamo problem", *Proc. Roy. Soc. A*, **274**, 274-283.

ELLIPTICAL INSTABILITY MODES IN RIGID CONTAINER GROWTH RATE AND REYNOLD STRESSES

Bin Bin Hu
Columbia University

Introduction

Oscillation in a rotating system has been studied for more than one hundred years by many people including Kelvin, Rayleigh and Poincaré, in a variety of geometric situations. Their theory and results are very well known (Greenspan). Poincaré studied eigenvalue problem in rigid rotating system, and found pure oscillation solution $e^{i\lambda t}$, where the eigenvalue $i\lambda$ is pure imaginary, and $|\lambda| < 2(\Omega = 1, \text{ angular velocity of system})$ in general container. In rigidly rotating spheroid, the inertial modes has been classified by Greenspan, Malkus, in terms of the products of Legendre's polynomials, in oblate spheroid coordinates. In general, dependence of the frequencies on the geometric parameters is very complicated.

When flow is not rigid rotating, but has elliptical streamlines, the behavior of the disturbance may be different. In 1986, Pierrehumbert discovered that a broad class of two-dimensional elliptical flow of an incompressible and inviscid fluid are unstable to three dimensional perturbation without short wave cutoff. Bayly gave a very detailed discussion on it in a infinite region. He found that the fundamental modes, which are also the exact solution of non-linear equations, are plane waves whose wave vector rotates elliptically around z axis with a period of $2\Omega \cos \Theta$.

However, real flows are always in a finite region. Questions have, therefore, been raised about the effect of the boundary conditions, in modifying, or perhaps even eliminating the instability. These questions involve the mechanism of energy transfer from mean flow to instability.

The object of this investigation is to study the general properties of the eigenvalues, and eigenfunction of elliptical flow in general containers. And also, we hope to get some knowledge of energy transfer through Reynold stresses between the mean flow and perturbation, from some particular eigensolutions.

General Properties of Instability Eigenmodes in Elliptical Flow

As pointed out before (Malkus and Greenspan), because of the complexity of the dependence of the frequency on the geometry in a rigidly rotating fluid, we expect it impossible, in general, to get the eigensolution of the problem analytically. This suggests that we look for some general properties of the instability problem following the treatment of Greenspan. These properties will help us understand the types of instability expected in elliptical flow.

Without loss of generality, the elliptical flow we have here is following, which also exact solution of $N.S$ equation.

$$\vec{U}_0 = (-Ey, E^2x, 0) \quad (2.1)$$

This velocity can also be described by

$$\vec{u}_0 = \lambda \cdot \vec{x} \quad (2.2)$$

where

$$\lambda = \begin{pmatrix} 0 & -E & 0 \\ E^{-1} & 0 & 0 \\ 0 & 0 & 0 \end{pmatrix} \quad (2.3)$$

in the inertial form.

The Navier-Stokes equations are

$$\partial_t \vec{u} + (\vec{u} \cdot \nabla) \vec{u} = -\nabla p \quad (2.4)$$

$$\nabla \cdot \vec{u} = 0 \quad \text{incompressibility} \quad (2.5)$$

$$\vec{u} \cdot \vec{n} = 0 \quad (2.6)$$

Boundary condition is satisfied on interior of the container.

Now consider the evolution of a small perturbation u^1 to the steady flow u^0 . Neglecting the quadratic terms in u , its evolution is given by linearized equation

$$\partial_t \vec{u}^1 + [(\vec{n} \cdot \vec{x}) \cdot \nabla] \vec{u}^1 + \vec{n} \cdot \vec{u}^1 = -\nabla p^1 \quad (2.7)$$

$$\nabla \cdot \vec{u}^1 = 0 \quad (2.8)$$

$$\vec{u}^1 \cdot \vec{n} = 0 \quad (2.9)$$

Assuming

$$\vec{u}^1(\vec{x}, t) = e^{\sigma t} \vec{v}(\vec{x}) \quad p^1 = e^{\sigma t} p^1(x) \quad (2.10)$$

(2.7) becomes

$$\sigma \vec{v} + [(\vec{n} \cdot \vec{x}) \cdot \nabla] \vec{v} + \vec{n} \cdot \vec{v} = -\nabla p^1 \quad (2.11)$$

$$\nabla \cdot \vec{v} = 0$$

(2.12)

F4.3

$$\vec{v} \cdot \vec{n} = 0$$

(2.13)

Multiplying (2.11) by v^* and integrating over domain, yields

$$\sigma \int |\vec{v}|^2 dV + \int \vec{v}^* \cdot (\nabla \vec{x}) \cdot \nabla \vec{v} dV + \int \vec{v}^* \cdot (\nabla \vec{v}) dV = 0 \quad (2.14)$$

Using the fact that $u^o \cdot n = 0$ i.e. $\Omega_{jk} x_k \cdot n_j = 0$ on the boundary the second term in (2.14), becomes

$$\begin{aligned} & \frac{1}{2} \int \Omega_{jk} x_k \partial_j |v_i|^2 dV - \int v_i \Omega_{jk} x_k \partial_j v_i^* dV \\ &= - \left[\int v_i^* \Omega_{jk} x_k \partial_j v_i dV \right]^* \end{aligned}$$

Hence, this term is pure image.

Third term in (2.14) involves Ω_{ij} , which can be split into symmetric, and anti-symmetric parts.

$$\Omega^S = \frac{1}{2} \begin{pmatrix} 0 & -E+E^{-1} & 0 \\ E^{-1}-E & 0 & 0 \\ 0 & 0 & 0 \end{pmatrix} \quad \Omega^A = \frac{1}{2} \begin{pmatrix} 0 & -(E+E^{-1}) & 0 \\ E+E^{-1} & 0 & 0 \\ 0 & 0 & 0 \end{pmatrix} \quad (2.15)$$

Obviously

$$\int dv_i^* \Omega_{ij}^S v_j = \text{real}$$

$$\int dv_i v_j^* \Omega_{ij}^A v_j = \text{Image}$$

So, if we let $\sigma = \sigma_r + i\sigma_I$, the real part of (2.14) becomes

$$\sigma_R \int |\vec{v}|^2 dv + \int dv v_i^* n_{ij}^s v_j = 0 \quad (2.16)$$

From (2.16) $\sigma_R > 0$ gives rise to instability:

$$\sigma_R = - \frac{\int v_i^* n_{ij}^s v_j dv}{\int |\vec{v}|^2 dv} \quad (2.17)$$

Now by triangle inequality:

$$|(\vec{v}_1, \vec{v}_2)| \leq \frac{(\vec{v}_1, \vec{v}_1) + (\vec{v}_2, \vec{v}_2)}{2}$$

we have

$$|\sigma_R| \leq \frac{1}{2} |E - E^{-1}| \quad (2.18)$$

(2.18) gives an upper bound to the perturbation growth rate. We can see, if we set $E = 1$, $\sigma_R = 0$, zero growth rate, this means circular flow is stable against all perturbations. Imaginary part of growth rate does not seem to be bounded.

Orthogonality Conditions

We are dealing with an eigenvalue problem with eigenvalue σ , eigenvector \vec{v} , and linear operation \hat{L}

$$\sigma \vec{v} + \hat{L} \vec{v} = -v p$$

$$\hat{L} = (\vec{n} \cdot \vec{\nabla}) \cdot \vec{v} + \vec{n}$$

Since \hat{L} is not Hermitian (self adjoint), and so, the eigenvectors are no longer necessarily orthogonal to each other.

Let's look for adjoint operator \hat{L}^+ .

By definition $(\vec{v}_1, \hat{L}\vec{v}_2) = (\hat{L}^+\vec{v}_1, \vec{v}_2)$

where \vec{v}_1, \vec{v}_2

are arbitrary vectors satisfying (2.12) and (2.13).

Then $(\vec{v}_1, \hat{L}\vec{v}_2) = \int [\vec{v}_1^* \cdot (\nabla \times \vec{v}_2 + \Omega \vec{v}_2)] dV.$

Upon integrating by parts, using the boundary condition and incompressibility condition, hence

$$(\vec{v}_1, \hat{L}\vec{v}_2) = \int dV [(-\nabla \times) \cdot \vec{v}_1 + \Omega^T \vec{v}_1] \cdot \vec{v}_2 = (\hat{L}^+\vec{v}_1, \vec{v}_2)$$

so

$$\hat{L}^+ = -(\nabla \times) + \Omega^T \quad (2.19)$$

For, $E = 1$ rigid rotation case: $\Omega^T = -\Omega$.

We have $\hat{L}^+ = -\hat{L}$, i.e. \hat{L} is anti-hermitian, which implies that the eigenfunction of the rigid rotation problem are indeed orthogonal (Greenspan).

Now suppose $\sigma_m, \vec{v}_m, P_m'$ is a set of eigens of operator \hat{L} , (where also $\nabla \cdot \vec{v}_m = 0$ $\vec{v}_m \cdot \vec{n} = 0$) i.e.

$$\sigma_m \vec{v}_m + \hat{L} \vec{v}_m = -\sigma P_m' \quad (2.20)$$

And μ_n, \vec{u}_n, P_n' , satisfying equations for \hat{L}^+ , that is

$$\mu_n \vec{u}_n + \hat{L}^+ \vec{u}_n = -\sigma P_n' \quad (2.21)$$

From (2.20), we have

$$\sigma_m (\vec{u}_n, \vec{v}_m) + (\vec{u}_n, \hat{L} \vec{v}_m) = 0 \quad (2.22)$$

From (2.21),

$$\mu_n^* (\vec{u}_n, \vec{v}_m) + (\hat{L}^+ \vec{u}_n, \vec{v}_m) = 0 \quad (2.23)$$

(pressure term vanish by integrating over domain).

Then subtracting (2.23) from (2.22), gives:

$$(\sigma_m - \mu_n^*) (\vec{u}_n, \vec{v}_m) = 0 \quad (2.24)$$

Hence either

$$\sigma_m = \mu_n^* \quad \text{or} \quad (\vec{u}_n, \vec{v}_m) = 0$$

In Rotating Frame

Using the same method, we can get almost the same conclusion for elliptical flow in a rotating frame.

The perturbation equation is:

$$\partial_t \vec{u} + (\vec{u}_0 \cdot \nabla) \vec{u} + (\vec{u} \cdot \nabla) \vec{u}_0 + 2\vec{\Omega} \times \vec{u} = -\nabla p \quad (2.25)$$

Here again

$$\vec{u}^0 = (-Ey, E^{-1}x, 0) = \begin{pmatrix} 0 & -E & 0 \\ E^{-1} & 0 & 0 \\ 0 & 0 & 0 \end{pmatrix} \begin{pmatrix} x \\ y \\ z \end{pmatrix} = A \vec{x} \quad (2.26)$$

together with incompressibility and boundary condition

$$\nabla \cdot \vec{u} = \vec{u} \cdot \vec{n} = 0$$

Assume $\vec{u} = \vec{v} e^{\sigma t}$ $p' = p' e^{\sigma t}$, we obtain.

$$\sigma \vec{v} + [A \vec{x} \cdot \nabla \vec{v}] + A \vec{v} + 2 \vec{n} \times \vec{v} = -\nabla p \quad (2.27)$$

we obtain

Looking for σ , we get
$$\sigma \int |\vec{v}|^2 dV + \int \vec{v}^* \cdot [A \vec{x} \cdot \nabla + A + 2 \vec{n} \times] \vec{v} dV = 0 \quad (2.28)$$

which is exactly the same as (2.14) except for an extra term which can be shown

to be purely imaginary. We get the same conclusion for σ . So exactly analogous orthogonal condition can be derived in this case also.

Note, in above, we are not limited to any specific geometric container. No matter what the geometry it has, the above results hold true. And these results put nontrivial constraints on the growth rate of perturbations to elliptical flows in general containers.

Polynomial Modes in Ellipsoid

In order to understand elliptical instability in a particular geometry, we should first get the normal modes. But, in general, it is tremendously difficult to discover these modes analytically. Bayly observed (following Greenspan) that finite order polynomials in x, y, z could satisfy the linearized stability equations in the interior of an ellipsoid whose surface can be given by a quadratic form. The coefficients of the polynomials and the mode growth rate can then be found numerically.

In general, we can describe an ellipsoid by

$$\frac{x^2}{a^2} + \frac{y^2}{b^2} + \frac{z^2}{c^2} = 1 \quad (3.1)$$

The problem we have is to find anomalous mode \vec{v} for the following equation.

$$\sigma \vec{v} + (\vec{u} \cdot \nabla) \vec{v} + (\vec{v} \cdot \nabla) \vec{u} = -\nabla p \quad (3.2)$$

$$\nabla \cdot \vec{v} = 0 \quad (3.3)$$

$$\vec{v} \cdot \vec{n} = 0 \quad (3.4)$$

Assuming

$$\vec{v} = u \hat{e}_x + v \hat{e}_y + w \hat{e}_z \quad (3.5)$$

we seek velocity component in the form

$$u, v, w = \sum_{l, m, n} C_{l, m, n}^{u, v, w} x^l y^m z^n \quad (3.6)$$

$$0 \leq l+m+n \leq N$$

with pressure field

$$p = \sum_{l+m+n \leq N+1} p_{l,m,n} x^l y^m z^n \quad (3.7)$$

pressure is given by solving

$$\nabla^2 p = - \nabla \cdot [(\vec{u}^0 \cdot \nabla) \vec{v} + (\vec{v} \cdot \nabla) \vec{u}^0] \quad (3.8)$$

with B.C.

$$\vec{n} \cdot \nabla p = + \vec{n} \cdot [(\vec{u}^0 \cdot \nabla) \vec{v} + (\vec{v} \cdot \nabla) \vec{u}^0] = -2U_0 y^0 \partial_z n_y \quad (3.9)$$

put u^0, v, P into equations, we can get a linear system from which we can get velocity growth rate σ and normal modes v numerically.

One of the normal modes found (by Bayly) is

$$u = 0.299175z - 0.211611x^2z + 0.202253xy^2z - y^2z \\ - 8.25841 \times 10^{-2} z^3$$

$$v = 0.237336z - 0.242064x^2z + 9.67917 \times 10^{-2} xy^2z \\ - 0.51885 y^2z - 5.8182 \times 10^{-2} z^3$$

$$w = -0.217363x - 0.596582y + 8.85462 \times 10^{-2} x^3 \\ + 0.281312x^2y + 0.295778 y^2x + 0.163216 xz^2 \\ + 0.877843 + 0.417428 yz^2$$

F4.10

together with pressure term.

$$P = 0.148949x^2z - 9.22106 \times 10^{-2}yz - 6.83489 \times 10^{-2}x^3z + 5.58857 \times 10^{-2}xy^2z \\ - 0.116707 \times y^2z - 3.54482 \times 10^{-2}x^3z + 0.116195y^3z + 2.44492 \times 10^{-2}yz^3$$

and growth rate

$$\sigma = 0.136470$$

To investigate the effect of the growing perturbation on the mean flow, we now allow the mean flow to evolve on a long time $\tau = \epsilon^2 t$ we write

$$\vec{u} = \vec{u}_{\text{mean}}(\vec{x}, \tau) + \epsilon \vec{u}' \quad (3.10)$$

$$p = p_0 + \epsilon p' + \epsilon^2 p'' \quad (3.11)$$

Also with

$$\nabla \cdot \vec{u}_m = \nabla \cdot \vec{u}' = \vec{n} \cdot \vec{u}' = \vec{u}_m \cdot \vec{n} = 0 \quad (3.12)$$

Put (3.10) and (3.11) into N.S. equation, we get

$$\vec{u}_m \cdot \nabla \vec{u}_m = -\nabla p_0 \quad (3.13)$$

$$\partial_t \vec{u}_m = -\nabla p' - \vec{u}' \cdot \nabla \vec{u}' \quad (3.15)$$

$$\partial_t \vec{u}' + \vec{u}_m \cdot \nabla \vec{u}' + \vec{u}' \cdot \nabla \vec{u}_m = -\nabla p' \quad (3.14)$$

From (3.14), we can choose u^1 to be a particular unstable velocity mode.

From (3.15), we obtain

$$\frac{d}{dt} \int dV \frac{1}{2} |\vec{u}_m|^2 = \int u_i^1 u_j^1 \partial_j u_{im}^1 dV = - \int S dV \quad (3.16)$$

where

$$S = -T_{ij} \partial_j u_{im}^1 = -u_i^1 u_j^1 n_{ij}$$

playing a role of energy source.

To see some interesting features of energy being transferred from mean flow to building up instability, for simplicity, we take an explicit normal mode described above and calculate T_{ij} and S . See plot.

We can see, S is symmetric about xoy plane, and for $Z = 0$ plane, $S = 0$, so no energy transfer happens.

For nonzero z , energy transfer substantially, especially near the ends of the ellipsoid. This may have some relevance to observation of Malkus that flow in an elliptical cylinder breaks down most violently near the ends.

Now, let's see how the higher order modes affect the mean flow amplitude.

Again the mean flow is denoted by u^0 which can be thought as the 0th order eigenvectors with zero growth rate. The velocity can be expressed as

$$\vec{u} = \vec{u}_0 + \sum_{n=0} a_n(t) \vec{u}_n e^{\sigma_n t} = \vec{u}_0 + \vec{u}^1 \quad (3.17)$$

$$p = p_0 + \sum C_n p_n = p_0 + p^1 \quad (3.18)$$

Substituting this into N.S. equation, we get

$$\sum_{n=0}^{\infty} \left[(\partial_t a_n) \vec{u}_n + a_n \sum_{m=0}^{\infty} a_m \left((\vec{u}_m \cdot \nabla) \vec{u}_n + (\vec{u}_n \cdot \nabla) \vec{u}_m \right) \right] = -\nabla p' \quad (3.19)$$

Hence we get the equation for the coefficients. And the difficulty is that we do not know the complete family of eigenfunctions. For simplicity, we seek for v_0 , for which

$$\hat{L}^+ \vec{v}_0 = -\nabla p_0$$

we know also from

$$\sigma_m - \mu_n^* \neq 0 \quad \text{that} \quad (\vec{u}_m, \vec{v}_0) = 0$$

Now recall that

$$\hat{L}^+ \vec{v}_0 = -(\vec{n} \cdot \nabla) \vec{v}_0 + \vec{n} \nabla \cdot \vec{v}_0 = -\nabla p_0$$

where

$$\vec{n} = \begin{pmatrix} 0 & -E & 0 \\ E^{-1} & 0 & 0 \\ 0 & 0 & 0 \end{pmatrix}$$

It can be verified $v_0 = u_0 = \Omega x$ since it satisfies that boundary condition and the adjoint momentum equation, with pressure field

$$p_0 \propto |\vec{x}|^2$$

So the evolution of mean flow is given by

$$\partial_t a_0 \int |\vec{v}_0|^2 dV + \sum_{n,m=0} a_n a_m \int \vec{v}_0^* \left[(\vec{u}_m \cdot \nabla) \vec{u}_n + (\vec{u}_n \cdot \nabla) \vec{u}_m \right] dV = 0 \quad (3.19)$$

scaling (3.19), $a_0 \sim \epsilon^2$ $a_n \sim \epsilon$

we have

$$\partial_t a_0 \int |\vec{v}_0|^2 dV + \sum_{n,m=1} \int \vec{v}_0^* \cdot \left[(\vec{u}_m \cdot \nabla) \vec{u}_n + (\vec{u}_n \cdot \nabla) \vec{u}_m \right] dV = 0 \quad (3.20)$$

Superposition in Elliptical Cylinder

Bayly, using the Floquet theory in infinite region, found the plane wave-like modes for instability. But if we look at high wave number modes in a large but finite region, we should still get some approximate results by superposition of plane waves. We look at a elliptical cylinder.

The modes we have from Bayly are

$$\vec{u} = e^{\sigma t} \vec{f}(nt + \varphi_0) e^{i\vec{k}_0 \cdot \vec{r}} \quad (4.1)$$

where φ_0 is an arbitrary phase constant and f satisfies

$$\frac{df_i(\varphi)}{d\varphi} = (2\varphi^{-2} f_i \varphi_j - \delta_{ij}) \bar{A}_{j\ell} f_\ell(\varphi) \quad (4.2)$$

and $\bar{A}_{j\ell} = \begin{pmatrix} 0 & -E & 0 \\ E & 0 & 0 \\ 0 & 0 & 0 \end{pmatrix} \quad (4.3) \quad f(\varphi) = f(\pi + \varphi) \quad (4.4)$

$$\vec{\varphi} = (\sin \theta \cos \varphi, E \sin \theta \sin \varphi, \cos \theta)$$

We seek a particular superposition of these waves to make u^1 satisfy the boundary conditions $u^1 \cdot \vec{n} = 0$.

A particularly simple superposition is to weight each phase constant φ equally, i.e.

$$\vec{u} = A e^{\sigma t} \left[\int_0^{2\pi} d\varphi_0 \vec{f}(nt + \varphi_0) \exp[i\vec{k}_0 \cdot \vec{r}] + c.c. \right] \quad (4.5)$$

Here, we use elliptical polar coordinates representation

$$\vec{r} = (rE\cos\chi, rE\sin\chi, z)$$

$$r^2 = \sqrt{x^2/E^2 + y^2}$$

$$\chi = \tan^{-1}(Ey/x)$$

with this representation we rewrite the integral as

$$\vec{u}_1 = Ae^{\sigma t} \left[\int_0^{2\pi} d\varphi_0 \vec{f}(\varphi_0 + \pi t) \exp \left[i k_0 z_0 r E \cos(\pi t + \varphi_0 - \chi) + i k_0 z_0 \omega t \right] \right] + c.c.$$

for $k_0 r \gg 1$. This is a rapidly changing phase function except near $\varphi = \begin{matrix} \chi, \chi + \pi \\ \chi_{st} \end{matrix}$. So the dominant contributions come from the vicinity of these points.

$$\begin{aligned} \vec{u}_1 = Ae^{\sigma t} & \int_0^{2\pi} d\varphi \left[\vec{f}(\chi) + \eta f'(\chi) + \dots \right] \exp(i k_0 r E \cos \varphi + i k_0 z_0 \omega t) \\ & \cdot \exp \left[-i k_0 r E \frac{1}{2} (\chi - \varphi)^2 + \dots \right] + \int_0^{2\pi} d\varphi \left[\vec{f}(\chi + \pi) + \eta f'(\chi + \pi) + \dots \right] \\ & \cdot \exp \left[-i k_0 r E \frac{1}{2} (\chi + \pi - \varphi)^2 + \dots \right] + c.c. \end{aligned}$$

Neglecting high order, we get

$$\begin{aligned} \vec{u}_1 \approx Ae^{\sigma t} & \vec{f}(\chi) \exp(i k_0 z_0 \omega t) \frac{1-i}{\sqrt{k_0 r E |\sin \chi|}} \frac{\sqrt{\pi}}{2} (e^{i k_0 r E \sin \chi} + e^{-i k_0 r E \sin \chi}) \\ & + c.c. \end{aligned} \quad (4.6)$$

F4.16

at surface of elliptical cylinder $r=R, z=0, L$

$$\vec{u}_1 \cdot \vec{n} = 0$$

we put

$$k_0 R E \sin \theta = (n + \frac{1}{2}) \pi$$

$$k_0 L \cos \theta = (m + \frac{1}{2}) \pi$$

The part we neglected is about

$$O\left(\frac{1}{k_0 R E \sin \theta}\right)$$

which is negligible as

$$k_0 R E \sin \theta \rightarrow \infty$$

As before the Reynold stress tensor

$$T_{ij} = \overline{u_i' u_j'}$$

(4.7)

where the overbar denote average over local region in which

$$k_0 a \gg 1$$

Using (4.6)

$$T_{ij} = \frac{\text{Const}}{r} f_i(x) f_j(x) \quad (4.8)$$

The force which Reynold stress exerts on the mean flow is

$$F_i = -\partial_j T_{ij} = -\text{Const} \left[-\frac{f_i f_j}{r^3} x_j + \frac{1}{r} (f'_i(x) f_j(x) + f_j(x) f'_i(x)) \right]$$

$$\nabla \chi = -\frac{\epsilon}{r^2} \begin{pmatrix} y \\ x \end{pmatrix}$$

Using the results Bayly got, from numerical calculations, for $f(x)$, (4.8), (4.9), we can plot energy dissipation versus angles, and force in various points as shown in Plot 2.

We can see, as before, energy dissipation peak at the ends of elliptical flow.

Acknowledgements

I greatly appreciate Dr. Bayly for directing me on this paper. Most of this was based on his thought. I also thank Prof. Malkus for his helpful discussion and encouragement.

References

Bayly, B.J. 1986. "Three-dimensional Instability of Elliptical Flow", *Phys. Rev. Lett.*, 57, 2160.

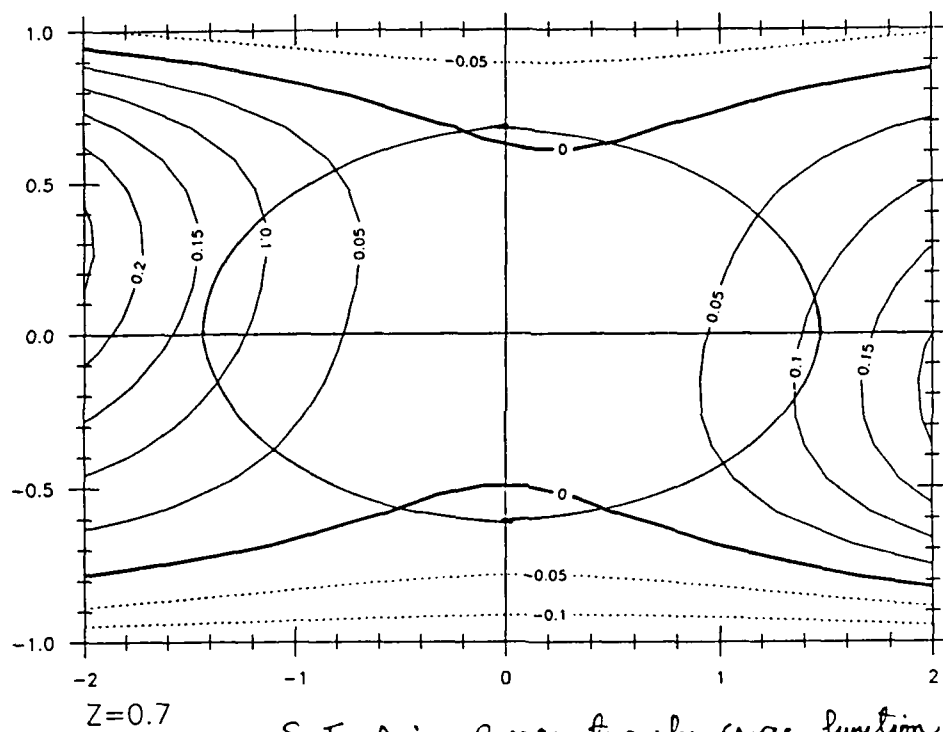
Greenspan, H.P. *The Theory of Rotating Fluids*.

Malkus, W.V.R. *Motions in the Fluid Core*.

Pierrehumbert, R.T., 1986. "Universal Short-Wave Instability of two dimensional Eddies in an inviscid fluid". *Phys. Rev. Lett.*, 57, 2157.

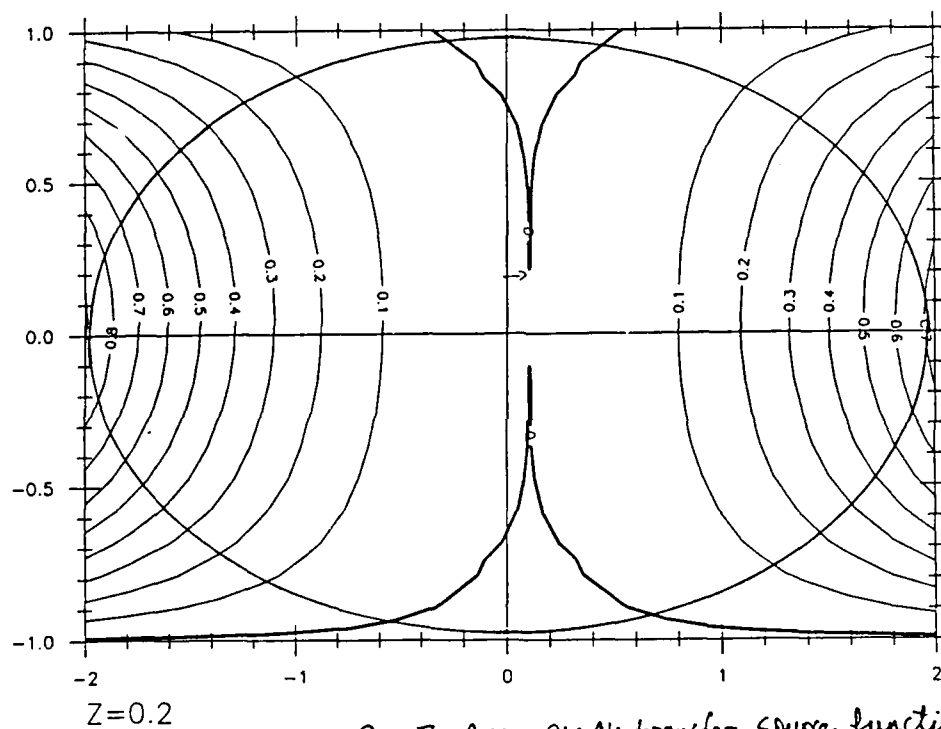
$$\frac{x^2}{4} + y^2 + z^2 = 1$$

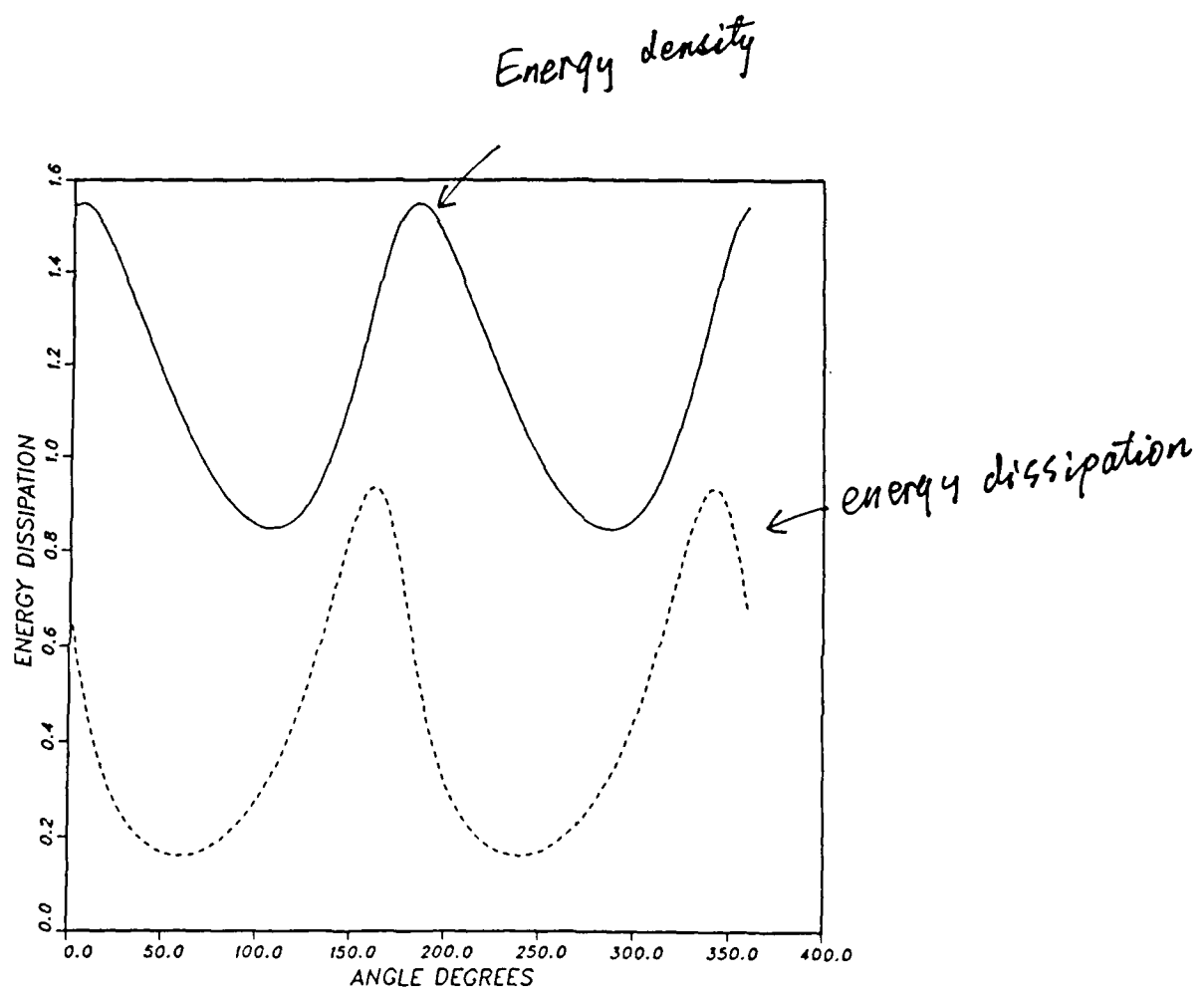
plot 1.a



$$\frac{x^2}{4} + y^2 + z^2 = 1$$

Plot. 1.6

 $S = T_{ij} n_{ij}$: energy transfer source function



Plot 2.

SYMMETRY BREAKING IN THE SOLAR DYNAMO

Richard Jennings
University of Newcastle-Upon-Tyne

Observations of the solar cycle show North, South asymmetries. A low order kinematic dynamo is formulated to examine a mechanism for such symmetry breaking. This model is then extended into the dynamic regime, and nonlinear equations valid in a thin layer are derived for the magnetic fields.

Introduction

The eleven year sunspot cycle is intimately related to the solar dynamo (e.g. Priest, p. 46). Examination of the butterfly diagrams shows that different numbers of spots can appear in *one or other* of the hemispheres during a cycle (Maunder, 1922; Kuiper, 1953). See Figure 1.

Spots are not acting dynamically in the dynamo but are merely indicators of magnetic field rising to the surface due to magnetic buoyancy (Priest, p. 291-299). Therefore, more spots appearing in either hemisphere indicates symmetry breaking in the magnetic fields.

A dynamo process for the production of magnetic field in stars seems highly likely (e.g. Priest, p. 325), and the likely stellar ingredients necessary for a dynamo are rotation and a turbulent convective envelope (Weiss, 1986). For this reason I shall adopt an $\alpha\omega'$ dynamo in my model:

ω' (differential rotation): Poloidal \rightarrow Toroidal

α (turbulence/helicity): Toroidal \rightarrow Poloidal

Parity Selection

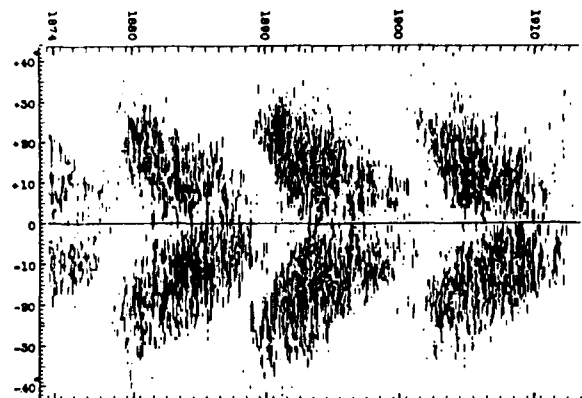
The stable existence of some quadrupole field, together with the dominant oscillatory dipole field (as shown by the sun in the cycles) would give North/South asymmetries as in Figure 2.

Marginality for these modes is considered even though in a star seed fields of infinitesimal amplitudes do not exist. However, the bifurcation structure of the equations is arguably related to the bifurcations that a star can undergo.)

Previous Work

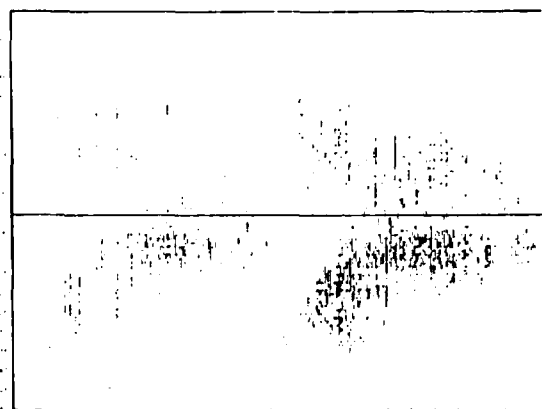
Parker 1955: suggests dynamo waves are responsible for the migration of spots towards the equator during a cycle. If the product $\alpha\omega' < 0$ in the Northern Hemisphere (N), then migration is pole \rightarrow equator.

Roberts 1972: examined kinematic dynamos by solving the induction equation in a sphere. For many models he found critical eigenvalues λ_c such that λ_c (dipole type) $\approx \lambda_c$ (quadrupole type).



"Butterfly" diagram representing the latitude distribution of sunspots from 1874 to 1913 (Maunder, 1922).

More Spots in Southern Hemisphere



Maunder's butterfly diagram showing the latitude distribution of sunspot occurrence as a function of time for two complete cycles.

More Spots in Northern Hemisphere

Figure F5.1: Butterfly Diagrams

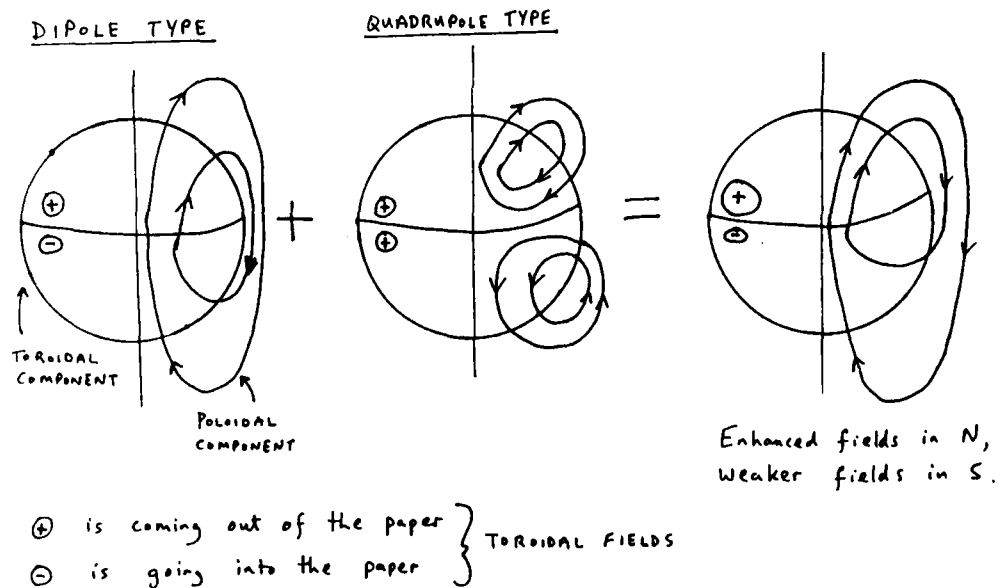


Figure F5.2

Proctor 1976: found a class of kinematic \mathbf{u} for which the eigenvalue problems for dipole and quadrupole types are identical (not the case for my model).

Stix 1972: isolated a marginal oscillatory dipole field by disallowing all other solutions. By introducing a cut-off in the α -effect and doing finite amplitude analysis he obtained spiky nonlinear dynamo waves.

The Model

Starting with the induction equation and a kinematic \mathbf{u}

$$\frac{\partial \underline{\mathbf{B}}}{\partial t} = \nabla \times (\underline{\mathbf{u}} \times \underline{\mathbf{B}}) + \nabla \times (\underset{\substack{\uparrow \\ \text{Forcing}}}{\alpha} \underline{\mathbf{B}}) + \eta \nabla^2 \underline{\mathbf{B}} \quad (1)$$

where η is a turbulent magnetic diffusivity.

$$\underline{\mathbf{u}} = v(r, \theta) \hat{\underline{\phi}}, \quad \underline{\mathbf{B}} = \underset{\text{Toroidal}}{B(r, \theta, t) \hat{\underline{\phi}}} + \underset{\text{Poloidal}}{\nabla \times (A(r, \theta, t) \hat{\underline{\phi}})} \quad (2)$$

for spherical coordinates (r, θ, ϕ) . All variables are independent of the azimuthal direction $\hat{\underline{\phi}}$.

The Form of α and ω'

Variation of \mathbf{u} in the radial direction gives ω' . Also, rotation rate is a function of latitude on the sun (fastest at equator). To model this take

$$v(r, \theta) = \omega' r \sin \theta$$

so that $\frac{\partial v}{\partial r} = \omega' \sin \theta$ independent of r . (3)

Alpha (α) is related to the helicity of turbulence (Moffatt) which has opposite sign in each hemisphere due to its relation with the Coriolis force. Alpha is taken to be zero at the equator i.e.

$$\alpha = \alpha_0 \cos \theta \quad \text{independent of } r. \quad (4)$$

For agreement with the pole \rightarrow equator migration we need $\alpha \omega' < 0$. Since $\alpha > 0$ in N , we need $\omega' < 0$ corresponding to faster rotation going into the sun.

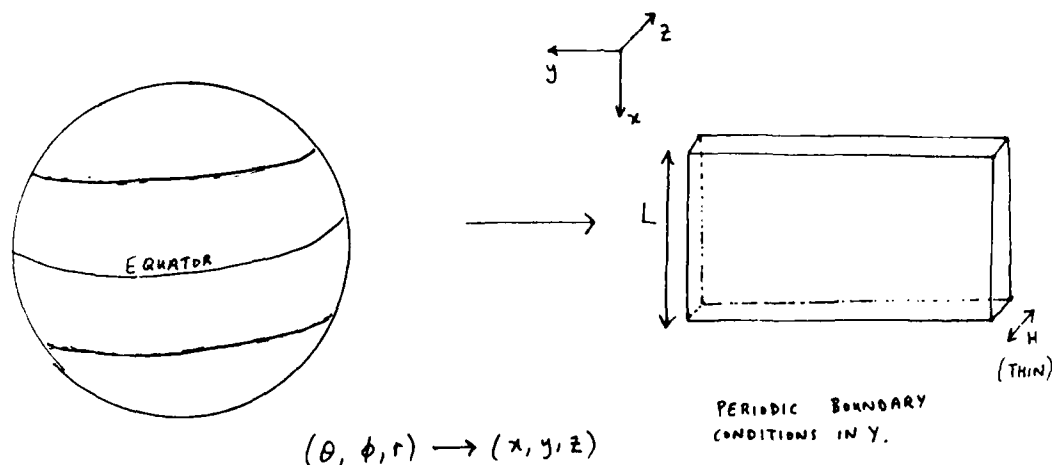


Figure F5.3: Coordinates

Coordinates

Cartesian geometry is used for convenience. This can be justified as almost all the dynamo action occurs between latitudes $\pm 25^\circ$ (Priest, p. 54) where curvature is less important.

A thin layer is considered as in Figure 3 and all z -dependence is averaged out.

Equations

$$\frac{\partial A}{\partial t} = \alpha_0 \cos x B + \eta \frac{\partial^2 A}{\partial x^2} \quad \text{(Toroidal} \rightarrow \text{Poloidal via } \alpha) \quad (5)$$

(obtained by uncurling one component)

$$\frac{\partial B}{\partial t} = \omega' \sin x \frac{\partial A}{\partial x} + \eta \frac{\partial^2 B}{\partial x^2} + [\text{Another } \alpha] \quad \left(\text{Poloidal} \rightarrow \text{Toroidal via } \omega' \right) \quad (6)$$

The second α -effect is ignored on the assumption that the regeneration of toroidal from poloidal field is dominated by differential rotation.

Rescaling the variables:

$$t \rightarrow \frac{L^2}{\eta} t^*, \quad x \rightarrow L x^*, \quad A \rightarrow \frac{\eta A^*}{\omega' L^3}, \quad B \rightarrow B^* \quad (7)$$

where L is on the scale of the solar radius, allows the equations to be written as:
(dropping stars)

$$\frac{\partial A}{\partial t} = -D \cos x B + \frac{\partial^2 A}{\partial x^2}, \quad \frac{\partial B}{\partial t} = \sin x \frac{\partial A}{\partial x} + \frac{\partial^2 B}{\partial x^2} \quad (8, 9)$$

with $A = A(x, t)$, $B = B(x, t)$ and a dimensionless dynamo number D :

$$D = \frac{\alpha_0 \omega' L^3}{\eta^2} \quad (10)$$

The minus sign in α with D is used for convenience. For $D < D_c$, $A = B = 0$ is the solution (no dynamo).

Boundary Conditions

$$B = 0, \quad x = 0, \pi$$

$$A = 0, \quad x = 0, \pi$$

$$\begin{array}{c} x=0 \\ \vdots \\ x=\pi/2 \\ \text{(equator)} \\ \vdots \\ x=\pi \end{array} \quad (11)$$

In general the potential A can be chosen to vanish at $x = 0$ and $x = \pi$ even though the poloidal field does not.

Seek solutions of the form:

Dipole Type:

$$\begin{aligned} B(x, t) &= B_1(t) \sin 2x + B_2(t) \sin 4x + \dots \\ A(x, t) &= A_1(t) \sin x + A_2(t) \sin 3x + \dots \end{aligned} \quad (12)$$

Quadrupole Type:

$$\begin{aligned} B(x, t) &= B_1(t) \sin x + B_2(t) \sin 3x + \dots \\ A(x, t) &= A_1(t) \sin 2x + A_2(t) \sin 4x + \dots \end{aligned} \quad (13)$$

Each parity has infinite modes, with each mode marginal at some value of D . These bifurcations can be either stationary or oscillatory. Furthermore, it can be shown that none of the A_n 's or B_n 's can be missing in any of the modes.

Reflection about $x = \pi/2$ by $x \rightarrow \pi - x$ gives:

$$\begin{array}{ll} \alpha \rightarrow -\alpha & \left. \begin{array}{l} A \rightarrow A \\ B \rightarrow -B \end{array} \right\} \text{DIPOLE} \\ \omega' \rightarrow \omega' & \left. \begin{array}{l} A \rightarrow -A \\ B \rightarrow B \end{array} \right\} \text{QUADRUPOLE} \end{array} \quad (14)$$

CRITICAL DYNAMO NUMBERS

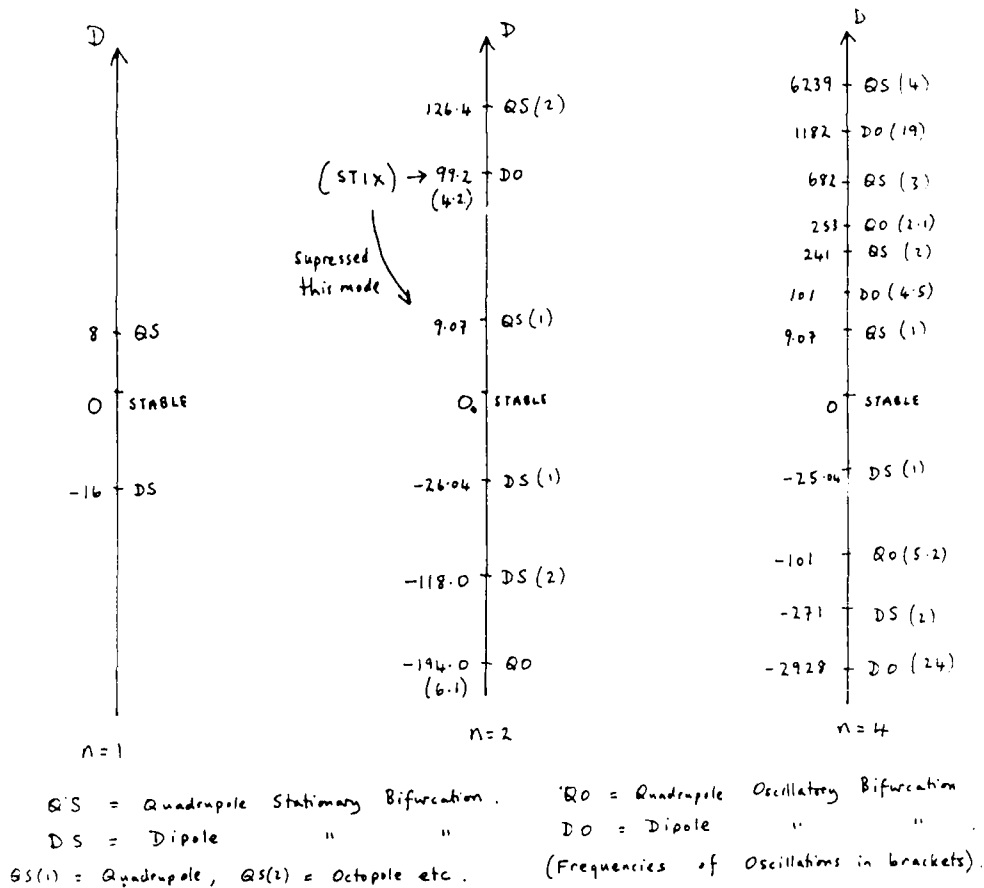


Figure F5.4

with the equations for the respective parities unchanged. Hence, we can solve for A and B in the range $x \in [0, \pi/2]$. Boundary conditions at $x = \pi/2$ become:

$$\left. \begin{aligned} B &= 0 \\ \frac{\partial A}{\partial x} &= 0 \end{aligned} \right\} \text{DIPOLE}, \quad \left. \begin{aligned} \frac{\partial B}{\partial x} &= 0 \\ A &= 0 \end{aligned} \right\} \text{QUADRUPOLE} \quad (15)$$

Assuming that the coefficients $A_n, B_n \rightarrow 0$ as $n \rightarrow \infty$ it is reasonable to truncate the series solutions 12 and 13. Truncating after n terms gives critical values of D (in qualitative agreement with Roberts). See Figure 4.

Clearly the most unstable modes are:

$$\begin{aligned} QS(D_c = +9.07) & \quad \text{if} \quad D > 0 \\ DS(D_c = -25.04) & \quad \text{if} \quad D < 0 \end{aligned} \quad (16)$$

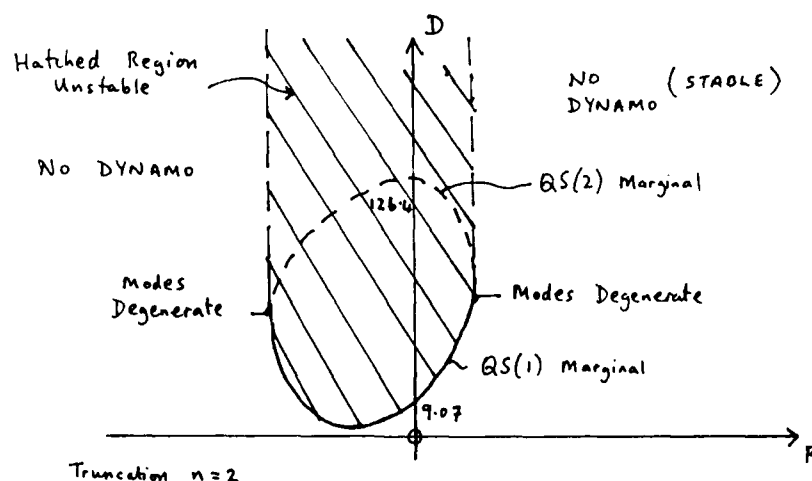


Figure F5.5

There is no possibility of simultaneously exciting dipole and quadrupole modes. Also, note that the oscillatory modes are excited long after the first stationary ones.

Meridional flows can influence dynamo behavior (see Roberts, Moffatt, and Priest, p. 18) and such a flow is now introduced to the model as $U_0 \sin 2x \hat{z}$ (kinematic).

An extra term results from $\nabla \times (u \times B)$, and equations 8 and 9 can be written in the form:

$$\frac{\partial A}{\partial t} = -D \cos x B - R \sin 2x \frac{\partial A}{\partial x} + \frac{\partial^2 A}{\partial x^2} \quad (17)$$

$$\frac{\partial B}{\partial t} = \sin x \frac{\partial A}{\partial x} - R \sin 2x \frac{\partial B}{\partial x} + \frac{\partial^2 B}{\partial x^2} \quad (18)$$

where R is a Reynold's number defined as $\frac{U_0 L}{\nu}$

Marginal Curves

Truncating after two terms in each series, the marginal curve for the first two QS modes in the R - D plane is as in Figure 5. At the degeneracies two modes are simultaneously excited and we have a bifurcation co-dimension two. However, the degeneracies of Figure 5 may only be a consequence of truncating with the true picture possibly as in Figure 6, where all the plane above the solid line is unstable. Further work is needed to clarify this issue.

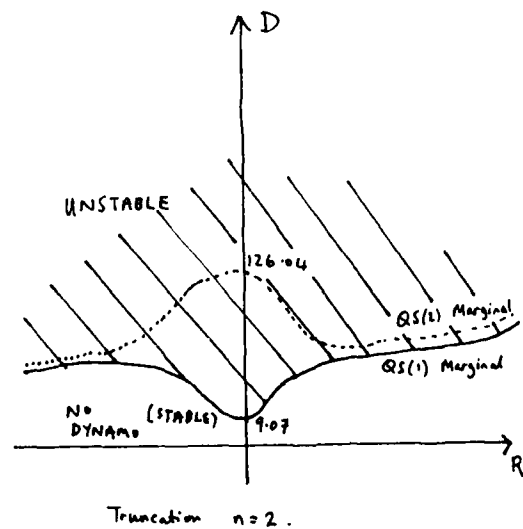


Figure F5.6

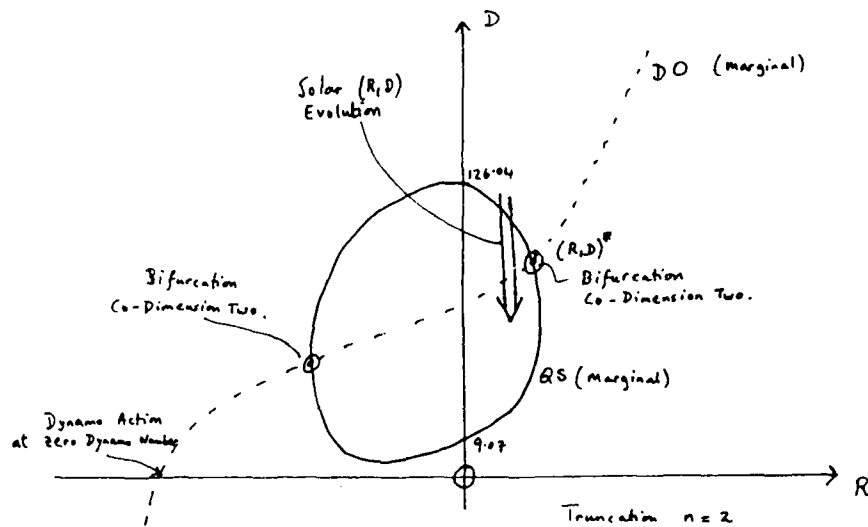


Figure F5.7

The simultaneous excitation of a QS and a DO field (see Figure 7) is interesting for the sun and this bifurcation is chosen for careful analysis in the next section. Solar values of (R, D) change with time (see arrow of Figure 7) e.g. D decreases with spindown, although it is unlikely that the solar (R, D) coincides with $(R, D)^*$. The reason we examine $(R, D)^*$ so carefully is that the local behavior is thought to extend far into the (R, D) plane.

Can a Dynamo Work at $D = 0$?

A quick analysis of equations 17 and 18 shows that steady solutions are impossible at $D = 0$ ($A = B = 0$ only solution), but non trivial oscillatory solutions are possible.

Other Marginal Modes

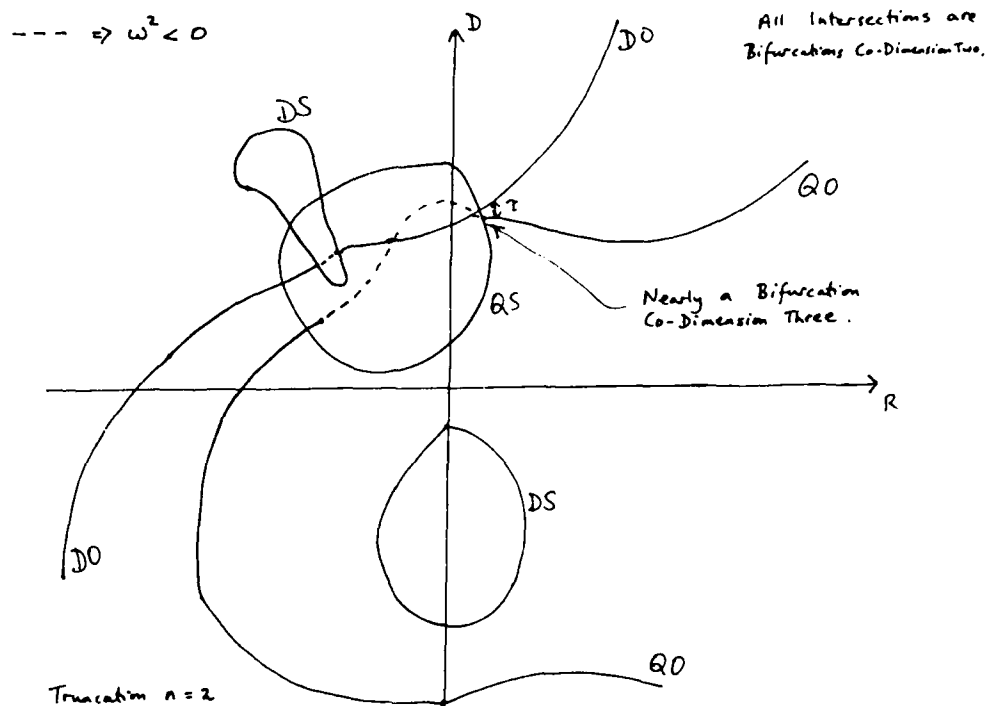


Figure F5.8

Other Modes

Marginal curves for all the other modes are as in Figure 8. There is evidence that a bifurcation co-dimension three analysis may be relevant to a region of the (R-D) plane. More resolution is required though and calculations for a less severe truncation need to be done. A separation parameters τ is needed also, since the three curves will not be exactly concurrent.

Nonlinear Evolution

Some of the possible mechanisms for arresting the initial growth of field are:

1. Quenching of the α -effect.
2. Quenching of ω' .
3. Enhanced diffusivity due to losses of $|B|$ through magnetic buoyancy.
4. Other feedbacks to the velocity field due to the Lorentz force.

The momentum equation can be analyzed to justify a particular form of the nonlinearity (e.g. Weiss et al., 1984), but it is not totally rigorous. When it comes to the quenching of α , it is hard to know whether the nonlinear term is

$$\alpha(B - \kappa |B|^3) \quad \text{or} \quad \alpha(B - \kappa |B|^{3/2}) \quad ? \quad (19)$$

where κ is a constant.

One way out of these uncertainties is to argue that there is no need to choose any particular nonlinearity because normal form theory immediately gives the amplitude equations for every type of bifurcation, independent of the nonlinear terms.

Normal forms are most easily found by looking in a book (e.g. GFD 1981, Guckenheimer and Holmes). The resulting amplitude equations are valid close to the bifurcation point on a surface called the centre manifold – a surface upon which all the important dynamics can be isolated. For a detailed theory of normal forms see Spiegel and Coullet (1983).

Example

For the bifurcation of Figure 7.

Let $x(t)$ be the amplitude of the QS field, and $z(t)$ the amplitude of DO field, $z \in \mathbb{C}$.

From texts:

$$\left. \begin{aligned} \dot{x} &= \nu x + f_1(x, z, \bar{z}) \\ \dot{z} &= (\lambda + i\Omega)z + z f_2(x, z, \bar{z}) \end{aligned} \right\} \begin{array}{l} \text{all nonlinearities must be} \\ \text{of the form in } f_1 \text{ and } f_2. \end{array} \quad (20, 21)$$

plus a conjugate equation for \bar{z}

Since $x \rightarrow \pi - x$ now alters the solution (see Figure 2) quadratic nonlinearities are permitted and will in general dominate. Converting to polars ($z = \rho e^{i\theta}$) and keeping only up to quadratic terms we get:

$$\dot{x} = \nu x + h_1 x^2 + h_2 \rho^2 \quad (22)$$

$$\dot{\rho} = \lambda \rho + h_3 x \rho \quad (23)$$

$$\dot{\theta} = \Omega \quad \text{coefficients } \nu, \lambda, \Omega, h_1, h_2, h_3 \in \mathbb{R} \quad (24)$$

The coefficients are not known unless a particular nonlinear mechanism is prescribed. If this is done, painful calculations will yield the sign and magnitude of the coefficients. Here, I choose to examine all possible solutions of equations 22 - 24, thus covering all nonlinear cut-offs.

Possible Evolutions

Stable Fixed Points ($\theta = \Omega t + \theta_0$ for all solutions)

1. $x = \text{const}, \rho = 0 \Rightarrow QS$ only
2. $x = \text{const}, \rho = \text{const} \Rightarrow$ both QS and DO co-existing with smooth secular variations in DO. Symmetry breaking occurs.

Other Solutions

1. All limit cycles found were unstable.
2. $x = 0, \rho = 0$ is impossible directly from the equations.
3. Solutions can run off to infinity ($x \rightarrow \infty, \rho \rightarrow \infty$). This can be prevented if cubic terms are included or by the use of Padé methods.

The equations cannot have chaotic solutions because the term $\dot{\theta} = \Omega$ is too simple. Yet it is highly probable that chaotic solutions would arise if the bifurcation is treated as co-dimension three (see Figure 8). Also, from Figure 8 it is apparent that there are many other types of bifurcations which can be analyzed similarly.

A Fully Dynamic Nonlinear Dynamo

By using the momentum equation, dynamic velocity fields can be treated. The geometry is unchanged from the previous model.

Momentum

$$\frac{\partial \underline{u}}{\partial t} + \left(f \hat{\underline{z}} + \underline{u} \right) \times \underline{\omega} = - \nabla \left(\frac{p}{\rho} + g \right) + \underline{j} \times \underline{B} + \nu \nabla^2 \underline{u} \quad (25)$$

\uparrow
Coriolis Force

\uparrow
Lorentz Force

(Traditional Approx. See Oceanography/Meteorology texts).

$$\underline{\omega} = \nabla \times \underline{u} \quad (\text{vorticity})$$

Induction

$$\frac{\partial \underline{B}}{\partial t} = \nabla \times (\underline{u} \times \underline{B}) + \nabla \times (\alpha \underline{B}) + \eta \nabla^2 \underline{B} \quad (26)$$

Forced by α

plus $\nabla \cdot \mathbf{u} = 0$ (incompressible) and $\nabla \cdot \mathbf{B} = 0$ (solenoid condition)

Using the divergence free properties of \mathbf{u} and \mathbf{B} write

$$\underline{u} = (-\psi_z, v, \psi_x) \quad , \quad \underline{B} = (-A_z, B, A_x) \quad (27)$$

Variables

A, B, v, ψ, p all functions of x, z, t ($\partial/\partial y = 0$, axisymmetric).

Prescribed Functions

$\alpha = \alpha(x, z)$ — antisymmetric about equator.

$f = f(x)$ — f models latitudinal variation of the Coriolis Force, $f(\pi/2) = 0$.

$g = g(z)$ — gravity. (28)

$\rho = \text{constant}$ — density.

ν, η are kinematic and magnetic diffusivities respectively, both constant in the layer.

Boundary Conditions

$\psi = 0$, $x = 0, \pi$ and $z = 0, H$.

$V_x = 0$, $x = 0, \pi$; $V_z = 0$, $z = 0, H$ (slippery boundaries).

$A = B = 0$, $x = 0, \pi$.

$A_z = B_z = 0$, $z = 0, H$.

The final conditions are required since the turbulent diffusivity η is taken to be a step function (constant in layer and zero outside). Therefore

$$\frac{\partial}{\partial t} \eta \frac{\partial B}{\partial z} \quad \text{and} \quad \frac{\partial}{\partial z} \eta \frac{\partial A}{\partial z} \quad (29)$$

are singular at the boundaries unless the above conditions are taken.

Four equations result for A, B, ψ, v .

1. y-component of the vorticity equation.

$$\partial_t (\nabla^2 \psi) + f v_z + J(\psi, \nabla^2 \psi) = \frac{1}{\mu_0 \rho} J(A, \nabla^2 A) + \nu \nabla^4 \psi \quad (30)$$

where $J(M, N) = M_x N_z - M_z N_x$ (A Jacobian),
and μ_0 is the permeability of the fluid (constant).

2. y-component of the momentum equation.

$$\partial_t (v) + J(\psi, v) - f \psi_z = \frac{1}{\mu_0 \rho} J(A, B) + \nu \nabla^2 v \quad (31)$$

3. y-component of the induction equation

$$\partial_t (B) + J(\psi, B) = J(v, A) - \nabla \alpha \nabla A + \eta \nabla^2 B \quad (32)$$

4. y-component of the uncurled induction equation

$$\partial_t (A) + J(\psi, A) = \alpha B + \eta \nabla^2 A \quad (33)$$

Make a formal thin layer approximation (see Figure 3).

Length scale of z is H , Length scale of x is L , put $H/L = \epsilon \ll 1$.

Considering a balance of Lorentz and Coriolis forces at leading order in equations 30 and 31 and choosing scales accordingly: (Ω is rotation frequency)

$$\frac{A^2}{\mu_0 \rho} = \Omega H R \eta A^*, \quad \frac{B^2}{\mu_0 \rho} = \Omega \eta B^*, \quad v = \frac{2}{R} v^*, \quad \psi = \epsilon \eta \psi^* \quad (34)$$

gives the following equations: (dropping stars)

$$J(A, \nabla^2 A) - \varepsilon^2 f v_z = \varepsilon^2 \left\{ Q [v_t + J(\psi, v)] - E \nabla^4 \psi \right\} \quad (35)$$

$\begin{matrix} \uparrow \\ O(\varepsilon^2) \\ \downarrow \end{matrix}$

$$J(A, B) + \varepsilon^2 f \psi_z = \varepsilon^2 \left\{ Q [v_t + J(\psi, v)] - E \nabla^2 v \right\} \quad (36)$$

$$B_{zz} = \varepsilon^2 \left[B_t + J(\psi, B) - J(v, A) + D \nabla_\alpha \nabla A - B_{xx} \right] \quad (37)$$

$$A_{zz} = \varepsilon^2 \left[A_t + J(\psi, A) - D \alpha B - A_{xx} \right] \quad (38)$$

where

$$E = \left(\frac{\nu}{\Omega H^2} \right), \quad Q = \left(\frac{\eta}{\Omega H^2} \right), \quad E, Q \ll 1.$$

$$D = \frac{\alpha_0 L^2}{\eta H} = O(1), \quad \text{Dynamo number.} \quad (39)$$

Immediately we have $A = a(x, t)$ and $B = b(x, t)$ at leading order. A series expansion in ε^2 of the usual form, with $v_o(x, z, t)$, and $\psi_o(x, z, t)$ both $O(1)$ with respect to ε^2 , and noting that $J(A, B)$ and $J(A, \nabla^2 A)$ both have leading terms of $O(\varepsilon^2)$, allows straight-forward calculations.

Solveability conditions (as used in Hughes) give the following relations between $a(x, t)$ and $b(x, t)$:

$$a_t = D \alpha b + a_{xx} \quad (40)$$

$$\text{where } \overline{T} = \int_0^1 T dz$$

$$b_t = \overline{V_0 z} a_x + b_{xx}$$

Average in z .

(Note similarity to kinematic model).

Using these conditions, nonlinear coupled partial differential equations are found for a and b .

$$a_t - a_{xx} = \frac{D b}{f(f^2 + a_x^4)} \left\{ (f^2 + a_x^4) [\bar{\alpha} - a_x b_x [\alpha]] + [\alpha] a_x^4 (f + b_x) \right\} \quad (41)$$

$$b_t - b_{xx} = \frac{D b}{f(f^2 + a_x^4)} \left\{ a_x^3 b_x \bar{\alpha} f + [\alpha] \left[b_x^2 (a_x^3 - (f^2 + a_x^4)) - a_x^2 f (f + b_x) \right] \right\} \quad (42)$$

where $[\alpha]$ = Jump in α across layer. Note that if $D = 0$, we have diffusion equations for both a and b . Alternatively, these two equations can be written

$$a_t - \psi_{0z} a_x = D \alpha b + a_{xx} \quad (43)$$

$$b_t - \psi_{0z} b_x = v_{0z} a_x + b_{xx} \quad (44)$$

$$f \psi_{zz} = -D \alpha' b b_x - v_z' a_x^2 \quad (45)$$

$$f v_z = -a_x \left[a_x \psi_{zz} + b D \alpha_z \right] \quad (46)$$

$$\text{where } \alpha = \bar{\alpha} + \alpha', \quad v_0 = \bar{v}_0 + v_0'.$$

A solvability condition gives the constraint $(a_x [B]_{z=0}^1 - [A]_{z=0}^1 b_x = 0)$ for the next order solution.

These equations have not been studied yet, but a numerical treatment is certainly required. It is likely that their behavior will be rich.

Acknowledgement

I am very grateful to Nigel Weiss for suggesting this project and guiding me through its initial stages. In steering the work to its conclusion I appreciated the advice and encouragement of Ed Spiegel and Bill Young.

Finally, I wish to thank the GFD program for such an enjoyable summer in the States.

References

Coullet, P.H., 1981. "Bifurcation and Chaos", Summer Program in Geophysical Fluid Dynamics, Woods Hole Oceanographic Institution, 81-102, 97.

Coullet, P.H. and Spiegel, E.A., 1983. "Amplitude Equations for Systems with Competing Instabilities", *S.I.A.M. J. Appl. Math.*, **43**, No. 4.

Guckenheimer, J. and Holmes, P., 1983. *Non-linear Oscillations, Dynamical Systems and Bifurcations of Vector Fields*, Springer-Verlag.

Hughes, D.W., 1987. "Finite-Amplitude Solutions for Interchange Instabilities Driven by Magnetic Buoyancy", *Geophys., Astrophys., Fluid Dynm.*, **37**, 297-343.

Kuiper, G.P., *The Solar System Vol. I The Sun*, Univ. Chicago Press.

Maunder, ??, 1922. *Ibid*, **82**, 534.

Moffatt, K., 1978. *Magnetic Field Generation in Fluids*, Cambridge Univ. Press.

Parker, E.N., 1955. "Hydromagnetic Dynamo Models", *Astrophys. J.*, **122**, 293-314.

Priest, E.R., 1984. *Solar Magneto-hydrodynamics*, Reidel.

Proctor, M.R.E., 1977. "The Role of Mean Circulation in Parity Selection by Planetary Magnetic Fields", *Geophys., Astrophys., Fluid Dynm.*, **8**, 311-324.

Roberts, P. H., 1972. "Kinematic Dynamo Models", *Phil. Trans. R. Soc. Lond.*, **A 272**, 663-697.

Stix, M., 1972. "Nonlinear Dynamo Waves", *Astron. and Astrophys.*, **20**, 9-12.

Weiss, N. O., 1986. "Stellar Dynamo Characteristics", *Highlights of Astronomy*, p. 385-392, IAU.

Weiss, N. O., Cattaneo, F., and Jones, C. A., 1984. "Periodic and Aperiodic Dynamo Waves", *Geophys., Astrophys., Fluid Dynam.*, **30**, 305- 341.

TOPOLOGY AND ERGODICS IN CHAOTIC FAST DYNAMOS

Isaac Klapper

Courant Institute of Mathematical Sciences

Introduction

Chaotic flows are flows such that almost any nearby particles diverge exponentially. If a magnetic field were placed in such a flow we would expect exponential stretching. This suggests fast dynamo action (Bayly, 1986). Unfortunately, however, exponential stretching is not sufficient to guarantee a fast dynamo. We must also consider how the stretched field is folded. There exists the possibility that folding will result in field cancellation, thereby preventing a fast dynamo. This paper will be an attempt to examine the issue of magnetic field folding in chaotic flow.

Brief Overview of Concepts from Ergodicity and Chaos

In this section I present a quick qualitative view of ideas that will be important. For more details see Arnold and Avez (1968), Ruelle and Eckmann (1985), Bayly (1987), and Bayly (this volume).

Dilating and contracting directions: These are two independent continuous direction fields defined at each point of a chaotic flow. Roughly speaking the dilating direction (also called stretching direction) is the direction in which an infinitesimal line element grows fastest, while the contracting direction is the direction in which such a line element shrinks most rapidly. Together with the flow direction they form a non-oriented basis at each point (i.e. these three directions are always independent). Now consider, say, the dilating directions; in any simply connected region (no holes) we can uniquely define two distinct continuous vector fields V_+ , V_- such that at any point in the region, the "+" and "-" vectors of the contracting direction are in V_+ , V_- respectively (figure 6.1).

In this paper we will be chiefly interested in the dilating direction for the reason that almost any vector placed in the flow will converge exponentially fast to the dilating direction.

Liapunov exponents: In a 3-d chaotic volume-preserving flow we have three Liapunov exponents λ , 0, and $-\lambda$ ($\lambda > 0$). Roughly these numbers are logarithms of growth rates in the dilating, flow, and contracting directions, respectively.

Ergodicity: The fact about ergodicity we need is that almost any flow line in a 3-d ergodic flow will fill out the entire volume of the flow (i.e. any flow line will come arbitrarily close to any point of the volume). Chaotic flows are ergodic.

Poincaré section: This is a handy method for studying chaotic flows. Consider a two dimensional cross section of the flow. We follow a flow line and mark each time it passes through the section. This defines a two dimensional map on the three dimensional flow. We see below (figure 6.2) a Poincaré section of the ABC flow (Dombre, et. al., 1986). The dense patches of points are from a single chaotic orbit.

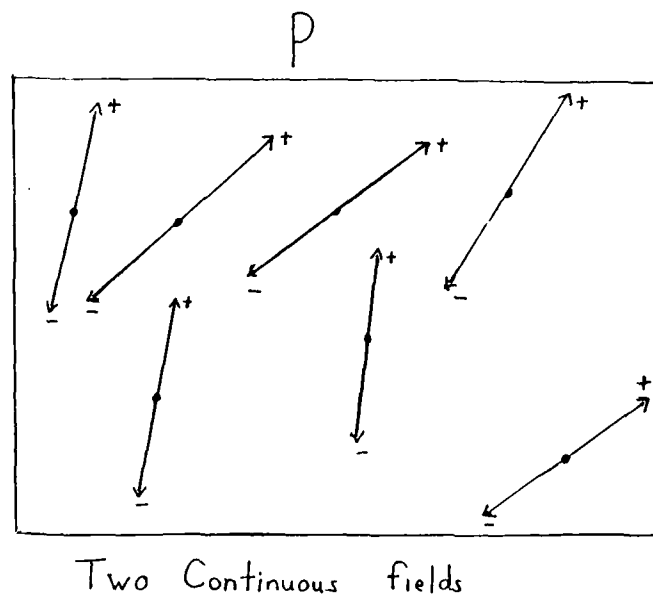


Figure F6.1

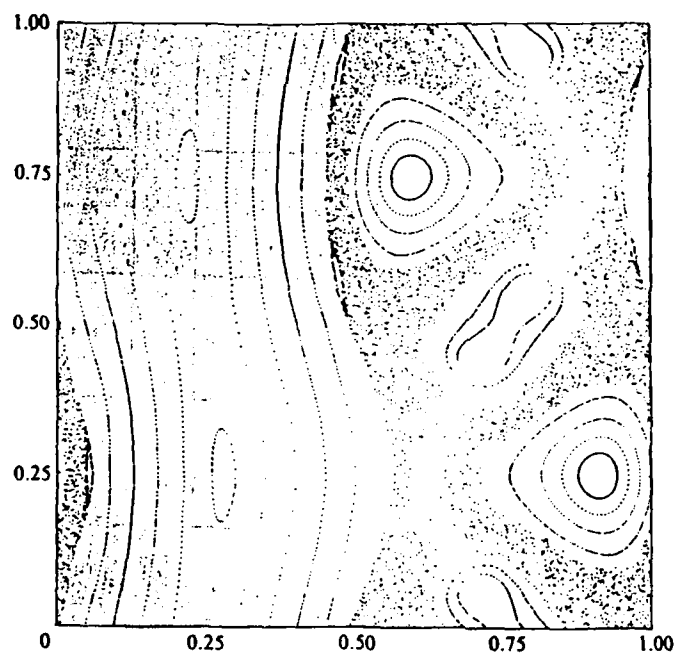


Figure F6.2

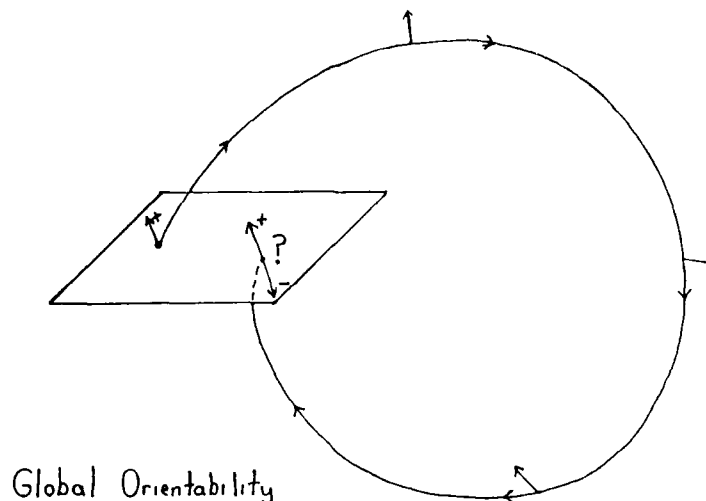


Figure F6.3

Types of Magnetic Field Cancellation

We now consider the problem of folding up the magnetic field. Since almost all vectors in a chaotic flow converge exponentially fast to the dilating direction, we will assume that the magnetic field almost always points in the dilating direction. This reduces the folding issue to a study of the dilating direction field. We can now split the problem into two basic questions.

1. *Global orientability:* Define V_+ , V_- in a small Poincaré section. Pick a point p in the section and follow through the flow the vector $v_p = V_+(p)$. On next return is $v_p \in V_+$ or $v_p \in V_-$ (figure 6.3)?

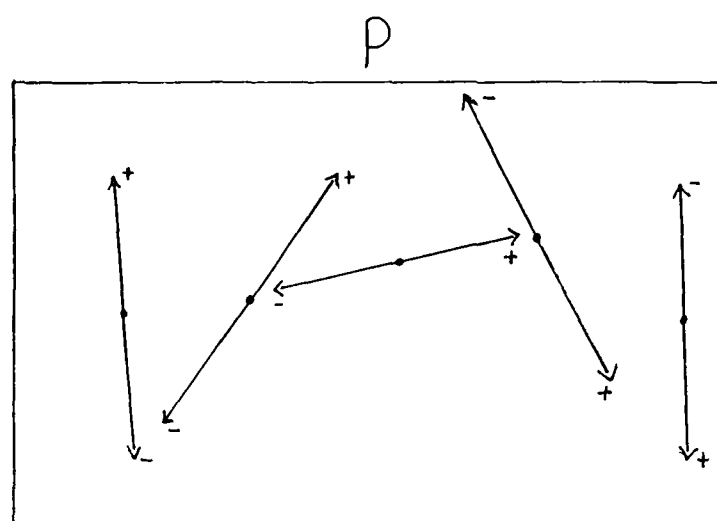
If $v_p \in V_-$ for any p , we say that the flow is orientation reversing. If $v_p \in V_+$ for all p then the flow is orientation preserving. Orientation reversing implies that at least some cancellation of magnetic field will occur since at any one time we would expect to have some magnetic field in V_+ and some in V_- . A corresponding reduction in dynamo efficiency results.

2. *Local rotation:* consider a small Poincaré section. Define V_+ and V_- . These vector fields are continuous but may be rapidly varying (figure 6.4).

In fact, if the dilating direction rotates 180° in a short distance (i.e. shorter than the diffusion length) we can expect to have considerable magnetic field cancellation, even if the flow is orientation preserving.

Global Orientability

The following theorem simplifies the question of global orientation.



Local Rotation

Figure F6.4

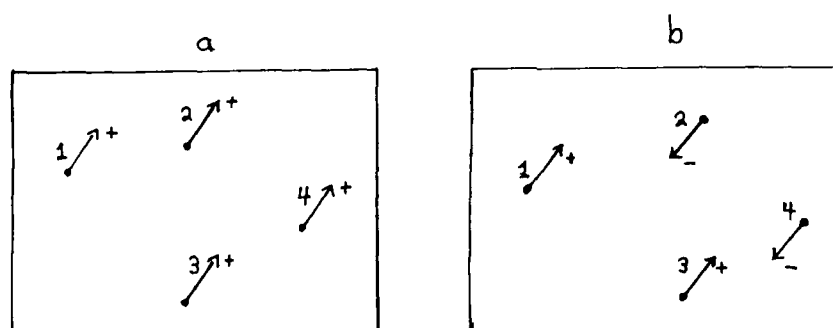


Figure F6.5

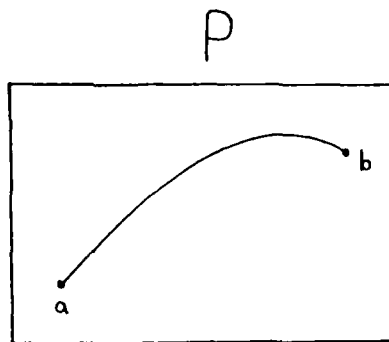


Figure F6.6

Theorem: Let P be a simply connected Poincaré section of a chaotic flow. Then each flow line through P either (figure 6.5)

- a. always preserves orientation of the dilating direction, or
- b. always reverses orientation of the dilating direction.

Furthermore every flowline through P is in the same class a or b. If we choose any other simply connected Poincaré section P' , then P' will have the same orientability class as P .

Proof: Let $f(p)$ be the function on P defined by

$$f(p) = \begin{cases} 1 & \text{if the flowline through } p \text{ preserves the dilating direction} \\ & \text{orientation on next return} \\ -1 & \text{if it reverses} \end{cases}$$

This function is clearly continuous on P . Now let

$$A = \{ x \in P \mid f(x) = 1 \}$$

$$B = \{ x \in P \mid f(x) = -1 \}$$

Assume that A and B are nonempty. Choose $a \in A$, $b \in B$ and draw a path $z(t) : [0, 1] \rightarrow P$ such that $z(0) = a$, $z(1) = b$ (figure 6.6).

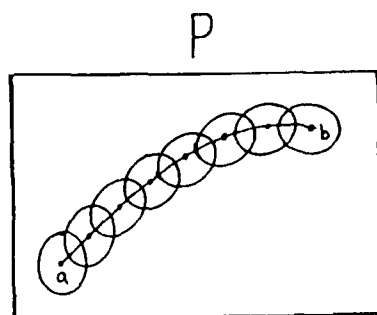


Figure F6.7

Each point of $z(t)$ is either in A or in B . Since f is continuous there exists an open set $\theta_{z(t')}$ around each $z(t')$, $0 \leq t' \leq 1$, such that

$$z(t') \in A, \theta_{z(t')} \subset A \quad \text{or} \quad z(t') \in B, \theta_{z(t')} \subset B$$

The $\{\theta_{z(t')}\}$ form an open cover of $z(t)$. Since $z(t)$ is compact we can choose a finite subcover (figure 6.7)

$$S = \{\theta_a, \theta_{z(t_1)}, \dots, \theta_{z(t_n)}, \theta_b\}$$

Now we do the following:

Since $\theta_a CA$ and $\theta_a \cap \theta_{2(t_1)} \neq \emptyset$ then $\theta_{2(t_1)} CA$
 Since $\theta_{2(t_1)} CA$ and $\theta_{2(t_1)} \cap \theta_{2(t_2)} \neq \emptyset$ then $\theta_{2(t_2)} CA$
 \vdots
 Since $\theta_{2(t_n)} CA$ and $\theta_{2(t_n)} \cap \theta_b \neq \emptyset$ then $\theta_b CA$
 Hence $b \in A$
 Contradiction

Thus either $A = \emptyset$ or $B = \emptyset$, so the Poincaré section P is strictly orientable or strictly non-orientable.

To extend this result to the entire flow notice that if P is orientation preserving/reversing, then $P(t)$ is orientation preserving/reversing where $P(t)$ is the time evolution of P through the flow for time t . Since the flow is ergodic then $P(t)$ sweeps out the entire flow, and the result follows. \square

(Note: using the same argument as above, facts concerning winding numbers, topology, etc. can be deduced about the flow.)

The above result allows us to classify chaotic flows as strictly orientation preserving or orientation reversing. The global character of this result suggests that flow orientability may be a topological property. To this end the following (partially proven) conjecture is offered:

Theorem

- a. Any chaotic flow on a non-orientable manifold is orientation reversing
- b. Any chaotic flow on an orientable manifold is orientation preserving

(A non-orientable manifold is one on which an orientation cannot be consistently defined, such as a Möbius strip.)

Proof - partial

- a. Suppose we have an orientation preserving chaotic flow on a non-orientable manifold. We can define an orientation at each point using the dilating, contracting, and flow directions. Since the flow is orientation preserving we can

define the pointwise orientations to be globally consistent. But this implies that the manifold is orientable. Contradiction. Hence the conclusion holds.

- b. (for the case in which the manifold is simply connected) The proof of this case uses a standard argument that involves contracting a loop to a point. This argument is fairly long and technical so that I will not include it here. To see an example, read the proof of the monodromy theorem, Ahlfors (1953). \square

Note that part (b) has not been proven for the general case.

At this point we can draw a conclusion. Since there are no 3-d non-orientable manifolds embeddable in 3-d, all 3-d chaotic flows embedded in 3-d are contained in orientable manifolds. If the theorem is true this implies that all 3-d chaotic flows are orientation preserving. We know at least that all 3-d chaotic flows in simply connected manifolds are orientation preserving.

Local Rotation of the Dilating Direction

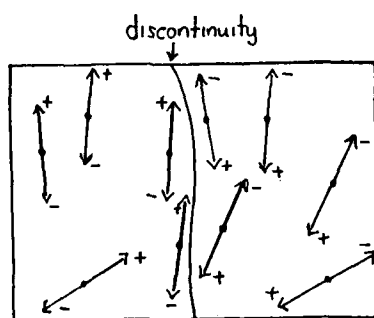
The question that arises here is – can the rotation of the dilating direction cause problems at finite diffusivity? The answer is “no” for the following reason: The dilating direction changes continuously; hence in any compact set it changes uniformly continuously. So we choose a compact set that contains 99.9% of the volume of the flow. In this set the rotation rate of the dilating direction is uniformly continuous, hence bounded. This implies that there is a minimum distance over the set in which a local reversal can occur. We set the diffusion length to be half of this distance (the rules of the fast dynamo game allow us to set this distance to be anything bigger than zero). Hence in 99.9% of the flow volume diffusion will not cause appreciable magnetic field dissipation. The remaining .1% is not enough to stop a fast dynamo. Therefore local rotation is not a problem for small enough diffusivity.

The arguments of the last two sections lead to this conclusion: all 3-d steady chaotic flows in simply connected manifolds are kinematic fast dynamos. In fact, it is possible that all 3-d steady chaotic flows whatsoever are kinematic fast dynamos.

Sheets of Discontinuity

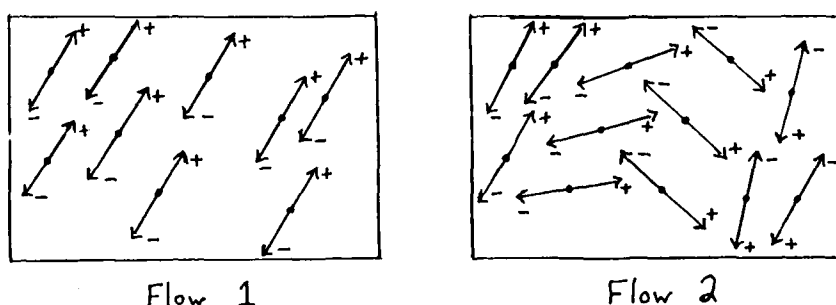
Up until now we have assumed continuity (and occasionally uniform continuity) of the dilating direction field almost everywhere. If, however, there are invariant sheets (such as KAM surfaces) running around inside our chaotic flow this assumption may break down. Across such a sheet we may have discontinuities in the dilating direction (figure 6.8) and a possibility of field cancellation. If these surfaces fill up too much of the chaotic flow volume (say with fractal dimension > 2), then presumably fast dynamo action could be prevented.

In fairness it must be pointed out that such a result is unlikely. We would require that the oriented dilating vector fields V_+ , V_- always exactly cancel each other across discontinuities. In general, however, we could only expect partial cancellation. Also, having invariant sheets filling up volume is not typical in chaotic flows. This



Cancellation across a discontinuity

Figure F6.8



Flow 1

Flow 2

Figure F6.9

pathological situation normally arises in the transition between non-chaotic and chaotic flow.

Speculations about Time Dependence

The previous results have been for the case of time independent chaotic flow. It would clearly be of interest to try to extend these results to time dependence.

Composition of time independent flows: in general we will get some magnetic field cancellation even if the individual flows are orientation preserving. Consider, for example, two orientation preserving flows (figure 6.9).

Let a magnetic field vector align itself with the V_+ direction of flow 1. Now switch to flow 2. Flow 2 will in general have a very different set of dilating directions from flow 1. Our field vector could end up in either of the V_+ or V_- fields of flow 2 as a function of position. This suggests that we will have some field cancellation. However, it is unlikely that all of the field will cancel; hence we are left with a reduced efficiency fast dynamo in most cases.

Continuous time dependent flow: We now have a chaotic flow which is evolving continuously in time. If we take a snapshot of the flow at time t we can define a

field of dilating directions $D(t)$ by letting $D(t)$ be the dilating direction field of the steady snapshot flow. Letting t vary we clearly get a continuously varying dilating direction field $D(t)$. Also, if a magnetic field vector is placed in the flow it will chase after the dilating direction. There are three possibilities:

1. in "slowly" evolving chaotic flow the vector will be able to keep up with the slowly changing dilating direction, and thus the old results apply.
2. in "quickly" evolving chaotic flow the vector cannot keep up with the quickly changing dilating direction. In this case the vector will seem to wander aimlessly.
3. the case where the flow evolves approximately as fast as the vector is able to follow is somewhat unpredictable. We might expect that sometimes the vector can catch the dilating direction, and other times it cannot. Thus the magnetic field might align itself sometimes in the V_+ direction and sometimes in the V_- direction, leading to possible cancellation.

Dynamics

The previous results have been kinematic. Naturally we are interested in dynamical effects. In particular, since exponential magnetic field growth cannot continue forever, we might want to know how such growth gets squelched. The following is a short (and incomplete) list of possibilities.

1. Chaotic motion gets damped out – no more stretching
2. Rotating length of dilating direction becomes smaller in time than the diffusion length – field cancellation
3. Time evolution of chaotic motion becomes too fast – field vectors wander, with no net stretching.

Numerical Results

1. Lorenz flow (not volume preserving) (see Sparrow, 1982).

$$\dot{x} = \sigma(y - x)$$

$$\dot{y} = rx - y - xz$$

$$\dot{z} = xy - bz$$

$$\text{where } \sigma = 10, b = \frac{8}{3}, r = 28$$

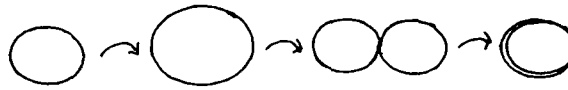


Figure F6.10

At these parameter values we see a strange attractor. By watching the growth of a vector in the flow an $O(1)$ Liapunov exponent was found. Furthermore, global orientation preserving was observed.

2. Stretch-twist-fold Dynamo. Moffatt and Proctor (1984) propose a flow to accomplish the motion of figure 6.10. However almost all flow lines escape to ∞ in finite time. They suggested adding a bounding factor to the flow potential to correct this problem. Unfortunately such a correction seems to alter the properties of the flow considerably.

As an alternative Bruce Bayly suggested the following series of maps in the sphere which simulate the stretch-twist-fold mechanism.

Rotation and stretch, figure 6.11a

$$\begin{pmatrix} x_2 \\ y_2 \\ z_2 \end{pmatrix} = \begin{pmatrix} 1 & 0 & 0 \\ 0 & \cos \omega(x_1) & -\sin \omega(x_1) \\ 0 & \sin \omega(x_1) & \cos \omega(x_1) \end{pmatrix} \begin{pmatrix} x_1 \\ y_1 \\ z_1 \end{pmatrix}$$

Fold (accomplished by two maps who composition is area preserving), figure 6.11b.

Invert

$$x_2 = x_3$$

$$y_2 = y_3 + f_x (x_3^2 + y_3^2 + z_3^2 - 1)$$

$$z_2 = z_3$$

and apply

$$\begin{pmatrix} x_4 \\ y_4 \\ z_4 \end{pmatrix} = \begin{pmatrix} \cos f(x) & \sin f(x) & 0 \\ -\sin f(x) & \cos f(x) & 0 \\ 0 & 0 & 1 \end{pmatrix} \begin{pmatrix} x_3 \\ y_3 \\ z_3 \end{pmatrix}$$

Change of coordinates

$$\begin{pmatrix} x_5 \\ y_5 \\ z_5 \end{pmatrix} = \begin{pmatrix} 0 & 1 & 0 \\ 0 & 0 & 1 \\ 1 & 0 & 0 \end{pmatrix} \begin{pmatrix} x_4 \\ y_4 \\ z_4 \end{pmatrix}$$

This map shows well-developed chaos with an $O(1)$ Liapunov exponent. The mapping can be represented in a 4-d flow. Orientation reversing was observed, but it appeared to be because of numerical error.

Acknowledgements

I would like to thank Bruce Bayly for his guidance in this study. Extremely helpful also were numerous conversations with the staff and fellows of the program. And most of all I would like to thank all of those who were responsible for a completely enjoyable summer.

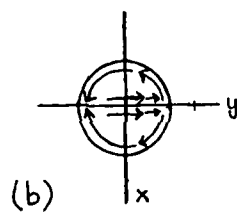
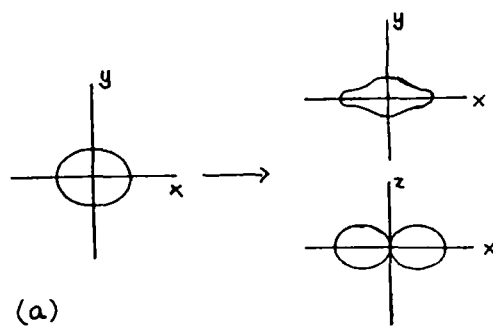


Figure F6.11

Bibliography

- Ahlfors, Lars V., 1953. *Complex Analysis*, McGraw-Hill Book Co., N.Y.
- Arnold, V.I. and Avez, A., 1968. *Ergodic Problems of Classical Mechanics*, W. A. Benjamin, Inc., N.Y.
- Bayly, Bruce, 1987. "Chaotic fast dynamos", this volume.
- Bayly, Bruce, 1987. *Kinematic and Dynamical Problems in Three Dimensional Steady Flows*, Ph.D. Thesis, Princeton University.
- Bayly, Bruce, 1986. "Fast magnetic dynamos in chaotic flows", *Phys. Rev. Lett.*, 57, 2160.
- Dombre, T., et al., 1986. "Chaotic streamlines in the ABC flows", *J. Fluid Mech.*, 167, 353.
- Moffatt, H.K. and Proctor, M.R.E., 1985. "Topological constraints associated with fast dynamo action", *J. Fluid Mech.*, 154, 493.
- Ruelle, D. and Eckmann, J.P., 1985. "Ergodic theory of chaos and strange attractors", *Rev. Mod. Phys.*, 57, 617-656.
- Sparrow, Colin, 1982. *The Lorenz Equations: Bifurcations, Chaos, and Strange Attractors*, Springer-Verlag, N.Y.

A QUASI-DYNAMICAL DYNAMO MODEL

Jack McMillan
University of Hawaii

Introduction

We investigate the possibility of dynamo action in a flow given by fluid velocity $\vec{u} = (\psi_y, -\psi_x, \frac{K(t)}{L} \psi)$ where the (time dependent) streamfunction $\psi = \frac{U(t)}{L} \sin \pi x \sin \pi y$. Note that ψ prescribes a Roberts cell, a flow spatially periodic in two dimensions and of constant helicity. Incompressibility is assured as $\nabla \cdot \vec{u} = 0$.

The case of steady Roberts cell flow has been previously studied as a kinematic dynamo, including in the limit of large magnetic Reynolds number $R_m \rightarrow \infty$ (Roberts 1972, Childress 1979, Soward 1987). Soward (1987) obtained a maximum growth rate (of magnetic field) $\frac{\ln(\ln R_m)}{\ln R_m}$ and concluded that the flow generates as "almost" fast dynamo.

Our effort here is to introduce, in a simple way, dynamics into the picture by deriving *global* axial (z -direction) force and torque (xy -plane) equations. These extra impositions on the flow require that degrees of freedom be allowed, hence as previously noted the velocity amplitudes will be functions of time: $U \rightarrow U(t)$, $KU \rightarrow K(t)U(t)$. A *scalar* magnetic induction equation for the mean field will be also formulated. Note that the streamlines, however, maintain the same "shape" in this admittedly idealized model. Thus the model will consist of three ordinary differential equations. Steady-state solutions are first found and the time evolution of perturbations from the steady-state will be investigated numerically (i.e., by computer using the standard Runge-Kutta method of numerical integration).

The Induction Equation

The time evolution of a magnetic field in a fluid of uniform conductivity σ and velocity \vec{u} is given by the hydromagnetic induction equation:

$$\partial_t \vec{B} = \nabla \times (\vec{u} \times \vec{B}) + \eta \nabla^2 \vec{B} \quad (2.1a)$$

$$\eta = (\mu_m \sigma)^{-1} = \text{magnetic diffusivity} \quad (2.1b)$$

$$\nabla \cdot \vec{B} = 0 \quad (\text{no monopoles, please!}) \quad (2.1c)$$

F7.2

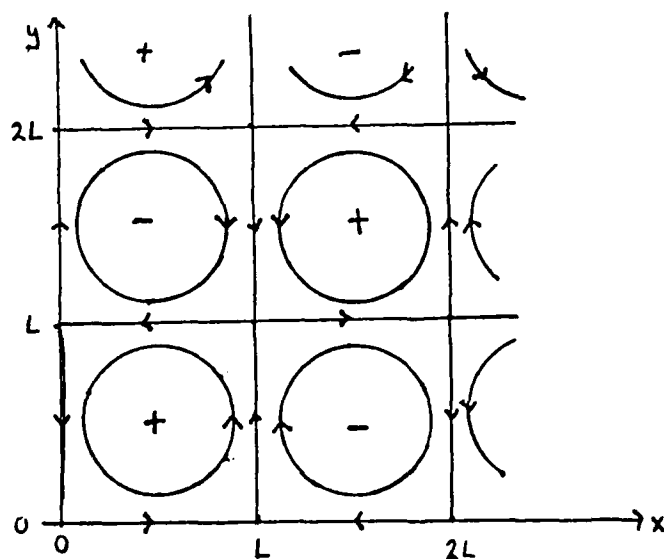


Figure F7.1: The Roberts cell. Positive and negative z -velocities are denoted by '+' and '-' respectively.

In our geometry, the field is expressed by

$$\vec{B} = (\partial_y a, -\partial_x a, b) \quad (1.2)$$

and hence by (2.1c) the z -component of the field, b , is independent of z .

The field is split into a "mean" and a "fluctuating" part where averaging is over the xy plane:

$$\vec{B} = \langle \vec{B} \rangle + \vec{B}' \quad (2.3a)$$

$$\langle \vec{B}' \rangle = 0 \quad (2.3b)$$

We prescribe a tensor α whereby $\langle \hat{u} \times \vec{B} \rangle = \alpha \langle \vec{B} \rangle$ and considering the symmetry of the flow $\alpha = \frac{1}{2}$. The constant α will be determined from a boundary layer analysis.

Therefore the mean field equation is given by:

$$\partial_t \langle \vec{B} \rangle = \hat{z} \partial_z \times \alpha \langle \vec{B} \rangle + \eta \partial_z^2 \langle \vec{B} \rangle \quad (2.4a)$$

$$\nabla \cdot \langle \vec{B} \rangle = 0 \quad (2.4b)$$

It is easily proveable that a solution of the following form is admissible:

$$\langle \vec{B} \rangle = (B_1(t), B_2(t), 0) e^{i n z} \quad (2.5)$$

The wavenumber n is such that $n \ll R_m^{1/2}/L$, i.e. the mean field is not varying in z much in the boundary layer (to be discussed in the next section).

A complex-valued, dimensionless scalar function B is defined by

$$B_0 B(t) = B_1(t) + i B_2(t) \quad (2.6)$$

where B_0 is a magnetic scale. The induction equation (2.4a) is now given in scalar form in terms of $B(t)$ by the following formula:

$$\partial_t B + n^2 \eta B = -\alpha n B \quad (2.7)$$

Boundary Layer Analysis

Determination of α is based upon the following considerations. In a conducting fluid, magnetic flux is expelled from an eddy (Weiss 1968) and is confined to a boundary layer of thickness $\sim R_m^{-1/2} L$ (Childress 1979, using Roberts cell flow). If we assume the timescale of the system (i.e., of U, V, B) to be large compared to eddy turnover time ($\sim U_0/L$) then α can be evaluated using a steady flow and "constant" magnetic field.

Recall that $\alpha = |\langle \hat{u} \times \hat{B} \rangle| / |\langle \hat{B} \rangle|$. For our purposes, let $\langle \hat{B} \rangle = 1 \hat{x}$. Then (2.8)

$$\alpha = L^{-2} \int_0^L \int_0^L (u_y B_z - u_z B_y) dx dy = L^{-2} \int_0^L \int_0^L \left(\frac{a_x K(t)}{L} \psi - b \psi_x \right) dx dy$$

Now, from (2.1a) assuming "constant" field.

$$\frac{\partial(a, \psi)}{\partial(x, y)} = \eta \nabla^2 a \quad (2.9a)$$

$$\frac{\partial(b, \psi)}{\partial(x, y)} - \eta \nabla^2 b = \frac{K(t)}{L} \frac{\partial(a, \psi)}{\partial(x, y)} \quad (2.9b)$$

(Compare with Childress 1979). We now show how to determine the integral in (2.8).

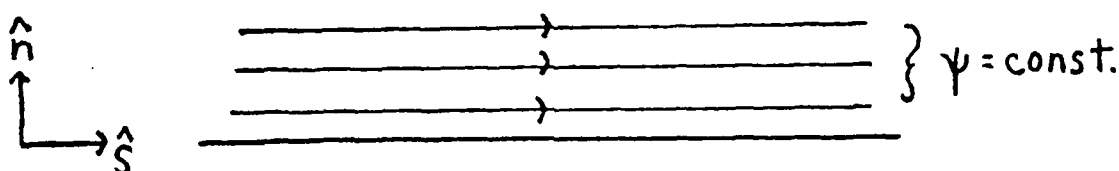
The magnetic boundary layer will be near the edges of the square cell ($R_m^{-1/2} \ll 1$). In this region, the z velocity is negligible and particles move along streamlines in the xy plane $\sin \frac{\pi x}{L} \sin \frac{\pi y}{L} = \text{const}$. Here the curvature of the streamlines is also negligible, so they lie parallel to the cell edge. Thus, locally, we can define rectangular coordinates \hat{n}, \hat{s} normal and parallel to the flow, respectively. The speed of the flow $q = |\nabla \psi| = \frac{\partial \psi}{\partial n}$. Whence $\nabla = \hat{n} \frac{\partial}{\partial n}$ implying that the Laplacian operation $\nabla^2 = \frac{\partial^2}{\partial n^2}$ in this region. We can then write

$$\nabla^2 a = \frac{\partial^2 a}{\partial n^2} \quad \nabla^2 b = \frac{\partial^2 b}{\partial n^2} \quad (2.10)$$

The Jacobians in (2.9 a, b) are treated like this in the boundary layer:

$$\frac{\partial(a, \psi)}{\partial(x, y)} = \frac{\partial a}{\partial s} \frac{\partial \psi}{\partial n} - \frac{\partial a}{\partial n} \frac{\partial \psi}{\partial s} \quad (2.11)$$

Figure F7.2: Coordinates used in the boundary layer. The 'flatness' of the streamlines occurs in the boundary layer of thickness $\sim R_m^{-1/2} L$.



and the same for b . But, $\frac{\partial \psi}{\partial s} = 0$ since \hat{s} is parallel to the streamlines, so

$$\frac{\partial(a, \psi)}{\partial(x, y)} = \frac{\partial a}{\partial s} \frac{\partial \psi}{\partial n} = q \frac{\partial a}{\partial s} \quad (2.12)$$

so, equations (2.9 a, b) now become:

$$q \frac{\partial a}{\partial s} - \eta \frac{\partial^2 a}{\partial n^2} = 0 \quad (2.13a)$$

$$q \frac{\partial b}{\partial s} - \eta \frac{\partial^2 b}{\partial n^2} = -\frac{k(t)}{L} q \frac{\partial a}{\partial s} \quad (2.13b)$$

We want to solve for α which involves an integral containing a_x , b_x , and ψ . To accomplish this we make some transformations (see Batchelor 1956) which hopefully will simplify equations (2.13 a, b). First, since $q = \partial \psi / \partial n$, we can write $\frac{\partial^2}{\partial n^2} = q^2 \frac{\partial^2}{\partial \psi^2}$. Also, we define a quantity σ such that $q \equiv \frac{\partial \sigma}{\partial s}$, thus (recall $q = \text{speed}$).

$$\frac{\partial}{\partial s} = q \frac{\partial}{\partial \sigma}$$

Under these transformations, we now have

$$\frac{\partial a}{\partial \sigma} - \eta \frac{\partial^2 a}{\partial \psi^2} = 0 \quad (2.14a)$$

$$\frac{\partial b}{\partial \sigma} - \eta \frac{\partial^2 b}{\partial \psi^2} = -\frac{k(t)}{L} \frac{\partial a}{\partial \sigma} \quad (2.14b)$$

The magnetic diffusivity η can be eliminated from the picture by one more (gasp!) set of transformations:

$$\bar{\psi} = R_m^{1/2} (UL)^{-1} \psi$$

$$d\bar{\sigma} = (UL) d\sigma$$

Note that $\bar{\psi}$ and $\bar{\sigma}$ are dimensionless; $R_m = UL/\eta$.

So our equations for a and b become:

$$\frac{\partial a}{\partial \bar{\sigma}} - \frac{\partial^2 a}{\partial \bar{\psi}^2} = 0 \quad (2.15a)$$

$$\frac{\partial b}{\partial \bar{\sigma}} - \frac{\partial^2 b}{\partial \bar{\psi}^2} = -\frac{k(t)}{L} \frac{\partial a}{\partial \bar{\sigma}} \quad (2.15b)$$

Now if a is a particular solution of (2.15a) (with relevant boundary conditions (see Childress 1979) then

$$b = \frac{1}{2} \frac{K(t)}{L} \bar{\psi} \frac{\partial a}{\partial \bar{\psi}}$$

Finally, plugging this all into the formula for α (eqn. 2.8)

$$\alpha = \frac{1}{2} L^{-2} \frac{U(t) K(t)}{R_m^{1/2}} \int \int_{y=0}^L a \bar{\psi} \bar{\psi} d\bar{\psi} dy = -k \sqrt{\frac{\eta}{L}} \frac{V(t)}{[U(t)]^{1/2}} \quad (2.16)$$

Soward (1987) obtains a value of $k \cong 0.533$, incidently, but our purposes its exact value is not so important. The "induction" equation (2.7) thereby becomes:

$$\partial_t B + n^2 \eta \tilde{B} = nk \left(\frac{\eta}{L} \right)^{1/2} \frac{V(t) B}{[U(t)]^{1/2}} \quad 2.17$$

This is the first equation of our model.

The Axial Force Balance

Now consider the global balance of z -momentum in the "tube".

$$(z\text{-momentum})/(\text{unit length}) = \rho_o \int_0^L \int_0^L \frac{K(t)}{L} \psi dx dy = \rho_o V(t) 4L^2/\pi^3 \quad (3.1)$$

where ρ_o = mass density

$$\text{Viscous Force/length} = F_{visc} = \int_0^L \int_0^L \nu_o \frac{K(t)}{L} \nabla^2 \psi dx dy = \frac{8}{\pi} \nu_o V(t) \quad (3.2)$$

where ν_o is the kinematic viscosity

$$\text{Pressure gradient } F_{press} = -4L \rho_o \Gamma / \pi^3 \quad (3.3)$$

$$\text{Lorentz Force/length } F_{mag} = \int_0^L \int_0^L (J_y B_x - J_x B_y) dx dy \quad (3.4)$$

$$\text{Now the current flux } \vec{J} = \frac{1}{\mu_m} (b_y + a_{xz}, -b_x + a_{yz}, -a_{xx} - a_{yy})$$

When averaged over the z -direction, the force becomes:

$$F_{mag} = \frac{1}{\mu_m} \int_0^L \int_0^L (a_x b_y - a_y b_x) dx dy$$

where the superscript 'bar' refers to the z -average and μ_m is the permeability. Thus the force can be expressed as (from boundary layer analysis, again):

$$\begin{aligned} F_{mag} &\sim \iint (a_{\bar{\sigma}} b_{\bar{\psi}} - a_{\bar{\psi}} b_{\bar{\sigma}}) d\bar{\sigma} d\bar{\psi} \\ &= k_m K(t) L B_0^2 |B|^2 \end{aligned} \quad (3.5)$$

So, putting this all together into a force eqn., and dividing through by $\frac{4L^2 \rho_0}{\pi^2}$:

$$\frac{dV}{dt} + \Gamma = \frac{2\pi^2 \rho_0 V(t)}{L^2} - \frac{k_m \pi^3 A_0^2 V(t) |B(t)|^2}{4L u(t)} \quad (3.6)$$

where $A_0 = \sqrt{\frac{B_0^2}{\rho_0 \mu_m}}$ is the Alfvén velocity. Eqn 3.6 is the second equation of our system.

The Global Torque Balance

$$\text{Angular momentum} = -\rho_0 \int_0^L \int_0^L (x\psi_x + y\psi_y) dx dy = \rho_0 u(t) 8L^3/\pi^2 \quad (4.1)$$

$$\text{Applied torque} = \tau_0$$

$$\text{Viscous torque} = \int_0^L \int_0^L (\hat{r} \times \nu_0 \nabla^2 \hat{u}) dx dy = k_v u(t) \nu_0 L \quad (4.2)$$

where k_v is a positive number

$$\text{Magnetic torque} \quad T_{\text{mag}} = \frac{-1}{\mu_m} \int_0^L \int_0^L (\hat{r} \times [\hat{B} \times \nabla \times \hat{B}]) dx dy \quad (4.3)$$

To simplify this, let's use the magnetic stress tensor $T_{ij} = B_i B_j$. The torque

can then be written as

$$T_i = -\frac{1}{\mu_m} \int_0^L \int_0^L \partial_j \epsilon_{ikl} x_k T_{lj} dx dy$$

$$= -\frac{1}{\mu_m} \oint_{\text{boundary}} \epsilon_{ikl} x_k T_{lj}$$

Using our boundary layer approximation, we have:

$$T_{\text{mag}} \approx -\frac{k_T B_o^2 |B|^2 L}{\mu_m} \quad (4.4)$$

The time evolution of $U(t)$ is given by

$$\frac{dU}{dt} + \frac{k_v v_o \pi^2 U}{8L^2} - \frac{T_o \pi^2}{8\rho_o L^2} + \frac{k_T \pi^2 A_o^2 |B|^2}{8L} = 0 \quad (4.5)$$

This is the third and last equation of the model.

Non-Dimensionalization of the Equations

Time: take the timescale as the magnetic diffusion scale $1/n^2 \eta$. Then define $t_* = n^2 \eta t$ so t_* is dimensionless. In the following, 'starred' quantities are dimensionless.

Velocities: $U(t) = U_0 U_*(t_*)$

$$V(t) = U_0 V_*(t_*)$$

Induction eqn: $\frac{dB}{dt_*} + B = \frac{\alpha_* V_* B}{|U|^{1/2}} \quad \alpha_* = \frac{k}{n\eta} \left(\frac{\eta U_0}{L} \right)^{1/2} \quad (5.1)$

momentum balance

$$\frac{dV_*}{dt_*} = \frac{\Gamma}{n^2 \eta U_0} - \frac{2\pi^2 \nu_* V_*}{n^2 \eta L^2} - \frac{k_m \pi^3 A_0^2 V_* |B|^2}{4L U_0 n^2 \eta U_*} \quad (5.2)$$

torque balance

$$\frac{dU_*}{dt_*} + \frac{k_v \pi^2 \nu_* U_*}{8L^2 n^2 \eta} - \frac{T_0 \pi^2}{8\rho_0 L^2 U_0 n^2 \eta} + \frac{k_T \pi^3 A_0^2 |B|^2}{8L U_0 n^2 \eta} = 0 \quad (5.3)$$

Now choose $U_0 = \frac{T_0 \pi^2}{8\rho_0 L^2 n^2 \eta}$

$$A_0^2 = \frac{8L n^2 \eta U_0}{k_T \pi^2}$$

Then

$$\frac{dU_*}{dt_*} + \mu_* U_* = 1 - |B|^2 \quad \mu_* = \frac{k_v \nu_* \pi^2}{8L^2 n^2 \eta} \quad (5.2a)$$

$$\frac{dV_{**}}{dt_*} + \nu_* V_{**} = 1 - \frac{\gamma_* V_{**} |B|^2}{U_*} \quad , V_{**} = \frac{\Gamma V_*}{U_0 n^2 \eta} \quad , \gamma_* = \frac{k_m \pi^3 A_0^2 \Gamma}{4L n^4 \eta^2 U_0^2} \quad (5.3a)$$

$$\frac{dB}{dt_*} + B = \frac{\alpha_{**} V_{**} B}{|U_*|^{1/2}} \quad , \quad \alpha_{**} = \frac{\alpha_* \Gamma}{n^2 \eta U_0} \quad (5.1a)$$

So, now, dropping all the 'stars', the three fully-nondimensionalized equations are:

$$\frac{dU}{dt} + \mu U = 1 - |B|^2 \quad (5.1b)$$

$$\frac{dV}{dt} + \nu V = 1 - \frac{\gamma V}{U} |B|^2 \quad (5.2b)$$

$$\frac{dB}{dt} + B = \alpha \frac{VB}{|U|^{1/2}} \quad (5.3b)$$

So we have three first order, non-linear, coupled ODE's characterized by four parameters μ, ν, α, γ .

Steady-State Solutions

Setting $\partial_t = 0$, our equations become

$$\mu U_e = 1 - z_e \quad (6.1)$$

$$\nu V_e = 1 - \frac{\gamma V_e}{U_e} z_e \quad (6.2)$$

$$0 = \left(1 - \frac{\alpha V_e}{|U_e|^{1/2}}\right) z_e \quad (6.3)$$

where $z = |B|^2$ and the subscript "e" refers to steady-state equilibrium values. Note that (6.3) gives rise to two cases.

Case I: no magnetic field: $z_e = 0$, $U_e = 1/\mu$, $V_e = 1/\nu$

Case II: non-zero magnetic field: $U_e = (1 - z_e)/\mu$, $V_e = (1 - z_e)/(\nu + k z_e)$

where $k = \gamma\mu - \nu$

The non-zero field case imposes the constraint $U_e = \alpha^2 V_e^2$; thus the field squared z_e must lie between zero and one: $0 \leq z_e \leq 1$. Solving for z_e , the equation is a simple quadratic:

$$k^2 z_e^2 + (2\nu k + \mu\alpha^2) z_e + \nu^2 - \mu\alpha^2 = 0$$

To insure a single positive value of z_e , it is sufficient that $\mu\alpha^2 > \nu^2$. This is the minimum condition for the zero field equilibrium to be unstable.

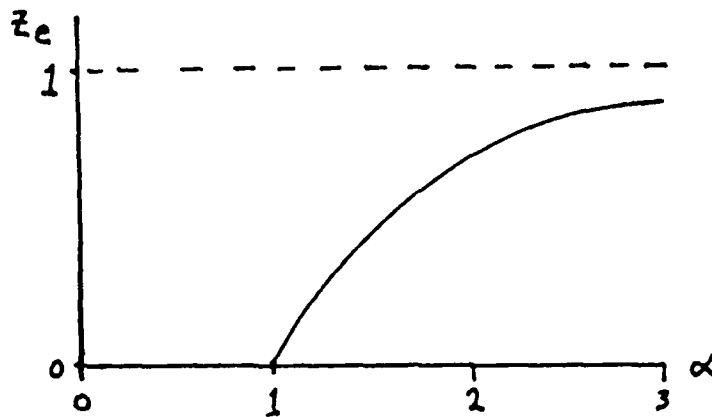


Figure F7.3: Plot of z_e versus α for the case $\mu = \nu = \gamma = 1$. Note that for $\alpha < 1$, only $z_e = 0$ is stable.

Some Special Cases

I. Inviscid case $\mu = \nu = 0$

$$z_e = 1$$

$$u_e = \gamma^2 / \alpha^2$$

$$v_e = \gamma / \alpha^2$$

Is this stable? Assume perturbations growing as e^{pt} and use linear stability analysis to solve for p . The eigenvalues (growth rates) are $p = -\alpha^2 \pm i\alpha$ for $\gamma = 1 \Rightarrow$ stable. For $\gamma > 1$, this is unstable: $\gamma = 1 + \epsilon \Rightarrow p \approx 2\epsilon\alpha^2 + i\alpha$.

II. $\mu = \nu = \gamma = 1$ ($k = 0$)

$$u_e = v_e = 1/\alpha^2$$

$$z_e = 1 - 1/\alpha^2$$

Is it stable? Yes, very much so! $p = -\alpha^2, -1/2 \pm 1/2\sqrt{5 - 4\alpha^2}$. So small perturbations, at least, always decay. Linear stability analysis doesn't tell us though what happens at values far from equilibrium (i.e., outside of 'limit cycle').

A Brief Digression: Linear Stability Analysis

Do perturbations from steady-state equilibrium tend to grow or decay with time? We consider a (generally complex) growth rate p and write $u = u_e + \delta u e^{pt}$, etc. This

leads to the three following equations:

$$(p + \mu) \delta U + \delta z = 0$$

$$-\gamma \frac{z_e V_e}{u_e^2} \delta U + (p + \nu + \gamma \frac{z_e}{u_e}) \delta V + \gamma \frac{V_e}{u_e} \delta z = 0$$

$$\frac{\alpha V_e z_e}{u_e^{3/2}} \delta U - \frac{2\alpha z_e}{u_e^{1/2}} \delta V + p \delta z = 0$$

In matrix form, this can be expressed as $\underline{A} \begin{pmatrix} \delta U \\ \delta V \\ \delta z \end{pmatrix} = 0$. Since we seek non-trivial solutions (i.e., $\delta U \neq 0$, etc.) the determinant of the matrix must vanish:

$$\det \underline{A} = 0$$

This will give a cubic equation in p of course. The 'leading' value of p , that is the p value with greatest real part, will determine the stability of the solution.

Case 2 Continued

As seen, the equilibrium values of z ($= |B|^2$ real) can be obtained from a quadratic equation. The solutions are given as follows:

$$z_e^{\pm} = \frac{\nu}{2k^2} \left\{ - \left[\left(\frac{2\gamma\mu}{\nu} - 1 \right) + \left(\frac{\mu\alpha^2}{\nu^2} - 1 \right) \right] \right. \\ \left. \pm \left[\left[\left(\frac{2\gamma\mu}{\nu} - 1 \right) + \left(\frac{\mu\alpha^2}{\nu^2} - 1 \right) \right]^2 + 4k^2 \left(\frac{\mu\alpha^2}{\nu^2} - 1 \right) \right]^{1/2} \right\}$$

Clearly, the combinations $2\alpha\mu/\nu$ and $\mu\alpha^2/\nu^2$ determine whether the z_e values are positive or negative, purely real or complex. This is shown graphically in Figure 7.4.

Bifurcations: Subcritical, Supercritical, Hopfian

Figure 7.4 has been divided into two regions by Roman numerals I and II. In Region I, $2\alpha\mu > \nu$ and a single positive z_e exists for $\mu\alpha^2 \geq \nu^2$. If α is less the 'critical' value $\nu/\sqrt{\mu}$, $z_e = 0$. This is a supercritical bifurcation and we have seen one example already ($\mu = \nu = \alpha = 1$). Solutions of z in this region are stable.

Simultaneous numerical integrations of the three ODE's for U , V , and z were performed using the Runge-Kutta method in a program executed on the WHOI VAX computer. Values of α , μ , ν , and γ as well as initial values of U , V , z were

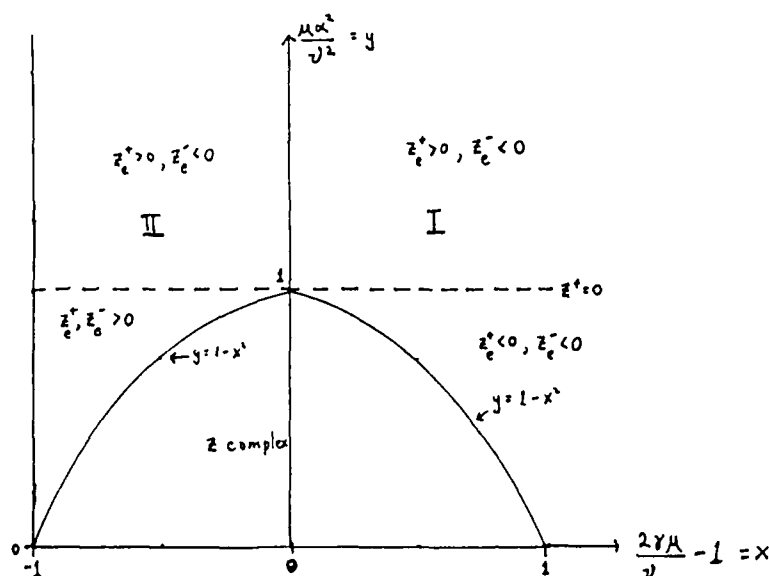


Figure F7.4: The range of equilibrium values z_e as determined by values of $2\alpha\mu/\nu$ and $\mu\alpha^2/\nu^2$. In the unshaded region, the only stable equilibrium value of z is zero.

entered. A typical example of a Region I case is shown in Figure 7.5. Note that initially z was far from its equilibrium value, but converged to it nicely.

Region II represents z_e values in which $2\gamma\mu < \nu$. For α less than the critical value there are two positive z_e 's. However, the 'lower' branch is unstable; while the upper branch is stable over a range of α 's. This region is denoted as a subcritical bifurcation. The two are shown in Figure 7.6

To investigate Region II, we considered several cases, one of which will be shown in detail here: $\gamma = 0.5$, $\mu = 1$, $\nu = 2$ (this is a 'typical' case and has no intrinsic peculiarities associated with it). A plot of z_e versus α is displayed in Figure 7.7. Note that for $\alpha < \sqrt{3}$, z_e is zero.

The lower branch is unstable; that is initial z values less than the equilibrium value (on the lower branch) tend to zero while those z 's initially larger than equilibrium grow, eventually reaching the upper branch equilibrium value (for a given choice of α). The velocity amplitudes U and V , in the computer simulations, were put initially at their respective equilibria. This is displayed in Figures 7.8 and 7.9 for the case in which α is set to 1.8. The lower branch $z_e = 0.41738$.

For the upper branch, the situation is stable; small perturbations of z from its steady-state values decayed. Larger perturbations produced limit cycles. A typical example of this phenomenon is illustrated in Figure 7.10 where $\alpha = 2.4$.

A program was written to ascertain whether Hopf bifurcations occurred along the z versus α curve. In our example, such a bifurcation did occur at $\alpha = 2.4099$.

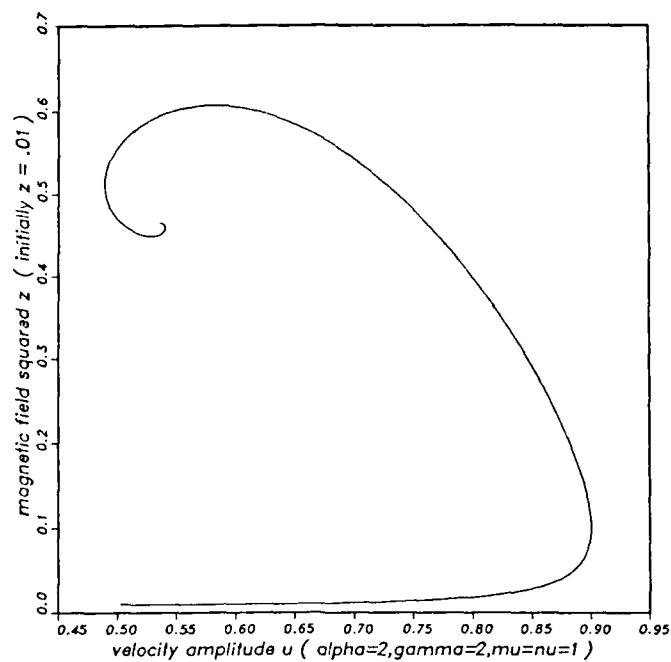


Figure F7.5: A plot of U versus z for a typical region I case. The region is 'stable' in that the equilibrium values are reached even for initially far values.

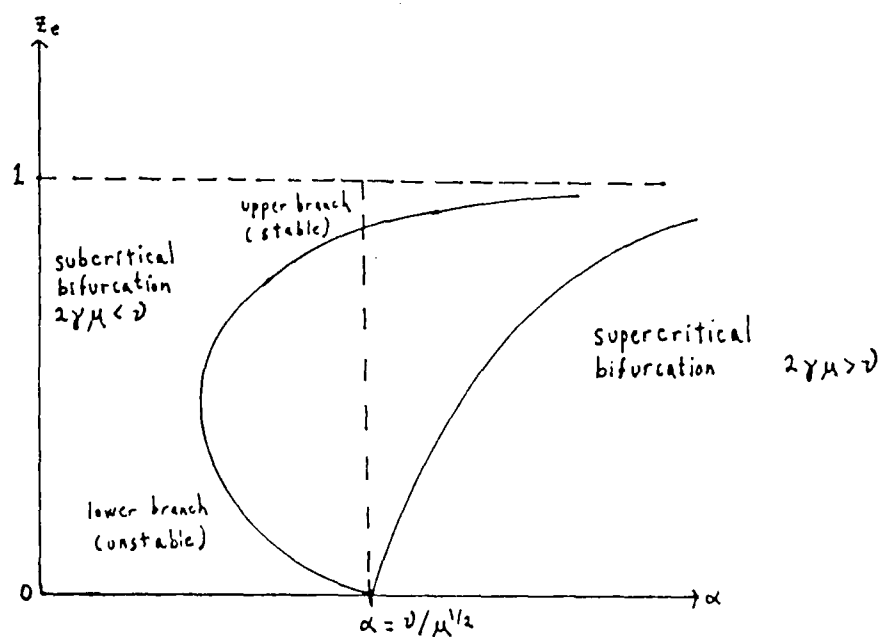


Figure F7.6: Plot of z_e vs α showing sub- and supercritical bifurcations.

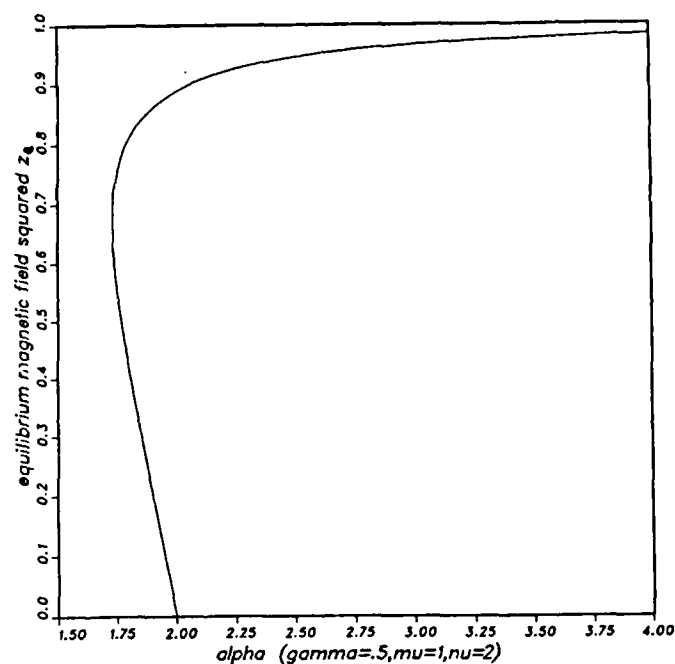


Figure F7.7: Plot of z_e versus α for $\gamma = 0.5$, $\mu = 1$, $\nu = 2$.

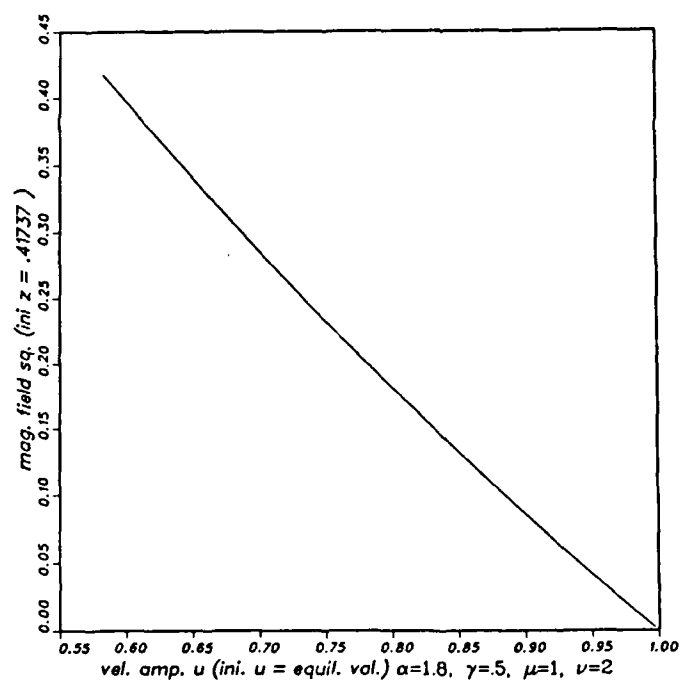


Figure F7.8: A plot of the time evolution of z versus U for z initially less than its equilibrium value on the lower branch of Figure 7.7.

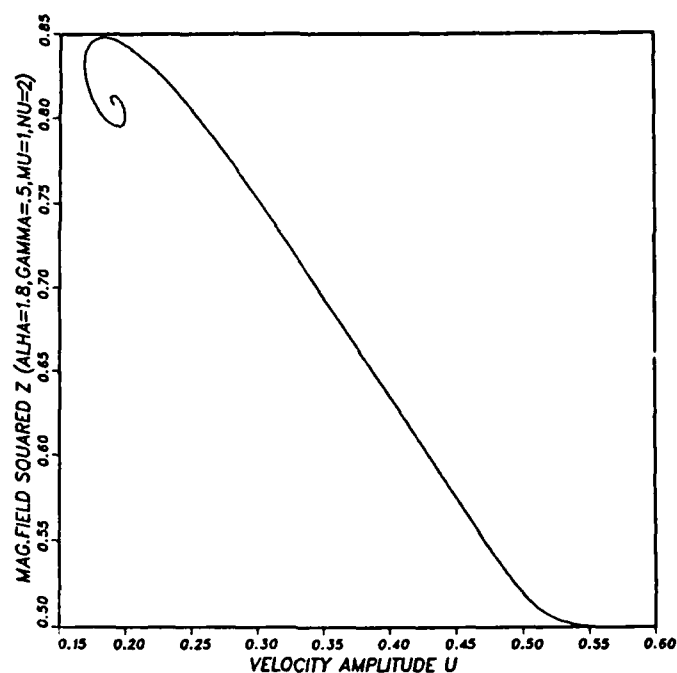


Figure F7.9: The parameters and initial values here are the same as in Figure 7.8 except that the initial z value is *greater* than the equilibrium value. z grows until it converges onto the upper branch value.

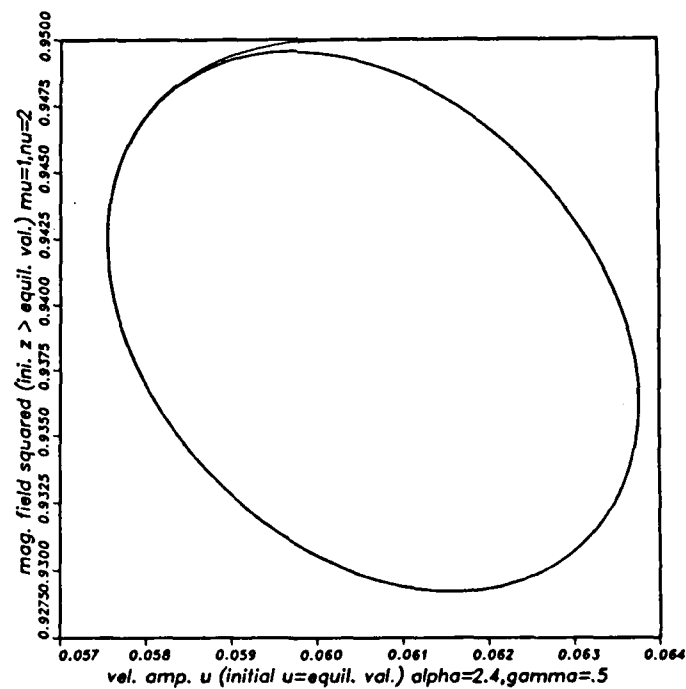


Figure F7.10: A limit cycle (non-linear oscillation) occurring of z versus U for $\alpha = 2.4$. Again U_e and V_e are initial values for those quantities respectively.

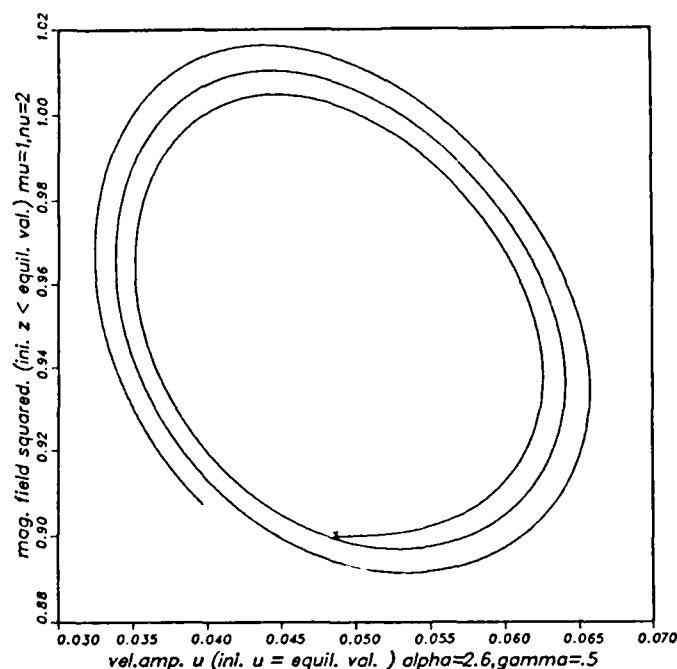


Figure F7.11: A plot of z versus U for $\alpha = 2.6 > \alpha_{\text{Hopf}}$ using the same μ, ν, γ values as before. The 'x' indicates starting point of time evolution of the two quantities.

Here the real part of the growth rate p passed through zero. Thus for values of α greater than α_{Hopf} , perturbations in z grew. This is shown in Figure 7.11. Note that as the perturbation grows, it is possible that a limit cycle may be 'hit' or U may eventually go to zero (at which point, a singularity occurs, as the boundary layer dissolves).

Conclusions

1. The system behaves as a simple attractor (with a large limit cycle 'radius') for the supercritical bifurcation branch (stable).
2. For the subcritical branch:
 - a. lower branch behaves as a simple repeller,
 - b. upper branch behaves as a simple attractor up to the Hopf bifurcation.
3. A minimum criterion ($\alpha > \mu\nu^{-1/2}$) is established to assure non-zero steady-state values of (magnetic field).²

Further Inquiries

1. Determine the critical magnetic Reynolds number for this system.
2. Consider the $R_m \rightarrow \infty$ limit of magnetic fields embedded in square (and possibly hexagonal) cells.
3. More as time proceeds.

I wish to thank Professor Stephen Childress who suggested this project and provided much help. His willingness to help (and patience!) I will always remember. Also, I express my gratitude to Dr. Willem Malkus, who provided me the opportunity of this very rewarding, enriching summer at Woods Hole. Also, I wish to thank Dr. Glenn Ierley for his much needed assistance with the computer graphics. Thank you all.

HOW I MANAGED TO SET AN ISOLATED MONOPOLE VORTEX IN QUASI-GEOSTROPHIC ZONAL SHEAR FLOW

Jun-Ichi Yano
Kyoto University

This is a story about a person who labored hard and obtained little results. His aim was to find general conditions for existence of isolated monopole vortices in geophysical zonal shear flow. First, he tried to find an isolated monopole vortex solution in the quasi-geostrophic periodic zonal flow, but it turned out to be unsuccessful. Finally, he managed to find isolated monopole vortex solution of constant anomalous potential vorticity in constant potential vorticity field. He has also managed to draw some implications.

Introduction

Anyone who knows Jupiter would be fascinated by the beauty of the Great Red Spot and every researcher would think about resolving its nature at least once. This problem is the basic motivation for the present study.

Because the Jovian atmospheres does not have the ground as its lower boundary as in the case of Earth, the Great Red Spot is expected to decay very slowly due to the viscosity. Even the radiative time scale is fairly long (c.a. 10^3 days; Gierasch and Goody, 1969) for Jupiter. This means that the dissipative time scale for the Great Red Spot is so long compared to the advective time scale (Yano, 1987) that it can be treated as a free vortex existing stably in the shearing zonal flow.

Intuitively, it might seem easy to place an isolated monopole vortex in the shearing zonal flow as in the case of the Great Red Spot. But, in fact, this is not so easy as it seems at first glance. It can be shown for a fairly general situation (for example, from primitive equations in isobaric coordinate systems for the atmosphere, see e.g. Holton, 1979) of the geophysical flow in the β -plane approximations that eddy component of the stream function ψ' , the difference between the total streamfunction and the zonal mean part, must satisfy the integral constraint

$$\int \psi' \rho dx dy dz = 0 \quad (1)$$

in order that ψ' decays "fast enough" for far from the center of the vortex (Flierl, et al, 1983). Here, ρ is the density and the integration is performed over a whole domain of the flow.

The integral constraint (1.1) means that if there is a monopole positive vortex in the domain, there must be a negative vortex somewhere. In particular, for the barotropic flow, this means that any isolated vortex must has a dipole structure (Flierl *et al*, 1983). On the other hand, in order that a horizontally isolated vortex has a monopole horizontal structure, the sign of vorticity of the upper layer must be opposite to that of the lower layer. However it is also found (Flierl, 1984a, b)

that this configuration is not always sufficient to obtain an isolated eddy in steady state; instead it may decay by radiating Rossby waves though slowly.

Hence, here, the question is what are the necessary and/or sufficient conditions to isolate a monopole vortex in the geophysical zonal flow in steady state. The aim of the present study is to at least partially answer this question.

An essential step in constructing a steady isolated vortex like the Great Red Spot is to make a localized closed streamline. For this purpose, it might be worth recalling the mathematical procedure to construct the solution of Taylor column, where the closed streamline is defined from the position of the obstacle from the beginning; because the stream function is defined by such an equation as Laplace equation that allows a fairly large generality for solutions, the essential mathematical procedure is to find a solution of stream function that *does* have the given closed streamline. Even without an obstacle, we can think in a similar manner: let us define a closed boundary of streamline we need first; next, we define a general solution of stream function of both the exterior and interior of a given closed streamline expanded in terms of the eigenfunctions satisfying a simple linear differential equation consistent with an original nonlinear governing equation; and finally determine the expansion coefficients so that the streamline does not cross the closed boundary and satisfies an appropriate continuity between the boundary. This is a basic idea of the "modon" theory (Flierl *et al.*, 1980), where the steady quasi-geostrophic potential vorticity equation is reduced to a set of linear differential equations by assuming that the potential vorticity is linearly related to the stream function.

In this report, I try to find monopole "modon" vortex in the zonal shear flow by using two-layer quasi-geostrophic model (e.g. Pedlosky, 1979, section 6.10). Here special attention will be paid to the conditions for the existence of the solution, because, as pointed out above, there are difficulties for existence of steady isolated monopole vortices in the geophysical flow due to the tendency to decay by radiating waves.

However, here, I must make a remark that the quasi-geostrophic system may not be an appropriate model to describe the dynamics of the Jovian atmospheres. Williams and Yamagata (1984) proposed the intermediate-geostrophic system (found by Flierl, 1980 and Yamagata, 1982 independently) as an appropriate model for isolated vortices of Jovian atmospheres; more recently, by careful scale analysis, Yano (1987) suggested that the dynamics of the Jovian atmospheres are more likely to be governed by the system named "thermo-geostrophic". Moreover, we must recognize from Charney and Flierl (1981) that the quasi-geostrophic system can be applicable only for a limited range of space and time scales of geophysical flows. Nevertheless, I believe that the quasi-geostrophic system is qualitatively appropriate, and it would give us insights for more general treatments.

The plan of the present report is as follows: in the next section, the case of periodic zonal flow is considered; in the following section, the case of parabolic zonal flow is considered; and in the final section, I will state several final remarks.

Model 1: Periodic Zonal Flow

I adopt the steady quasi-geostrophic potential vorticity equation of the two-layer model

$$J(\psi_1 + \epsilon c y, \nabla^2 \psi_1 + (\psi_2 - \psi_1) + \epsilon y) = 0, \quad (2.1a)$$

$$J(\psi_2 + \epsilon c y, \nabla^2 \psi_2 + \delta(\psi_1 - \psi_2) + \epsilon y) = 0, \quad (2.1b)$$

where ψ_1 and ψ_2 are the stream functions for upper and lower layers, respectively c the phase velocity of eddy, and J the Jacobian

$$J(a, b) \equiv \frac{\partial a}{\partial x} \frac{\partial b}{\partial y} - \frac{\partial a}{\partial y} \frac{\partial b}{\partial x},$$

in which x and y are the coordinates measured in eastward and northward directions, respectively. The governing equations (2.1) are already appropriately non-dimensionalized in terms of nondimensional parameters defined by

$$\epsilon \equiv \beta L^2 / U, \quad (2.2a)$$

$$\delta \equiv H_1 / H_2, \quad (2.2b)$$

where β is the rate of the change of Coriolis parameters in the y -direction, L the horizontal scale taken to the Rossby radius of deformation of upper layer ($g'H_1/f^2$), U the magnitude of the flow, H_1 and H_2 are the mean thickness of the upper and lower layers, respectively.

Equation 2.1 can be reduced to the form

$$\nabla^2 \psi_1 + (\psi_2 - \psi_1) + \epsilon y = F_1(\psi_1 + \epsilon c y), \quad (2.3a)$$

$$\nabla^2 \psi_2 + \delta(\psi_1 - \psi_2) + \epsilon y = F_2(\psi_2 + \epsilon c y), \quad (2.3b)$$

where F_1 and F_2 are the functionals to be defined. In the present section, I assume

$$F_1(\xi) = \begin{cases} \mu_1 \xi & \eta > \eta(0) \\ D_1 + \nu_1 \xi & \eta < \eta(0) \end{cases}, \quad (2.4a)$$

$$F_2(\xi) = \begin{cases} \mu_2 \xi & \eta > \eta(0) \\ D_2 + \nu_2 \xi & \eta < \eta(0) \end{cases}, \quad (2.4b)$$

where $\mu_1, \mu_2, D_1, D_2, \nu_1$, and ν_2 , are the constants to be chosen appropriately, r is the distance from the origin $(0, 0)$, and $r(\theta)$ the boundary depends on the azimuthal angle θ . Note that the assumption of linear stream function - potential vorticity relationship permits only rather special forms of the mean flows.

In the following, I shall assume ϵ is a small perturbation quantity and also assume the zonal flow is of order ϵ . Hence the streamfunctions are decomposed into eddy part ϕ_1, ϕ_2 and the zonal-flow part $\Psi_1(y), \Psi_2(y)$ by

$$\psi_1 = \phi_1 + \epsilon \Psi_1(y) \quad , \quad (2.5a)$$

$$\psi_2 = \phi_2 + \epsilon \Psi_2(y) \quad , \quad (2.5b)$$

and further decompose the stream functions of both layers into (pseudo-) baroclinic part Φ_{BC}, Ψ_{BC} and (pseudo-) barotropic part Φ_{BT}, Ψ_{BT} :

$$\phi_1 = \begin{cases} \phi_{BC}^{ex} + \phi_{BT}^{ex} \\ \phi_{BC}^{int} + \phi_{BT}^{int} \end{cases} \quad , \quad \phi_2 = \begin{cases} r_1 \phi_{BC}^{ex} + r_2 \phi_{BT}^{ex} \\ s_1 \phi_{BC}^{int} + s_2 \phi_{BT}^{int} \end{cases} \quad \begin{matrix} \text{in } r > r(\theta) \\ \text{in } r < r(\theta) \end{matrix} \quad , \quad (2.6a)$$

$$\Psi_1 = \begin{cases} \Psi_{BC}^{ex} + \Psi_{BT}^{ex} \\ \Psi_{BC}^{int} + \Psi_{BT}^{int} \end{cases} \quad , \quad \Psi_2 = \begin{cases} r_1 \Psi_{BC}^{ex} + r_2 \Psi_{BT}^{ex} \\ s_1 \Psi_{BC}^{int} + s_2 \Psi_{BT}^{int} \end{cases} \quad \begin{matrix} \text{in } r > r(\theta) \\ \text{in } r < r(\theta) \end{matrix} \quad , \quad (2.6b)$$

where superscripts *ex* and *int* imply the solutions for exterior and interior of the boundary $r = r(\theta)$ and coefficients r_1, r_2 are defined by

$$r_1 = \frac{1 - \delta + \mu_1 - \mu_2}{2} - \sqrt{\left(\frac{1 - \delta + \mu_1 - \mu_2}{2}\right)^2 + \delta} \quad ,$$

$$r_2 = \frac{1 - \delta + \mu_1 - \mu_2}{2} + \sqrt{\left(\frac{1 - \delta + \mu_1 - \mu_2}{2}\right)^2 + \delta} \quad ,$$

and similar definitions for s_1 and s_2 . We have called the components of the stream functions (pseudo-) baroclinic and (pseudo-) barotropic parts because $r_1 < 0$ and $s_1 < 0$, $r_2 > 0$ and $s_2 > 0$ and hence these parts roughly correspond to baroclinic and barotropic modes, respectively. It may be worth remarking that when $\mu_1 = \mu_2$ we obtain $r_1 = -\delta$, $r_2 = 1$ hence these indeed correspond to the baroclinic and the barotropic modes, respectively.

Consequently, the governing equations are written by

$$\left[\begin{array}{ll} (\nabla^2 - \lambda_1^2) \phi_{bc}^{ex} = 0, & (\nabla^2 - \lambda_1^2) \bar{\psi}_{bc}^{ex} = \gamma_1 y, \end{array} \right. \quad (2.7a, b)$$

$$\left[\begin{array}{ll} (\nabla^2 - \lambda_2^2) \phi_{bt}^{ex} = 0, & (\nabla^2 - \lambda_2^2) \bar{\psi}_{bt}^{ex} = \gamma_2 y, \end{array} \right. \quad (2.7c, d)$$

$$\left[\begin{array}{ll} (\nabla^2 + k_1^2) \phi_{bc}^{int} = 0, & (\nabla^2 + k_1^2) \bar{\psi}_{bc}^{int} = \beta_1 y, \end{array} \right. \quad (2.8a, b)$$

$$\left[\begin{array}{ll} (\nabla^2 + k_2^2) \phi_{bt}^{int} = 0, & (\nabla^2 + k_2^2) \bar{\psi}_{bt}^{int} = \beta_2 y, \end{array} \right. \quad (2.8c, d)$$

where the various parameters can be found in terms of those used previously.

We assume the boundary conditions

$$\psi_i^{ex} - \psi_i^{int} = 0 \quad (i=1,2) \quad \text{at} \quad r = r(\theta), \quad (2.9a)$$

$$\hat{n} \cdot \nabla (\psi_i^{ex} - \psi_i^{int}) = 0 \quad (i=1,2) \quad \text{at} \quad r = r(\theta), \quad (2.9b)$$

where \hat{n} is the unit vector in the normal direction to the boundary. We also assume that there is a closed streamline along the boundary in the upper layer, i.e.

$$\psi_1^{ex} = \psi_1^{int} = \text{const.} \quad \text{at} \quad r = r(\theta). \quad (2.9c)$$

From the conservation of potential vorticity along the flow, we have

$$\mu_2 = \nu_2, \quad D_2 = 0, \quad (2.10)$$

but we retain the parameters ν_2 and D_2 in most parts of manipulations for later modification of the condition.

Now, the eddy solution must satisfy $\Phi \rightarrow 0$ as $r \rightarrow \infty$ so that either $\lambda_1^2 > 0$ or $\lambda_2^2 > 0$ is required from equation (2.7a,c). On the other hand, in order that the zonal flow is bounded for $y \rightarrow \pm\infty$ (or more specifically, is periodic in y -direction), either $\lambda_1^2 < 0$ or $\lambda_2^2 < 0$ is required. Because $\lambda_1^2 > \lambda_2^2$ from the definition:

$$\lambda_1^2 = S + \mu_2 + \tau_2 \quad ,$$

$$\lambda_2^2 = S + \mu_2 + \tau_2 \quad ,$$

it is required that $\lambda_1^2 \equiv \lambda^2 > 0$ and $\lambda_2^2 \equiv -l^2 < 0$, and hence

$$\phi_{BT}^{ex} \equiv 0 \quad (2.11)$$

must be imposed. On the other hand, we can have only a uniform baroclinic zonal-flow part and uniform plus periodic barotropic zonal-flow in the exterior from (2.7b,d)

$$\psi_{BC}^{ex} = -\frac{\sigma_2}{\lambda^2} y \quad , \quad (2.12a)$$

$$\psi_{BT}^{ex} = \frac{\sigma_2}{l^2} y + \psi_0 \cos l(y-y_0) \quad , \quad (2.12b)$$

and correspondingly for the interior from (2.8b,d),

$$\psi_{BC}^{int} = \frac{\beta_2}{k_1^2} y + \psi_{BC} \cos k_1(y-y_0) \quad , \quad (2.12c)$$

$$\psi_{BT}^{int} = \frac{\beta_2}{k_2^2} y + \psi_{BT} \cos k_2(y-y_0) \quad , \quad (2.12d)$$

where Ψ_0 , Ψ_{BC} and Ψ_{BT} are the amplitudes which might be specified later. As a convention, we assume $\bar{\Psi}_{BC} = 0$ and/or $\bar{\Psi}_{BT} = 0$ when k_1 and/or k_2 is purely imaginary.

To sum up, our aim is to find a solution with an isolated vortex which is monopolar in each layer, embedded in the barotropic periodic zonal flow. However, a difficulty is that we must satisfy five boundary conditions (2.9) with only four dependent variables Φ_{BC}^{ex} , Φ_{BC}^{int} , Φ_{BT}^{int} , and $r(\theta)$. We look for necessary or sufficient conditions for existence of the solution within this restriction in the following.

Because it is formidable to find the solutions of equation (2.7) and (2.8) such that satisfy the boundary condition (2.9), I assume that the boundary $r(\theta)$ is nearly circular and modulated only at $O(\epsilon)$:

$$r(\theta) = r_0 + \epsilon \eta(\theta), \quad (2.13)$$

and make Taylor expansion of the boundary conditions around $r = r_0$ (see Swenson, 1982). Hence, we obtain

$$\phi_1^{ex(0)} - \phi_1^{int(0)} = 0, \quad \phi_2^{ex(0)} - \phi_2^{int(0)} = 0, \quad (2.14 a, b)$$

$$\frac{\partial}{\partial r}(\phi_1^{ex(0)} - \phi_1^{int(0)}) = 0, \quad \frac{\partial}{\partial r}(\phi_2^{ex(0)} - \phi_2^{int(0)}) = 0 \quad (2.14 c, d)$$

at $r = r_0$ for $O(1)$, and

$$\frac{\partial}{\partial r}(\phi_1^{ex(0)} - \phi_1^{int(0)})\eta + (\phi_1^{ex(1)} - \phi_1^{int(1)}) + (\bar{\psi}_1^{ex} - \bar{\psi}_1^{int}) = 0,$$

$$\frac{\partial}{\partial r}(\phi_2^{ex(0)} - \phi_2^{int(0)})\eta + (\phi_2^{ex(1)} - \phi_2^{int(1)}) + (\bar{\psi}_2^{ex} - \bar{\psi}_2^{int}) = 0,$$

$$\frac{\partial^2}{\partial r^2}(\phi_1^{ex(0)} - \phi_1^{int(0)})\eta + \frac{\partial}{\partial r}(\phi_1^{ex(1)} - \phi_1^{int(1)}) + \frac{\partial}{\partial r}(\bar{\psi}_1^{ex} - \bar{\psi}_1^{int}) = 0,$$

$$\frac{\partial^2}{\partial r^2}(\phi_2^{ex(0)} - \phi_2^{int(0)})\eta + \frac{\partial}{\partial r}(\phi_2^{ex(1)} - \phi_2^{int(1)}) + \frac{\partial}{\partial r}(\bar{\psi}_2^{ex} - \bar{\psi}_2^{int}) = 0$$

$r = r_0$ at for $O(\epsilon)$. Here I have expanded all eddy quantities in ϵ , e.g.

$$\phi_1^{ex} = \phi_1^{ex(0)} + \epsilon \phi_1^{ex(1)} + O(\epsilon^2).$$

In accordance with my purpose to find an isolated monopole vortex, I assume the radially symmetric solutions of the form

$$\phi_{BC}^{ex(0)} = a_0 K_0(\lambda r), \quad (2.17a)$$

$$\phi_{BC}^{ind(0)} = \frac{d_1}{k_1^2} + b_0 J_0(k_1 r), \quad (2.17b)$$

$$\phi_{BT}^{ind(0)} = \frac{d_2}{k_2^2} + c_0 J_0(k_2 r) \quad (2.17c)$$

at $O(1)$. Here, when k_1 and/or k_2 is purely imaginary, the Bessel function

$$J_0(k_1 r) \quad \text{and/or} \quad J_0(k_2 r)$$

should be replaced by the modified Bessel function

$$I_0(\chi_1 r) \quad \text{and/or} \quad I_0(\chi_2 r)$$

in which

$$\chi_1 = |\operatorname{Im}(k_1)|, \quad \chi_2 = |\operatorname{Im}(k_2)|,$$

and the similar procedure should be applied in the higher order (see Flierl *et al.*, 1980). The coefficients a_0, b_0, c_0 are determined by

$$\Delta_1 a_0 K_0(\lambda r_0) - b_0 J_0(k_1 r_0) = \frac{d_1}{k_1^2}, \quad (2.18a)$$

$$\Delta_2 a_0 K_0(\lambda r_0) - c_0 J_0(k_2 r_0) = \frac{d_2}{k_2^2}, \quad (2.18b)$$

$$\Delta_1 a_0 \lambda K_1(\lambda r_0) - b_0 k_1 J_1(k_1 r_0) = 0, \quad (2.18c)$$

$$\Delta_2 a_0 \lambda K_1(\lambda r_0) - c_0 k_2 J_1(k_2 r_0) = 0, \quad (2.18d)$$

where we have introduced

$$\Delta_1 = \frac{S_2 - r_1}{S_2 - S_1}, \quad \Delta_2 = \frac{S_1 - r_1}{S_1 - S_2}. \quad (2.19)$$

In order that four conditions (2.18) are satisfied by three coefficients a_0, b_0, c_0 , we require

$$\Delta_1 \tilde{W}_0(\lambda, k_1) \frac{d_2}{k_2} = \Delta_2 \tilde{W}_0(\lambda, k_2) , \quad (2.20)$$

where

$$\tilde{W}_m(\lambda, k_i) \equiv \frac{\lambda K'_m(\lambda r_0)}{K_m(\lambda r_0)} - \frac{k_i J'_m(k_i r_0)}{J_m(k_i r_0)} \quad (i=1,2) .$$

This is a first condition to be satisfied in order that we have an isolated vortex solution.

Because the lowest order solution (2.17) is radially symmetric, we have

$$\eta(\theta) = - \frac{\phi_i^{ext(1)} + \bar{\psi}_i^{ext}}{\frac{\partial \phi_i^{ext(1)}}{\partial r}} \bigg|_{r=r_0} = - \frac{\phi_i^{int(1)} + \bar{\psi}_i^{int}}{\frac{\partial \phi_i^{int(1)}}{\partial r}} \bigg|_{r=r_0}$$

from (2.15e,f). These two expressions for $\eta(\theta)$ are consistent, because denominators and numerators are identical, respectively, from (2.14c) and (2.15a).

The solutions of the $O(\epsilon)$ equations consistent with boundary conditions (2.15, a-d) are given by

$$\phi_{BC}^{ext(1)} = \sum_{m=0}^{\infty} [a_{2m}^{(1)} \cos 2m\theta K_{2m}(\lambda r) + a_{2m+1}^{(1)} \sin(2m+1)\theta K_{2m+1}(\lambda r)] , \quad (2.22a)$$

$$\phi_{BC}^{int(1)} = \sum_{m=0}^{\infty} [b_{2m}^{(1)} \cos 2m\theta J_{2m}(k_1 r) + b_{2m+1}^{(1)} \sin(2m+1)\theta J_{2m+1}(k_1 r)] , \quad (2.22b)$$

$$\phi_{BT}^{int(1)} = \sum_{m=0}^{\infty} [c_{2m}^{(1)} \cos 2m\theta J_{2m}(k_2 r) + c_{2m+1}^{(1)} \sin(2m+1)\theta J_{2m+1}(k_2 r)] , \quad (2.22c)$$

by invoking the fact that the boundary value of zonal-flow part can be written in terms of Bessel function by the relation

$$\begin{aligned} \cos[l(r_0 \sin \theta - \vartheta_0)] &= \cos l \vartheta_0 \cdot J_0(lr_0) + 2 \cos l \vartheta_0 \sum_{m=1}^{\infty} J_{2m}(lr_0) \cos 2m\theta \\ &\quad + 2 \sin l \vartheta_0 \sum_{m=0}^{\infty} J_{2m+1}(lr_0) \sin (2m+1)\theta \end{aligned}$$

(see e.g. Abramowitz and Stegun, 1964). The boundary conditions (2.15a-d) can be re-written in terms of conditions of continuity of both the baroclinic and the barotropic parts of interior to the exterior. Put into Eq. (2.22) into them, we obtain

$$\Delta_1 a_n'' K_n(\lambda r_0) - b_n'' J_n(k_1 r_0) = g_{1,n}, \quad (2.23a)$$

$$\Delta_2 a_n'' K_n(\lambda r_0) - c_n'' J_n(k_2 r_0) = g_{2,n}, \quad (2.23b)$$

$$\Delta_1 \{ \tilde{W}_1(\lambda, k_1) K_n(\lambda r_0) - \lambda K_n'(\lambda r_0) \} a_n'' + k_1 J_n'(k_1 r_0) b_n'' = g_{3,n}, \quad (2.23c)$$

$$\Delta_2 \{ \tilde{W}_1(\lambda, k_2) K_n(\lambda r_0) - \lambda K_n'(\lambda r_0) \} a_n'' + k_2 J_n'(k_2 r_0) c_n'' = g_{4,n}, \quad (2.23d)$$

where $g_{i,n}$ ($i = 1, 2, 3, 4$) are given in Appendix. Again we have four conditions for three coefficients for every n .

In particular, for $n = 1$, we have

$$\Delta_1 a_1'' K_1(\lambda r_0) - b_1'' J_1(k_1 r_0) = g_{1,1},$$

$$\Delta_2 a_1'' K_1(\lambda r_0) - c_1'' J_1(k_2 r_0) = g_{2,1},$$

$$-k_1 J_1'(k_1 r_0) / J_1(k_1 r_0) [\Delta_1 a_1'' K_1(\lambda r_0) - b_1'' J_1(k_1 r_0)] = g_{3,1},$$

$$-k_2 J_1'(k_2 r_0) / J_1(k_2 r_0) [\Delta_2 a_1'' K_1(\lambda r_0) - c_1'' J_1(k_2 r_0)] = g_{4,1}.$$

Obviously, the determinant vanishes for this case and, hence,

$$k_1 J_1'(k_1 r_0) / J_1(k_1 r_0) \cdot g_{1,1} + g_{3,1} = 0, \quad (2.24a)$$

$$k_2 J_1'(k_2 r_0) / J_1(k_2 r_0) \cdot g_{2,1} + g_{4,1} = 0 \quad (2.24b)$$

are required in order the solution to exist. These are the second and the third condition for existence of the solution.

In order that (2.23) have solutions, we have

$$\begin{aligned} & \Delta_1 \lambda \tilde{W}_1(\lambda, k_1) \{ \Delta_2 \tilde{W}_m(\lambda, k_2) - \Delta_4 \tilde{W}_m(l, k_2) \} \\ & - \Delta_2 \lambda \tilde{W}_1(\lambda, k_2) \{ \Delta_1 \tilde{W}_m(\lambda, k_1) - \Delta_3 \tilde{W}_m(l, k_1) \} \\ & + \Delta_1 \Delta_4 \tilde{W}_m(\lambda, k_1) \tilde{W}_m(l, k_2) - \Delta_2 \Delta_3 \tilde{W}_m(\lambda, k_2) \tilde{W}_m(l, k_1) = 0 \end{aligned}$$

for every n except $n \neq 1$, where

$$\tilde{W}_m(l, k_i) \equiv \frac{l J'_m(l k_i r_0)}{J_m(l k_i r_0)} - \frac{k_i J'_m(l k_i r_0)}{J_m(l k_i r_0)} \quad (i=1, 2)$$

Apparently, four functions of n

$$\Delta_2 \tilde{W}_m(\lambda, k_2) - \Delta_4 \tilde{W}_m(l, k_2) \quad , \quad (2.26a)$$

$$\Delta_1 \tilde{W}_m(\lambda, k_1) - \Delta_3 \tilde{W}_m(l, k_1) \quad , \quad (2.26b)$$

$$\tilde{W}_m(\lambda, k_1) \tilde{W}_m(l, k_2) \quad , \quad (2.26c)$$

$$\tilde{W}_m(\lambda, k_2) \tilde{W}_m(l, k_1) \quad (2.26d)$$

seem to be independent of each other. If that is true then

$$\Delta_1 \lambda \tilde{W}_1(\lambda, k_1) \{ \Delta_2 \tilde{W}_m(\lambda, k_2) - \Delta_4 \tilde{W}_m(l, k_2) \} = 0 \quad , \quad (2.27a)$$

$$\Delta_2 \lambda \tilde{W}_1(\lambda, k_2) \{ \Delta_1 \tilde{W}_m(\lambda, k_1) - \Delta_3 \tilde{W}_m(l, k_1) \} = 0 \quad , \quad (2.27b)$$

$$\Delta_1 \Delta_4 \tilde{W}_m(\lambda, k_1) \tilde{W}_m(l, k_2) = 0 \quad , \quad (2.27c)$$

$$\Delta_2 \Delta_3 \tilde{W}_m(\lambda, k_2) \tilde{W}_m(l, k_1) = 0 \quad (2.27d)$$

are the necessary and sufficient conditions for (2.25). Unfortunately, I could not prove the independence of four functions (2.26). Nevertheless, if the above argument is right, an only possible non-trivial choice of parameters is

$$h_2 = l, \quad S_1 = \gamma_1, \quad S_2 = \gamma_2. \quad (2.28)$$

I attempted to find a solution with this choice of parameters, but the solution has been possible only for the case without periodic zonal-flow part i.e. $\Psi_0 = 0$, which is not interest here and hence I have not considered this case further.

I have also examined the relations between conditions (2.20), (2.24) and (2.25) and the integral constraint (1.1) or the other integral constraint derived for this model,

$$\iint_{\gamma \leq \gamma(0)} \phi_1 dx dy = \frac{\pi D_2 \gamma_0^2}{\gamma_2 - \gamma_1},$$

when $\mu_1 = \mu_2 = \nu_2$, and $D_2 = 0$ are assumed. However, I could not find the clear correspondences between them. Nevertheless, the results imply that an infinite number of constraints (2.25) are required in addition to the integral constraint (1.1) in order that the monopole vortex is to be isolated locally in general. Thus it seems almost impossible to set a monopole isolated vortex in the periodic geostrophic zonal flow, as in the case of the Great Red Spot, within this model.

Model 2: Homogeneous Potential Vorticity Field

In order to find the way to resolve the difficulty, now I turn into a much simplified model in the present section. I assume that the value of the potential vorticity is constant in both interior and exterior but of different values. The solution for the one-layer model is readily evaluated (Flierl, personal communication from Seattle, Aug. 5, 1987). In the present section, I consider the two layer model given by

$$F_1(\xi) = \epsilon \alpha + q_1 H(\gamma_b^1 - \gamma), \quad (3.1a)$$

$$F_2(\xi) = \epsilon \alpha + q_2 H(\gamma_b^2 - \gamma), \quad (3.1b)$$

instead of (2.4). Here, H is the step function and I have assumed different boundaries

$$\gamma_b^1 = \gamma_0 + \epsilon \gamma_1(0),$$

$$\gamma_b^2 = \gamma_0 + \epsilon \gamma_2(0)$$

for upper and lower layers, otherwise the isolated monopole solution is not possible in general even within this simplified model.

The boundary conditions (2.9a) and (2.9c) are replaced at $r = r_b^1$ and (2.9b) is replaced by $r = r_b^2$, and in addition I assume the closed streamline also in the lower layer, i.e.

$$\psi_a^{\text{ext}} = \psi_a^{\text{int}} = \text{const.} \quad \text{at} \quad r = r_b^2(\theta), \quad (3.2)$$

which means that vortex is so strong that it can exist even against the opposite sign of vorticity of shear flow.

I separate the eddy part Φ_1, Φ_2 and the zonal flow part Ψ , instead of (2.5), by

$$\psi_1 = g_1 \phi_1 + \epsilon \Psi, \quad (3.3a)$$

$$\psi_2 = g_1 \phi_1 + e \Psi, \quad (3.3b)$$

where the zonal flow in the homogeneous potential vorticity is given by

$$\Psi = -\frac{y^3}{6} + \alpha \frac{y^2}{2} + \gamma y; \quad (3.4)$$

γ is a constant. Note that in this model the zonal flow Ψ is no longer bounded at infinity $y \rightarrow \pm \infty$. This artificial configuration of flow may be modified into more realistic one by assuming latitudinal bands of constant potential vorticity field (see Stern and Flierl, 1987 for basic idea), but I do not consider this case in this report.

The eddy part Φ_1, Φ_2 of stream functions are decomposed into the baroclinic and barotropic parts by

$$\phi_1 = \phi_{BT} + \phi_{BC}, \quad (3.5a)$$

$$\phi_2 = \phi_{BT} - \delta \phi_{BC}. \quad (3.5b)$$

The point is that, though the barotropic part Φ_{BT} of the stream function still does not decay with the distance in the exterior, barotropic part of the velocity *does* decay in the far field. Hence, we do not assume the barotropic part to be vanished in the exterior in the present model.

The procedure to obtain the solutions are similar and much more easier than that of the previous section. The results are

$$\phi_{BC} = \phi_{BC}^{(0)} + \epsilon \left[\phi_{BC,1}^{(1)} \sin \theta + \phi_{BC,2}^{(1)} \cos 2\theta + \phi_{BC,3}^{(1)} \sin 3\theta \right], \quad (3.6a)$$

$$\phi_{BT} = \phi_{BT}^{(0)} + \epsilon \left[\phi_{BT,1}^{(1)} \sin \theta + \phi_{BT,2}^{(1)} \cos 2\theta + \phi_{BT,3}^{(1)} \sin 3\theta \right], \quad (3.6b)$$

and

$$\gamma_b^1 = \gamma_0 + \epsilon (\gamma_{1,1} \sin \theta + \gamma_{1,2} \cos 2\theta + \gamma_{1,3} \sin 3\theta), \quad (3.7a)$$

$$\gamma_b^2 = \gamma_0 + \epsilon (\gamma_{2,1} \sin \theta + \gamma_{2,2} \cos 2\theta + \gamma_{2,3} \sin 3\theta), \quad (3.7b)$$

where

$$\phi_{BC}^{(0)} = \begin{cases} -\frac{1-g}{(1+g)^2} + \frac{1-g}{(1+g)^2} \gamma_0 K_2(\nu r_0) I_1(\nu r) & \text{for } r < \min(r_b^1, r_b^2) \\ \left[-\frac{1-g}{(1+g)^2} + \frac{1-g}{(1+g)^2} \gamma_0 K_2(\nu r_0) I_1(\nu r_0) \right] \frac{K_0(\nu r)}{K_0(\nu r_0)} & \text{for } r > \max(r_b^1, r_b^2), \end{cases} \quad (3.8a)$$

$$\phi_{BC,m}^{(1)} = \begin{cases} -\frac{\gamma_{1,m} - g\gamma_{2,m}}{1+g} \gamma_0 K_m(\nu r_0) I_m(\nu r) & \text{for } r < \min(r_b^1, r_b^2) \\ -\frac{\gamma_{2,m} - g\gamma_{1,m}}{1+g} \gamma_0 I_m(\nu r_0) K_m(\nu r) & \text{for } r > \max(r_b^1, r_b^2), \end{cases} \quad (3.8b)$$

$$\phi_{BT}^{(0)} = \begin{cases} \frac{g+g}{4(1+g)} \gamma_0^2 \left[\left(\frac{r}{r_0} \right)^2 - 1 + 2 \ln r_0 \right] & \text{for } r < \min(r_b^1, r_b^2) \\ \frac{g+g}{2(1+g)} \gamma_0^2 \ln r & \text{for } r > \max(r_b^1, r_b^2), \end{cases} \quad (3.9a)$$

$$\phi_{BT,m}^{(1)} = \begin{cases} -\frac{g\gamma_{1,m} + g\gamma_{2,m}}{2m(1+g)} \gamma_0 \left(\frac{r}{r_0} \right)^m & \text{for } r < \min(r_b^1, r_b^2) \\ -\frac{g\gamma_{1,m} + g\gamma_{2,m}}{2m(1+g)} \gamma_0 \left(\frac{r_0}{r} \right)^m & \text{for } r > \max(r_b^1, r_b^2), \end{cases} \quad (3.9b)$$

$$\eta_{1,m} = \frac{1}{\text{Det}} \left[-\frac{\delta+g}{2} - g(1+\delta) K_m(\nu r_0) I_m(\nu r_0) + \delta(1-g) k_1(\nu r_0) \right. \\ \left. I_1(\nu r_0) \right] \Delta_m, \quad (3.10a) \quad \text{F8.15}$$

$$\eta_{2,m} = \frac{1}{\text{Det}} \left[-\frac{\delta+g}{2} - (1+\delta) K_m(\nu r_0) I_m(\nu r_0) - (1-g) k_1(\nu r_0) I_1(\nu r_0) \right] \Delta_m, \\ (3.10b)$$

where

$$g = g_2/g_1, \quad \nu = (1+\delta)^{1/2}, \quad (3.11a,b)$$

and

$$\text{Det} = -\left(1 - \frac{1}{m}\right) \left(\frac{\delta+g}{2}\right)^2 + \frac{1}{2} \left[-\frac{\delta^2-g}{m} + (\delta-1)(\delta+g) \right] (1-g) K_1(\nu r_0) I_1(\nu r_0) \\ - \frac{1}{2} \left[-\frac{(1+\delta)^2}{m} g + (1+\delta g)(\delta+g) \right] K_m(\nu r_0) I_m(\nu r_0) \\ + \delta(1-g)^2 K_1(\nu r_0) I_1(\nu r_0) [K_m(\nu r_0) I_m(\nu r_0) + k_1(\nu r_0) I_1(\nu r_0)], \quad (3.11c)$$

$$\Delta_1 = \left(\gamma - \frac{\gamma_0^2}{g}\right) \gamma_0, \quad \Delta_2 = -\frac{\alpha \gamma_0^2}{2}, \quad \Delta_3 = \frac{\gamma_0^3}{24}. \quad (3.11d)$$

I must point out here that streamlines have been determined for

$$r < \min(\gamma_b^1, \gamma_b^2) \quad \text{and} \quad r > \max(\gamma_b^1, \gamma_b^2),$$

but not for

$$\min(\gamma_b^1, \gamma_b^2) < r < \max(\gamma_b^1, \gamma_b^2), \quad (3.12)$$

because I have assumed deformation of the boundaries η_1, η_2 are small enough so that these parts are narrow enough to neglect. It is also worth mentioning that the case with $q = 1$ does not have baroclinic part and identical to the one-layer results.

A special interest is the case with $q = -\delta$ when leading order $\Phi_{BT}^{(0)}$ of the barotropic part vanishes so that vortex is isolated in a stronger sense, and on the other hand there is no baroclinic eddy part $\Phi_{BC}^{(1)}$ in higher order, which means that eddy is adjusted against zonal flow and β -effect only by barotropic part. Because the eddy of lowest order is purely baroclinic we have

$$\phi_2^{(0)} = -\delta \phi_1^{(0)}, \quad (3.13)$$

so that thicker the lower layer weaker the lowest order eddy of the lower layer; however we must note that higher order eddy is of same magnitude for both layer. It is also worth to take notice that deformation η_1, η_2 of the boundary satisfy the relation

$$\eta_1 = -\delta \eta_2, \quad (3.14)$$

which means that the direction of the deformation of upper layer is completely of opposite to that of the lower layer and its ratio is proportional to the ratio of the thickness of two layers.

The boundaries $\eta_{i,1}$ proportional to $\sin \theta$ is due to the homogeneous part γ of the zonal flow, which just move the center of the vortex in the latitudinal direction, but in different direction and magnitude at each layer. Note that by choosing

$$\gamma = \frac{\gamma_0^2}{8},$$

vorticity is not displaced in the latitudinal direction.

The term $\eta_{i,2}$ proportional to $\cos 2\theta$ is due to the shear α of the zonal flow. Within the cyclonic shear flow ($\alpha > 0$), positive upper-layer vortex (by assuming $q_1 > 0$ hereinafter) is elonged in the longitudinal direction and negative lower-layer vortex is shrunk longitudinal direction (figure 1a). Within the anticyclonic shear flow ($\alpha < 0$), the opposite is true (figure 1b).

The term $\eta_{1,3}$ proportional to $\sin 3\theta$ is due to the curvature of the zonal flow. The positive upper-layer vortex is deformed to the triangular form, because the vortex must rotate in the direction against that of the zonal flow, and hence shrunk in longitudinal direction at the northern part. From the same reason, the negative lower-layer vortex is deformed to inverse triangular form (figure 1c).

I have shown streamline of the barotropic eddy part $\Phi_{BT}^{(1)}$ with $r_0 = 1$, $\delta = 1$, $q = -1$, $\alpha = 1/8$ for several cases in figure 2. We can see that purely radially symmetric *baroclinic* eddy is adjusted to β -effect and barotropic zonal flow by *barotropic* multipole eddy. Note that $\Phi_{BT}^{(1)}$ has opposite sign to η_1 .

I also performed the numerical calculations of time evolution of contour of the boundary of constant potential vorticity area by using the program prepared by Flierl (personal communication from M.I.T., Aug. 21, 1987) in order to examine the reliability and stability of the linear analytical solutions obtained above. The basic zonal flow $u(y)$ is given by

$$\bar{u}(y) = \frac{\hat{\beta}}{2} y^2 + \hat{\alpha} y + \hat{\gamma} \quad (3.15)$$

in numerical calculations. In comparison with (3.4), we have

$$\hat{\beta} = \epsilon, \quad \hat{\alpha} = -\epsilon\alpha, \quad \hat{\gamma} = -\epsilon\gamma.$$

As an initial condition, I assume a circular vortex of radius r_0 in belief that the form of vortex would approach to the analytical result $r_b^1(\theta)$ and $r_b^2(\theta)$ as a equilibrium if it is a stable state. The computational results are summarized in Table 1. The parameters used for computations are summarized in Table 2.

First let us consider the case only with shear $\hat{\alpha}$. When the thickness of two layers is the same (i.e. $\delta = 1$) with weak shear, ($|\hat{\alpha}| \leq 0.2$), the vortex is elongated into elliptical shape in accordance with linear theory, though it rotates with time and does not reach equilibrium state within computational time ($t_{max} = 60$). However, with stronger shear ($\hat{\alpha} = -0.4$, figure 3a), the north-south (N-S) elongated vortex can not endure against shear flow, becomes unstable, and continuously stretched to form a dipole-structure. (In figure 3a, the fourth counter has been broken down numerically.) When the ratio δ of thickness of two-layers is decreased from unity, the vortex of lower layer is expected to deform in larger extent from relation (3.14). This tendency is also observed in numerical calculations. But for very small δ , the vortex of the lower layer is so weak (the strongness of vorticity is δ of that of the upper layer, see (3.13)) that it can not be sustained in the shear flow and is

stretched continuously in east-west direction, even for the case of negative shear flow when the vortex should be elongated in latitudinal direction (figure 3b). When the scale r_0 of vortex is enlarged from unity with $\delta = 1$, the vortex becomes unstable again and tend to assume a dipole structure in the upper (figure 3c) or lower layers depending on the sign (positive or negative) of shear flow.

Turn to the case only with $\hat{\beta}$, next: With $\delta = 1$, the vortex deforms to the triangular form as expected from linear theory. However as δ is decreased, the vortex of the lower layer tends to be unstable (figure 3d) as in pure shear flow case.

Finally, when both shear $\hat{\alpha}$ and β -effect are taken into account: when $\delta = 1$, $r_0 = 1$ with strong $\hat{\beta}$ and weak shear, vortex tends to deform triangular shape, and with strong shear and weak $\hat{\beta}$, vortex tends to deform elliptical shape (figure 3e). In any case, vortex tends to move latitudinally to the axis of the parabolic flow, which imply that vortex is most stable without shear. Again when r_0 is increased, vortex becomes unstable and tends to assume a diapole structure.

Concluding Remarks

Several remarks are made in this final section.

Firstly, I tried to find an isolated monopole vortex solution in the periodic zonal flow within two-layer quasi-geostrophic model. However, it turned out to be unsuccessful due to a mathematical difficulty, which might imply that very delicate conditions are indeed required in order to isolate vortex in *physical* geostrophic flow. Anyway, it is apparent that additional infinite number of constraints are required to isolate an eddy, and hence the integral constraint (1.1) is not sufficient condition for existence of isolated vortex.

Next, I turn into the constant potential vorticity vortex model. I managed to find an isolated vortex solution by assuming different boundaries ($\tau_b^1 \neq \tau_b^2$) for both layers. Though, I have not tried same procedure ($\tau_b^1 = \tau_b^2$) for the periodic zonal flow case, it may make it possible to obtain an isolated eddy solution. If that were case, the result implies that in order the monopole vortex isolate in the periodic zonal flow its vorticity should be strong enough so that it can maintain a closed streamline in the zonal flow that has opposite vorticity to the eddy.

On the other hand, Ingersoll and Cuong (1981) has obtained an isolated monopole vortex solution within periodic zonal flow under the similar formulation as the second section with deep lower layer (i.e. $\delta \ll 1$), but numerically by assuming

$$|\phi_1| \gg |\phi_2| \sim \delta \quad (4.1)$$

so that upper layer ϕ_1 , can be treated without taking into account the lower layer eddy. They did not examine the consistency of the solution. In the case of simple

constant-potential-vorticity vortex model with $q = -\delta$, though the assumption (4.1) is satisfied in the lower order solution, eddy is adjusted to the β -effect and the deep barotropic zonal flow by purely barotropic part in the higher order, and hence the assumption (4.1) is not valid for this case. It is likely to be the general tendency of the baroclinic monopole eddy that is adjusted to the β -effect and the barotropic zonal flow by barotropic mode, hence the effect of lower eddy to upper eddy is not always negligible. In this sense, Ingersoll and Cuong's numerical calculations are not posed correctly.

Williams and Yamagata (1984) has also demonstrated numerically the stability of isolated eddies in a system different from quasi-geostrophic. However, the same argument can be applied to their numerical calculations, because they have also implicitly assumed the eddy of the deep lower layer is so weak that it is negligible.

The results of constant-potential-vorticity vortex model show that within the restriction of the integral constraint the circular baroclinic monopole solution adjusts to the β -effect and the zonal shear flow by horizontal redistribution of vorticity in higher order. The higher order eddy part, which is solely barotropic and of multiple-pole structure, deforms the circular monopole vortex structure. The results of numerical calculations of counter of vortex show that within strong shear and/or β -term the vortex indeed tends to assume dipole structure stretched by zonal flow. This implies the instability of the monopole vortex within strong zonal shear flow. Hence, the stability of the Great Red Spot is of much more enigma than before.

Acknowledgements

The present work was suggested by and performed under the guidance of Glenn R. Flierl. I express my sincere thanks to Glenn, who also performed most of the numerical computations and made grammatical corrections of this manuscript for me. Discussions with Melvin Stern and other G.F.D. participants were quite helpful. My thanks go to all of them. And finally, but not least, I express my gratitude to Mary Berry, who typed the manuscript in haste, but precisely, so that I could leave Woods Hole in time.

References

Abramowitz, M. and Stegun, I.A., 1964. *Handbook of Mathematical Functions with Formulas, Graphs, and Mathematical Tables* U. S. Dept. of Commerce.

Charney, J.G. and Flierl, G.R., 1981. "Oceanic analogues in large-scale atmospheric motions", in *Evolution of Physical Oceanography*, ed. by B. Warren and C. Wunsch, MIT Press, 502-546.

Flierl, G.R., 1980. "Introduction to coherent features", Summer Study Program in Geophysical Fluid Dynamics, Woods Hole Oceanographic Institution, WHOI 80-53, 1-12.

Flierl, G.R., Larichev, V.D., McWilliams, J.C. and Rezmik, G.M., 1980. "The dynamics of baroclinic and barotropic solitary eddies", *Dyn. Atmos. Oceans*, 5, 1-41.

Flierl, G.R., Stern, M.E. and Whitehead, J.A., Jr., 1983. "The physical significance of modons: laboratory experiments and general integral constraints", *Dyn. Atmos. Oceans*, 7, 233-263.

Flierl, G.R., 1984a. "Model of the structure and motion of a warm-core ring", *Aust. J. Mar Freshw. Res.*, 35, 9-23.

Flierl, G.R., 1984b. "Rossby wave radiation from a strongly nonlinear warm eddy", *J. Phys. Ocean.*, 14, 47-58.

Holton, J.R., 1979. *An Introduction to Dynamic Meteorology*, 2nd ed., Academic Press, New York.

Ingersoll, A.P., and Cuong, P.G., 1981. "Numerical model of long-lived Jovian vortices", *J. Atmos. Sci.*, 38, 2067-2076.

Pedlosky, J., 1979. *Geophysical Fluid Dynamics*, Springer-Verlag, New York.

Stern, M.E. and Flierl, G.R., 1987. "On the interaction of a vortex with a shear flow", preprint.

Swenson, M., 1982. "Isolated 2-D Vortices in the Presence of Shear", Summer Study Program in Geophysical Fluid Dynamics, Woods Hole Oceanographic Institution, WHOI 82-45, 324-336

Yamagata, T., 1982. "On nonlinear planetary waves: a class of solutions missed by the traditional quasi-geostrophic approximation", *J. Oceanogr. Soc. Japan*, 38, 236-244.

Yano, J.-I., 1987. "Rudimentary considerations of the dynamics of the Jovian atmospheres. Part II: Dynamics of the atmospheric-layer", *J. Met. Soc. Japan*, 65, 329-340.

Williams, G.P., and Yamagata, T., 1984. "Geostrophic regimes, intermediate solitary vortices and Jovian eddies", *J. Atmos. Sci.*, 41, 453-478.

Appendix

Coefficients $q_{i,n}$ of (2.23) are defined by

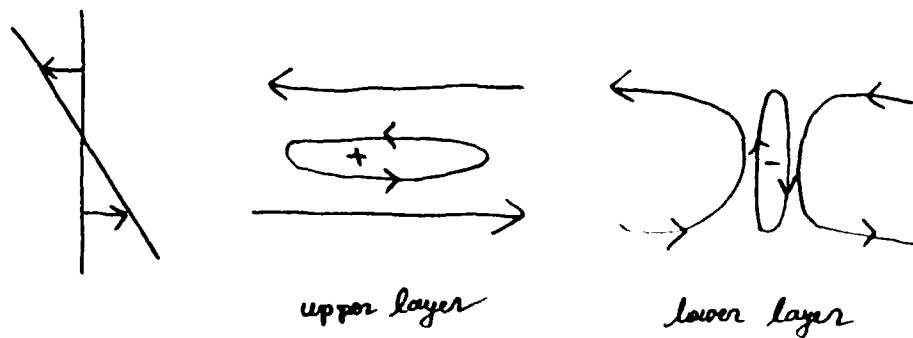
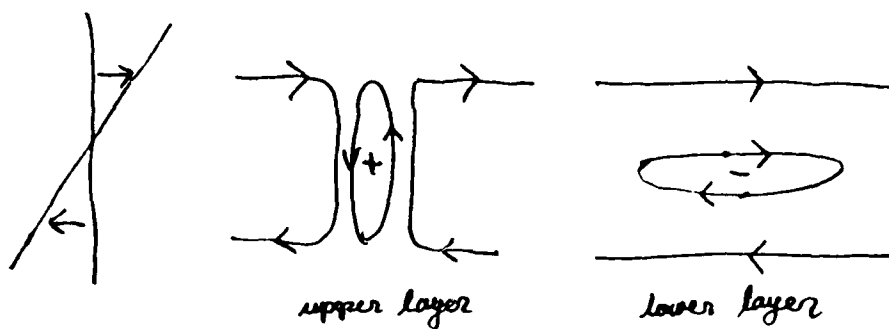
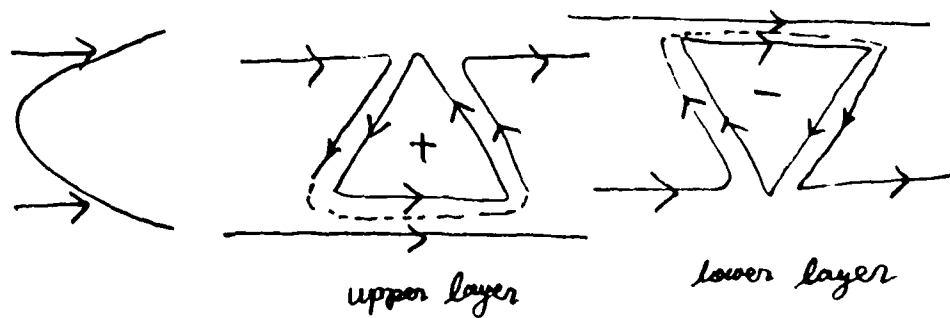
$$\begin{aligned} q_{1,n} &= \left(\Delta_1 \frac{\alpha_1}{\lambda^2} - \Delta_3 \frac{\alpha_3}{\lambda^2} + \frac{\beta_1}{k_1^2} \right) \tau_0 \delta_{n,1} - 2\tilde{\Psi}_0 \sin l y_0 J_n(l r_0) + 2\tilde{\Psi}_{BC} \sin k_1 y_0 J_n(k_1 r_0), \\ q_{2,n} &= \left(\Delta_2 \frac{\alpha_1}{\lambda^2} - \Delta_4 \frac{\alpha_3}{\lambda^2} + \frac{\beta_2}{k_2^2} \right) \tau_0 \delta_{n,1} - 2\tilde{\Psi}_0 \sin l y_0 J_n(l r_0) + 2\tilde{\Psi}_{BT} \sin k_2 y_0 J_n(k_2 r_0), \\ q_{3,n} &= \left\{ \Delta_1 \tilde{W}_1(\lambda, k_1) \left(\frac{\alpha_1}{\lambda^2} - \frac{\alpha_3}{\lambda^2} \right) \tau_0 - \left(\Delta_1 \frac{\alpha_1}{\lambda^2} - \Delta_3 \frac{\alpha_3}{\lambda^2} + \frac{\beta_1}{k_1^2} \right) \right\} \delta_{n,1} \\ &\quad - 2\Delta_1 \tilde{W}_1(\lambda, k_1) \tilde{\Psi}_0 \sin l y_0 J_n(l r_0) + 2\Delta_3 \tilde{\Psi}_0 l \sin l y_0 J_n'(l r_0) - 2\tilde{\Psi}_{BC} k_1 \sin k_1 y_0 J_n'(k_1 r_0), \\ q_{4,n} &= \left\{ \Delta_2 \tilde{W}_1(\lambda, k_2) \left(\frac{\alpha_1}{\lambda^2} - \frac{\alpha_3}{\lambda^2} \right) \tau_0 - \left(\Delta_2 \frac{\alpha_1}{\lambda^2} - \Delta_4 \frac{\alpha_3}{\lambda^2} + \frac{\beta_2}{k_2^2} \right) \right\} \delta_{n,1} \\ &\quad - 2\Delta_2 \tilde{W}_1(\lambda, k_2) \tilde{\Psi}_0 \sin l y_0 J_n(l r_0) + 2\Delta_4 \tilde{\Psi}_0 l \sin l y_0 J_n'(l r_0) - 2\tilde{\Psi}_{BT} k_2 \sin k_2 y_0 J_n'(k_2 r_0) \end{aligned}$$

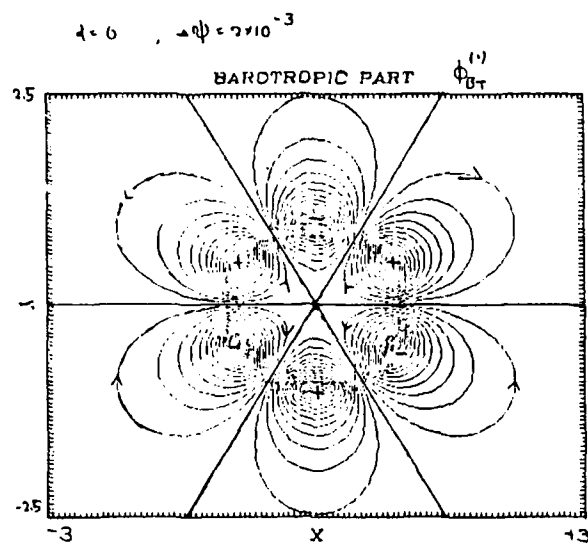
for odd n and

$$\begin{aligned} q_{1,n} &= -(2 - \delta_{n,0}) \tilde{\Psi}_0 \cos l y_0 J_n(l r_0) + (2 - \delta_{n,0}) \tilde{\Psi}_{BC} \cos k_1 y_0 J_n(k_1 r_0), \\ q_{2,n} &= -(2 - \delta_{n,0}) \tilde{\Psi}_0 \cos l y_0 J_n(l r_0) + (2 - \delta_{n,0}) \tilde{\Psi}_{BT} \cos k_2 y_0 J_n(k_2 r_0), \\ q_{3,n} &= -(2 - \delta_{n,0}) \Delta_1 \tilde{W}_1(\lambda, k_1) \tilde{\Psi}_0 \cos l y_0 J_n(l r_0) \\ &\quad + (2 - \delta_{n,0}) \Delta_3 \tilde{\Psi}_0 l \cos l y_0 J_n'(l r_0) - (2 - \delta_{n,0}) \tilde{\Psi}_{BC} k_1 \cos k_1 y_0 J_n'(k_1 r_0), \\ q_{4,n} &= -(2 - \delta_{n,0}) \Delta_2 \tilde{W}_1(\lambda, k_2) \tilde{\Psi}_0 \cos l y_0 J_n(l r_0) \\ &\quad + (2 - \delta_{n,0}) \Delta_4 \tilde{\Psi}_0 l \cos l y_0 J_n'(l r_0) - (2 - \delta_{n,0}) \tilde{\Psi}_{BT} k_2 \cos k_2 y_0 J_n'(k_2 r_0) \end{aligned}$$

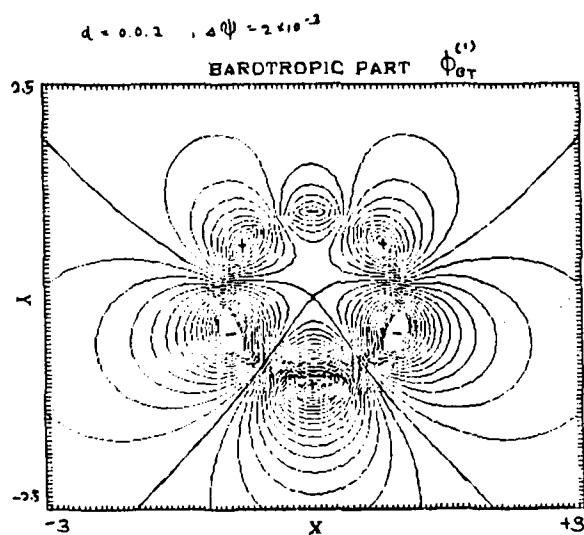
for even n .

Figures and Tables

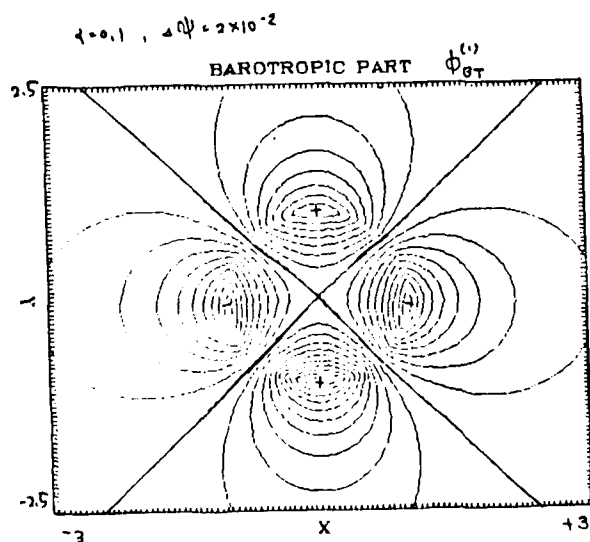
Fig. 1(a) cyclonic shear ($d > 0$)(b) anticyclonic shear ($d < 0$)(c) parabolic shear ($d = 0$)



8.2 (a)

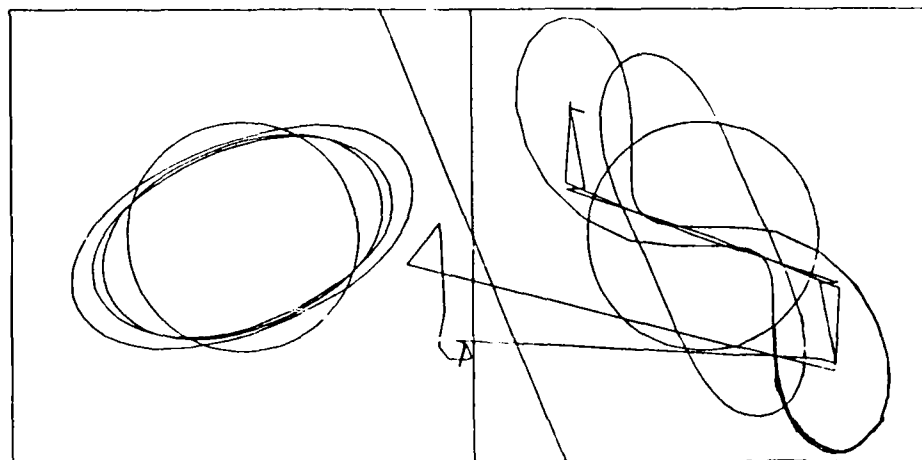


8.2 (b)



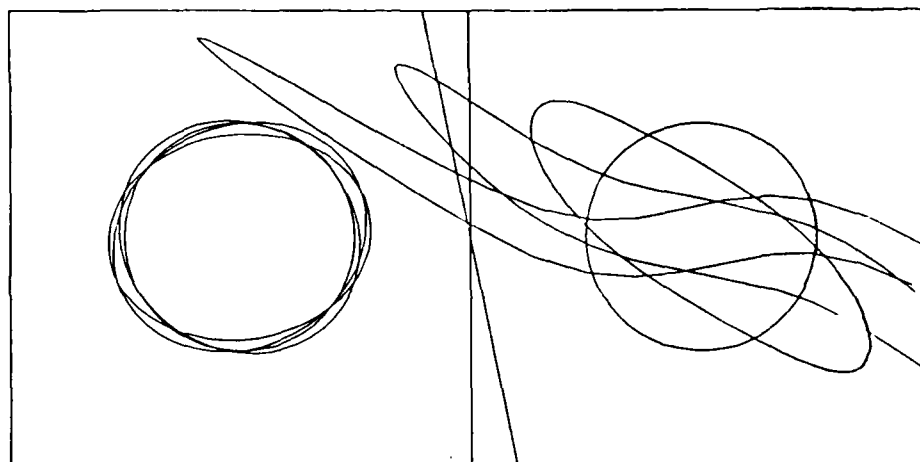
8.2 (c)

50,0.1,30,10.0, 0.0,-0.4,0.0, 1.0,-1.0,1.0, 2.0
 n,dt,ns,tmax, beta,shear,u0, delta,qratio,gamma, scale



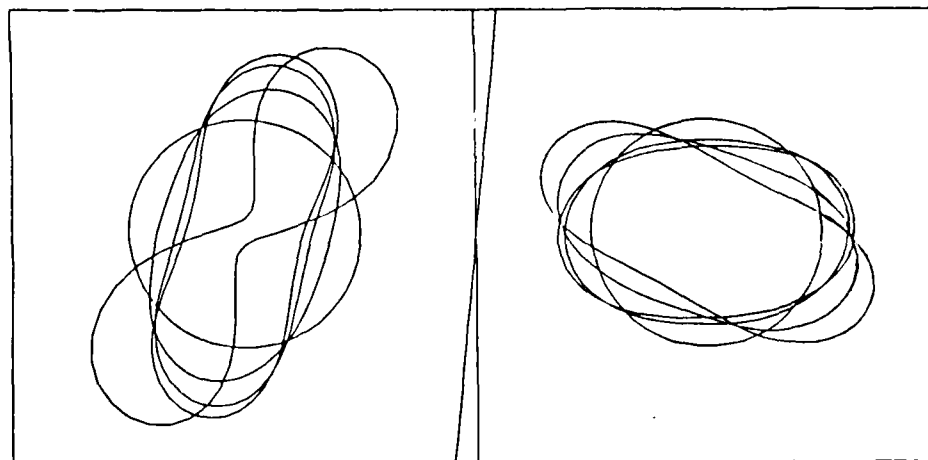
8.3 (a)

50,0.1,60,20.0, 0.0,-0.2,0.0, 0.1,-0.1,1.0, 2.0
 n,dt,ns,tmax, beta,shear,u0, delta,qratio,gamma, scale



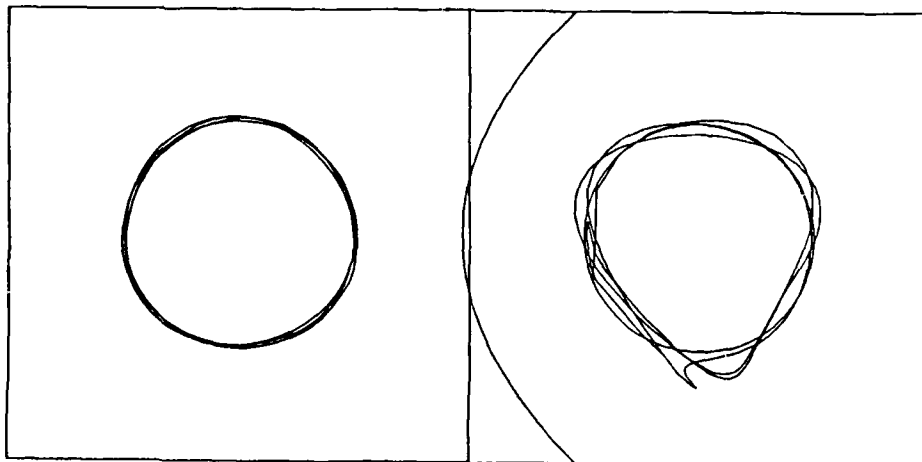
8.3 (b)

50,0.1,40,20.0, 0.0,0.1,0.0, 1.0,-1.0,1.5, 2.0
 n,dt,ns,tmax, beta,shear,u0, delta,qratio,gamma, scale



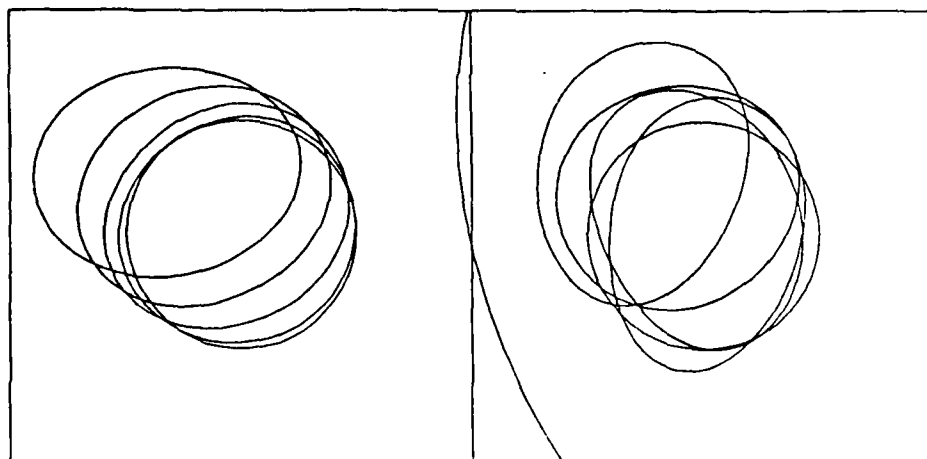
8.3 (c)

50,0.05,60,10.0,0.5,0.0,-0.0625,0.3,-0.3,1.0,2.0
n,dt,ns,tmax,beta,shear,u0,delta,qratio,gamma,scale



8.3 (d)

50,0.1,40,20.0,0.2,-0.2,-0.025,1.0,-1.0,1.0,2.0
n,dt,ns,tmax,beta,shear,u0,delta,qratio,gamma,scale



8.3 (e)

TABLE 1
SUMMARY OF NUMERICAL RESULTS

1. Only with shear ($\hat{\beta} = 0$)

1.1 $r_o = 1$, $\delta = 1$

<i>shear</i> $\hat{\alpha}$	<i>upper layer</i>	<i>lower layer</i>
0.2	N-S elongated (rotate with time)	E-W elongated
- 0.2	E-W elongated (rotate with time)	N-S elongated
* - 0.4	E-W elongated	N-S elongated (unstable)

1.2 $r_o = 1$, $\delta \neq 1$

δ	<i>shear</i> $\hat{\alpha}$	<i>lower layer</i>
0.5	- 0.1	N-S elongated (rotate with time)
0.2	0.2	E-W elongated (in larger magnitude than upper layer)
0.1	0.2	vortex continuously stretched in E-W
* 0.1	-0.2	vortex continuously stretched in NW-SE

1.3 $\delta = 1$, $r_o \neq 1$

r_o	<i>shear</i> $\hat{\alpha}$	<i>upper layer</i>	<i>lower layer</i>
1.2	- 0.2	E-W elongated	N-S elongated
* 1.5	0.1	N-S dipole	E-W elongated
1.5	- 0.2	N-S elongated (rotate)	N-S dipole

2. Only with β (shear $\hat{\alpha} = 0$)

2.1 $r_o = 1$

δ	$\hat{\beta}$	upper layer	lower-layer
1	0.5	triangular shape	inverse-triangular shape
0.5	0.5	triangular shape	inverse-triangular shape
* 0.3	0.5	triangular shape	inverse-triangular shape (unstable)
0.3	0.3	triangular shape	inverse-triangular shape

2.2 $r_o = 2$

δ	$\hat{\beta}$	upper layer	lower-layer
1	0.5	E-W dipole (unstable)	E-W elongated dipole structure

3. Both β and shear, $\delta = 1$

3.1 $r_o = 1$

$\hat{\beta}$	shear	direction of displacement	shape of deformation
0.1	- 0.1	northward	elongation (weak)
0.1	0.1	southward	elongation (weak)
* 0.2	- 0.2	northward	triangular/elongation
0.2	0.2	southward	elongation
0.5	- 0.2	(northward)	triangular
0.5	- 0.1	northward	triangular
1.5	0.2	southward	triangular

3.2 $r_o = 1.5$

$\hat{\beta}$	shear $\hat{\alpha}$	
* 0.1	- 0.2	lower layer: E-W dipole
	- 0.1	northward movement, elongated
	0.1	upper layer: NE-SW dipole

* The run with * is represented in figure.

TABLE 2
The Parameters Used for Computations

n:	number of points taken along the contour
dt:	time step (in nondimensional unit)
ns:	the interval in number of time steps that the contour is drawn
tmax:	computations 1 time (nondimensional unit)
beta:	$\hat{\beta}$
shear:	$\hat{\alpha}$
u0:	$\hat{\gamma}$
delta:	$\hat{\delta}$
qratio:	q ; note $q_1 = 1$ is assumed
gamma:	r_0
scale:	parameter giving the domain of representation by $(-\text{scale} \cdot r_0, \text{scale} \cdot r_0) \times (-\text{scale} \cdot r_0, \text{scale} \cdot r_0)$

DOCUMENT LIBRARY

August 21, 1987

Distribution List for Technical Report Exchange

Attn: Stella Sanchez-Wade
Documents Section
Scripps Institution of Oceanography
Library, Mail Code C-075C
La Jolla, CA 92093

Hancock Library of Biology &
Oceanography
Alan Hancock Laboratory
University of Southern California
University Park
Los Angeles, CA 90089-0371

Gifts & Exchanges
Library
Bedford Institute of Oceanography
P.O. Box 1006
Dartmouth, NS, B2Y 4A2, CANADA

Office of the International
Ice Patrol
c/o Coast Guard R & D Center
Avery Point
Groton, CT 06340

Library
Physical Oceanographic Laboratory
Nova University
8000 N. Ocean Drive
Dania, FL 33304

NOAA/EDIS Miami Library Center
4301 Rickenbacker Causeway
Miami, FL 33149

Library
Skidaway Institute of Oceanography
P.O. Box 13687
Savannah, GA 31416

Institute of Geophysics
University of Hawaii
Library Room 252
2525 Correa Road
Honolulu, HI 96822

Library
Chesapeake Bay Institute
4800 Atwell Road
Shady Side, MD 20876

MIT Libraries
Serial Journal Room 14E-210
Cambridge, MA 02139

Director, Ralph M. Parsons Laboratory
Room 48-311
MIT
Cambridge, MA 02139

Marine Resources Information Center
Building E38-320
MIT
Cambridge, MA 02139

Library
Lamont-Doherty Geological
Observatory
Columbia University
Palisades, NY 10964

Library
Serials Department
Oregon State University
Corvallis, OR 97331

Pell Marine Science Library
University of Rhode Island
Narragansett Bay Campus
Narragansett, RI 02882

Working Collection
Texas A&M University
Dept. of Oceanography
College Station, TX 77843

Library
Virginia Institute of Marine Science
Gloucester Point, VA 23062

Fisheries-Oceanography Library
151 Oceanography Teaching Bldg.
University of Washington
Seattle, WA 98195

Library
R.S.M.A.S.
University of Miami
4600 Rickenbacker Causeway
Miami, FL 33149

Maury Oceanographic Library
Naval Oceanographic Office
Bay St. Louis
NSTL, MS 39522-5001

ADA 196554

REPORT DOCUMENTATION PAGE	1. REPORT NO. WHOI-88-16	2.	3. Recipient's Accession No.
4. Title and Subtitle Summer Study Program in Geophysical Fluid Dynamics Order and Disorder in Planetary Dynamos		5. Report Date May 1988	
7. Author(s) Willem V.R. Malkus; Edited by Mary Evans Berry		8. Performing Organization Rept. No. WHOI-88-16	
9. Performing Organization Name and Address The Woods Hole Oceanographic Institution Woods Hole, Massachusetts 02543		10. Project/Task/Work Unit No.	
		11. Contract(C) or Grant(G) No. (C) N000114-82-G-0079 (G) DMS-85-04166	
12. Sponsoring Organization Name and Address The Office of Naval Research; and the National Science Foundation		13. Type of Report & Period Covered Technical Report	
		14.	
15. Supplementary Notes This report should be cited as: Woods Hole Oceanog. Inst. Tech. Rept., WHOI-88-16.			
16. Abstract (Limit: 200 words) This volume contains the lectures of Stephen Childress on the kinematic properties of the "fast" dynamo, one whose growth rate is insensitive to electrical conductivity. These novel studies and the extended seminar abstracts by Andrew Soward and others that follow offer assurance of more mechanistic understanding of evolving magnetic fields in stars and planets. The timely juxtaposition of Childress' lectures on kinematic fast dynamos and the seminars by Bruce Bayly on inertial three-dimensional instabilities of shear flow, may lead soon to a dynamic fast-fast dynamo. The final section contains the fellows' reports, which were more confined to the summer topic than is usual. Several of the Fellows reported on exciting discoveries of the season, several reported on sound extensions of work discussed in the principal lectures, and several struggled with problems which resisted swift resolution.			
17. Document Analysis a. Descriptors 1. Planetary dynamos 2. Geophysical Fluid Dynamics NE b. Identifiers/Open-Ended Terms c. COSATI Field/Group			
18. Availability Statement Approved for publication; distribution unlimited.		19. Security Class (This Report) UNCLASSIFIED	21. No. of Pages 164
		20. Security Class (This Page)	22. Price